WL-TR-92-2023

COMBUSTION DIAGNOSTICS BY PHOTO-DEFLECTION SPECTROSCOPY

DR RAJENDRA GUPTA
UNIVERSITY OF ARKANSAS
Dept of Physics/105 Physics Bldg
Fayetteville, Arkansas 72701

MARCH 1992

FINAL REPORT FOR PERIOD OCTOBER 1984 - SEPTEMBER 1988

Approved for public release; distribution is unlimited

Aero Propulsion and Power Directorate
Wright Laboratory
Air Force System Command
Wright-Patterson Air Force Base, Ohio 45433-6563

NOTICE

When Government drawings, specifications, or other data are used for any purpose other than in connection with a definitely Government-related procurement, the United States Government incurs no responsibility or any obligation whatsoever. The fact that the government may have formulated or in any way supplied the said drawings, specifications, or other data, is not to be regarded by implication, or otherwise in any manner construed, as licensing the holder, or any other person or corporation; or as conveying any rights or permission to manufacture, use, or sell any patented invention that may in any way be related thereto.

This report is releasable to the National Technical Information Service (NTIS). At NTIS, it will be available to the general public, including foreign nations.

This technical report has been reviewed and is approved for publication.

Sigmund W. Kizirnis

SIGMUND W. KIZIRNIS
Power Components Branch
Aerospace Power Division
Aero Propulsion and Power Directorate

Lowell D. Massie

LOWELL D. MASSIE
Chief, Power Components Branch
Aerospace Power Division
Aero Propulsion and Power Directorate

Michael D Brayboy

MICHAEL D. BRAYBOY, Lt Col, USAF
Deputy Director
Aerospace Power Division
Aero Propulsion & Power Directorate

If your address has changed, if you wish to be removed from our mailing list, or if the addressee is no longer employed by your organization please notify WL/POOC , WPAFB, OH 45433-6563 to help us maintain a current mailing list.

Copies of this report should not be returned unless return is required by security considerations, contractual obligations, or notice on a specific document.

REPORT DOCUMENTATION PAGE

Form Approved
OMB No. 0704-0188

1a. REPORT SECURITY CLASSIFICATION UNCLASSIFIED	1b. RESTRICTIVE MARKINGS N/A
2a. SECURITY CLASSIFICATION AUTHORITY N/A	3. DISTRIBUTION/AVAILABILITY OF REPORT Approved for public release; distribution is unlimited.
2b. DECLASSIFICATION/DOWNGRADING SCHEDULE N/A	
4. PERFORMING ORGANIZATION REPORT NUMBER(S)	5. MONITORING ORGANIZATION REPORT NUMBER(S) WL-TR-92-2023
6a. NAME OF PERFORMING ORGANIZATION Univ. of Arkansas 6b. OFFICE SYMBOL (If applicable)	7a. NAME OF MONITORING ORGANIZATION Aero Propulsion & Power Dir. (WL/POOC) Wright Laboratory
6c. ADDRESS (City, State, and ZIP Code) Dept of Physics / 105 Physics Bldg Fayetteville, Arkansas 72701	7b. ADDRESS (City, State, and ZIP Code) Wright-Patterson AFB, OH 45433-6563
8a. NAME OF FUNDING/SPONSORING ORGANIZATION 8b. OFFICE SYMBOL (If applicable)	9. PROCUREMENT INSTRUMENT IDENTIFICATION NUMBER F33615-84-K-2437
8c. ADDRESS (City, State, and ZIP Code)	10. SOURCE OF FUNDING NUMBERS

PROGRAM ELEMENT NO.	PROJECT NO.	TASK NO.	WORK UNIT ACCESSION NO.
61102F	2301	S1	26

11. TITLE (Include Security Classification)

Combustion Diagnostics by Photo-Deflection Spectroscopy

12. PERSONAL AUTHOR(S)
Gupta, Rajendra

13a. TYPE OF REPORT	13b. TIME COVERED	14. DATE OF REPORT (Year, Month, Day)	15. PAGE COUNT
Final	FROM 10/84 TO 9/88	9203XX	98

16. SUPPLEMENTARY NOTATION

17. COSATI CODES			18. SUBJECT TERMS (Continue on reverse if necessary and identify by block number)
FIELD	GROUP	SUB-GROUP	Photo-Deflection Spectroscopy Photo-Acoustic Deflection Spect., Photo-Thermal Defl. Spect., Flames, Combustion
	2		
7	3		

19. ABSTRACT (Continue on reverse if necessary and identify by block number)

Experimental and theoretical investigations of photocoustic deflection spectroscopy (PADS) and photo thermal deflection spectroscopy (PDTS) have been carried out for the application of these techniques to combustion diagnostics. The investigations have been two-pronged: (i) To determine the range of applicability of these techniques to combustion diagnostics, and (ii) to develop a good theoretical and experimental understanding of these techniques so that quantitative measurements can be made. Both techniques (PADS and PTDS) are very useful for combustion diagnostics and absolute measurements of the species concentrations. Also, simultaneous measurements of species concentrations, local temperature, and flow velocity can be made. With these techniques the most stringent tests of the theoretical models of combustion can be done. PTDS is about an order of magnitude more sensitive than PADS, and therefore PTDS was chosen for a thorough theoretical and experimental investigation. The results showed a good agreement between the theory and the experiment. Where disagreement existed, reasons for the discrepancies were determined.

20. DISTRIBUTION/AVAILABILITY OF ABSTRACT	21. ABSTRACT SECURITY CLASSIFICATION
☐ UNCLASSIFIED/UNLIMITED ☐ SAME AS RPT. ☒ DTIC USERS	Unclassified

22a. NAME OF RESPONSIBLE INDIVIDUAL	22b. TELEPHONE (Include Area Code)	22c. OFFICE SYMBOL
Sigmund Kizirnis	(513) 255-2923	WL/POOC

Table of Contents

Summary

Experimental and theoretical investigations of photoacoustic deflection spectroscopy (PADS) and photothermal deflection spectroscopy (PDTS) have been carried out for the application of these techniques to combustion diagnostics. The investigations have been two-pronged: (i) To determine the range of applicability of these techniques to combustion diagnostics, and (ii) to develop a good theoretical and experimental understanding of these techniques so that quantitative measurements can be made. Both techiques (PADS and PTDS) have been found to be extremely useful for combustion diagnostics and absolute measurements of the species concentrations are possible. Morevoer, simultaneous measurements of species concentrations, local temperature and flow velocity can be made. Thus, using these techniques, the most stringent tests of the theoretical models of combustion can be performed. PTDS has been found to be about an order of magnitude more sensitive than PADS, and therefore a thorough theoretical and experimental investigation of PTDS has been carried out. In general, very good agreement between the theory and the experiment has been found, and where disagreements exist, possible reasons for the disagreements have been determined.

I. Introduction

We have investigated two interrelated techniques, photoacoustic deflection spectroscopy (PADS) and photothermal deflection spectroscopy (PTDS), as combustion diagnostic techniques. The main goal of this work was two-fold: (i) To determine the range of applicability of those techniques to combustion diagnostics and (ii) to develop rigorous theoretical models and to verify the models experimentally so that the techniques may be used for quantitative measurements. Section II describes our investigations of PADS and Section III describes those of PTDS. Major accomplishments of this work are summarized in Section IV and lists of publications and presentations based on work done under this contract are given in Sections V and VI, respectively.

II. Photoacoustic Deflection Spectroscopy

Application of PADS to a combustion environment was demonstrated by observation of PADS signals generated in OH produced in the combustion of methane and air (Appendix 1). Relative concentration profile of OH radical in a natural gas/air flame was also measured (Appendix 2). Temperature measurement by PADS was demonstrated by generating the signal on soot particles in an oxyacetylene flame (Appendix 3). In order to make quantitative measurements using PADS, it is necessary that a quantitative understanding of the size and shape of PADS signals exist. For this purpose, a theoretical model of PADS was developed. The results of this model are given in Appendix 4. An experiment was performed under well characterized conditions to verify the model. This result is also described in Appendix 4. A discrepancy of about a factor of three between the thoeory and the experiment can be ascribed to the limited bandwidth of our optical deflection. We have determined that the sensitivity of PADS is about an

order of magnitude smaller than that of PTDS (See Section III below). Therefore, no further work was performed on PADS and most of the effort was devoted to the investigation of PTDS.

III. Photothermal Deflection Spectroscopy

Application of PTDS to combustion diagnostics was demonstrated by us in 1982 (Appendix 5) and the concentration profile of OH radical in a propane/air flame was measured in 1984 (Appendix 6). Moreover, since one of the most important combustion parameters is the flow velocity of the medium, we have devised two techniques based on PTDS to measure flow velocities. The first technique makes use of the transit time of a heat pulse between two laser beams and it is particularly suitable for flow-velocity measurements in a combustion medium (Appendix 7). We have demonstrated this technique experimentally by measuring the flow velocity profile of a laminar oxyhydrogen glass-blowing torch (Appendix 7). The second technique, which depends on the amplitude of the PTDS signal, is particularly suitable for very slow velocities (Appendix 8). However, the use of this technique in a combustion medium is problematic. The use of PTDS for flow velocity and soot concentration measurements was also demonstrated by applying the techniques to a sooting oxyacetylene flame (Appendix 3). Recently, we have also detected NH_2 radical in an ammonia/oxygen/nitrogen flame using PTDS. Reliable temperature measurements using PTDS have not yet been possible due to a non-Gaussian spatial profile of our pump laser.

Having demonstrated the usefulenss of PTDS for velocity and concentration measurements in flames, our next task was to obtain quantitative understanding of the sizes and shapes of PTDS signals under a variety of conditions so that quantitative measurements can be performed. For this purpose we have developed

a theoretical model of PTDS under most general conditions (Appendix 9). Our model is valid for a flowing as well as a stationary medium, and for laser pulses of arbitrary length. Experimental verification of the theoretical model has also been attempted (Appendix 9). This work has also been extended to CW excitation (Appendix 10). For the pulsed case, which is what is relevant for combustion diagnostics, we have found that in general the theory and the experiment are in very good agreement, except in one case: The width of the PTDS signal for a stationary medium was found to be too narrow compared to the theoretical predictions (Appendix 9). This disagreement between the theory and the experiment is believed to be due to either one of the following two causes: (i) The spatial profile of our laser is not Gaussian, as assumed in the theoretical model. The actual spatial profile was measured and found to be a mixture of higher order modes. For this purpose we devised a method of measurement, using PTDS itself (Appendix 11). However, this method could only measure the average profile of a large number of pulses. Therefore, a second method was devised, again using PTDS, to measure the spatial profile of individual laser pulses in real time (Appendix 12). Thus, pulse-to-pulse instability could be monitored. It was found that less than 10% of the pulses from our laser were even close to being Gaussian (Appendix 12). (ii) It is possible that the observed signal was not a pure PTDS signal, and that it had an admixture of photothermal lensing spectroscopy (PTLS) signal. For this purpose, a thorough investigation of PTLS signal size and shapes was carried out (Appendix 13). At this point, we have all the background information available, and if a laser with good spatial profile (e.g., Nd:YAG pumped dye laser) becomes available, we will be able to definitely establish the cause of the discrepancy between the theory and the experiment mentioned above. Once this is accomplished, absolute measurements of species concentration, temperature, and flow-velocity can be performed.

IV. Major Accomplishments

1. Experimentally demonstrated the applicability of photothermal technique to flames for the measurements of species concentration, temperature, and flow velocity.

2. Developed a rigorous and complete theoretical model of the photothermal technique under the most general conditions (flowing medium, arbitrary excitation function, etc.). This covers all three detection schemes, that is, photothermal phase-shift spectroscopy, photothermal deflection spectroscopy, and photothermal lensing spectroscopy.

3. Subjected the theoretical model of pulsed photothermal deflection spectroscopy to experimental tests. Absolute measurements were made and compared with the predictions of the theoretical model without using any adjustable parameter. Very good agreement was found.

4. All the background work is now complete, and the technique can now be applied to absolute measurements of minority species concentrations, temperature, and flow velocities in flames. All three parameters can be obtained simultaneously in a single laser shot. Species such as OH, CN, CH, NO can be measured.

5. The photothermal signal depends critically on the spatial profile of the pump laser, which changes from pulse to pulse. We have developed a new method for the measurement of spatial profile of a pulsed laser. Using this method, spatial profile of a single pulse can be measured in real time.

6. Work done under this contract resulted in 19 refereed publications, and 13 presentations at national and internatonal conferences, including six invited talks.

V. Publications

1. Photoacoustic Detection of OH Molecules in a Methane-Air Flame," A. Rose, J.D. Pyrum, G.J. Salamo, and R. Gupta, Applied Optics 23, 781 (1984).

2. "Photoacoustic Deflection Spectroscopy: A New Species-Selective Method for Combustion Diagnostics," A. Rose, G.J. Salamo, and R. Gupta, Applied Optics 23, 781 (1984).

3. "Hydroxyl (OH) Distributions and Temperature Profiles in a Premixed Propane Flame Obtained by Laser Deflection Techniques," S.W. Kizirnis, R.J. Brecha, B.N. Ganguly, L.P. Goss, and R. Gupta, Applied Optics 23, 3873 (1984).

4. "The Photoacoustic and Photothermal Techniques as Probes in Combustion Studies," K. Tennal, A. Rose, J. Pyrum, C. Muzny, R. Gupta, and G. Salamo, in Lasers as Reactants and Probes in Chemistry, Eds. W.M. Jackson and A.B. Harvey (Howard University Press, 1985).

5. "Combustion Diagnostics by Photo-Deflection Spectroscopy," A. Rose and R. Gupta, Proceedings of the Twentieth International Symposium on Combustion (The Combustion Institute, Pittsburgh, PA, 1985).

6. "Application of Photothermal Deflection Technique to Flow Velocity Measurements in a Flame," Optics Letters 10, 532 (1985).

7. "Application of Photothermal and Photoacoustic Deflection Techniques to Sooting Flames; Velocity, Temperature, and Concentration Measurements," Optics Communications 56, 303 (1986).

8. "Laser Beam Profile Measurement by Photothermal Deflection Technique," A. Rose, Y.-X. Nie, and R. Gupta, Applied Optics 25, 1738 (1986).

9. "A Quantitative Investigation of Pulsed Photothermal and Photoacoustic Deflection Spectroscopy for Combustion Diagnostics," R. Gupta, in Advances in Laser Science-I, eds. W.C. Stawley and M. Lapp, AIP Conference Proceedings #146 (AIP, N.Y., 1986).

10. "Measurement of Very Slow Gas Flow Velocities by Photothermal Deflection Spectroscopy," Y.-X. Nie, K. Hane, and R. Gupta, Applied Optics 25, 3247 (1986).

11. "A Quantitative Investigation of Pulsed Polythermal Deflection Spectroscopy in a Flowing Medium," A. Rose, Reeta Vyas, and R. Gupta, Applied Optics 25, 4626 (1986).

12. "Combustion Diagnostics by Photothermal Deflection Spectroscopy and Photoacoustic Deflection Spectroscopy," R. Gupta and Y.-X. Nie, Wuli 16, 202 (1987).

13. "Theory of the Photothermal Effect in Fluids," R. Gupta, in Photothermal Investigations in Solids and Fluids, ed. J. Sell (to be published by Academic Press, 1988).

14. "Combustion Diagnostics by Photothermal Deflection Spectroscopy," R. Gupta, in Photothermal Investigations in Solids and Fluids, ed. J. Sell (to be published by Academic Press, 1988).

15. "Photothermal Deflection Spectroscopy in Fluid Media: A Review", R. Gupta, in Proceedings of International Conference on Lasers '86, Ed. R. McMillan, STS Press, McLearn, VA, 1987.

16. "Continuous Wave Photothermal Deflection Spectroscopy in a Flowing Medium, Reeta Vyas, B. Monson, Y.-X. Nie, and R. Gupta, Appl. Optics 27, 3914 (1988).

17. "Real-time Measurements of the Spatial Profile of a Pulsed Laser by Photothermal Spectroscopy," Karen Williams, Paul Glezen, and R. Gupta, Optics Letters 13, 740 (1988).

18. "Photothermal Lensing Spectroscopy in a Flowing Medium: Theory," Reeta Vyas and R. Gupta, Applied Optics 27, 4701 (1988).

19. "Pulsed and Continuous Wave Photothermal Phase-shift Spectroscopy in a Fluid Medium: Theory," Applied Optics (submitted, 1988).

VI. Presentations at Conferences

"Photoacoustic Deflection Spectroscopy: A Purely Optical Method of Photoacoustic Signal Detection, "A. Rose and R. Gupta, Bull. Am. Phys. Soc. 29, 822 (1984). DEAP meeting 1984.

"An Experimental Investigation of Pulsed Photo-Deflection Spectroscopy," A. Rose and R. Gupta, Bull. Am. Phys. Soc. 30, 866 (1985). DEAP Meeting 1985.

"Combustion Diagnostics by Photo-Deflection Spectroscopy," A. Rose and R. Gupta, Twentieth International Symposium on Combustion, U of Michigan, Ann Arbor, MI, August 1984.

"Measurement of Species Concentration, Temperature and Flow Velocities in Flames by Photothermal and Photoacoustic Deflection Spectroscopy," A Rose and R. Gupta, Gordon Research Conference on Laser Combustion Diagnostics, July 1985.

"Application of Photothermal and Photoacoustic Deflection Spectroscopy to Flame Diagnostics," A. Rose and R. Gupta, Congre Photoacoustique 1985, Montreal, Canada, August 1985.

**"Application of Photoacoustic and Photothermal Deflection Spectroscopy to Flames," R. Gupta, Annual Meeting, Optical Society of America, Washington, DC, 1985.

**"An Investigation of Pulsed Photothermal and Photoacoustic Deflection Spectroscopy for Combustion Diagnostics," A. Rose and R. Gupta, First International Laser Science Conference, Dallas, TX, 1985.

"Flow Velocity Measurements Using Photothermal Deflection Spectroscopy,' R. Gupta, XIII Annual Meeting of the Federation of Analytical Chemistry and Spectroscopy Societies, St. Louis, 1986.

**"Photothermal Deflection Spectroscopy in a Gaseous Medium," R. Gupta, International Conference on Lasers '86, Orlando, FL, 1986.

"Photoacoustic Measurements by a Michelson Interferometer," Y.-X. Nie, K. Hane, and R. Gupta, International Conference on Lasers '86, Orlando, FL, 1986.

**"Absolute Measurements Using Photothermal Deflection Spectroscopy," R. Gupta †, International Conference on Lasers '87, Lake Tahoe, 1987.

**"Photothermal Lensing Spectroscopy in a Flowing Medium: Theory and Experiment," R. Gupta †, International Conference on Lasers '88, Lake Tahoe, 1988.

** Invited papers

† Also organizer of a session & session chair.

Appendix I

Reprinted from Applied Optics, Vol. 23, page 781, March 15, 1984

Photoacoustic deflection spectroscopy: a new specie-specific method for combustion diagnostics

A. Rose, G. J. Salamo, and R. Gupta

University of Arkansas, Physics Department, Fayetteville, Arkansas 72701.
Received 15 October 1983.
0003-6935/84/060781-04$02.00/0.

Recently we have shown that photothermal deflection spectroscopy has an excellent potential for developing into a sensitive combustion diagnostic technique for minority species concentration measurements.[1] In this technique a dye laser (pump beam), tuned to an absorption line of the molecule (or atom) of interest, is directed through the combustion region. Most of the optical energy absorbed by the molecules is rapidly converted into heat due to quenching collisions. Heating of the dye laser irradiated region is accompanied by refractive-index gradients due to the spatial profile of the dye laser beam and diffusion of this heat. The refractive-index gradient is probed by observing the deflection of a He–Ne laser (probe) beam. This deflection can be correlated with the concentration of absorbing molecules. Application of this technique to a combustion environment was demonstrated by observing a photothermal signal from NO_2 produced in the combustion of methane and oxygen.[1] In this Letter, by application to OH molecules in a methane–oxygen flame, we show that the pressure change accompanying the heating of the dye laser irradiated region can also be detected by the deflection of the probe beam placed a small distance from the pump beam. This technique, photoacoustic deflection spectroscopy (PADS), can be used as a sensitive technique for minority species and local temperature measurements. If significant concentration gradients are present in the flame, application of photothermal deflection spectroscopy (PTDS) is not straightforward. The PTDS signal in this case may be proportional to the concentration gradients rather than concentration of the absorbing molecules if the pump and probe beams overlap. The problem may be largely alleviated if the pump and probe beams are spatially separated.[1] However, the PTDS signal amplitude decreases very fast with increasing probe–pump beam distance[2] reducing the sensitivity of the technique. In this case (i.e., when significant concentration gradients are present) PADS can be used with advantage because the PADS signal does not decrease with probe–pump beam distance very fast, and its sensitivity for spatially separated beams is much higher than that for PTDS. Moreover PADS also offers a simple way to measure simultaneously local temperature by measurement of the acoustic velocity in the flame. In this respect, PADS is related to Tam's recently developed "Optoacoustic Laser Deflection (OLD)" technique for temperature measurements.[3] A more detailed discussion of OLD and its comparison with PADS will be given later in the Letter.

PADS is similar to conventional photoacoustic spectroscopy (PAS)[4,5] except that the pressure change is detected optically and not by a microphone (or a piezoelectric transducer). PADS has several advantages over PAS while retaining the sensitivity of PAS: (1) The optical detector that measures the deflection of the probe beam can be placed as far away from the flame as necessary without adversely affecting the sensitivity. The SNR depends on the separation between the probe and pump beams inside the flame and not on the position of the detector. This permits application of this technique to hostile environments. (2) The acoustic signal never

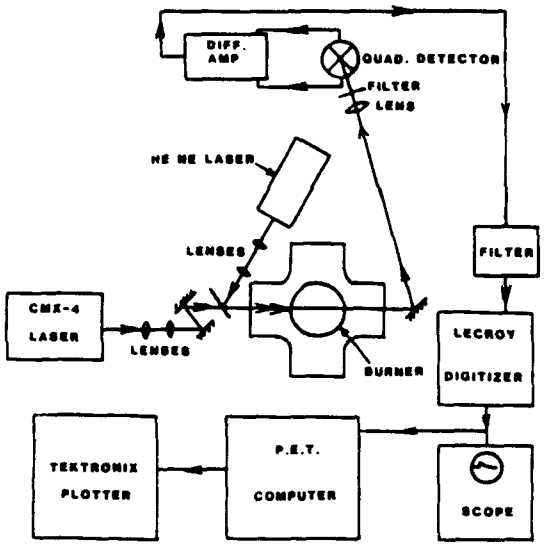

Fig. 1. Schematic illustration of our experimental arrangement.

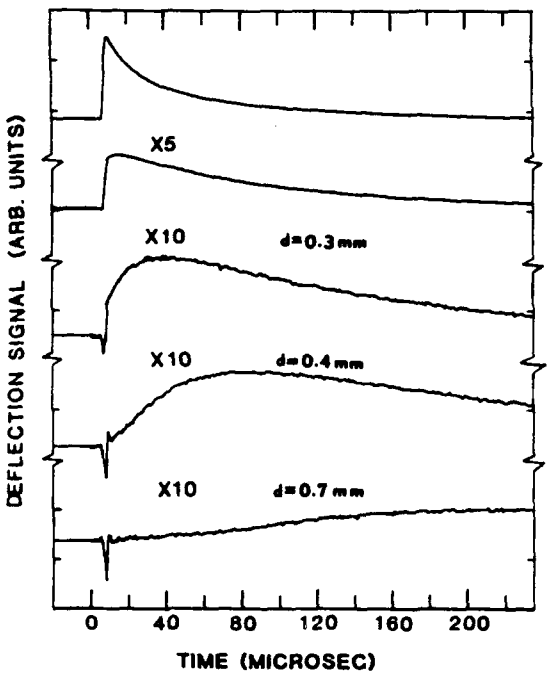

Fig. 2. Deflection of the probe beam as a function of time after the pump laser firing for various pump–probe beam distances d. The distance d was estimated from the measurements of acoustic travel times; d for top two curves could not be estimated. Laser fires 5.3 μsec after the trigger pulse ($t = 0$). The second curve from the top has been magnified by a factor of 5, and the three bottom curves have been magnified by a factor of 10. The broad curves represent the photothermal deflection signal, while the sharp spike in the bottom three curves is the photoacoustic deflection signal. The laser was tuned to the $Q_1(8)$ line of OH molecules at 3092 Å and delivered 7 μJ of energy per pulse.

has to cross the flame boundaries where modifications of the acoustic wave front may occur—a problem with microphone detection.[6] (3) Microphones have a limited bandwidth (typically <100 kHz), which limits the usefulness of PAS considerably. Piezoelectric transducers may be obtained with higher bandwidth, but they have poor sensitivity due to acoustic impedence mismatch. On the other hand, optical detectors have a much larger bandwidth, and this limitation does not occur. (4) It is not an easy matter to measure local temperature in a flame using PAS in real time. In PADS, however, measurement of the acoustic travel time between the pump and probe beams directly yields the local temperature on a single-shot basis. (5) Finally, it is difficult to get spatial resolution using PAS because one detects the integrated signal from the entire flame–laser beam interaction length. However, PADS has a good potential for obtaining spatial resolution by using probe and pump laser beams nearly at right angles.

We would like to describe our preliminary experiments in which we have observed PADS signals from OH in a methane–oxygen flame. Our apparatus is shown in Fig. 1. A stainless steel flat flame burner with methane, oxygen, and nitrogen is used. The burner, ~6 cm in diameter, operated at atmospheric pressure, produces a faint blue pancake-shaped ~1.5-mm thick flame. The burner is enclosed inside a glass chamber with four quartz windows and an exhaust at the top. Laser radiation from a Chromatix CMX-4 flashlamp pumped dye laser, frequency doubled by an intracavity ADP second harmonic crystal, is used to excite the $X^2\Pi$–$A^2\Sigma$ band of OH molecules. The laser produces 1-μsec pulses, and in the experiments reported in this paper, operated with ~10 μJ of energy/pulse at 3100 Å. A He–Ne laser beam used as a probe beam also passed through the flame close to the pump beam. The deflection of the probe beam caused by refractive-index gradients produced by the passing acoustic pulse is detected by a position sensitive detector. The position sensitive detector consists of four quadrants, two of which are used in our experiments. The difference signal from the two quadrants is proportional to the position of the probe beam. The difference signal is digitized by a LeCroy WD 8256 transient digitizer and transferred to a Commodore PET microcomputer for signal averaging. The averaged signal is viewed on the microcomputer screen and plotted on a Tektronix plotter.

Figure 2 shows some of our typical data. The deflection of the probe laser beam has been plotted as a function of time after the pump beam firing for various pump–probe beam distances. The top curve corresponds to overlapping probe and pump beams, and successive curves toward the bottom of the diagram correspond to increasing probe and pump beam distances, as indicated on the diagram. The pump–probe beam distances were estimated by measurements of the acoustic travel times (see below). The dye laser was tuned to the $Q_1(8)$ line of OH molecules at 3092 Å, and it delivered 7 μJ energy per pulse. The dye laser and He–Ne beams were collimated in the flame region. After collimation the He–Ne beam was ~1 mm in diameter. The UV dye laser beam had an oblong shape with its short dimension (along the direction of overlap of the probe–pump beams) being ~1 mm. In the top curve of Fig. 2, the probe beam suffers a deflection at the instant of pump laser firing due to photothermal effect and returns to its original position on the time scale of the thermal diffusion time. The deflection in the top curve of Fig. 2 corresponds to ~8 μrad. As the pump–probe beam distance is increased, the PTDS signal gradually decreases. Moreover, when the two beams begin to separate, the PTDS signal is primarily produced by thermal diffusion of heat from the dye

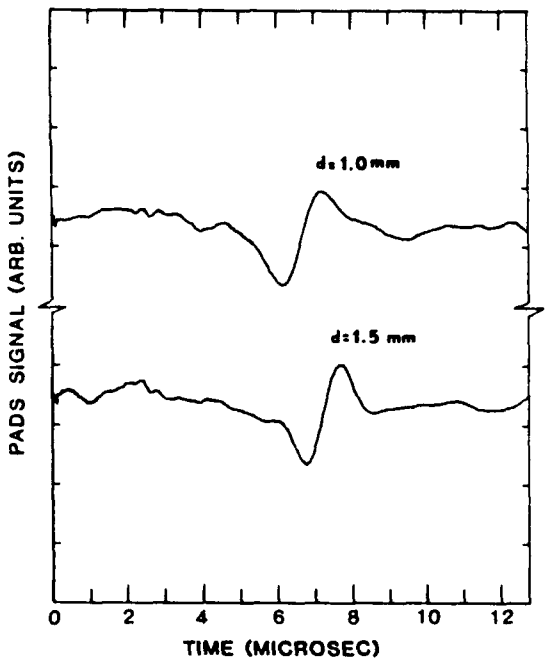

Fig. 3. Photoacoustic deflection signal from OH molecules in our methane–air flame shown on an expanded scale for two pump–probe beam distances. The trigger pulse corresponds to time $t = 0$, and the pump laser fires at $t = 5.3$ μsec. All other parameters are the same as for Fig. 2.

laser irradiated region to the probe beam and consequently arrives at a later time. By the time the two beams are separated by ~0.7 mm, the PTDS signal has almost disappeared. As the two beams are separated, one observes a sharp spike develop shortly after the dye laser firing due to the photoacoustic effect. Note that the PADS signal is quite strong even when the PTDS signal has almost disappeared (bottom curve), and the PADS signal decreases slowly for larger probe pump beam distances (not shown). In Fig. 3 we show the PADS signal on an expanded time scale for pump probe beam separation of ~1 mm (upper curve) and 1.5 mm (lower curve). The PADS signal occurs on a characteristic time scale of ~1 μsec. When these curves (Figs. 2 and 3) were taken, our laser was giving an extremely small amount of output energy (7 μJ/pulse) so that signal averaging was needed. In particular, these curves represent an integration over 300 pulses. We have calibrated the PADS signal in terms of OH density by absorption measurements. We observe ~43% attenuation of laser when tuned to the $Q_1(5)$ transition at 3085 Å for a 6-cm path length through the flame. This gives an OH density of $\sim 9 \times 10^{14}$ molecules/cm^3 in the flame. We are attempting to develop a model of PADS, which will allow us to obtain the number density without calibration.

We have also measured the temperature in the luminous region of our flame using PADS. The temperature was measured in the following way: A small fraction of the pump beam was allowed to leak into the quadrant detector. This gave a signal at the instant of laser firing. The time interval between the instant of laser firing and arrival of the acoustic pulse at the probe beam was thus measured. If the distance between the pump and probe beams is precisely known, acoustic velocity, and thus the temperature of the flame, may be determined from this information. We have, however, determined the flame temperature T_f simply from the ratio of the acoustic travel times between the probe and pump beams, t_f and t_r, respectively, at flame temperature and at room temperature:

$$\frac{T_f}{T_r} = \left(\frac{v_f}{v_r}\right)^2 = \left(\frac{t_r}{t_f}\right)^2 . \quad (1)$$

Here T_r is the room temperature and v_f and v_r are the acoustic velocities at flame and room temperatures, respectively. In Eq. (1) we have neglected some minor corrections.[3] We have measured t_r in the following way: With the burner turned off, we placed a piece of thin wire in the pump beam. The pump laser energy was absorbed by the wire, heating the wire, and resulting in an acoustic signal which was detected a time t_r later by deflection of the probe beam. We have measured the temperature of our oxygen-rich flame (equivalence ratio = 0.76) to be 1500 ± 60 K. This temperature is considerably below that for stoichiometric flame (2130 K) because (1) the fuel ratio was not stoichiometric in our case, (2) N_2 flow rate was larger in our case than it would have been if methane–air were used, and (3) perhaps the cooling of the flame by the burner head.

As noted before, recently Tam and collaborators[3] have developed a related technique for temperature measurements in a flame. In this technique an intense beam of Nd:YAG laser produces a weak plasma via breakdown within the flame. The acoustic pulse emerging from the plasma spark is detected by the transient deflection of a He–Ne beam. The temperature of the flame is obtained by measuring acoustic travel time between two spatially separated probe beams. We would like to point out two important differences between PADS and Tam's "Opto-acoustic Laser-beam Deflection (OLD)" technique. First, OLD is not species selective, and it can only be used for temperature measurements. PADS, on the other hand, yields both species concentrations and temperature. Second, OLD breaks down the flame gases and thus produces a significant perturbation in the flame. On the other hand, PADS is nonperturbing as the typical pressure change produced in our experiments is of the order of 1 mTorr.

In conclusion, PADS has a high potential for developing into an excellent combustion diagnostic technique for *in situ* measurement of minority species concentration and local temperature with both high temporal and spatial resolution. Our experiment has a demonstrated sensitivity of 1×10^{14} OH molecules/cm^3 (for a SNR of 3) on a single-shot basis or 4×10^{12} OH molecules/cm^3 for integration over 1000 pulses (30 sec with CMX-4), when the laser is delivering full energy specified by the manufacturer at 3100 Å (200 μJ/pulse). Note that our data were taken with only 7 μJ of laser energy because the second harmonic crystal in our laser was defective. Moreover, in these preliminary experiments, we have made no special attempt to optimize the SNR. The SNRs in Figs. 2 and 3 were not limited by the flame noise but were primarily limited by ~400-kHz noise on our He–Ne laser. With a noise-free He–Ne laser and noise-free amplifiers, the detection sensitivity can be significantly improved above the figures given above. Work is in progress to develop a theoretical model of PADS and also to apply this technique to a variety of combustion situations.

We would like to thank Larry Goss, Sigmund Kizirnis, and Bishwa Ganguly for many helpful discussions. This work was supported by AeroPropulsion Laboratory, Air Force Wright Aeronautical Laboratories, Wright-Patterson AFB, Ohio.

References

1. A. Rose, J. D. Pyrum, C. Muzny, G. J. Salamo, and R. Gupta, Appl. Opt. **21**, 2663 (1982).
2. A. Rose, J. D. Pyrum, G. J. Salamo, and R. Gupta, in *Proceedings, International Conference on Lasers '82* (Society of Optical and Quantum /Electronics, McLean, Va., 1983).
3. W. Zapka, P. Pokrowsky, and A. C. Tam, Opt. Lett. **7**, 477 (1982).
4. Y.-H. Pao, Ed., *Optoacoustic Spectroscopy and Detection* (Academic, New York, 1977).
5. K. Tennal, G. J. Salamo, and R. Gupta, Appl. Opt. **21**, 2133 (1982).
6. A. Rose, J. D. Pyrum, G. J. Salamo, and R. Gupta, Appl. Opt. **23** (15 May 1984), in press.

Twentieth Symposium (International) on Combustion/The Combustion Institute, 1984/pp. 1339–1345

COMBUSTION DIAGNOSTICS BY PHOTO-DEFLECTION SPECTROSCOPY*

A. ROSE AND R. GUPTA
Department of Physics
University of Arkansas
Fayetteville, AR 72701

Preliminary investigations of photo-deflection spectroscopy (PDS) indicate a very good potential of these techniques for combustion diagnostics. PDS consists of two separate but interrelated techniques, photothermal deflection spectroscopy (PTDS) and photoacoustic deflection spectroscopy (PADS). Both of these techniques can measure both minority species concentrations and local temperatures. In addition, PTDS can also be used for a measurement of flow velocities. These techniques are suitable for *in situ* measurements, are nonperturbing, and have high sensitivity. Moreover, they are capable of giving a high degree of spatial and temporal resolution. Also, these techniques are simple and do not require expensive instrumentation. In this paper, by application to OH molecules in a natural-gas-air flame, we demonstrate the potential of these techniques for local temperature and minority species concentration measurements.

I. Introduction

There is presently considerable interest in the development of good combustion diagnostic techniques. These techniques should be able to measure both the local temperatures and the majority and minority species concentrations. In addition, an "ideal" technique should satisfy the following criteria: (i) It should be capable of making *in situ* measurements, (ii) it should be non-perturbing, (iii) it should have a high sensitivity, (iv) it should have a high degree of spatial resolution, and (v) it should have a high degree of temporal resolution. In general, optical techniques satisfy the first two criteria, and many optical techniques have been investigated which satisfy the five criteria enumerated above to varying degrees. A few of the techniques have been quite successful; among them is coherent anti-Stokes Raman scattering (CARS). CARS is a very useful technique for majority species; however, it has a rather limited usefulness for a large variety of minority species due to its relatively low sensitivity, although efforts are under way to increase its sensitivity using resonance effects. As a matter of fact, no ideal technique seems to exist and all of the techniques appear to have relative advantages and disadvantages over each other. If one technique is most suitable for one situation, another one is more suitable for another situation. Therefore, there is a need for continued investigations for newer and better techniques.

In the last two years we have made some preliminary investigations of photothermal deflection spectroscopy (PTDS) and photoacoustic deflection spectroscopy (PADS) for combustion diagnostics. The two techniques are closely related to each other and we shall refer to these together as photo-deflection spectroscopy (PDS). Our preliminary results have been very encouraging. These techniques satisfy all five criteria enumerated above. The basic idea behind PDS techniques is quite simple: A dye laser beam (pump beam) passes through the region of interest (flame in this case). The dye laser is tuned to one of the absorption lines of the molecules that are to be detected, and the molecules absorb the optical energy from the laser beam. Due to fast quenching rates in a flame, most of this energy quickly appears in the rotational-translational modes of the flame gases [1,2]. For most molecules, only a negligible fraction of the energy is reemitted as fluorescence. Thus the dye laser irradiated region gets slightly heated, leading to changes in the refractive index of the medium in that region. If the density of absorbing molecules is uniform over the width of the dye laser beam, the refractive index will have the same spatial profile as the dye laser beam (generally assumed to be Gaussian). Now if a probe laser beam, generally a He-Ne beam, overlaps the pump beam, as shown in Fig. 1(a), the probe beam will be deflected due to the gradient in the refractive index of the medium created by the spatial profile of the pump beam. This deflec-

*This work was supported by AeroPropulsion Laboratory, Air Force Wright Aeronautical Laboratories, Wright-Patterson AFB, OH 45433.

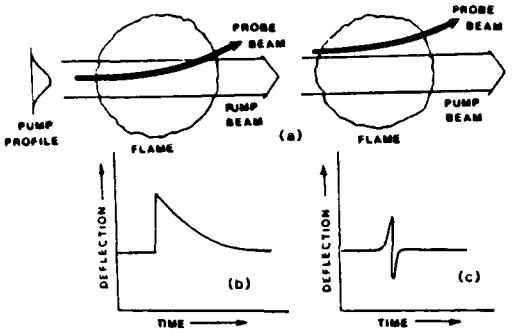

FIG. 1. (a) Deflection of a probe beam due to refractive index gradients produced by the absorption of pump beam. (b) Sketch of the photothermal deflection spectroscopy (PTDS) signal. (c) Sketch of the photoacoustic deflection spectroscopy (PADS) signal.

tion can be easily measured by a position-sensitive optical detector. The deflection of the probe beam, among other things, is also proportional to the number density of absorbing molecules. If a pulsed pump laser is used, a signal similar to that sketched in Fig. 1(b) is obtained. The probe beam gets deflected shortly after the instant of laser firing, as discussed above, and gradually returns to its original position on the time scale of the diffusion time of the heat from the irradiated region. Thus the width of the signal depends on the thermal diffusion time constant, and consequently on the local temperature of the flame. Therefore, both the concentration of the molecules of interest and local temperature of the flame may be determined simultaneously from the size and width of the signal, respectively. This technique, called photothermal deflection spectroscopy (PTDS), has recently been investigated in solids, liquids, and gases by Amer and collaborators [3]. To test the applicability of this technique to a combustion environment, we have recently applied it to a laboratory flame [4]. These preliminary experiments have been very successful and indicate that PTDS has a very good potential as a combustion diagnostic technique. Recently, Sell [5] has demonstrated that PTDS can also be used for flow velocity measurements.

We have also investigated a closely related technique, photoacoustic deflection spectroscopy (PADS). The heating of the pump beam irradiated region is accompanied by an increase in pressure. If the pump beam is pulsed, as ours is, a pressure pulse travels outward from the pump beam irradiated region. This pressure pulse causes changes in the refractive index of the medium which may be detected by the deflection of a probe beam placed a few mm away from the pump beam. A typical signal is sketched in Fig. 1(c). We shall refer to this technique as photoacoustic deflection spectroscopy (PADS). The strength of the PADS signal is proportional to the concentration of the absorbing molecules. Moreover, acoustic velocity in the flame can also be measured by measuring the arrival time of the PADS signal after the instant of laser firing, and from a knowledge of the pump and probe beam separation. Since acoustic velocity depends on the temperature, this information directly yields the local flame temperature. We have applied PADS to a combustion environment to determine its usefulness for combustion diagnostics [6,7]. Our preliminary experiments have been very successful and indicate that PADS also has a very good potential.

PADS is very similar to the conventional photoacoustic spectroscopy (PAS) where the pressure changes are measured by a microphone rather than by the deflection of a probe beam. Our group [1,2] and Crosley's group [8,9] have applied PAS to a combustion environment, and find it to be a very sensitive diagnostic technique for minority species measurements. PADS, however, has several advantages over PAS: (1) The optical detector that measures the deflection of the probe beam can be placed as far away from the flame as necessary without adversely affecting the sensitivity. The signal-to-noise ratio depends on the separation between the probe and pump beams inside the flame, and not on the position of the detector. This permits the application of this technique to hostile environments. (2) The acoustic signal never has to cross the flame boundaries where modifications of the acoustic wavefront may occur—a problem with microphone detection. (3) Microphones have a limited bandwidth (typically less than 100 KHz) which limits the usefulness of PAS considerably. Piezoelectric transducers may be obtained with higher bandwidth but they have poor sensitivity due to acoustic impedance mismatch. On the other hand, optical detectors have a much larger bandwidth and this limitation does not occur. (4) It is not an easy matter to measure local temperature in a flame using PAS in *real time*. In PADS, however, measurement of the acoustic travel time between the pump and probe beams directly yields the local temperature on a single-shot basis. (5) Finally, it is difficult to get spatial resolution using PAS because one detects the integrated signal from the entire flame-laser beam interaction length. On the other hand, one may obtain good spatial resolution in PADS by using probe and pump laser beams nearly at right angles. On the negative side, PADS has a somewhat lower sensitivity than PAS. For collinear pump and probe beams the sensitivity of PADS is approximately a factor of four lower than that of PAS, and decreases further as the angle between the pump and probe beams is increased in order to in-

crease the spatial resolution. The above result is purely an experimental one; we have not yet explored the theoretical limits of detection sensitivities.

Both of the PDS techniques satisfy all five of the criteria for an "ideal" combustion diagnostic technique. These techniques are suitable for *in situ* measurements of both the minority concentrations and local temperatures. They are non-perturbing since only negligible temperature and pressure changes are induced by the pump beam. They have a high sensitivity and therefore they are particularly suitable for minority species. The region from which the signal is observed can be localized by crossing the pump and probe beams at an angle. Three dimensional spatial resolution can thus be obtained, the best resolution case being when the two beams cross at or near right angles. In general, PTDS with overlapping beams offers better spatial resolution than PADS, since the PTDS signal decreases faster with increasing pump and probe distance than does the PADS signal [6]. Finally, temporal resolution is achieved by using a pulsed pump laser. The PADS signal is obtained within a few microseconds and PTDS is obtained typically in less than 100 microseconds. Signal-to-noise ratios are sufficiently high that both the specie concentrations and local temperatures can be measured simultaneously on a single shot basis. Therefore, the signal can be acquired at about a 10 KHz rate provided that a laser with this repetition rate is available. In addition to these attributes, PDS techniques are simple and do not require expensive instrumentation. For example, in order to measure the temperature of the flame, one does not need to measure the Boltzmann distribution which requires an expensive optical multichannel analyzer. The relative merits of PTDS and PADS will be discussed in Sec. IV.

In the preliminary reports referred to above [4,6,7], we had used a methane-air flat-flame burner to observe PTDS and PADS signals from OH molecules. This flat-flame burner, which was very stable and gave a constant OH density across the flame, was suitable for the first observation of these signals in a combustion environment. In this report, we have applied these techniques to a different kind of burner, operated with natural-gas and air, where considerable spatial variation of OH density and temperature exist. We thus demonstrate the use of these techniques to map out specie concentration and temperature profile of a flame. We demonstrate, for the first time, the dependence of the PTDS signal width on the local temperature of the flame. We must point out, however, that PDS techniques are still in their infancy, and not all of the necessary theoretical models have been developed. Therefore the results presented in this paper represent only a starting point for the future work.

II. Apparatus

A diagram of our burner is shown in Fig. 2. The burner was fabricated out of stainless steel and it is approximately 5 cm in diameter. A mixture of natural gas and air was used. A light blue conical flame approximately 30 cm tall was produced. A chimney, as shown, helped stabilize the flame. The burner was mounted on a linear translator and it was moved across the laser beams to determine the spatial profile of the flame. The measurements reported in this paper were taken at about 1 cm above the flame base, as indicated by the dotted line. The experiment is shown schematically in Fig. 3. Laser radiation from a Chromatix CMX-4 flash lamp pumped dye laser was frequency doubled by an intracavity ADP second harmonic crystal, and it was used to excite the $X^2\Pi - A^2\Sigma$ band of OH molecules. The laser produced 1 μsec pulses, and in the experiments reported in this paper, operated with approximately 40 μJ of energy/pulse in a 10 GHz bandwidth at 3100 Å. A He-Ne laser beam, used as a probe beam, also passed through the flame close to the pump beam. The deflection of the probe beam caused by refractive index gradients produced by the heating of the pump irradiated region (PTDS) or by the passing acoustic pulse (PADS) was detected by a position-sensitive detector. The po-

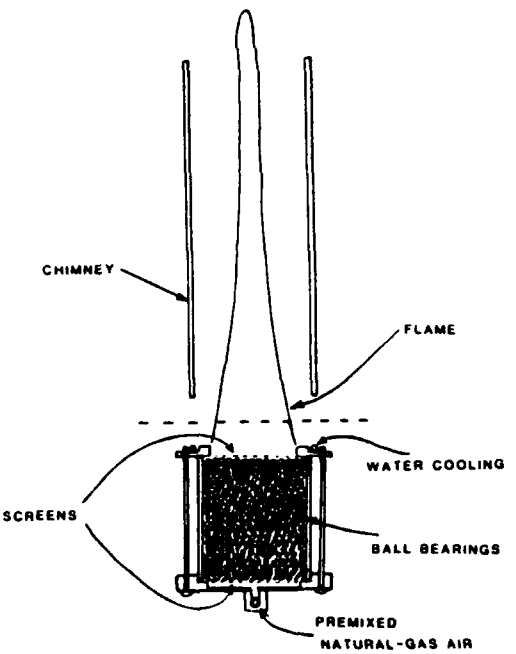

FIG. 2. A sketch of the burner and the flame. A chimney was used to stabilize the flame. Dotted line indicates the position where data were taken.

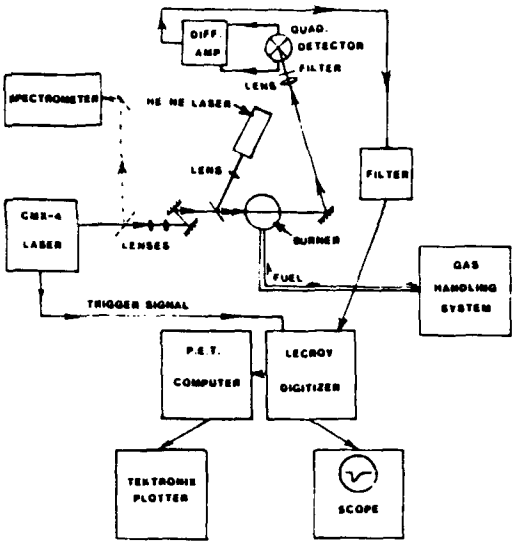

FIG. 3. Schematic illustration of the experimental apparatus.

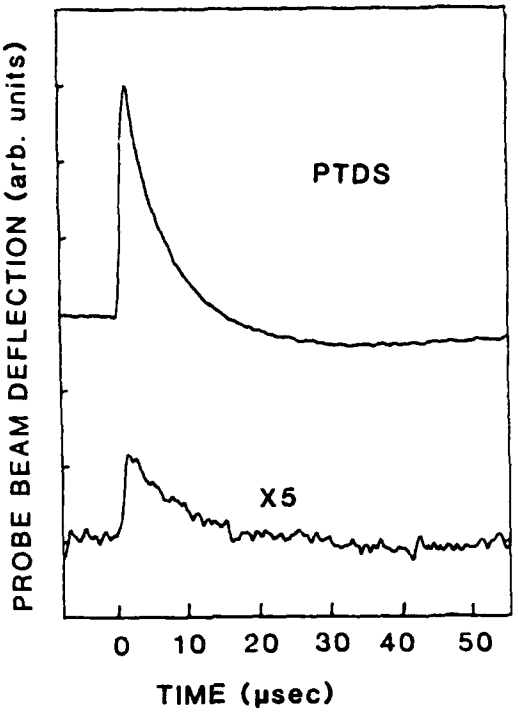

FIG. 4. Photothermal deflection signal at two different positions in the flame. The upper curve was taken where the OH density was high and it is narrower than the lower one indicating higher local temperature at that position. The lower curve was taken 3 mm inward (toward the center) from the position of the upper curve.

sition sensitive detector consisted of four quadrants, two of which were used in our experiments. The difference signal from the two quadrants was proportional to the position of the probe beam. The difference signal was digitized by a LeCroy WD 8256 transient digitizer, and transferred to a Commodore PET microcomputer for signal averaging. The averaged signal was viewed on the microcomputer screen and plotted on a Tektronix plotter.

III. Experiment

Fig. 4 shows a typical PTDS signal due to OH molecules at two different positions in our flame. The upper curve was taken near the edge of the flame where the OH density was apparently the highest. The lower curve was taken 3 mm inward (toward the center of the flame) from the position corresponding to the upper curve and it is shown expanded by a factor of five. The dye laser was tuned to the $Q_1(8)$ line of OH molecules at 3092.4 Å and delivered approximately 40 μJ of energy per pulse. Both probe and pump beams were mildly focused (using long focal length lenses) to approximately 1 mm diameter and crossed in the flame region at a small angle of 4° giving relatively low spatial resolution of approximately 0.5 mm^3 (0.3 mm × 0.3 mm × 5 mm). Data in Fig. 4 represent averaging over 200 pulses. The probe beam deflected sharply shortly after the laser fired and returned to its original position on the time scale of the diffusion time of the heat out of the laser irradiated region, as expected. We note that the upper curve indicates a larger density of OH molecules than the lower one. We also note that the upper curve is narrower, indicating that the thermal diffusion time is smaller, and therefore the temperature is higher, than for the lower one. In Fig. 5 we have plotted the OH density and the local temperature of the flame as a function of the burner position. Zero of the abscissa corresponds to the center of the flame. Only the relative OH density is measured by PTDS in this experiment. Absorption measurements were used to put the curve on an absolute scale. An absorption of 27% measured when the laser was tuned to the $Q_1(7)$ line of OH at 3089.7 Å, together with the relative OH density as given by PTDS, gave the OH density at peak (near the edges) to be 6×10^{15} cm^{-3}. We should point out that absolute density can be measured directly without the need for calibration when the necessary theoretical models have been developed; this is not a limitation of the technique. Moreover, in many situations it is not necessary to know the absolute numbers, the relative numbers themselves are of considerable in-

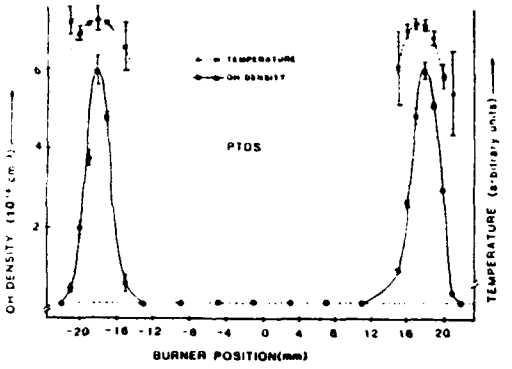

FIG. 5. OH density and temperature profile at about 1 cm above the base of the flame taken by PTDS. Zero of the abscissa corresponds to the center of the flame. The error bars represent one standard deviation of 3 measurements.

terest. In Fig. 5, the dashed base line gives the detectivity limit ($\sim 1 \times 10^{14}$ cm^{-3}) in this particular experiment. The low detectivity limit in this experiment was imposed by a defective second harmonic crystal in our dye laser and by a noisy He-Ne laser (see below). All points on the baseline represent an OH density of 1×10^{14} cm^{-3} or less. We note that the OH density in the center of the flame was very low, although the entire flame was luminous (faint blue). Fig. 5 also shows the relative temperature profile of this flame deduced from the relative widths of PTDS signals. The temperature could only be measured near the edges of the flame where the OH density was high and consequently the S/N ratio was sufficient. The width of the PTDS signal, in addition to the local temperature, also depends on the spatial profile of the pump beam, on the degree and manner of the overlap between the probe and pump beams, etc. We have not yet developed the necessary theoretical model to quantitatively determine the dependence of the signal width on these parameters. Therefore we have not yet been able to determine the absolute temperature of the flame with any certainty; the temperature curves in Fig. 5 simply show that signal width does vary with temperature and it can in principle be used to measure the temperature. The temperature near the peak of OH density, as determined by PADS (see below) is 2060 K.

It should be pointed out that if significant concentration gradients of the molecules of interest exist over the dimensions of the pump beam, complications arise. In this case, refractive index gradients may also be produced by the concentration gradients of the molecules of interest. Consequently, the probe beam deflection would depend not only on the concentration of the molecules but also on their gradient. In this case it would be a difficult task to obtain concentration measurements from the observed data. However, one can still use PTDS if the pump and probe beams are spatially separated by a very small distance. In this case, the observed PTDS signal is relatively insensitive to the pump beam spatial profile and the concentration gradients of the absorbing molecules. The refractive index gradients which cause a deflection of the probe beam, in the case of spatially separated beams, are caused primarily by the diffusion of heat from the pump beam irradiated region to the probe beam. The price to be paid, of course, is a decrease in signal-to-noise ratio over that obtainable for the overlapping case. We have observed PTDS signals with spatially separated pump and probe beams [4,6], however, in Fig. 5 we have used overlapping beams for ease of detection. A comparison of OH density profile obtained by PTDS and that obtained by PADS (see below) indicates, however, that the effect of density gradients is not too severe in our case.

Fig. 6 shows one of our typical PADS data and it is seen to have a dispersion shape. The experimental setup was exactly the same as that for PTDS with the following exception: The probe and pump beams crossed at 4° in the horizontal plane but were separated by about 1 mm in the vertical plane. That

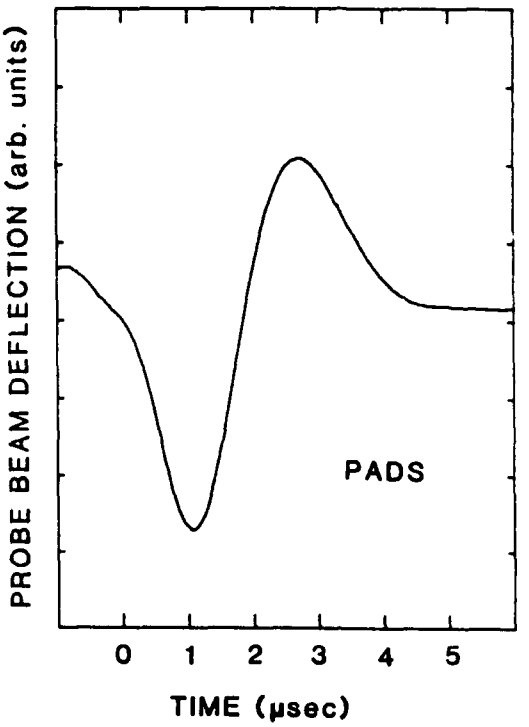

FIG. 6. A typical photoacoustic deflection signal. The signal has a dispersion shape.

is, the closest separation between the two beams was 1 mm and that occurred when one beam was directly above the other. The signal in Fig. 6 represents averaging over 300 pulses. In this case the PTDS signal is so small that it cannot be seen. The PADS signal can very easily be distinguished from the PTDS signal because its width is much smaller, on the order of a microsecond. Moreover, the PADS signal travels with acoustic velocity and arrives at the probe beam earlier than the PTDS signal which travels by thermal diffusion. The size of the signal is proportional to the OH density while its arrival time is proportional to the temperature.

Fig. 7 shows the OH density and temperature profile of the flame determined by PADS, and it is seen to be similar to that found by PTDS. Comparison of Fig. 7 with Fig. 5 shows that in Fig. 7 the OH peaks near the edges are broader and OH density in the center of the flame is higher than that in Fig. 5. We believe that this is due to lower spatial resolution of PADS than that of PTDS in our experiment. Of course, spatial resolution could have been increased by crossing the beams at a larger angle. In this experiment, however, this was not done due to accompanying decrease in sensitivity. As in PTDS, only the relative number density of OH was determined by PADS; the curve was put on an absolute scale by calibration using absorption measurements. The necessary theoretical models of PADS which will allow us to measure absolute number densities without the need for calibration are still being developed. We have also made a measurement of the temperature of the flame using PADS. In this case two He-Ne laser probe beams separated by about 1 mm were used. A measurement of the arrival times of the PADS signal at the two probe beams gave the acoustic travel time between the two probe beams. The acoustic travel time, along with a measurement of the separation between the two beams, gave the acoustic velocity which was used to deduce the local temperature of the flame. Since the PADS signal has dispersion shape and it is not obvious where on the curve the timing measurements should be performed, use of two probe beams eliminates this uncertainty. The separation between the two probe beams was determined from a measurement of the acoustic travel time between the two beams at room temperature. The photoacoustic signal in this case was generated by the pump beam hitting a piece of thin wire. We found the temperature of the flame near the edge (at the peak of the OH density curve) to be 2060 ± 100 K. The uncertainty represents one standard deviation of four measurements. The large uncertainty is due to pulse-to-pulse fluctuations in the timing of the laser pulse with respect to the trigger pulse (which was derived from the flashlamp circuitry of the laser). This uncertainty can and will be reduced in the future work.

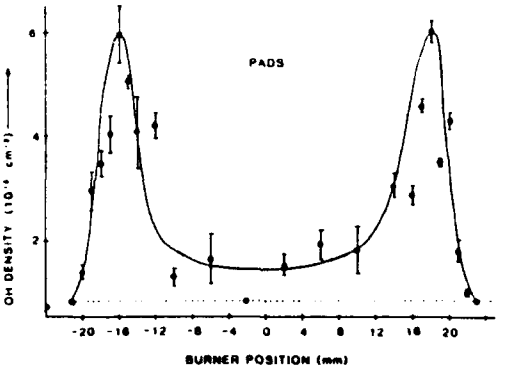

FIG. 7. OH density profile of the flame determined by PADS. The error bars represent one standard deviation of 3 measurements.

IV. Conclusions

We have made preliminary investigations of two new and interrelated techniques: photothermal deflection spectroscopy (PTDS) and photoacoustic deflection spectroscopy (PADS). These techniques are suitable for minority species concentrations and simultaneous local flame temperature measurements. These techniques satisfy all five of the criteria required of an "ideal" combustion diagnostic technique. An additional advantage of PDS techniques is that they have the potential of monitoring the temperature and specie concentration along the entire length of the pump beam, on a single shot basis, by employing multiple probe beams.

Our PADS experiment has a demonstrated sensitivity of 1×10^{14} OH molecules/cm^3 (for a signal-to-noise ratio of 3) on a single shot basis, or 4×10^{12} OH molecules/cm^3 for integration over 1000 pulses (30 secs with CMX-4), when the laser is delivering full energy specified by the manufacturer at 3100 Å (300 μJ/pulse). Under similar conditions, the demonstrated sensitivity of PTDS is about 3×10^{12} OH molecules/cm^3 on a single shot basis or 1×10^{11} molecules/cm^3 for integration over 1000 pulses. The above figures are for collinear beams and naturally the sensitivity decreases as spatial resolution is increased by increasing the angle between the two beams. Note that our data were taken with only 40 μJ of laser energy because the second harmonic crystal in our laser was defective. Moreover, in these preliminary experiments, we have made no special attempt to optimize the signal-to-noise ratio. The signal-to-noise ratios in Figs. 4 and 6 were not limited by the flame noise but were pri-

marily limited by 50 KHz noise on our He-Ne laser. With a noise-free He-Ne laser and noise-free amplifiers, the detection sensitivity can be significantly improved above the figures given above. We should emphasize that PDS techniques are still in their infancy and that more work, both theoretical and experimental, is required. Therefore this report does not represent a comprehensive investigation; rather it is presented here to stimulate more interest in this potentially very useful technique.

Finally, it is desirable to compare PTDS with PADS. PTDS and PADS have complementary advantages. For example, if large concentration gradients of absorbing molecules are present, PTDS can only be effectively used with spatially separated beams. Since the sensitivity of PTDS decreases very rapidly with increasing separation of pump-probe beams, it is clearly desirable to use PADS in this situation. Moreover, when the pump beam spatial profile is difficult to measure, it is advantageous to use PADS for absolute concentration measurements (relative concentration measurements present no difficulty). On the other hand, PTDS (for overlapping beams) has higher sensitivity and higher spatial resolution than PADS. The two techniques are thus complementary.

REFERENCES

1. Tennal, K., Salamo, G. J., and Gupta, R., Applied Optics *21*, 2133 (1982).
2. Rose, A., Pyrum, J. D., Salamo, G. J., and Gupta, R., Applied Optics 23, 1573 (1984).
3. Boccara, A. C., Fournier, D., Jackson, W., and Amer, N. M., Opt. Lett. 5, 377 (1980); Fournier, D., Boccara, A. C., Amer, N. M., and Gerlach, R., Appl. Phys. Lett. *37*, 519 (1980); Jackson, W. B., Amer, N. M., Boccara, A. C., and Fournier, D., Appl. Opt. *20*, 1333 (1981).
4. Rose, A., Pyrum, J. D., Muzny, C., Salamo, G. J., and Gupta, R., Applied Optics *21*, 2663 (1982).
5. Sell, J. A., Applied Optics 23, 1586 (1984).
6. Rose, A., Pyrum, J. D., Salamo, G. J., and Gupta, R., *Proceedings of the International Conference on Lasers '82* (Society of Optical and Quantum Electronics, McLean, VA, 1983).
7. Rose, A., Salamo, G. J., and Gupta, R., Applied Optics 23, 7811 (1984).
8. Allen, J. E., Anderson, W. R., and Crosley, D., Opt. Lett. *1*, 118 (1977).
9. Smith, G. P., Dyer, M. J., Crosley, D. R., Applied Optics 22, 3995 (1983).

COMMENTS

J. A. Sell, General Motors Research Labs, USA. It seems like it should be possible to measure the temperature in a sooting flame by the photoacoustic deflection technique. By focussing a YAG or other high power laser on the soot, thereby generating acoustic pulses, and measuring the time delay between the deflection of two probe beams giving the velocity of sound. In your opinion would the velocity of sound propagating through this inhomogeneous media still be proportional to $\sqrt{T}$?

Authors' Reply. It appears that it should be possible to measure the temperature in a sooting flame by generating the acoustic signal on soot particles. It is an interesting possibility that we have not previously thought about. It is not possible to tell whether the sound velocity will still be proportional to $\sqrt{T}$ without detailed investigation. There are a few other things that must be considered also. The reflection of the acoustic pulse by soot particles may create some problems, although these problems may be minor due to the fact that the size of the soot particles is very small compared to the acoustic wavelengths involved. Extinction of the probe and pump beams due to reflection and absorption by soot particles is likely to be a serious problem in a heavily sooting flame. Nevertheless it is an interesting idea that should be pursued further.

Volume 56, number 5 OPTICS COMMUNICATIONS 1 January 1986

APPLICATION OF PHOTOTHERMAL AND PHOTOACOUSTIC DEFLECTION TECHNIQUES TO SOOTING FLAMES; VELOCITY, TEMPERATURE, AND CONCENTRATION MEASUREMENTS

A. ROSE and R. GUPTA

Department of Physics, University of Arkansas, Fayetteville, AR 72701, USA

Received 27 August 1985

Photothermal and photoacoustic deflection techniques have been applied for the first time to sooting flames. The values of these techniques for combustion diagnosis is demonstrated by measurements of velocity, temperature, and soot concentration profiles in a C_2H_2/O_2 flame.

1. Introduction

There is a need for the development of diagnostic techniques that can be applied to sooting flames. One is generally interested in the measurements of flow velocity, temperature, and soot concentration. An ideal technique is one that would measure all three parameters simultaneously, be nonintrusive, and have a high degree of spatial and temporal resolution. In this communication, we show that large photothermal deflection (PTD) signals and photoacoustic deflection (PAD) signals can be generated from the absorption of a laser beam by soot particles, and these signals can be used to do diagnostics in a flame. We demonstrate the usefulness of PTD and PAD techniques by measurements of flow velocity, temperature, and concentration profiles in a sooting oxyacetylene (C_2H_2/O_2) flame. The techniques meet all three of the criteria enumerated above for an ideal technique.

2. Experiment

The set up for our experiment is shown schematically in fig. 1. The flame is produced by an oxyacetlyne welding torch which has an inner column of soot as shown. All measurements presented in this paper were made within this column. Soot particles absorb radiation from a Chromatix CMX-4 flashlamp-pumped dye-laser, hereafter called the pump beam. The dye laser is generally tuned to 590 nm and typically delivers ~6 mJ of energy in ~1 μs long pulses. The soot particles are heated due to the absorption of the pump beam and most of this heat is transferred to the flame gases due to thermal conduction. When the laser fluence is larger than a critical value (as it was in our case), soot particles start evaporating [3]. While most of the laser energy goes into breaking the c–c bonds, hot vaporization products heat the medium. The heating modifies the refractive index of the flame gase. A HeNe laser beam, hereafter called the probe beam, monitors the changes in the refractive index. Whenever a change in the refractive index of the medium occurs, the probe beam gets deflected by an amount proportional to the gradient of the refractive index at the position of the probe beam. This method is known as the photothermal deflection (PTD) [1]. Our experiments were performed using a pulsed dye laser, therefore the PTD signals consisted of a transient deflection of the probe beam. The deflection of the probe beam was detected by a quadrant detector when the beam was deflected from the quiescent position producing a difference signal between the two quadrants. The difference signal was digitized by a LeCroy WD256 transient digitizer and transferred to a Commodore PET microcomputer for signal averaging, if

0 030-4018/86/$03.50

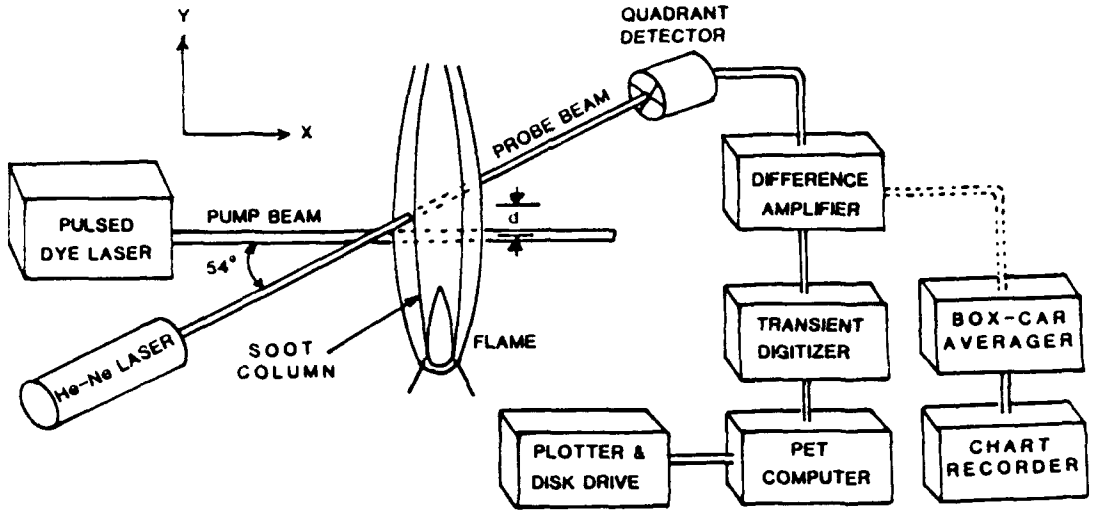

Fig. 1. Schematic illustration of the experimental arrangement. The pump and probe beams made an angle of 54° and were separated by a variable distance d in the vertical (y) direction.

necessary, and for data storage. In some of our experiments the difference signal was sent to a box-car integrator. The pump beam could be translated up and down to observe the PTD signal as a function of the distance between the probe and pump beams. The probe and pump beams had diameters of ~0.5 mm and ~0.3 mm, respectively, and made an angle of 54° with respect to each other to provide a good spatial resolution.

The heating of the pump-beam irradiated region also results in a thermal expansion of that region. The thermal expansion gives rise to an increase in pressure, and in our pulsed experiments, a pressure pulse propagates outwards. The pressure pulse is also accompanied by a change in the refractive index, which is detected by a transient deflection of the probe beam similar to that described above. This method is known as the photoacoustic deflection (PAD) technique [2].

Fig. 2 shows typical PTD signals for several positions of the probe beam, as indicated by the value of d. The top curve corresponds to the probe and the pump beams overlapping but the center of the probe beam being slightly upstream from the center of the pump beam. In this case we observe a deflection of the probe beam at the instant of laser firing, followed by the return of the beam to its original position. The time scale of the return is governed by the diffusion constant and the flow velocity of the flame gases. Superimposed on this signal is another signal, which is caused by increased transmission of the probe beam due to laser vaporization of soot particles. Dasch [4] refers to this signal as MALV: Modulated Absorption due to Laser Vaporization. Unfortunately, it is not easily possible to separate the PTD signal from the MALV signal for overlapping beams. The next curve

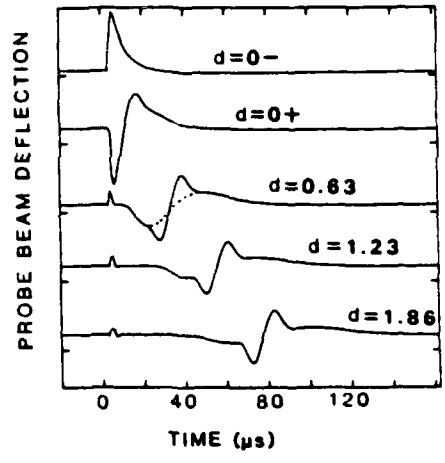

Fig. 2. The photothermal deflection signal for five different pump beam positions. MALV signal is superimposed on the PTD signal (see text). d is the separation between the pump and probe beams. Each curve represents an average of 50 shots. Signal averaging was not necessary; it was performed simply for convenience in data acquisition.

corresponds to the probe and the pump beams still overlapping, but the center of the probe beam being shifted slightly downstream from the center of the pump beam. Successive curves correspond to the pump beam being displaced downstream by 0.63 mm each. The dispersion-like shape of these curves can easily be understood. The heat pulse has roughly the same shape as the spatial profile of the pump beam (assumed gaussian). As the heat pulse passes by the probe beam position (blown by the flow of the flame gases), one observes a signal proportional to the spatial gradient of the heat pulse. The second curve ($d = 0+$) is asymmetric due to the effects of heat diffusion [‡]. Unfortunately, the MALV signal is superimposed on the PTD signal here also. In the third and the subsequent curves the two signals, although still overlapping, can be distinguished: A strong and narrow signal, and a weak and broad signal. We have drawn a dotted line on the third curve to aid in the visualization of the two signals. We have observed these signals for values of d as large as 5.6 mm (not shown) and we find that the narrow signal maintains its shape throughout, while the broad signal continues to get broader with increasing d. The broad signal is the PTD signal which broadens out due to thermal diffusion, while the narrow signal is the MALV signal [6]. The MALV signal does not show any change in its width or shape with increasing pump-probe separation because the diffusion rate of soot particles is extremely small. We have confirmed that the narrow signal is indeed caused by increased transmission (MALV) by arranging the probe beam to lie entirely on one quadrant of the detector. In this case the PTD signal disappeared and the shape of the MALV signal was the same as that of the spatial profile of the pump beam, as expected. The transit time of the PTD signal between two probe beam positions can be used to measure the flow velocity of the flame gases. Moreover, the velocity of the soot particles (which is the same as the flow velocity of the flame gases if there is no particle lag), can be measured from the transit time of the MALV signal, as pointed out by Dasch [7]. The magnitude of the PTD signal at $d = 0$ is a measure of the absorption of laser energy by soot particles, and therefore it is proportional to the soot concentration.

‡ Effects of the thermal diffusion will be covered in a forthcoming comprehensive article [5].

When the probe beam is outside the pump beam ($d > 0.5$ mm), it will be noted from fig. 2 that another transient signal arrives at the probe beam position before the PTD signal arrives. This is the photoacoustic deflection signal and is considerably smaller than the PTD signal. Since the PAD signal travels essentially with the acoustic velocity (which is much larger than the gas flow velocity in our case), the PAD signal arrives much earlier than the PTD signal. The temperature of the flame may be obtained from a measurement of the acoustic velocity (see section 4).

3. Velocity measurements

A velocity profile of our flame, determined from the measurements of arrival times of the PTD signals at two probe-beam positions a distance Δd apart, is shown in fig. 3. The flow velocity in the y-direction is plotted against the flame position in the x-direction. The flow rates of acetylene and oxygen were 34 cm^3/s and 10 cm^3/s, respectively, representing an equivalence ratio $\phi = 8.5$. The inner diameter of the torch nozzle was 1.7 mm. The velocity measurements were taken 40 mm above the nozzle, where the flame diameter was ~8 mm and the diameter of the soot column was ~4 mm. The error bars represent one standard

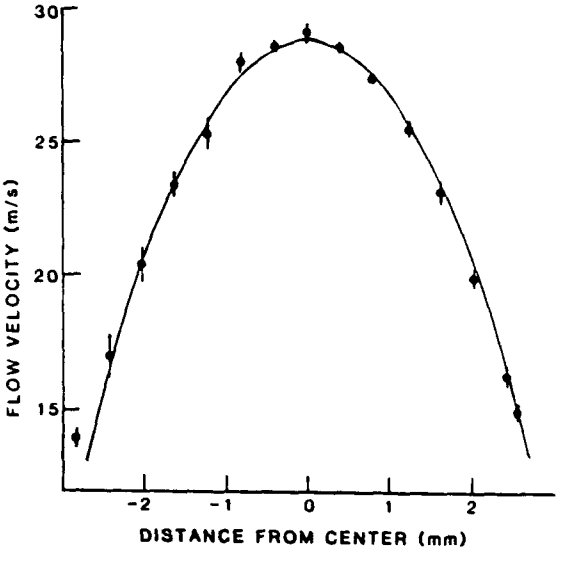

Fig. 3. The velocity profile of a laminar C_2H_2/O_2 flame 40 mm above the torch tip.

deviation of the mean of three measurements. The solid line is a least-squares fit to the data by a curve $V(r) = V_0(1 - r^2/R^2)$, where R is the radius of the flame and V_0 is the peak velocity. The data fits very well to a parabolic flow and the fitted values of V_0 and R were found to be 29 m/s and 3.7 mm, respectively. A crude estimate based on a simple model, which uses the cold gas flow, flame diameter, and flame temperature, gives 17 m/s for the maximum flow in the center of the flame. Our experience with this technique in a N_2 jet [8] shows that this technique gives accurate values for the velocity of a flow.

The spatial resolution in this experiment was $\sim 1 \times 10^{-4}$ cm^3, given by the widths of the pump and probe beams (transverse direction) and by the separation between the two positions of the probe beam (longitudinal direction). The technique is capable of giving a high degree of temporal resolution, given by the transit time of the PTD signal between the two positions of the pump beam (20 μs in this experiment). No attempt to obtain temporal resolution was made in this experiment due to the lack of proper instrumentation. Temporal resolution could have been obtained by employing two probe beams simultaneously with their own difference amplifiers and transient digitizers. A computer interfaced with the digitizers could then measure the time interval between the arrival times of the PTD pulses at the two probe beams within a single laser pulse. A simpler method would be to use time-to-digital converters instead of the transient digitizers.

To our knowledge, the only method which has received any attention for flow velocity measurements in flames is laser Doppler velocimetry [9] (LDV). In order to use LDV one needs to seed the flame with particles. However, it may be possible to do LDV measurements in a sooting flame by simply scattering laser light from soot particles. A major disadvantage of LDV is that one measures the particle velocity, not the gas velocity, and it is well known that seeded particles sometimes lag behind the gas flow. In our technique, we measure *both* the particle velocity and the gas velocity. The gas velocity is measured from the transit time of the PTD signal, while the particle velocity is measured from that of the MALV signal. In our case, the narrow and the broad signals overlap (fig. 2) indicating that the soot and gas velocities are equal. In LDV, the velocity is measured by a measurement of the Doppler shift, which makes its use difficult for low velocities. PTD technique, on the other hand, gives accurate results even for slow velocities, the ultimate lower limit being imposed by the thermal diffusion rate of the heated media and the widths of the laser beams [5].

4. Temperature measurements

As pointed out in section 2, the temperature of the flame can be measured by a measurement of the acoustic velocity v_f. For this purpose, the travel time Δt_f of the PAD signal between two probe beams, a distance Δd apart, was measured. The temperature of the flame T_f is given by

$$T_f = k_f v_f^2 = k_f(\Delta d/\Delta t_f)^2, \quad (1)$$

where the subscript f refers to the flame, and k_f depends on the composition of the flame. A similar measurement was made in air at the room temperature. In this case, the PAD signal was generated by letting the pump beam hit a thin piece of wire. The room temperature T_r is related to the acoustic travel time Δt_r between the two probe beams by

$$T_r = k_r(\Delta d/\Delta t_r)^2. \quad (2)$$

The flame temperature is derived from the ratio of eqs. (1) and (2):

$$T_f = T_r(k_f/k_r)(\Delta t_r/\Delta t_f)^2. \quad (3)$$

In the absence of soot, k_r and k_f can be calculated since the majority composition of both the air and the flame is known. In the presence of soot, however, its effect on the acoustic velocity must be theoretically investigated. In the present work, we have only measured the relative temperatures and set $(k_f/k_r) = 1$. We have assumed, of course, that eq. (1) is valid in the presence of a small number of soot particles.

A temperature profile of our flame with $\phi = 8.8$, 40 mm above the torch nozzle, is shown in fig. 4. For this measurement, the two probe beams, a distance $\Delta d = 4.5$ mm apart, were below the pump beam. Thus the measured velocity was not the true acoustic velocity but the difference between the acoustic and flow velocities. Since the flow velocity profile of our flame was known, the temperature measurements were corrected for the effect of flow. In retrospect, the problem could have been avoided by arranging the pump

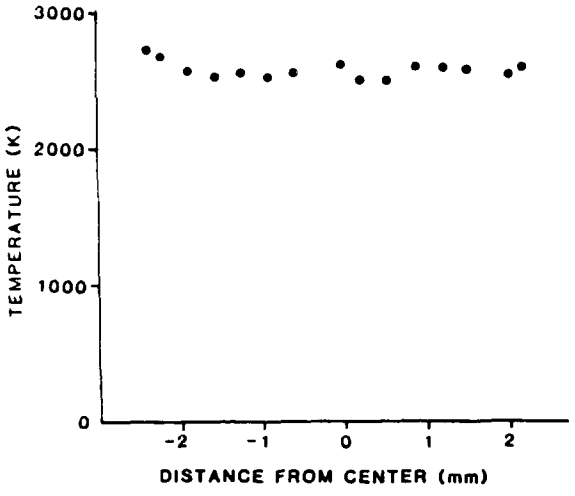

Fig. 4. The temperature profile of a laminar C_2H_2/O_2 flame, $\phi = 8.8$, 40 mm above the torch tip. The error bars are within the widths of the points. The temperature scale is not absolute (see the text).

and the probe beams in a horizontal plane. In fig. 4, the error bars, representing one standard deviation of the mean of three runs, are within the widths of the points. Within the limits of the error, there does not seem to be any appreciable variation in the temperature across the flame. The measured temperature ~2600 K is reasonable for a fuel-rich oxyacetylene flame [10]. However, these measurements should only be considered relative, as noted above.

The spatial resolution in this experiment was $\sim 1 \times 10^{-3}$ cm^3. Although no attempt to obtain temporal resolution was made for reasons described previously, a temporal resolution of ~5 μs given by the transit time between the two probe beams could be obtained in a straightforward manner.

Other nonintrusive methods of temperature measurement in a flame rely on a measurement of the Boltzmann distribution among the rotational levels of a flame molecule [11,12]. In order to get temporal resolution, however, one must use an expensive optical multichannel analyzer. Moreover, one must assume that a thermal equilibrium exists, which is not always the case [11]. The PAD technique, to our knowledge, is the only nonintrusive technique (proposed or demonstrated) capable of giving a direct measurement of the kinetic temperature of a flame. We hope this work will stimulate theoretical investigation of the acoustic velocity in a sooty medium so that absolute measurements of the temperature can be made.

5. Concentration measurements

The PTD signal amplitude is a direct measure of the absorption by soot particles in the region where probe and pump beams overlap. In our case, the PTD signal is superimposed on MALV signal due to soot vaporization. However, both the PTD signal and the MALV signal are proportional to the soot concentration (mass density).

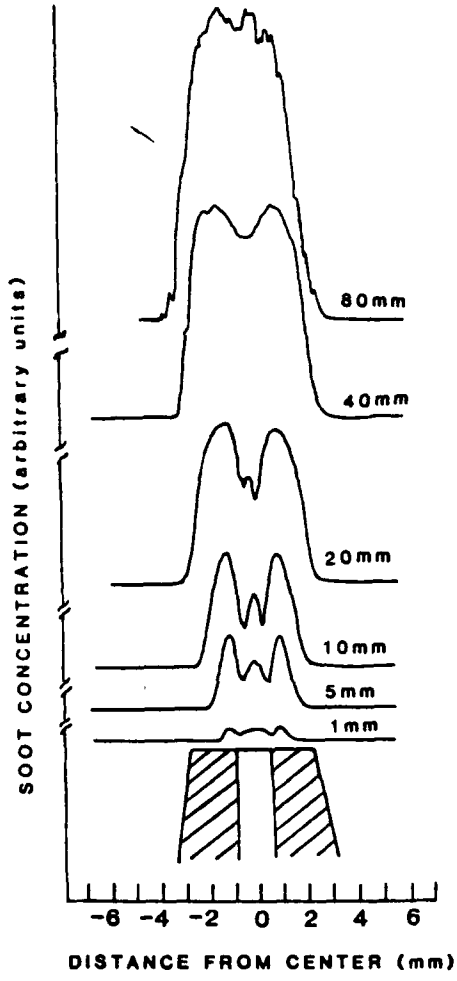

Fig. 5. The soot concentration profiles measured by PTD in a C_2H_2/O_2 flame, $\phi = 8.5$, for several heights above the torch tip. An extinction of 14% was measured at 40 mm above the torch tip.

Fig. 5 shows concentration profiles of soot particles at several heights above the torch tip. The equivalence ratio ϕ was equal to 8.5. For this experiment, the probe and pump beams were overlapping ($d \approx 0$) and, for historical reasons, crossed at an angle of 7°. The output of the difference amplifier was connected to a box-car integrator with its gate set on the PTD signal. The output was recorded on a strip chart recorder as the torch was translated horizontally under the crossing beams.

In general, one needs to know both the number density and the size distribution of soot particles in a flame. This information can be obtained if both the light scattering and the absorption from soot are measured simultaneously [4]. While spatial resolution in scattering can be obtained easily, a measurement of the absorption is generally obtained from a measurement of the extinction, which is a line-of-sight measurement. MALV is one method for obtaining spatial resolution in absorption measurements [4] and PTD offers another method of obtaining spatial resolution in absorption measurements. A combination of scattering and PTD would yield the desired number density and size distribution of soot particles with spatial resolution. The concentration profile shown in fig. 5 represents only a relative measurement of soot concentration. A quantitative measurement would require further theoretical development of pulsed PTD generated by the absorption of laser light on soot particles, and we hope that this communication would stimulate this work.

The spatial resolution in this experiment, determined by the overlap volume of the two laser beams, was $\sim 1.5 \times 10^{-3}$ cm^3. When the signal was recorded on the transient digitizer, a temporal resolution of ~ 30 μs given by the width of the PTD signal was obtained. The temporal resolution was lost, however, in fig. 5 because we used a box-car integrator for convenience of recording the profiles.

6. Conclusions

The value of the PTD and PAD techniques for combustion diagnostics in a sooting environment has been demonstrated by measurements of velocity, temperature, and soot concentration profiles. These techniques are nonintrusive, have a high degree of spatial and temporal resolution, and have many advantages over other techniques. Moreover, all three parameters (velocity, temperature, and soot concentration) can be measured simultaneously. Further theoretical work is required to obtain absolute measurements of the temperature and soot concentration.

Acknowledgements

We are thankful to Jeffrey Sell for suggesting that PTD signals generated by soot may be useful for combustion diagnostics and to C. Dasch for suggesting that the narrow signal in fig. 2 may be due to soot vaporization. This work was supported by Air Force Wright Aeronautical Laboratories.

References

[1] W.B. Jackson, N.M. Amer, A.C. Boccara and D. Fournier, Appl. Optics 8 (1981) 1333.
[2] A. Rose, G.J. Salamo and R. Gupta, Appl. Optics 23 (1984) 781.
[3] C. Dasch, Appl. Optics 23 (1984) 2209.
[4] C. Dasch, Optics Lett. 9 (1984) 214.
[5] A. Rose and R. Gupta, to be published.
[6] C. Dasch, private communication.
[7] C. Dasch, in: Twentieth Symposium on Combustion (The Combustion Institute, Pittsburgh, PA, 1985) pp. 1231–1237.
[8] A. Rose and R. Gupta, Optics Lett., to be published.
[9] See, for example, R.K. Cheng and T.T. Ng, Phys. Fluids 28 (1985) 473.
[10] A.G. Gaydon and H.G. Wolfhard, Flames, their structure, radiation, and temperatures (Chapman and Hall, London, 1979).
[11] L.P. Goss, G.L. Switzer, D.D. Trump and P.W. Schreiber, J. Energy 7 (1983) 403.
[12] C. Chan and J.W. Dally, Appl. Optics 19 (1980) 1963.
[13] K.E. Shuler, J. Phys. Chem. 57 (1953) 3961.

Appendix 4

A QUANTITATIVE INVESTIGATION OF PULSED PHOTOTHERMAL AND PHOTOACOUSTIC DEFLECTION SPECTROSCOPY FOR COMBUSTION DIAGNOSTICS

R. Gupta
Department of Physics, University of Arkansas, Fayetteville, AR 72701

ABSTRACT

A quantitative investigation of pulsed photothermal and photoacoustic deflection spectroscopy in a flowing medium has been performed with a view of applying these techniques for absolute measurements of minority species concentration, temperature, and flow velocity in flames.

INTRODUCTION

There is presently a large interest in the research on combustion phenomena. In order to test the theoretical models of combustion, one needs to be able to measure local temperatures, flow velocities, and concentrations of various combustion products. Hence, there is a need for the development of diagnostic techniques capable of measuring these parameters. In the last few years we have made some investigations of photothermal deflection spectroscopy (PTDS) and photoacoustic deflection spectroscopy (PADS) for combustion diagnostics. Both of these techniques are non-perturbing techniques suitable for in situ measurements and have a high degree of spatial and temporal resolution.

The basic idea behind the PTDS technique is quite simple: A dye laser beam (pump beam) passes through the region of interest (flame in this case). The dye laser is tuned to one of the absorption lines of the molecules that are to be detected, and the molecules absorb the optical energy from the laser beam. Due to quenching collisions this energy appears as heating of the dye laser irradiated region, leading to changes in the refractive index of the medium in that region. Now if a probe laser beam, generally a He-Ne beam, overlaps the pump beam, the probe beam is deflected due to the gradient in the refractive index of the medium created by the heating. This deflection can be easily measured by a position sensitive optical detector. The deflection of the probe beam is proportional to the number density of absorbing molecules. If a pulsed pump laser is used, the probe beam gets deflected shortly after the instant of laser firing, as discussed above, and gradually returns to its original position on the time scale of the diffusion time of the heat from the irradiated region. Thus the width of the signal depends on the thermal diffusion time constant, and consequently on the local temperature of the flame. In the presence of a flow, the heat pulse produced by the absorption of the dye laser travels downstream with the medium. The transit time of the heat pulse between two positions of the probe beam a distance Δd apart is measured. The flow velocity is derived simply from $v = \Delta d/\Delta t$, where Δt is the measured transit time.

We have also investigated the closely related PADS technique. The heating of the pump beam irradiated region is accompanied by an

increase in pressure. If the pump beam is pulsed, a pressure pulse travels outward from the pump beam irradiated region. This pressure pulse causes changes in the refractive index of the medium which may be detected by the deflection of a probe beam placed a few mm away from the pump beam. The strength of the PADS signal is proportional to the concentration of the absorbing molecules. Moreover, acoustic velocity in the flame can be measured by measuring the arrival time of the PADS signal after the instant of laser firing, and from a knowledge of the probe-pump-beam separation. Since acoustic velocity depends on the temperature, this information directly yields the local flame temperature. In the presence of a flow, the acoustic velocity is modified. Therefore if two probe beams are used, one upstream and one downstream from the pump beam, then both the flow velocity and the acoustic velocity can be measured simultaneously.

In order to be able to apply these techniques for absolute measurements in a flame, we need to have a quantitative understanding of the size and the shape of the signals in a flowing medium. We have attempted to gain such an understanding by solving the appropriate equations and subjecting the theories to experimental tests. This paper describes some of the theoretical and experimental results.

THEORY

We have derived an approximate analytical expression to predict the shape and strength of the PTDS signals in a flowing medium. Although this expression is approximate, it gives excellent agreement with the exact numerical results.[1] The deflection angle is given by

$$\phi_T(t) = \frac{2\alpha E_o (\partial n/\partial T)}{\sqrt{2\pi}\, t_o \rho C_p [4Dx + v_x a^2 + 4Dv_x(t - t_o)]}$$

$$\{[a^2 + 8D(t - t_o)]^{1/2} \exp(-2[x - v_x(t - t_o)]^2 / [a^2 + 8D(t - t_o)])$$

$$-[a^2 + 8Dt]^{1/2} \exp(-2[x - v_x t]^2/[a^2 + 8Dt])\} \qquad (1)$$

In the derivation of Eq.(1) we have assumed that the pump laser propagates along the z-axis and the probe beam propagates along the y-axis. The flow velocity v_x is directed along the x-axis, and the deflection ϕ_T in the x-direction is measured as a function of time t. The separation between the probe and the pump beams is x, and the $(1/e^2)$-radius of the pump beam is a. E_o and t_o are the energy and the duration of the laser pulse. α, n, ρ, C_p, T and D are, respectively, the absorption coefficient, refractive index, density, specific heat, temperature, and the diffusion constant of the medium.

The photoacoustic deflection signal $\phi_A(t)$ has been derived for a static medium since the typical flow velocities in a laboratory flame ($\sim$1 m/s) do not appreciably affect the size and shape of the PADS signal. The deflection angle is given by[2]

$$\phi_A(t) = -\frac{\ell E_o(\partial n/\partial p)}{n(2\pi\epsilon)^{3/2}} \frac{\alpha\beta}{C_p}\left(\frac{v}{x}\right)^{\frac{1}{2}} \left[\frac{1}{2x}F(\xi) + \frac{1}{v\epsilon}F'(\xi)\right] \quad (2)$$

where

$$F(\xi) = \left[M(-\tfrac{1}{4},\tfrac{1}{2},\xi^2)\Gamma(\tfrac{3}{4}) - 2\xi M(\tfrac{1}{4},\tfrac{3}{2},\xi^2)\Gamma(\tfrac{5}{4})\right]e^{-\xi^2} \quad (3)$$

and

$$\epsilon = (t_o^2 + a^2/2v^2)^{\frac{1}{2}} \; ; \; \xi = (t - x/v)/\epsilon \quad (4)$$

Here ℓ is the interaction length, v is the acoustic velocity, p is the pressure and β is the coefficient of thermal expansion. $F'(\xi)$ is the derivative of $F(\xi)$ with respect to ξ, M is the degenerate hypergeometric function and Γ is the Gamma function.

RESULTS

Our experimental setup is shown in Fig. 1. The pump beam is provided by a flash-lamp-pumped dye-laser (1 μsec duration pulses) and the probe beam is provided by a He-Ne laser. PTDS experiments were performed on an open jet of N_2 seeded with 1000 ppm NO_2. Seeding was required because N_2 does not have optical absorption in the dye-laser spectral range. PADS experiments were performed in a quartz cell filled with N_2 and 1000 ppm NO_2. When the dye laser is fired, a transient deflection of the probe beam is produced

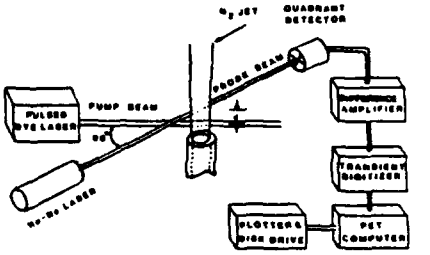

Fig. 1. Experimental setup.

Fig. 2. PTDS signals.

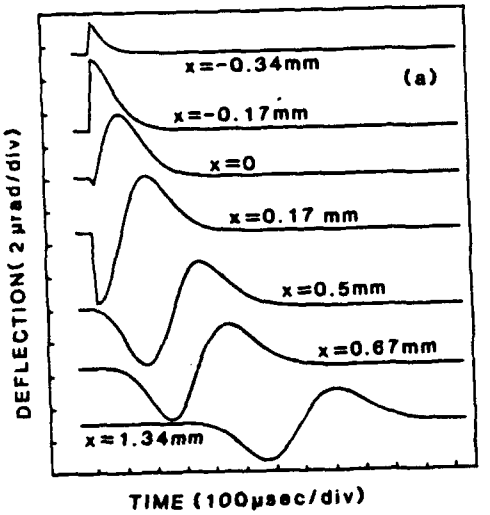

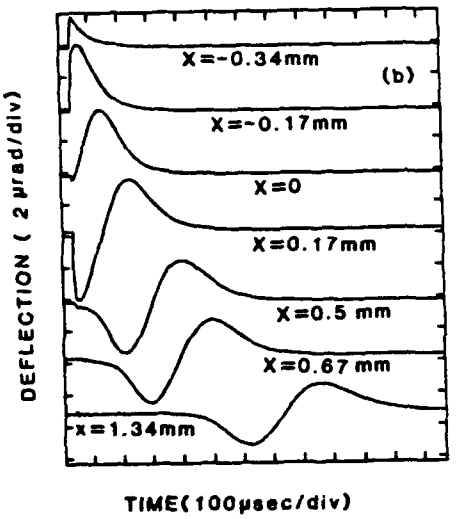

which is detected as a difference signal from a quadrant detector. The distance between the probe and pump beams, x, is variable.

Fig. 2 shows the (a) theoretical and the (b) experimental PTD signals as a function of time for v_x = 1.96 m/s with x as a parameter. Different values of x are given on each curve. Negative x represents probe beam upstream from the pump beam and positive x represents probe beam downstream. We note that as the probe beam is moved upstream, the signal becomes smaller and narrower because the heat has to diffuse against the gas flow. As the probe beam is moved downstream, the signal gets stronger at first and then acquires a shape which is essentially the derivative of the spatial profile (assumed Gaussian here) of the pump beam. As x is increased further, the signal becomes smaller and broader due to the thermal diffusion effects. There is an excellent agreement between theoretical prediction and the experimental results. Note that the theoretical results are absolute with no adjustable parameters. Preliminary results of PADS are shown in Fig. 3. The agreement between the theory and the experiment is fair, considering the uncertainties associated with the spatial profile of our pump beam.[2]

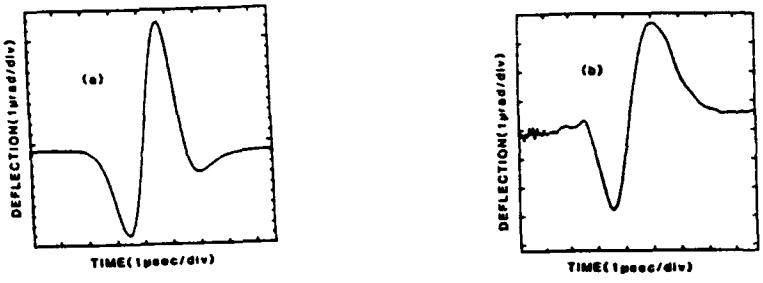

Fig. 3. PADS signals. (a) Theoretically predicted signal. (b) Experimental signal.

This work was performed in collaboration with Allen Rose, Reeta Vyas, and Yu-Xin Nie, and was supported by Air Force Wright Aeronautical Laboratories.

REFERENCES

1. A. Rose, Reeta Vyas, and R. Gupta, Applied Optics (to be published).
2. A. Rose, Y.-X. Nie, and R. Gupta, Applied Optics (to be published).

Reprinted from **Applied Optics**, Vol. 21, page 2663, August 1, 1982

Application of the photothermal deflection technique to combustion diagnostics

A. Rose, J. D. Pyrum, C. Muzny, G. J. Salamo, and R. Gupta

University of Arkansas, Physics Department, Fayetteville, Arkansas 72701.
Received 19 April 1982.
0003-6935/82/152663-03$01.00/0.

There is considerable interest[1,2] in development of combustion diagnostic techniques for minority species concentration measurements which (1) are nonperturbing, (2) have temporal resolution, and (3) have spatial resolution. In this Letter we report on the first application of photothermal deflection spectroscopy[3] to combustion diagnostics. The technique meets all three of the above requirements and has the potential of developing into an excellent combustion diagnostic tool for measurements of very low concentrations of molecules in flames. In particular, we report on preliminary experiments in which we have detected low concentrations of NO_2 produced in the combustion of a monomethylamine-seeded methane–air flame.

Several techniques are presently under extensive investigation for species concentration measurements in flames. Coherent anti-Stokes Raman scattering (CARS) is a very successful technique for majority species concentration measurements.[4] Fluorescence techniques have a high sensitivity; however, for these techniques to be useful combustion diagnostic tools one must either eliminate the effect of or quantitatively account for all quenching collisions. The saturated fluorescence technique[5] has recently received a lot of attention. In this technique the effect of quenching collisions is practically eliminated by making the absorption and stimulated emission rate much higher than the quenching rate by using high laser intensities. Following the work of Crosley,[6] we have recently shown[7] that the photoacoustic technique has a high potential of developing into an excellent technique for measurements of very low concentrations of molecules in combustion environments. Parts per million sensitivity (with a resolution of few microseconds) has been obtained for NO_2 molecules, and parts per billion sensitivity can easily be achieved for strongly absorbing molecules like OH. Achievement of spatial resolution, however, is not very easy in the photoacoustic technique, although these attempts are in progress in our laboratory. Photothermal deflection technique in many ways is similar to the photoacoustic technique but eliminates use of a microphone for signal detection, and both spatial and temporal resolution may easily be achieved.

The photothermal deflection technique has been pioneered by Amer and collaborators.[8] The basic idea behind the technique is quite simple. Two laser beams, a dye laser beam (pump beam) and a He–Ne laser beam (probe beam), intersect in the region where the molecules of interest are to be detected. The pump beam is tuned to an absorption line of the molecules of interest. Laser energy is absorbed by the molecules, who lose most of that energy by quenching collisions with other flame molecules. Most of this energy eventually appears in the heating of the flame gases, thereby changing the refractive index of the medium. The probe beam suffers a deflection due to the refractive-index gradient that is produced, which is detected by a position sensitive optical detector. The amplitude of the signal, among other things, is also proportional to the concentration of the molecules of interest. Spatial resolution is obtained because the intersection of the pump and probe beams localizes the region where the signal is observed. The temporal resolution is obtained by using a pulsed laser.

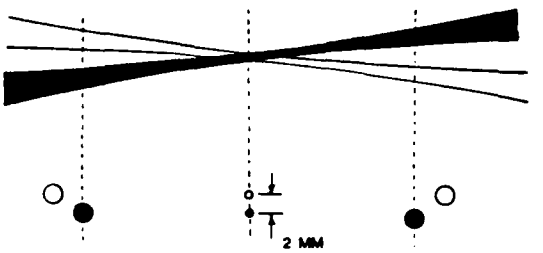

Fig. 1. Pump (dark) and probe laser beams as viewed from above (top part of the figure). The bottom part shows the cross sections of the two beams in three vertical planes.

Application of this technique to a combustion environment produces complications because of the existence of the concentration gradients of the absorbing molecules. In particular, if the pump and probe beams intersect, a deflection of the probe beam may also be produced by the refractive-index gradients due to the concentration gradients of the absorbing molecules. In this case, deflection is proportional to the concentration gradients rather than the concentration of the absorbing molecules. In our experiment the two beams do not intersect but pass close to each other as shown in Fig. 1. The top part of the figure shows how the two beams look when viewed from above. The bottom part shows cross sections of the two beams in vertical planes at three different positions. In other words, the two beams are in two different horizontal planes. The detector is arranged in such a way that it detects only the vertical component of the deflection of the probe beam. Under our experimental arrangement, the vertical deflection of the beam is proportional only to the concentration of the absorbing molecules and not to the concentration gradients.

Figure 2 shows our experimental setup. A stainless steel flat flame burner with methane, oxygen, nitrogen, and 70-ppm monomethylamine is used. The addition of small amounts of monomethylamine increases the concentrations of NO_2 in the flame for ease of detection.[9] The burner, ~6 cm in diameter and operated at atmospheric pressure, produces a faint blue pancake shaped and ~1.5-mm thick flame. Part of the burner head is masked by a stainless steel sheet to give a straight edge to the flame as shown. The straight edge was not essential to this experiment and was there for historical

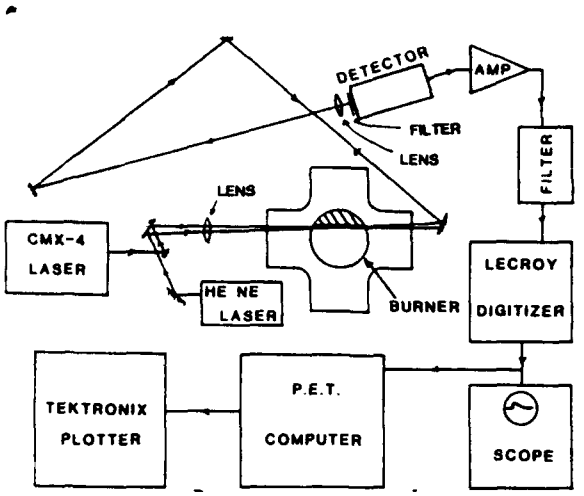

Fig. 2. Schematic diagram of our experimental arrangement.

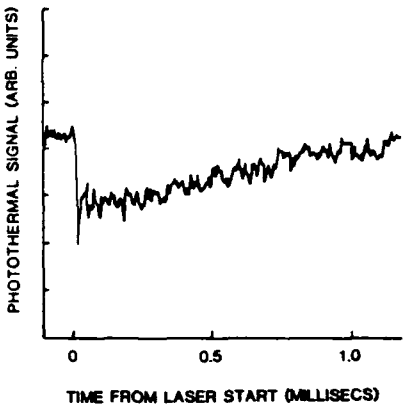

Fig. 3. Photothermal deflection signal due to NO_2 generated in a monomethylamine seeded methane–air flame. This signal was observed at the straight edge of the flame (Fig. 2), ~2 mm above the burner head, with near collinear laser beams. Laser energy was 8 mJ/pulse, and the signal was averaged over 4000 pulses.

reasons.[7] The burner is enclosed inside a glass chamber with four quartz windows and an exhaust at the top. Laser radiation from a Chromatix CMX-4 flashlamp pumped dye laser is used to excite the NO_2 molecules produced in the combustion process. The laser produces 5–10 mJ of laser energy in a 1-μsec pulse. NO_2 molecules have a quasi-continuum of absorption throughout the visible region which is peaked in the blue.[10] In the experiments reported in this paper we have used radiation at 490 nm (LD 490 dye). A 0.5-mW He–Ne beam is deflected due to the refractive-index gradients produced by the absorption of dye laser radiation by NO_2 molecules. This deflection is measured by a position sensitive gradient detector.[11] The output of the detector, after amplification, goes to a LeCroy WD 8256 transient digitizer interfaced to a Commodore PET microcomputer for signal averaging. The averaged signal is viewed on the microcomputer screen and plotted on a Tektronics plotter.

Figure 3 shows a typical photothermal deflection signal due to NO_2 generated in the flame. The detector signal is proportional to the deflection of the probe beam, which returns to its original position on the time scale of the thermal diffusion time in a flame. The curve in Fig. 3 is obtained with the pump laser beam right on the edge of the flame (where the NO_2 density is apparently high), ~2 mm above the burner head, and represents an integration over 4000 pulses. We have estimated the concentration of NO_2 molecules in this region by calibrating the size of the signal with known concentrations NO_2 in an atmospheric pressure of N_2. To be able to use the room temperature calibration to deduce the concentration of NO_2 molecules in a flame, three assumptions must be made: (1) the quenching rate of NO_2 molecules, both for flame and nonflame conditions, is much faster than the radiative rates; (2) the optical absorption by NO_2 at flame temperatures does not significantly differ from that at room temperature; and (3) the relative shift of the two beams due to beam steering effects at the flame interface is negligible. While the first assumption is good,[12] the second and third assumptions may not be strictly valid. The effect of the first two assumptions on photothermal signals and photoacoustic signals are similiar, and we have discussed these assumptions in detail in Ref. 7 in connection with the photoacoustic effect. Making the above assumptions we find that the number density of NO_2 molecules in the region investigated is $\sim 3 \times 10^{14}$ molecules/cm^3 (~50 ppm). In the above experiment, the probe and pump beams make an angle of ~2.6° (near collinear as in Fig. 2) giving low spatial resolution. To get good spatial resolution, the pump and probe beams must make a right angle with each other (crossed beam). We have determined that the sensitivity of the technique for the crossed beam case is lower by only a factor of 5 compared with that for the collinear beam case.

Further work is required to obtain reliable and accurate number densities in flames using this technique. Due to a low-absorption cross section (5×10^{-3} cm^{-1} Torr^{-1}),[13] low-number densities (few ppm),[9] and the complexity of the spectrum[10] of NO_2 molecules, quantitative work has been difficult in our experiment. Nevertheless we have successfully applied the technique to a combustion environment, and we have determined that it has an excellent potential for developing into a good combustion diagnostic tool. Future work in our laboratory on OH molecule (a molecule of considerable interest in combustion) will yield the required quantitative information. Based on our data on NO_2, we conclude that we can obtain sensitivities of a fraction of a ppm for OH molecules with good spatial resolution (crossed beam) and good temporal resolution (single shot). Also local temperature measurements in flames may be possible by measurement of thermal diffusion times.

The assistance of Kevin Tennal on this experiment is gratefully acknowledged.

This work was supported by Air Force Aero Propulsion Laboratory, Wright Aeronautical Laboratories, Wright-Patterson Air Force Base.

References

1. P. W. Schreiber, R. Gupta, and W. B. Roh, in *Laser Spectroscopy-Applications and Techniques*, Howard Schlossberg, Ed. (Society of Photo-Optical Instrumentation Engineers, Washington, D.C., 1978).
2. A. C. Eckbreth, P. A. Bonczyk, and J. F. Verdieck, *Progress in Energy and Combustion Science, Vol. 5* (Pergamon, London, 1979), pp. 253–322.
3. A. C. Boccara, D. Fournier, and J. Badoz, Appl. Phys. Lett. **36**, 130 (1980).
4. R. J. Hall and A. C. Eckbreth, in *Laser Spectroscopy-Application and Techniques*, Howard Schlossberg, Ed. (Society of Photo-Optical Instrumentation Engineers, Washington, D.C., 1978).
5. See, for example, A. P. Baronavski and J. R. McDonald, J. Chem. Phys. **66**, 3300 (1977); Appl. Opt. **16**, 1897 (1977).

6. J. E. Allen, W. R. Anderson, and D. Crosley, Opt. Lett. 1, 118 (1977).
7. K. Tennal, G. J. Salamo, and R. Gupta, Appl. Opt. 21, 2133, (1982).
8. A. C. Boccara, D. Fournier, W. Jackson, and N. M. Amer, Opt. Lett. 5, 377 (1980); D. Fournier, A. C. Boccara, N. M. Amer, and R. Gerlach, Appl. Phys. Lett. 37, 519 (1980); W. B. Jackson, N. M. Amer, A. C. Boccara, and D. Fournier, Appl. Opt. 20, 1333 (1981).
9. E. L. Merryman and A. Levy, in *Fifteenth Symposium (International) on Combustion* (The Combustion Institute, Pittsburgh, 1975), pp. 1073–83.
10. D. K. Hsu, D. L. Monts, and R. N. Zare, *Spectral Atlas of Nitrogen Dioxide 5530 to 6480 Å* (Academic, New York, 1978).
11. Silicon Detector Corp., Newbury Park, Calif.
12. V. M. Donnelly, D. C. Keil, and F. Kaufman, J. Chem. Phys. 71, 659 (1979).
13. T. C. Hall, Jr., and F. E. Blacet, J. Chem. Phys. 20, 1745 (1952); V. M. Donnely and F. Kaufman, J. Chem. Phys. 66, 4100 (1977).

Reprinted from Applied Optics, Vol. 23, page 3873, November 1, 1984

Hydroxyl (OH) distributions and temperature profiles in a premixed propane flame obtained by laser deflection techniques

Sigmund W. Kizirnis, Robert J. Brecha, Biswa N. Ganguly, Larry P. Goss, and Rajendra Gupta

OH-concentration distributions and temperature profiles have been measured on a premixed propane–air flame by laser deflection techniques. Photothermal deflection spectroscopy has been utilized for the measurement of the OH radical. Both a low-spatial-resolution (near collinear) and high-spatial-resolution (crossed-beam) scheme were used to profile the premixed flame. An optoacoustic deflection technique was utilized for thermometry. Both average-temperature profiles and probability distribution functions were determined by this technique. A comparison with data obtained by the CARS technique demonstrated that no significant flame perturbation was occurring.

I. Introduction

The availability of tunable high-peak-power laser sources has stimulated research in the area of combustion diagnostics, with the goal being to understand the basic fluid and chemical properties of combustion. Thermometry and majority species are usually detected by means of Raman techniques,[1,2] while radical intermediates in a much lower concentration are often probed using laser-induced fluorescence (LIF).[3-5] Raman methods, however (with the exception of electronically enhanced Raman techniques),[6,7] are insensitive to trace species; and LIF techniques often suffer from collisional quenching of the fluorescence in high-pressure combustion environments.[5] As a result emphasis has recently been placed on the development and application of techniques which are not only sensitive to minor flame species but also free from uncertainties due to collisional quenching. Newly developed techniques include optoacoustic spectroscopy,[8,9] photoacoustic deflection spectroscopy (PADS)[10,11] and photothermal deflection spectroscopy (PTDS).[10,12,13] These techniques not only complement the well-established Raman and LIF techniques but also widen the applicability of laser diagnostics in the area of combustion studies.

Photothermal deflection spectroscopy (PTDS), as pioneered by Amer and co-workers,[13] has been shown recently to have excellent potential for minority-species concentration measurements,[12] as demonstrated by observation of the PTDS signal from NO_2 produced in a methane–air premixed flame. It was further demonstrated that the OH radical could be observed in a premixed methane–air flame by the PTDS technique.[10] In this technique two laser beams, a dye laser (pump) beam and a He–Ne (probe) beam, intersect in the region where the molecules of interest are to be detected. The pump beam is tuned to an absorption line of the molecules of interest, and the laser energy absorbed by these molecules is lost through quenching collisions with other flame molecules, resulting in the heating of the flame gases. Due to the spatial profile of the laser (generally assumed to be Gaussian) and thermal diffusion of heat, a refractive-index gradient is produced. The probe beam is deflected due to this gradient which is observed by a position-sensitive optical detector. The amplitude of the signal is proportional to the concentration of the probed molecules. The technique has high sensitivity,[10,12] which is appropriate for minority species, and displays good spatial resolution if the two beams intersect at approximate right angles. Temporal resolution can be achieved by using a pulsed laser. The technique is nonperturbing, a typical temperature change produced by the absorption of laser energy being of the order of 1 K.

Another technique which has been shown to have high potential for the measurement of very low concentrations in combustion environments is the opto-

Rajendra Gupta is with University of Arkansas, Physics Department, Fayetteville, Arkansas 72701; L. P. Goss is with Systems Research Laboratories, Inc., 2800 Indian Ripple Road, Dayton, Ohio 45440; the other authors are with AFWAL Aero Propulsion Laboratory, Wright-Patterson AFB, Ohio 45433.

Received 29 March 1984.
0003-6935/84/213873-09$02.00/0.

acoustic (photoacoustic) technique. Parts-per-million sensitivity has been obtained with NO_2 molecules,[9] and higher sensitivity can be achieved for strongly absorbing OH molecules.[14] Crosley[15] recently demonstrated that OH, NH_2, CO_2, and H_2O could be monitored by means of this technique. Achievement of spatial resolution through the use of a microphone as the acoustic detector, however, is difficult. A detection method employing laser beam deflection (PADS) has been used in an attempt to improve the spatial resolution of this technique.[10,11] PADS has some advantages over PTDS, although its sensitivity is lower.[11]

One interesting application of the optoacoustic technique which was demonstrated by Tam[16] involved determination of flame temperature by measurement of the sound velocity between two probe beams. In this method an intense sound pulse was generated by a plasma spark created by focusing an intense 1064-nm, 10-nsec Nd:YAG laser. Two probe beams were employed to monitor the speed of the sound pulse over a distance defined by the probe-beam separation. Since the velocity of sound varies with the square root of the temperature, the temperature can be determined from the sound transit time. However, the spark as well as the blast wave generated by the gas breakdown can greatly disrupt the flow and, in the case of unburnt fuel and air mixtures, even cause ignition of the gases. In the present study a small wire was employed for the target of the pump laser for sound production, which reduced the perturbation of the flame and the requirements for high peak powers. The sound pulse produced with a wire target is of sufficient amplitude to permit thermometry with laser powers as low as 2 mJ/pulse.

Studies with both the optoacoustic and the PTDS techniques on a premixed propane–air flame are reported in this paper. The PTDS technique was employed to determine OH distributions, while the optoacoustic technique was used to determine the temperature profile.

II. Apparatus

The experimental setup for the PTDS studies is shown schematically in Fig. 1. A Quanta-Ray model PDL dye laser was pumped by a frequency-doubled Quanta-Ray Nd:YAG laser. The DCM dye employed typically delivered 7 mJ of energy in a pulse length of 10 nsec at 6200 Å. The dye laser output at 6200 Å was frequency doubled by an Inrad autotracking harmonic generator assembly. The typical UV output at 3100 Å was ~200 μJ/pulse in a spectral width of ~18 GHz. The frequency-doubled UV output was tuned to one of the main branch transitions of the OH molecule and allowed to pass through a propane–air flame. Radiation from a Spectra-Physics model 233 He–Ne laser intersected the dye-laser beam inside the flame. These beams were focused in the flame using long-focal-length lenses (~50 cm). The beam diameter near the focal point was ~1 mm. Both a low-spatial-resolution near-collinear and a high-spatial-resolution 12° crossed-beam configuration were used to profile the premixed flame. Most of

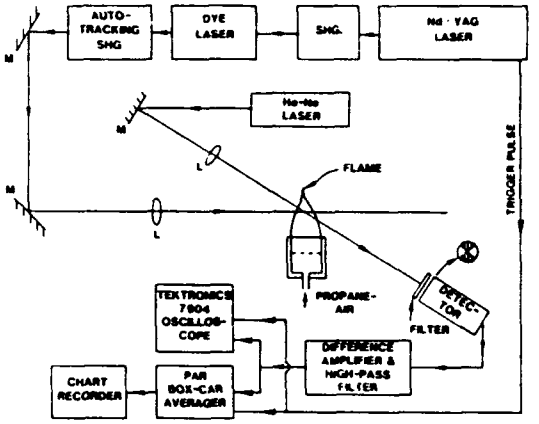

Fig. 1. Schematic illustration of the PTDS experimental arrangement.

the dye-laser energy absorbed by the OH molecules eventually appeared as heat in the irradiated region due to collisional de-excitation. Refractive-index gradients were produced in the medium due to the spatial profile of the pump-laser beam, which causes the overlapped probe beam to be deflected. This deflection was monitored by a Silicon Detector Corp. model SD-380-23-21 position-sensitive detector having four quadrants; the two quadrants oriented in the direction of the deflection were used in the present experiment. The signals from the individual quadrants were passed through a current-to-voltage amplifier and fed into a difference amplifier which was used to gain the difference signal. The output of the difference amplifier was filtered by a high-bandpass filter (3-dB point at 10 kHz) to reduce low-frequency signal fluctuations due to the He–Ne instabilities and the index-of-refraction gradients in the flame. The signal shape was observed on a Tektronix model 7904 oscilloscope equipped with a programmable digitizer (model 7D20) and triggered by the Q-switch pulse from the Nd:YAG laser. The signal was measured by a PAR model boxcar integrator which was also triggered by the Nd:YAG laser. The boxcar gate was set at 20 μsec to envelop most of the PTDS signal, and the output of the boxcar was recorded on a chart recorder.

Before measurements were made, the He–Ne quiescent position was adjusted to give a zero difference signal. This insured that the maximum deflection was observed and aided in minimizing the high-frequency noise of the probe laser. A deflection of the probe laser would result in an imbalance between the two quadrants and produce a difference signal.

The arrangement for the optoacoustic experiment is shown in Fig. 2. The frequency-doubled output from the Quanta-Ray Nd:YAG laser was mildly focused (50-cm focal length) on a small 500-μm wire. Two He–Ne lasers were used for the probe beams; each beam was imaged onto a separate PIN diode detector. The electronics for the PIN diodes were similar to those of the quadrant detector, except that no difference-amplifier stage was employed. The probe beams were located 2 cm upstream of the wire sound source to mini-

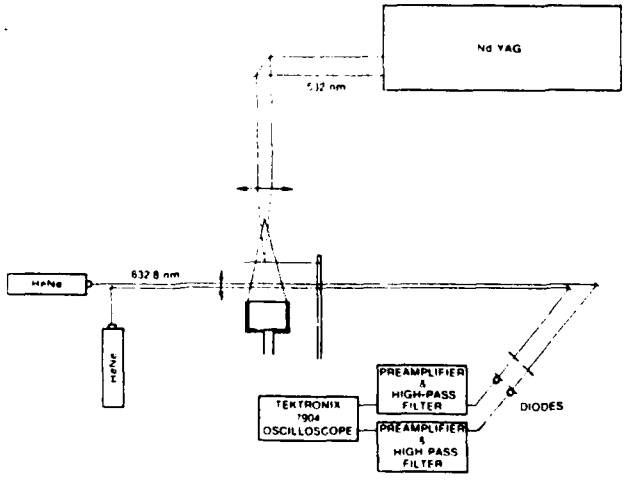

Fig. 2. Schematic illustration of the optoacoustic experimental arrangement.

mize flow disturbances within the probe region. The probe beams were placed 2 mm apart, resulting in an estimated spatial resolution of 0.5 mm^3. A 2-mJ 532-nm laser pulse, mildly focused in ambient air, resulted in a deflection signal of 0.2 V.

The burner was fabricated from stainless steel and is ~7.6 cm (~3 in.) in diameter. A fuel-rich mixture of propane and air with an equivalence ratio of 1.48 was used. The flame extends ~18 cm (~7 in.) above the burner head. A chimney, which was used to help stabilize the flame, greatly limited the accessibility of the upper part of the flame for optical measurements. Some of the experiments were conducted without the chimney, and the flame in these conditions was unstable. The burner was mounted on a motor-driven X-Y translator to permit horizontal and vertical movements.

III. OH Measurements

A typical single-shot OH photothermal signal deflection is shown in Fig. 3(a). The frequency-doubled dye laser was tuned to the $Q_1(7)$ absorption line of the $v'' = 0$ to $v' = 0$ band of the $X^2\pi$—$A^2\Sigma^+$ electronic transition of OH at 3089.6 Å. The pump and probe beams were arranged in the near-collinear configuration, resulting in low spatial resolution. At the instant of laser firing, the probe beam was deflected due to refractive-index gradients produced by the adsorption of laser energy by the OH molecules and subsequent heating of the irradiated region due to quenching collisions. The deflection of the probe beam gave rise to a difference signal at the quadrant detector. The probe beam returned to its original position on the time scale of the thermal diffusion. The deflection of the probe due to absorption of the OH molecules can be distinguished from refractive-index gradients produced by the flame (even in the case of high turbulence) in two ways. First, as seen in Fig. 3, the frequency of the PTDS signal is of the order of 15–50 kHz, while the maximum fluctuations in a turbulent flame are 10 kHz (typically 1–2 kHz). Thus, electronic filtering, as em-

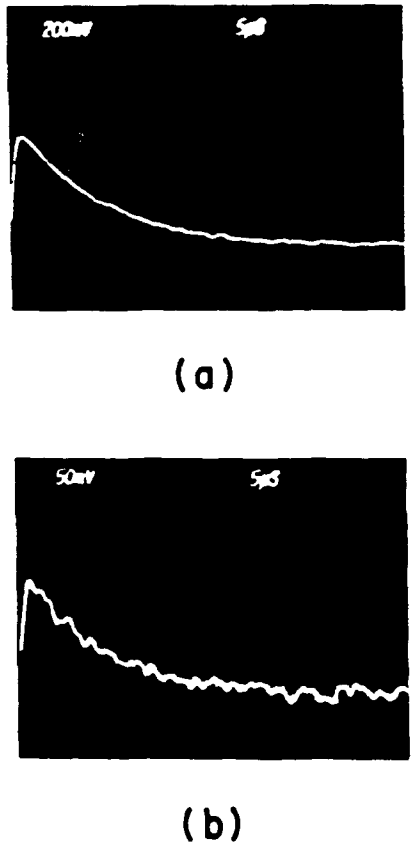

Fig. 3. Typical single-shot photothermal signal from OH molecules in propane–air flame with probe and pump beams (a) near-collinear and (b) 12° crossed. Pump laser tuned to $Q_1(7)$ of OH at 3089.6 Å.

ployed, can remove turbulence-induced refractive indices. Second, the PTDS signal occurs immediately after the laser pulse, thus allowing for a narrow window to minimize laser and detector noise.

By routing the amplified and filtered difference output of the quadrant detector into a boxcar integrator, the relative signal strength of the photothermal deflection could be recorded and plotted on a strip-chart recorder as the flame was traversed. This allowed the OH profiles shown in Fig. 4 to be measured. The boxcar integrator gate was set at 20 μsec with a 1-msec integration time constant. The zero of the abscissa of Fig. 4 corresponds approximately to the center of the flame. These measurements were repeated at different heights above the burner head, as indicated in the diagram. Since the beam configuration was not changed and only the flame was moved through the beams, the photothermal signal strength was directly proportional to the OH density (neglecting any corrections for the temperature nonuniformity across the flame). Note that the OH density is highest near the edges of the flame. The asymmetric OH density was reproducible and consistent from run to run and believed to be characteristic of the burner employed. Due to the presence of the chimney, measurements at heights >35 mm above the burner head could not be made. The observed profiles are quite similar to OH profiles obtained by

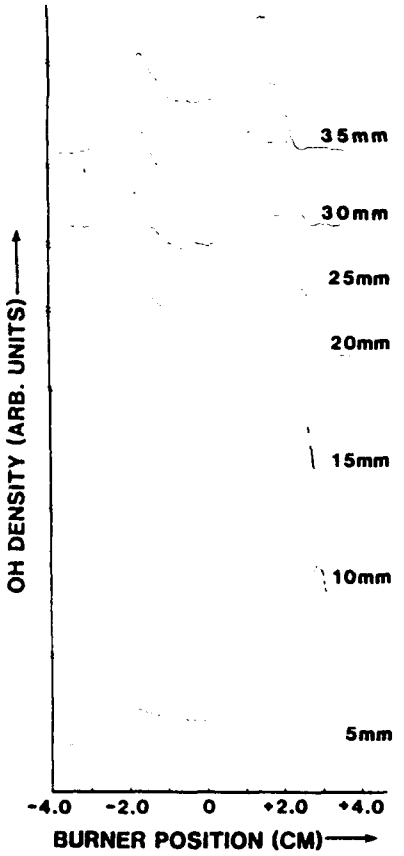

Fig. 4. OH concentration profiles in propane–air flame at various heights above burner head. Probe and pump beams were near-collinear, giving low spatial resolution. Zero of abscissa represents center of burner.

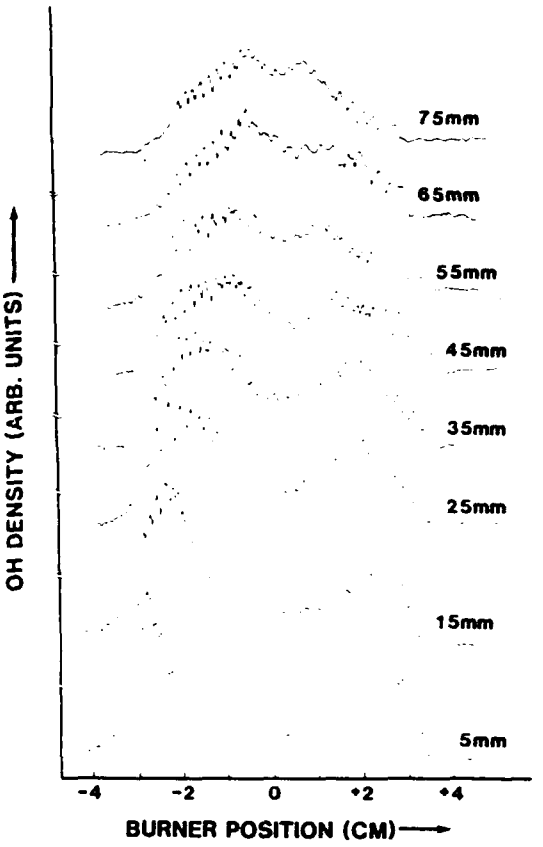

Fig. 5. Results similar to those of Fig. 4, with the flame being operated without a chimney. In these conditions, the flame was flickering at the rate of a few hertz; small oscillations in the figure represent the effect of flicker on OH density. OH peaks are reversed compared with those in Fig. 4, since the direction of the flame scan was reversed.

Alden *et al.*[17] and Dyer and Crosley[18] on premixed hydrocarbon–air flames.

To facilitate measurements at heights >35 mm above the burner head, the stabilizing chimney was removed and the flame flickered at the rate of a few hertz. Figure 5 shows the OH profiles at various heights above the burner in the nonsteady flame. The OH concentration at the edges appears to be reversed; however, it was the direction of scan which was reversed. The periodic oscillations in the signal are believed to be due solely to flicker of the flame and do not represent laser perturbations or detector noise. If laser perturbations were indeed occurring, they would also have been displayed in Fig. 4. The likelihood of laser perturbations of this flame is small due to the low powers used for the measurements and the large size of the burner. Small jets, however, are very sensitive to acoustic perturbations, and care must be taken with these systems when measurements are made close to the jet nozzle.[19] The flame flicker in our experiment can be avoided by using a transparent quartz chimney.

While the measurements made with the collinear arrangement displayed strong signals, indicating good detectivities of OH in the flame, the spatial resolution of the measurements greatly limits the usefulness of the data—especially in the area of combustion-model evaluation where high spatial resolution is required and a cross-beam configuration must be employed. To demonstrate that the signal-to-noie ratio was sufficiently large—even with a small overlap between the pump and probe beams—a crossing angle of 12° was chosen as a test case. In the near-collinear configuration case, the interaction zone over which the measurement was made consisted of a substantial part of the 8-cm flame width. With a 12° crossed-beam configuration, the interaction length is ~3 mm (3 mm^3 vol). The observed signal drop shown in Fig. 3(b) on changing from the near-collinear to the 12° crossed-beam configuration was a factor of 4.

The spatially resolved OH distribution in the premixed flame, as measured by the crossed-beam technique, is shown in Figs. 6 and 7. In Fig. 6 the chimney was replaced on the burner to permit a relatively stable flame to be profiled. Several points should be noted in Fig. 6 relative to the low-resolution profile shown in Fig. 4. The two peaks in OH concentration near the edge of the burner are much sharper in the crossed-beam case than in the collinear case, while the central regions of the flame, <35 mm high, show a much lower OH number density. This is due to the large interaction region in the low-resolution case which acts to smear and broaden the observed profiles.

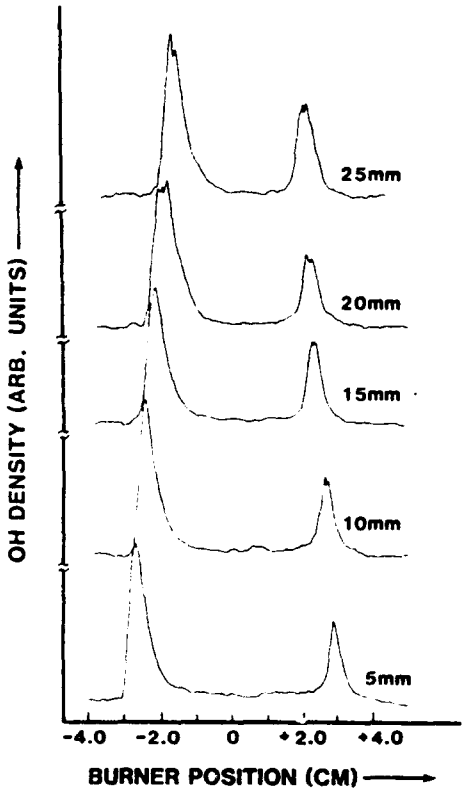

Fig. 6. OH density profile of flame with higher spatial resolution (3 mm³). Note that OH density is lower in the center of the flame and OH density peaks at the edges are sharper than low-resolution data indicate.

Figure 7 shows the effect of the flame flicker when the chimney is removed. Note that the OH profile breaks up into four peaks at about the midpoint of the flame. This is most evident in the 65–85-mm range in Fig. 7. The four peaks are believed to be an artifact of the synchronization of the low-frequency flame flicker with the 10-Hz data acquisition. As one moves higher up the flame, the four peaks collapse into one. Most of the low-frequency noise at heights above 25 mm in Fig. 7 is caused by flame instability. This breakup of the OH distribution was not observed in Fig. 5 due to the spatial averaging that was occurring with the small-angle beam overlap.

To put the OH concentration measurements on an absolute scale, the absolute OH density was determined at one place in the flame by absorption measurements. The laser was tuned to the $Q_1(7)$ line of OH molecules at 3089.6 Å, and absorption of the laser energy was measured by a Scientec power meter. The absorption was measured to be 8.6% at a height of 5 mm above the burner head which corresponds to an OH density of $\sim 5 \times 10^{14}$ molecules/cm³ at the edge of the flame. The flame in the present study was used in fuel-rich conditions (equivalence ratio = 1.48).

In Fig. 8 the photothermal deflection spectrum of OH molecules is shown. The PTDS signal was recorded using a boxcar averager, as above, at a fixed point in the flame while scanning the frequency of the dye-laser

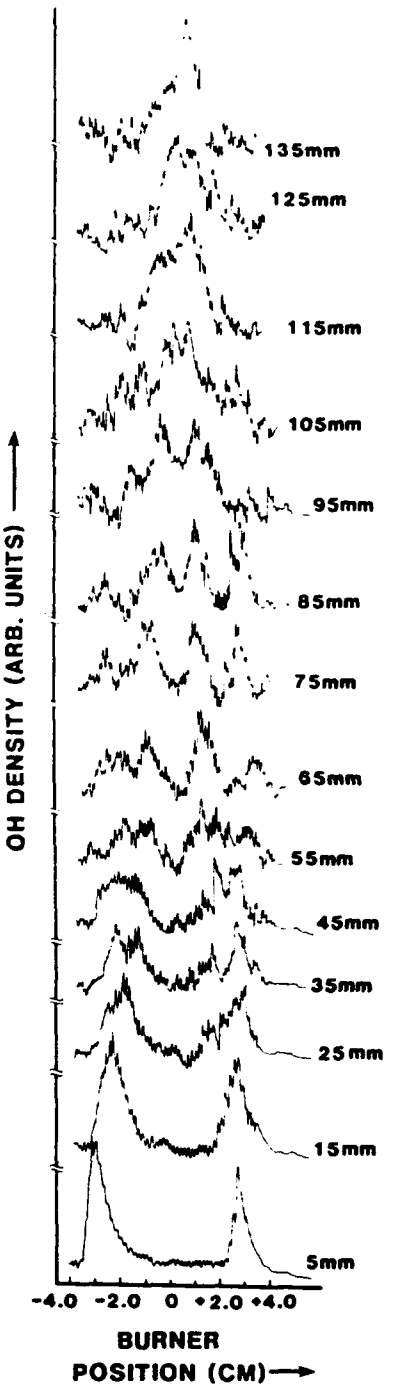

Fig. 7. Data similar to that of Fig. 6 with chimney removed. The flame, in this case, was flickering and wandered near the top.

beam. The autotracker rotated the second harmonic crystal for optimum UV output as the dye-laser frequency was scanned, giving a smooth UV output as a function of frequency. The features in Fig. 8 can be identified with known transitions in the OH spectrum. These results demonstrate that PTDS can be used as a sensitive spectroscopic technique for atomic and molecular species.

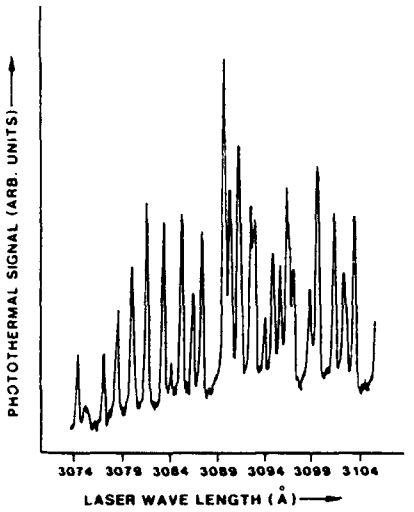

Fig. 8. Absorption spectrum of OH molecules. Photothermal signal strength was plotted as the pump laser frequency was scanned.

IV. Thermometry

As mentioned previously, the velocity of an acoustic wave which is propagating through a flame is dependent on the temperature of the flame. The relationship between the temperature and the acoustic-wave-propagation velocity is given by

$$T = \frac{V_0^2 \overline{m}}{R\left[1 + \frac{R}{\overline{C_v}(T)}\right]}, \tag{1}$$

where $\overline{m}$ is the average molecular weight of the gases in the flame, R is the universal gas constant, V_0 is the sound velocity, and $C_v(T)$ is the temperature-dependent average molar specific heat at constant volume in the flame.

The solution of Eq. (1) for temperature T requires that $\overline{m}$ and $\overline{C_v}(T)$ be known. In a premixed propane–air flame in the experimental conditions of the present study, the main gaseous component is N_2, with the other major components being CO_2 and H_2O. An adiabatic flame code[20] can be used to yield the gaseous composition of the flame as a function of temperature from which $\overline{m}$ and $\overline{C_v}(T)$ can be calculated and used to extract a temperature from a sound-velocity measurement. In the most accurate case, this is the approach of choice. However, to a first approximation the composition can be assumed to be constant with temperature; and by simply ratioing the velocity measured by ambient conditions to that in the flame, a temperature can be determined,

$$\frac{T_f}{T_a} = \left(\frac{V_f}{V_a}\right)^2. \tag{2}$$

If the gas velocity is small compared to the speed of sound, Eq. (2) can be simply written as

$$\frac{T_f}{T_a} = \left(\frac{\Delta t_a}{\Delta t_f}\right)^2, \tag{3}$$

where Δt_a and Δt_f are the measured times required for the acoustic pulse to travel between the two probe beams with and without the flame. Equation (3) is found to give only a small underestimate of the correct T value (in the present flame conditions) compared with Eq. (1) which uses the appropriate $\overline{m}$ and $\overline{C_v}(T)$ values as well as takes into account the gas velocities of the flame. In general, this will not be the case in a turbulent diffusion flame where $\overline{m}$ can vary greatly, and thus, Eq. (1) must be employed.

The basic experiment is to measure the velocity of an acoustic pulse as it travels through the flame. A small wire which was pulsed with a low-power, <2 mJ/pulse, mildly focused frequency-doubled Nd:YAG laser was used as the acoustic source (see Fig. 2). Absorption of the pump beam by the wire produces a localized heating of the wire which acts to heat the surrounding gases, giving rise to a pressure increase. This acoustic pulse travels outward, causing a change in the refractive index of the medium. The arrival of the acoustic pulse at a beam was measured by an observation of the deflection of that beam. Two probe beams separated by 2 mm were used to monitor the sound velocity. The probe beams were arranged upstream of the wire in order that no significant perturbation of the flame would be produced by the wire at the position of the probe beams.

The photoacoustic deflection signals in the absence and presence of the flame are shown in Fig. 9. Note the drop in amplitude of the acoustic signal with temperature. This effect is due to the lower number density at the elevated temperature. The width of the acoustic deflection is primarily determined by the transit time of the sound pulse across the He–Ne probe beam. The probe beams were focused to decrease their size and increase the time resolution (spatial resolution) of the acoustic measurement. The acoustic deflection signals were recorded on a transient digitizer which allowed the acoustic transit time to be determined. Both single-shot and averaged transit times were recorded and compared. The temperature profiles shown in Fig. 10 were determined in this manner. Note that the temperature profile across the premixed flame was essentially constant, with a slight drop in temperature at the center. As the flame is profiled at different heights above the burner, the temperature results clearly reveal the narrowing of the flame along with a gradual drop in temperature. Similar results have been obtained with the CARS technique on a propane–air premixed flame.[21]

To demonstrate that the beam steering of the flame did not adversely affect the temperature measurements, the stabilizing chimney was removed from the burner and three sets of 100 single-shot temperatures were taken above the flickering flame. The resulting temperature probability distribution functions (pdfs) are shown in Fig. 11. Low in the flame (4 cm above burner surface), a single-mode pdf is observed with an average temperature of 1831 K ± 67 K. At a position 7 cm above the burner, the pdf begins to show signs of a bimodal distribution. The average temperature has dropped to 1525 K. At the 11-cm position, a distinctive bimodal distribution is observed with an average temperature of 1196 K. The index-of-refraction gradients

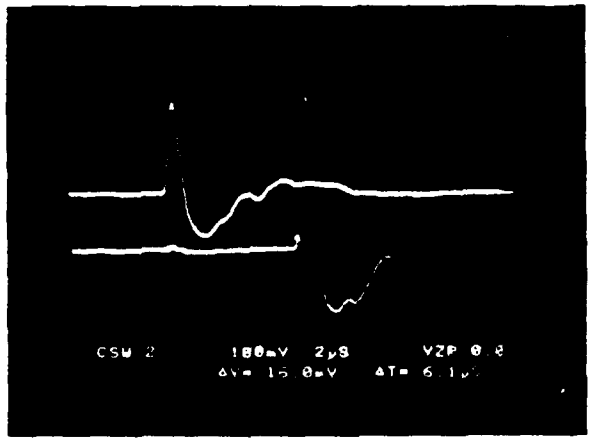

(a)

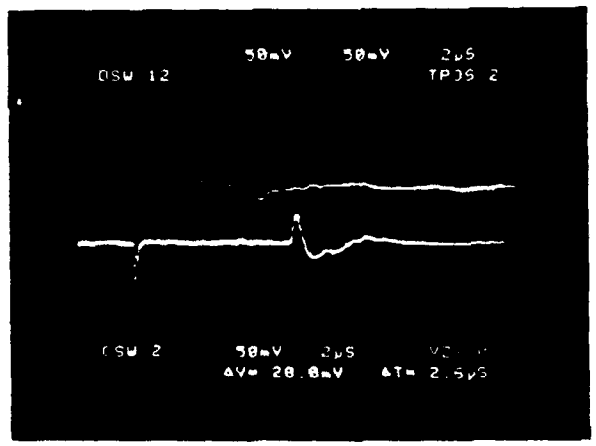

(b)

Fig. 9. Optoacoustic deflection signals (a) in room air and (b) in a propane–air flame.

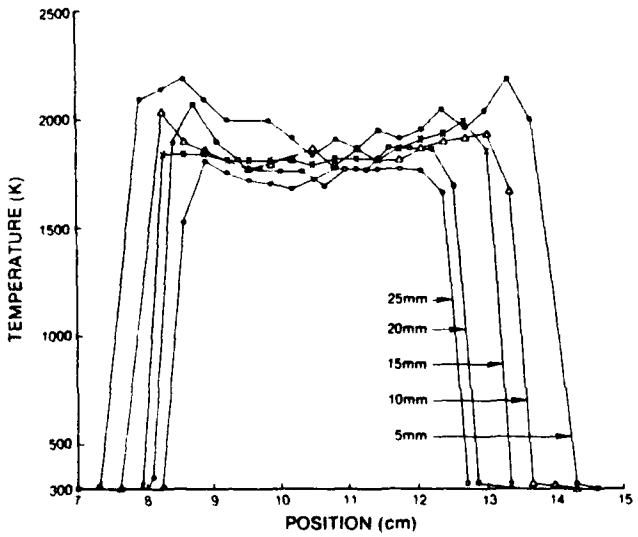

Fig. 10. Average-temperature profiles taken in a propane–air flame by the optoacoustic technique.

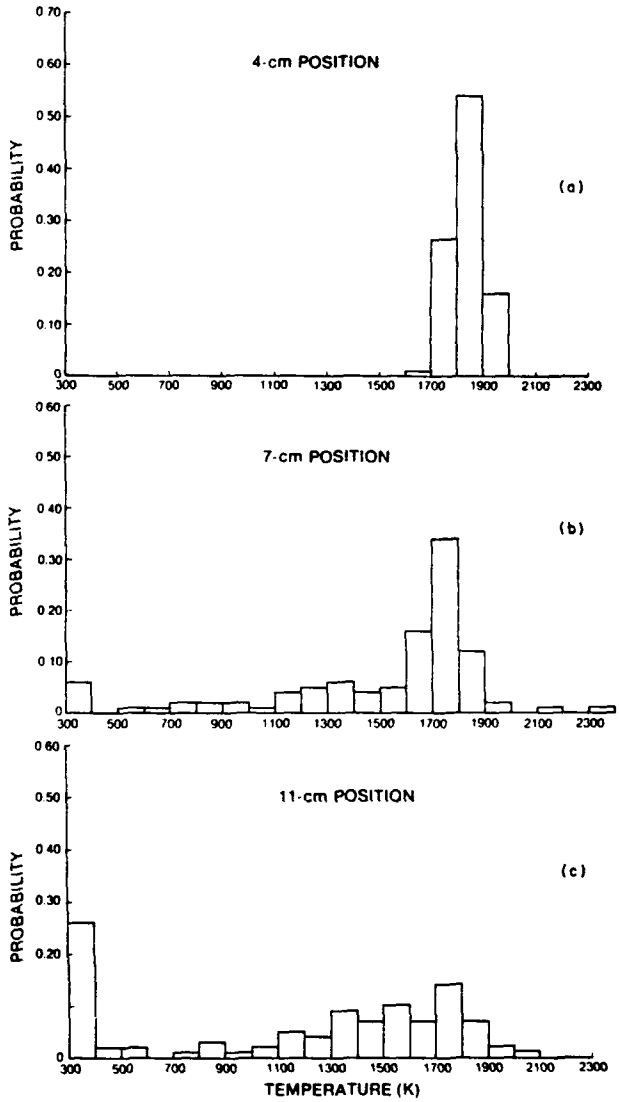

Fig. 11. Probability distribution functions obtained at flame locations (a) 4 cm, (b) 7 cm, and (c) 11 cm above the burner surface.

in the upper part of the flame are severe due to the large temperature variation which occurs there. However, electronic filtering of the signal which blocked the low-frequency fluctations below 10 kHz and passed the higher frequencies associated with the acoustic signal (500 kHz) allowed the acoustic signals to be measured without interference from the flame turbulence. The observed pdf's in this flame are very similar to reported results on a turbulent flame obtained by the CARS technique.[22,23]

This method of temperature measurement was compared with CARS, which is an established technique for temperature measurements. The optoacoustic technique indicated a temperature of 1950 K, at a position 5 mm above the burner surface, while the CARS technique indicated 1970 K. Both methods yielded consistent results, proving the reliability of this technique. Also, for the stoichiometry of the flame, both methods yielded results in agreement with theoretical predictions[20] (equivalence ratio = 1.48, T = 1968 K),

proving that the presence of the thin wire caused no significant perturbation of the flame at the site of measurement (region between the two probe beams).

This technique of temperature measurement is closely related to photoacoustic deflection spectroscopy (PADS)[11] and to optoacoustic laser deflection (OLD).[16] In PADS the acoustic signal is generated by the absorption of the pump-laser energy by the flame molecules themselves (the pump laser being tuned to a transition of the molecules). The PADS technique was not utilized as the sound source in these experiments due to the limited distribution of the OH molecules. However, with a more uniformly distributed absorbing species, the PADS technique could be employed. The OLD technique was not employed because of the perturbation to the flame caused by optical breakdown, as discussed earlier.

V. Conclusions

It has been demonstrated that PTDS can be used to measure concentration profiles of a minority combustion species. In particular, OH concentration profiles have been measured in a propane–air flame. The technique is nonperturbing and possesses both spatial and temporal resolution. The temporal capabilities of this technique have not been exploited in this particular experiment. However, an examination of Fig. 3 shows that complete concentration information at a point in the flame can be obtained in ~40 μsec. Therefore, data can be acquired at a 10-kHz rate if a suitable laser is available. Local temperatures of the flame can be deduced from a measure of the thermal diffusion times. PTDS was not used for this purpose in the present study because of the lack of a quantitative theoretical model. By using several probe beams at right angles to the pump beam along the length of the pump beam, one can, in principle, measure concentration and temperature simultaneously at several points along a line in the flame. Moreover, a theoretical model of the PTDS is being developed which will permit absolute temperature and concentration measurements of OH without the need for calibration by absorption measurements.

It has also been demonstrated that the optoacoustic deflection technique can be employed for thermometry, in both a laminar and a turbulent flame environment. The advantages of acoustic deflection thermometry over other thermometry techniques are that it is relatively simple to implement, it does not require the high-peak-power pulsed laser necessary for nonlinear Raman techniques, and it potentially can be extended to the analysis of high-frequency temperature fluctuations if a suitable laser is utilized for the sound production. However, because of the dependence of the sound velocity on $\overline{m}$, a knowledge of the flame composition–especially in the case of a turbulent-diffusion flame—is necessary. It is in the high-frequency-thermometry area that the acoustic deflection technique will be extended in the near future.

The authors would like to thank D. Linder for his excellent technical help and K. Herren for his generous loan of several instruments. R. Gupta would like to thank the Plasma Physics Group of the Air Force Wright Aeronautical Laboratories/Aero Propulsion Laboratory for their kind hospitality while this work was being performed. This work was entirely supported by and performed at the Aero Propulsion Laboratory at Wright-Patterson AFB, Ohio.

References

1. M. D. Drake, M. Lapp, C. M. Penney, S. Warshaw, and B. W. Gerhold, "Measurements of Temperature and Concentration Fluctuations in Turbulent Diffusion Flames Using Pulsed Raman Spectroscopy," in *Proceedings, Eighteenth Symposium (International) on Combustion* (Combustion Institute, Pittsburgh, Pa., 1981), p. 1521.
2. A. C. Eckbreth and R. J. Hall, "CARS Concentration Sensitivity With and Without Nonresonant Background Suppression," Combust. Sci. Technol. **25**, 175 (1981).
3. J. W. Daily, "Saturation Effects in Laser Induced Fluorescence Spectroscopy," Appl. Opt. **16**, 568 (1977).
4. R. P. Lucht, D. W. Sweeney, and N. M. Laurendeau, "Saturated-Fluorescence Measurements of the Hydroxyl Radical," in *Laser Probes for Combustion Chemistry*, D. R. Crosley, Ed. (American Chemical Society, Washington, D.C., 1980), Vol. 134, p. 145.
5. D. R. Crosley, "Collisional Effects on Laser-Induced Fluorescence Flame Measurements," Opt. Eng. **20**, 511 (1981).
6. B. Attal, K. Muller-Dethlefs, D. Debarre, and J. P. E. Taran, "Resonant CARS Spectroscopy of C_2," Appl. Phys. B **28**, 121 (1982).
7. B. Attal, D. Debarre, K. Muller-Dethlefs, and J. P. E. Taran, Rev. Phys. Appl. **18**, 39 (1983).
8. J. E. Allen, Jr., W. R. Anderson, and D. R. Crosley, "Optoacoustic Pulses in a Flame," Opt. Lett. **1**, 118 (1977).
9. K. Tennal, G. J. Salamo, and R. Gupta, "Minority Species Concentration Measurements in Flames by the Photoacoustic Techniques," Appl. Opt. **21**, 2133 (1982).
10. A. Rose, J. D. Pyrum, G. J. Salamo, and R. Gupta, in *Proceedings, International Conference on Lasers '82*, R. C. Powell, Ed. (STS Press, McLean, Va., 1983).
11. A. Rose, G. J. Salamo, and R. Gupta, "Photoacoustic Deflection Spectroscopy: A New Specie-Specific Method for Combustion Diagnostics," Appl. Opt. **23**, 781 (1984).
12. A. Rose, J. D. Pyrum, C. Muzny, G. J. Salamo, and R. Gupta, "Application of the Photothermal Deflection Technique to Combustion Diagnostics," Appl. Opt. **21**, 2663 (1982).
13. W. B. Jackson, N. M. Amer, A. C. Boccara, and D. Fournier, "Photothermal Deflection Spectroscopy and Detection," Appl. Opt. **20**, 1333 (1981).
14. A. Rose, J. D. Pyrum, G. J. Salamo, and R. Gupta, "Photoacoustic Detection of OH Molecules in a Methane–Air Flame," Appl. Opt. **23**, 1573 (1984).
15. G. P. Smith, M. J. Dyer, and D. R. Crosley, "Pulsed Laser Optoacoustic Detection of Flame Species," Appl. Opt. **22**, 3995 (1983).
16. W. Zapka, P. Pokrowsky, and A. C. Tam, "Noncontact Optoacoustic Monitoring of Flame Temperature Profiles," Opt. Lett. **7**, 477 (1982).
17. M. Alden, H. Etner, G. Holmstedt, S. Svanberg, and T. Högberg, "Single-Pulse Laser-Induced OH Fluorescence in an Atmospheric Flame, Spatially Resolved with a Diode Array Detector," Appl. Opt. **21**, 1236 (1982).
18. D. J. Dyer and D. R. Crosley, "Two-Dimensional Imaging of OH Laser-Induced Fluorescence in a Flame," Opt. Lett. **7**, 382 (1982).

19. See, for example, D. C. Fourguette and M. B. Long, "Highly Localized Pressure Perturbations Induced by Laser Absorptive Heating in the Shear Layer of a Gas Jet," Opt. Lett. 8, 605 (1983), and references therein.
20. S. Gordon and B. J. McBride, "Computer Program for Calculation of Complex Equilibrium Composition Rocket Performances, Incident and Reflected Shocks, and Chapman-Junget Detonations," NASA SP-273-1971, NTIS N71-37775 (NTIS, Springfield, Va., 1971).
21. L. P. Goss, G. L. Switzer, and P. W. Schreiber, "Flame Studies with the Coherent Anti-Stokes Raman Spectroscopy Technique," J. Energy 7, 389 (1983).
22. L. P. Goss, G. L. Switzer, D. D. Trump, and P. W. Schreiber, "Temperature and Species-Concentration Measurements in Turbulent Flames by the CARS Techniques," J. Energy 7, 403 (1983).
23. L. P. Goss, B. G. MacDonald, D. D. Trump, and G. L. Switzer, "10-Hz Coherent Anti-Stokes Raman Spectroscopy Apparatus for Turbulent Combustion Studies," Paper No. AIAA-83-1480 presented at the AIAA Eighteenth Thermophysics Conference, June 1983, Montreal, Canada.

Reprinted from Optics Letters, Vol. 10, page 532, November, 1985

Application of photothermal deflection technique to flow-velocity measurements in a flame

A. Rose and R. Gupta

Department of Physics, Universtiy of Arkansas, Fayetteville, Arkansas 72701

Received July 15, 1985; accepted August 27, 1985

A new method for a measurement of flow velocities in flames using the photothermal deflection technique is demonstrated. The technique has been applied to measure the velocity profile of a laminar H_2/O_2 flame. The method is nonintrusive and has a high degree of spatial and temporal resolution.

There is extensive interest in the development of nonintrusive techniques for a measurement of flow velocities in flames and other combustion media. These techniques should be capable of giving a high degree of spatial and temporal resolution. Many techniques have recently been developed to measure flows, although few have been applied to combustion. Miller and Hanson[1] and Cheng *et al.*[2] have made use of the Doppler shift in laser-induced fluorescence to obtain flow-field measurements in gas flows seeded with I_2 and Na, respectively. Gustafson *et al.*[3] and Moosmüller *et al.*[4] have demonstrated the use of Raman techniques in supersonic flows for velocity measurements. Schenck *et al.*[5] have measured flow velocities in an analytical flame seeded with Na using laser-enhanced ionization (LEI). An important class of techniques is based on seeding the medium with particles, the most widely used of these being laser Doppler velocimetry (LDV).[6] However, to our knowledge, only the applications of LDV and LEI to flames have been demonstrated. In this Letter, we demonstrate the application of a new method based on the photothermal deflection (PTD) technique for flow-velocity measurements in a flame. The flow-velocity profile of a laminar H_2/O_2 flame has been obtained. This method is nonintrusive and has excellent spatial and temporal resolution. This technique has some important advantages over other (proposed or demonstrated) techniques, and in one aspect it is complementary to other techniques. Undoubtedly, this technique will also find use in many other areas, e.g., fluid mechanics and aerodynamics.

In this technique a dye laser is tuned to an absorption line of a species of the medium. In this case the two media used were a N_2 jet seeded with NO_2 and a H_2/O_2 flame. The absorbing species were NO_2 in the jet and an OH radical in the flame. The absorbed optical energy is quickly transferred into translational modes of the flame gases because of quenching collisions. That is, the dye-laser-irradiated region gets slightly heated, and a pulse of heat is produced if a pulsed dye laser is used. The heat pulse is accompanied by changes in the refractive index of the medium, which can be detected by deflection of a probe (usually a He–Ne laser) beam. The arrival time of the heat pulse is measured downstream at two points a known distance apart. A measurement of the transit time between the two positions of the probe beam yields the flow velocity of the medium.

Sell[7] has demonstrated the use of the PTD technique for flow-velocity measurements in an ethylene jet. In his method, however, the flow velocity is derived from a measurement of the *amplitude* of the PTD signal. Therefore, his method can easily be applied only to media that have uniform and constant concentrations of the absorbing species. This precludes the application of this technique to combustion media, in which large spatial and temporal variations in species concentrations may exist. In our technique the flow velocity is derived from the transit time of the heat pulse, which depends on the flow velocity alone (in the limit that the thermal diffusion can be neglected, a condition that generally prevailed in our experiments). While this work was in progress we learned of a similar technique used simultaneously and independently by Sontag *et al.*[8] for a measurement of flow velocity in an aerosol stream. This Letter, however, represents the first reported demonstration of the applicability to, and measurements in, a flame.

The technique demonstrated here has several important advantages over other techniques mentioned in the first paragraph. All the other techniques, with the exception of Raman techniques, rely on seeding the medium, either by a fluorescing species or by particles. Seeding may not always be possible in a practical combustion device, and there is a question whether the seeding alters the combustion parameters. Moreover, it is well known that particles sometimes lag behind the gas flow. Raman techniques require expensive instrumentation, and difficult phase-matching conditions must be met. All these techniques, with the exception of LEI, depend on Doppler shift, which makes their use at slow velocities difficult. PTD in this sense is complementary to the Doppler techniques, as it can measure slow velocities accurately, the ultimate lower limit being imposed by thermal-diffusion effects.[9] Again, the use of most of the above techniques in a combustion environment still remains

0146-9592/85/110532-03$2.00/0

to be demonstrated. Finally, the PTD technique has an additional advantage in that species concentration can be measured from the size of the signal and local temperature can be deduced from the diffusion constant.[10] Thus this technique has the potential of yielding species concentration, temperature, and the flow velocity simultaneously.

The experiment is shown schematically in Fig. 1. A laminar H_2/O_2 flame produced by a glassblowing torch was used for convenience. The OH radical produced in the combustion was excited by frequency-doubled radiation from a Chromatix CMX-4 flash-lamp-pumped dye laser. The laser was tuned to the $Q_2(5)$ line of OH at 309.2 nm, and it typically gave ~130 μJ of energy in a ~5.5-cm^{-1} bandwidth and a ~1-μsec-duration pulse. A 0.8-mW He–Ne laser provided the probe beam. The probe beam could be translated up or down to record the arrival time of the photothermal pulse at different heights above the pump beam. Deflection of the probe beam was monitored by a quadrant detector. The difference signal from two quadrants was amplified and fed to a LeCroy WD8256 transient digitizer. The digitized signal was transferred to a Commodore PET microcomputer for signal averaging, if necessary, and for data storage.

In order to check the reliability of results given by this technique, it was first applied to a gas jet where the flow velocity and its profile were well known. For this experiment, the torch was replaced by a 4.6-mm inside-diameter × 25-cm-long tube through which N_2 seeded with 500 parts in 10^6 of NO_2 passed. Seeding was necessary because N_2 does not have optical absorption in the dye-laser range. The dye laser was tuned to 490 nm, where NO_2 has high absorption. The insert in Fig. 2 shows PTD signals for three positions of the probe beam. The flow velocity was derived from the travel time of these signals. The signal shape can be understood easily, and it is simply the derivative of the spatial profile of the laser beam.[9]

Data similar to those shown in the insert were taken across the jet to determine the velocity profile shown in Fig 2. The X component of the velocity is plotted against the Y position in the jet. The data were taken 4 mm downstream from the nozzle. The experimental data were least-squares fitted to a theoretical curve,[11] $v(r) = v_0(1 - r^2/R^2)$, where v_0 is the velocity at the center of the jet and R is the radius of the jet. v_0 and R were treated as parameters, and the fitted value of v_0 = 4.1 m/sec is in excellent agreement with that derived from the measured flow rate of the gases F and the area of the nozzle A. The measured values of F and A were, respectively, 32.9 cm^3/sec and 0.16 cm^2, giving $v_0 = 2F/A$ = 4.0 m/sec. The fitted value of R was 2.5 mm, slightly larger than the inside diameter of the nozzle, owing to the expansion of the jet, as expected. With such excellent agreement between the theoretical and experimental value of the velocity and its profile, we have every confidence in the measurements made in a flame.

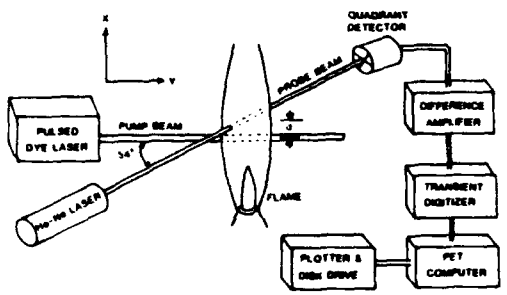

Fig. 1. Schematic illustration of the experimental arrangement. The pump and probe beams made an angle of 54° to provide good spatial resolution and were separated by a variable distance d in the vertical (X) direction.

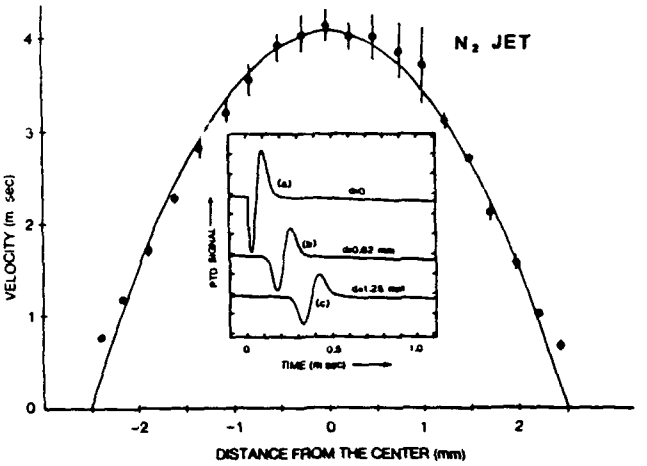

Fig. 2. Velocity profile of a jet measured by the PTD technique. The solid line is the theoretical fit to the experimental data points. The error bars represent one standard deviation of the mean of three runs. The two data points near the edge of the jet were not included in the fit, as they were affected by thermal diffusion. The insert shows the photothermal signal for three positions of the probe beam. Each curve represents an average of 50 shots. Signal averaging was not necessary, it was performed simply for convenience in data acquisition. Curve (a) corresponds to nearly overlapping probe and pump beams, and curves (b) and (c) represent successive displacements of the probe beam by 0.62 mm each. The asymmetric shape of the top curve is caused by thermal-diffusion effects.[9] Only curves (b) and (c) were used in the analysis.

A velocity profile, similar to that described above, was obtained for a H_2/O_2 torch by generating the PTD signals on OH, and it is shown in Fig 3. The velocity profile was measured 40 mm above the torch tip, which was ~30 mm above the inner cone of the flame. Since the diffusion constant increases with temperature, a small correction for diffusion effects was made to each data point in Fig. 3.[9] Surprisingly, the velocity profile in this flame fits a parabola very well, except near the center of the flame, as shown in the figure. It should be pointed out that there was considerable turbulence at the measurement points near the center of the flame (which was directly above the tip of the inner cone), which is also indicated by larger error bars on these points in Fig. 3. The least-squares-fitted values of v_0 and R were found to be 55.4 m/sec and 4.2 mm, respectively. The fitted value of R is in good agreement with that obtained by a visual observation of the flame.

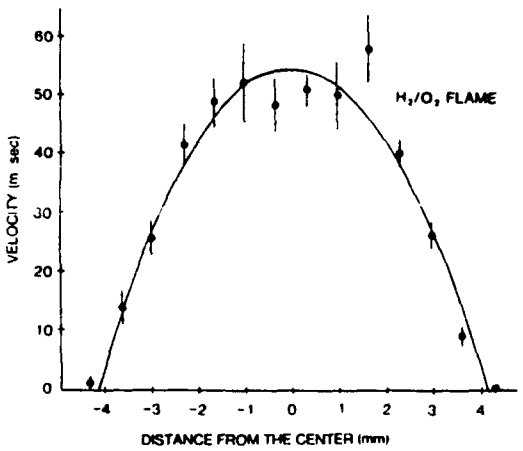

Fig. 3. Velocity profile of a laminar H_2/O_2 flame, 40 mm above the tip of the torch. The inside diameter of the tip was 2.5 mm, and it was operated with H_2 and O_2 flow rates of 98.6 and 49.2 cm^3/sec, respectively, representing an equivalence ratio of one. The experimental data fitted a parabolic curve quite well. The error bars represent one standard deviation of the mean of three runs.

The fitted value of v_0 is in good agreement with a value 55 m/sec, obtained by a simple-minded estimate based on the flow rates of H_2 and O_2, the area of cross section of the flame at the point of observation, and the temperature of the flame.

The spatial resolution in the transverse directions is given by the widths of the pump and probe beams (0.4 and 0.2 mm, respectively) and the angle between them (54°). The spatial resolution in the longitudinal direction is given by the distance between the two positions of the probe beam (0.3 mm). Thus the three-dimensional spatial resolution in our flame experiment was about 10^{-4} cm^3. Much higher spatial resolution can easily be achieved without any significant change in the signal-to-noise ratio. In principle, a high degree of temporal resolution, given by the transit time of the heat pulse between the two positions of the probe beam, can be achieved. Since this experiment was primarily a demonstration of the technique, and because different instrumentation would have been required, no attempt was made to obtain a high degree of temporal resolution. Temporal resolution, if desired, could be obtained in the following way: Instead of translating one probe beam up and down, two separate probe beams, a certain distance apart, would be used. Each beam would have its own detector, difference amplifier, and transient digitizer. The outputs of the transient digitizers would be fed to one computer, which would determine the transit time of the heat pulse between the two probe beams. The temporal resolution would be determined by this transit time, which in our flame experiment was ~5 μsec. This, of course, assumes that a sufficient signal-to-noise ratio can be obtained in a single shot. Sufficiently strong single-shot photothermal signals from OH can routinely be obtained with commercial dye lasers in hydrocarbon flames.[12] In principle one can even obtain an entire velocity profile (similar to that of Fig. 3) in a single shot with proper (and expensive) instrumentation. By using cylindrical diverging lenses, the probe beams can be expanded along the direction of the pump beam and deflections can be recorded by a diode array interfaced with a multichannel device. Time-resolved studies of turbulent flames by this technique would be particularly valuable.

In summary, we have demonstrated a new nonintrusive technique for flow-velocity measurements in a flame. A high degree of spatial resolution was achieved, and a high degree of temporal resolution can be achieved in a straightforward manner. The technique should also find use in many other areas.

This research was supported by the U. S. Air Force Wright Aeronautical Laboratories.

References

1. B. Miller and R. K. Hanson, Opt. Lett. **5**, 206 (1985).
2. S. Cheng, M. Zimmerman, and R. B. Miles, Appl. Phys. Lett. **43**, 143 (1983).
3. E. K. Gustafson, J. C. McDaniel, and R. L. Byer, IEEE J. Quantum Electron. **QE-17**, 2258 (1981).
4. M. Moosmüller, G. C. Herring, and C. Y. She, Opt. Lett. **9**, 536 (1984); C. Y. She, W. M. Fairbanks, Jr., and R. J. Exton, IEEE J. Quantum Electron. **QE-17**, 2 (1981).
5. P. K. Schenck, J. C. Travis, G. C. Turk, and T. C. O'Haver, Appl. Spectrosc. **36**, 168 (1982).
6. L. E. Drain, *The Laser Doppler Technique* (Wiley, New York, 1980).
7. J. A. Sell, Appl. Opt. **23**, 1586 (1984).
8. H. Sontag, I. Hussla, and A. C. Tam (preprint, IBM Research Laboratory, San Jose, Calif., 1985).
9. A more complete description, including the effects of thermal diffusion, will be given in a comprehensive article later.
10. A. Rose and R. Gupta, *Twentieth Symposium (International) on Combustion* (Combustion Institute, Pittsburgh, Pa.,1985).
11. See, for example, W. Kaufmann, *Fluid Mechanics* (McGraw-Hill, New York, 1963).
12. S. W. Kizirnis, R. J. Brecha, B. N. Ganguly, L. P. Goss, and R. Gupta, Appl. Opt. **23**, 3873 (1984), and yet unpublished results from our laboratory.

Reprinted from Applied Optics, Vol. 25, Page 3247, September 15, 1986

Measurements of very low gas flow velocities by photothermal deflection spectroscopy

Y.-X. Nie, K. Hane, and R. Gupta

A technique for measurement of gas flow velocity using photothermal deflection spectroscopy is described. This technique is especially suited for measurements of very low velocities. An extensive investigation of the technique has been carried out. This all-optical technique is nonintrusive and has high degrees of spatial and temporal resolution.

I. Introduction

There is extensive interest in the development of nonintrusive techniques for measurement of flow velocities. In many applications, these techniques are required to have high spatial and temporal resolution. Several nonintrusive techniques have recently been developed. For example, Cheng *et al.*[1] have used Doppler shift in laser-induced fluorescence to obtain flow-field measurements in a gas flow seeded with sodium vapor. Hiller and Hanson[2] have used I_2 seeding instead. Moosmüller *et al.*[3] and Gustafson *et al.*[4] have demonstrated the use of Raman techniques for flow velocity measurements in supersonic flows. Nevertheless, laser Doppler velocimetry[5] is the most widely used technique for flow measurements. In this method, the medium is seeded with small particles, and the velocity is derived from the Doppler shift in Mie scattering. However, seeding with particles may not be possible in many applications, making use of this technique impractical. All the above methods depend on Doppler shift measurements. Therefore, their use for measurements of low velocities is very difficult, if not impossible. Recently, application of photothermal deflection spectroscopy (PTDS) to flow velocity measurements has been demonstrated. Flow velocity measurement techniques based on PTDS are free from the objection cited above. Sell[6] has used the variation of the amplitude of the PTDS signal with the flow velocity of the medium to measure flow velocity in a jet of ethylene. In a recent paper,[7] Sell has used the change in shape of the PTDS signal to deduce the flow velocity in a jet of ethylene. Weimer and Dovichi,[8] on the other hand, have used the change in shape of the thermal lensing signal (thermal lensing is closely related to PTDS) to deduce flow velocity in a liquid flow. Sontag and Tam,[9] Rose and Gupta,[10] and Sell[7] have demonstrated a novel method for flow velocity measurements in gas flows using a measurement of the transit time of a photothermal pulse between two probe beam positions. Zharov and Amer[11] have used a similar method to measure flow velocity in liquids. The use of the transit time method for very low velocities in gases is difficult, however, due to broadening of the PTDS signal by thermal diffusion. In this paper, we demonstrate a new method based on PTDS for measurement of very low velocities when the transit time method becomes difficult to use. In this method the probe and pump beams are aligned so that the centers of the two beams coincide giving a null PTDS signal in a stationary medium (see below). In the presence of a flow, a nonzero signal is obtained whose magnitude is proportional to the flow velocity.

The basic principle of the PTDS technique is simple and can be explained with the aid of Fig. 1. A pulsed dye laser beam (hereafter referred to as the pump beam) passes through the medium of interest, and it is tuned to one of the absorption lines of the medium. The medium absorbs the optical energy from the pump beam, and, if the pressure is sufficiently high (i.e., if the quenching rates are sufficiently fast), most of this energy quickly appears in the rotational–translational modes of the medium. In a medium at atmospheric pressure, this condition is easily satisfied, and only a negligible fraction of the energy appears as fluorescence. The dye-laser-irradiated region thus gets slightly heated, leading to changes in the refractive index in that region. If the density of the absorbing molecules is uniform over the width of the dye laser beam, the refractive index acquires the same spatial profile as the dye-laser beam (e.g., a Gaussian profile if the dye laser is working in the TEM_{00} mode). Now, if another laser beam (called the probe beam) overlaps the pump beam, it is deflected due to changes in the

The authors are with University of Arkansas, Physics Department, Fayetteville, Arkansas 72701.

Received 14 April 1986.
0003-6935/86/183247-06$02.00/0.

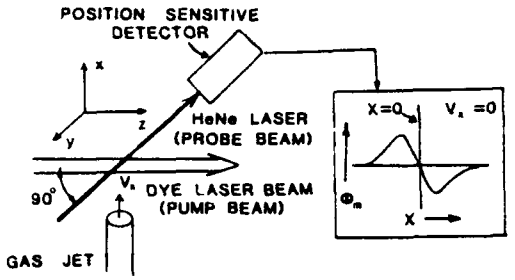

Fig. 1. Schematic illustration of a photothermal deflection experiment. A probe beam is deflected by the refractive-index change produced by the absorption of a dye laser in the medium. The inset shows the amplitude of the photothermal deflection signal in a stationary medium plotted against the distance between the pump and probe beams.

refractive index created by absorption of the pump beam. This deflection is easily measured by a position sensitive optical detector. If a pulsed dye laser is used, as that considered in this paper, a transient deflection of the probe beam is obtained. Consider first the behavior of the signal in a stationary medium. Assume that the pump beam has a Gaussian spatial profile and that the center-to-center distance between the pump and probe beams is x. If the magnitude (i.e., the peak value) of the probe deflection in a stationary medium ϕ_m is plotted against the position of the probe beam with respect to the pump beam x, a curve of the type shown in the inset in Fig. 1 is obtained. This curve is approximately proportional to the x-derivative of the spatial profile of the pump beam, because the deflection of the probe beam depends on the gradient of the refractive index. We note that the signal is zero at $x = 0$, i.e., when the centers of the two beams coincide. In the presence of a flow, however, the symmetry with respect to the center is destroyed, the curve shown in Fig. 1 is distorted, and a nonzero signal at $x = 0$ is obtained. Physically, of course, this is because heat is blown in the direction of the gas flow, and the gradient of the refractive index at $x = 0$ is no longer zero. The deflection signal at $x = 0$ is then directly proportional to the flow velocity. Since the pump and the probe beams overlap in this method, the peak of the PTDS signal (which is used to deduce the flow velocity) occurs shortly after the pump laser firing. Therefore, thermal diffusion effects are not as important as in the transit time method where the pump and probe beams are, by necessity, separated by a finite distance. This makes this method particularly suited for measurements of very low flow velocities. As a matter of fact, this method is complementary to the transit-time method because its sensitivity decreases for high velocities where the transit-time method is more suitable. High spatial and temporal resolution can be obtained by this method, just as they can be by the transit-time method. For the pump and probe beams crossing at 90° (as in Fig. 1), the spatial resolution of $\sim 10^{-5}$ cm^3, defined by the overlap volume of the two beams, can be obtained with mild focusing of the beams. If the spatial resolution is not important in a particular application, the angle between the pump and probe beams can be decreased, resulting in a larger interaction length and a correspondingly larger SNR. Temporal resolution is given by the duration of the PTDS signal, if the SNR is large enough to permit single-shot measurements. This is generally of the order of a few milliseconds. Single-shot measurements are possible in most applications due to the high sensitivity of the technique. In principle, the technique can also be applied with modulated cw pump beam, although temporal resolution is then lost. In this paper, however, we will only consider pulsed PTDS.

Our method can be thought of as a variant of Sell's technique.[6] We are, however, presenting a comprehensive treatment of the subject in which Sell's method becomes one special case (long pulse lengths and a restricted velocity range). For completeness, a brief account of the relevant theory will be given in Sec. II, the apparatus will be described in Sec. III, and the results and conclusion will be given in Sec. IV.

II. Theory

Rose *et al.*[12] have recently given the theory of PTDS in a flowing medium. We will not rederive their results here. However, for completeness, we will give below a very brief outline of the relevant theory. Deflection of a laser beam propagating in an inhomogeneous medium is given by the equation[13]

$$\frac{d}{ds}\left(n_0 \frac{d\mathbf{r}}{ds}\right) = \nabla_\perp n(x,y,z,t), \tag{1}$$

where s is the beam path, $\mathbf{r}$ is the perpendicular displacement of the beam, $n(x,y,z,t)$ is the (inhomogeneous) refractive index, and n_0 is the unperturbed refractive index of the medium. $\nabla_\perp$ designates the gradient in a direction perpendicular to the beam path. For our geometry (see Fig. 1) and small deflections, we may write the deflection angle $\phi(x,y,t)$ as

$$\phi(x,t) = \frac{1}{n_0}\frac{\partial n}{\partial T}\int \frac{\partial T(x,y,t)}{\partial x}\, dy. \tag{2}$$

The temperature distribution $T(x,y,t)$ is given by the solution of the partial differential equation

$$\frac{\partial T(x,y,t)}{\partial t} = D\nabla^2 T(x,y,t) - v_x \frac{\partial T(x,y,t)}{\partial x} + \frac{1}{\rho C_p} Q(x,y,t). \tag{3}$$

In Eq. (3), the first term on the right represents the effect of the thermal diffusion, D being the thermal diffusion constant of the medium. The second term represents the effect of the flow with v_x as the flow velocity assumed to be in the x direction. The last term represents the source term. ρ and C_p are the density and heat capacity of the medium, respectively, and $Q(x,y,t)$ is given by

$$Q(x,y,t) = \begin{cases} \dfrac{2\alpha E_0}{\pi a^2 t_0} \exp[-2(x^2+y^2)/a^2] & \text{for } 0 \le t \le t_0 \\ 0 & \text{for } t > t_0. \end{cases} \quad (4)$$

Here α is the absorption coefficient of the medium, and the medium is assumed to be weakly absorbing so that linear absorption can be considered a good approximation. E_0 is the energy in the dye laser pulse, t_0 is the pulse duration, and the dye laser is assumed to have a Gaussian spatial profile with $(1/e^2)$ radius a. The solution of Eq. (3) has been found by Rose *et al.*[12] to be

$$T(x,y,t) = \frac{2\alpha E_0}{\pi t_0 \rho C_p} \int_0^{t_0} \times \frac{\exp(-2|[x - v_x(t-\tau)]^2 + y^2|/|a^2 + 8D(t-\tau)|)}{|a^2 + 8D(t-\tau)|} d\tau. \quad (5)$$

The solution is valid for $t > t_0$. Substitution of Eq. (5) into Eq. (2) gives the final expression for the probe beam deflection,

$$\phi(x,t) = -\frac{1}{n_0}\frac{\partial n}{\partial T}\frac{8\alpha E_0}{\sqrt{2\pi} t_0 \rho C_p} \int_0^{t_0} \frac{[x - v_x(t-\tau)]}{[a^2 + 8D(t-\tau)]^{3/2}} \times \exp|-2[x - v_x(t-\tau)]^2/[a^2 + 8D(t-\tau)]| d\tau. \quad (6)$$

Sell[6] has numerically solved Eq. (3) by neglecting thermal diffusion effects ($D = 0$) and has presented the results graphically. It is worth pointing out that if D is set equal to zero in Eq. (5), one can write $\phi(x,t)$ in closed form as

$$\phi(x,t) = \frac{1}{n_0}\frac{\partial n}{\partial T}\frac{2\alpha E_0}{\sqrt{2\pi} t_0 \rho C_p a v_x} (\exp|-2[x - v_x(t-t_0)]^2/a^2| - \exp[-2(x - v_x t)^2/a^2]). \quad (7)$$

Equation (6) has been integrated using a standard International Mathematical and Statistical Library (IMSL) subroutine which uses the adaptive Romberg method. Figure 2 shows the prediction of Eq. (6). The peak value of the probe beam deflection $\phi_m(x)$ has been plotted as a function of the pump–probe distance x for $v_x = 0$, $v_x = 0.5$ m/s, and $v_x = 2.0$ m/s. Gas flow is along a positive x, that is, a positive value of x corresponds to a probe beam being downstream from the pump beam. For $v_x = 0$, as expected, the PTDS signal is zero at $x = 0$, and it is antisymmetric about $x = 0$. For larger values of v_x, we find that the symmetry of the curve about $x = 0$ is broken, as expected, and a nonzero deflection signal is obtained at $x = 0$. As a matter of fact, the signal at $x = 0$ rises monotonically with v_x. We also note that the curve in Fig. 2 splits in two branches for $v_x > 0$ and $x > 0$. This can be understood with the aid of Figs. 3 and 4. In Fig. 3, the probe beam deflection $\phi(t)$ has been plotted as a function of time for several different values of the velocity v_x. Figure 3(a) shows the curves for $x = 0$ while (b) shows similar curves for $x = a/2$. For $x = 0$, the signal is zero at $v_x = 0$ and increases monotonically with v_x as the flow blows the positive gradient of the heat pulse past the probe beam, as shown in Fig. 4(a). Now consider $x = a/2$ shown in Fig. 3(b). For $v_x = 0$ the

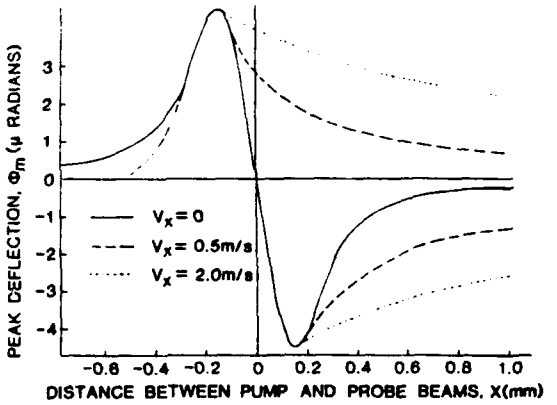

Fig. 2. Peak value of the probe beam deflection ϕ_m plotted as a fucntion of the pump–probe distance x for $v_x = 0$, $v_x = 0.5$ m/s, and $v_x = 2.0$ m/s. The pump laser was assumed to have a pulse length of 1 μs and a pulse energy equal to 1.4 mJ, and the radius of the pump beam was assumed to be 0.3 mm. The medium was assumed to be N_2 at atmospheric pressure with 1025-ppm NO_2 (absorption coefficient $\alpha = 0.39$ m^{-1}).

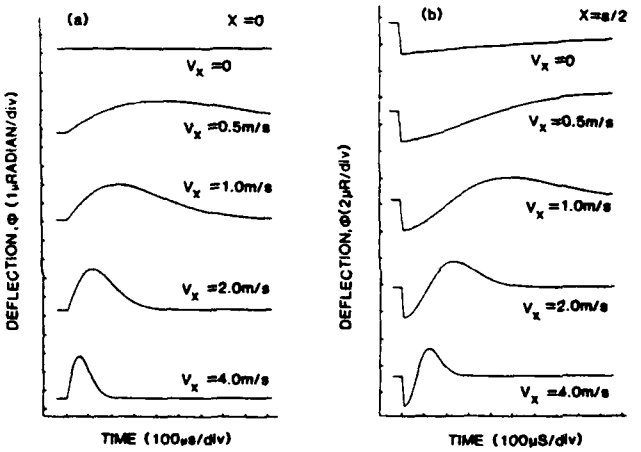

Fig. 3. Probe beam deflection $\phi(x,t)$ as a function of time for several different values of the velocity v_x: (a) is for $x = 0$, while (b) is for $x = a/2$. The pump beam radius a is assumed to be 0.46 mm. The pulse energy of the laser was 1.65 mJ, the pulse length was 1 μs, and the medium was assumed to be N_2 with 1025-ppm NO_2.

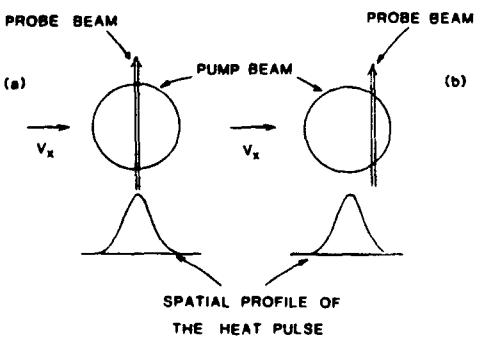

Fig. 4. Configuration of the pump and the probe beams for (a) $x = 0$ and (b) $x = a/2$.

probe beam suffers a deflection shortly after the dye-laser firing, and it returns to its original position on the time scale of the diffusion of heat out of the probe region. The deflection is negative because the probe beam experiences a negative gradient of the heat pulse as shown in Fig. 4(b). For $v_x > 0$, the negative gradient is blown out of the probe region by the gas flow, and a positive gradient is blown in [see Fig. 4(b)]. This results in a sharper negative deflection signal followed by a positive deflection signal. As the velocity increases, the deflection signals become narrower. The positive and negative branches of the signal in Fig. 2 for $v_x > 0$ and $x > 0$ correspond to the positive and negative peaks in Fig. 3(b), respectively.

Figure 5 shows the peak signal at $x = 0$, $\phi_m(0)$, as a function of v_x for several different laser pulse lengths t_0. For short laser pulses, $\phi_m(0)$ increases almost linearly with v_x at first and then seems to reach a saturation. Our technique is most valuable for low velocities, for example, $v_x < 1$ m/s. For longer pulse lengths and moderate velocities, even the qualitative behavior of these curves changes. It is interesting to point out that the qualitative behavior of these curves remains the same even for $x > 0$. However, the slope for low velocities is smaller resulting in a lower sensitivity for velocity measurements. This can be seen easily by an examination of Fig. 2. Sell[6] has carried out some experiments in a very restricted velocity range (1 m/s < v_x < 5 m/s) using a 0.2-ms pulse-length laser. Although he has not specified the distance between the probe and pump beams in this experiment, his result should still be in qualitative agreement with Fig. 5. In the restricted velocity range that he has taken his data, he finds that ϕ_m is proportional $1/v_x$ in agreement with Fig. 5. We wish to point out, however, that the inverse dependence of ϕ_m on v_x is not a general behavior, and it is restricted to a very small velocity range. As a matter of fact, one can see that the last point on the low-velocity side in Sell's data starts to deviate from $1/v_x$ dependence. ϕ_m depends on v_x in a rather complicated manner on the value of v_x and the laser pulse length. Even for a 1-ms laser pulse, ϕ_m shows a nearly linear dependence on v_x for low velocities, and $1/v_x$ dependence occurs in a very limited velocity range. In his recent paper,[7] Sell has extended the measurements to lower velocities when ϕ_m increases with velocity. However, it appears that Sell was not able to account for this behavior theoretically (Fig. 15 in Ref. 7).

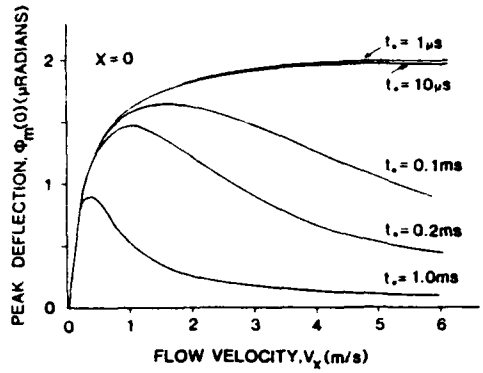

Fig. 5. Peak value of the probe beam deflection at $x = 0$, ϕ_m (0), plotted as a function of v_x for several different laser pulse lengths t_0.

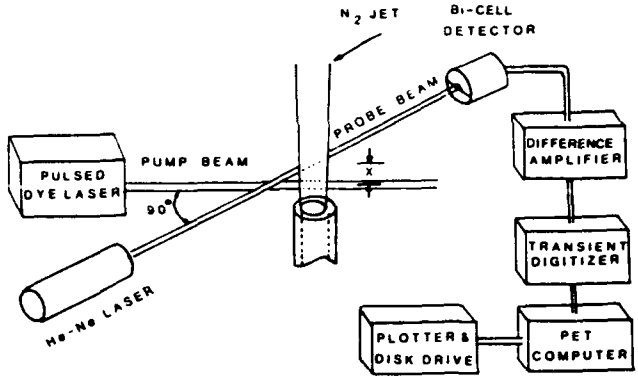

Fig. 6. Schematic illustration of the experimental arrangement.

III. Apparatus

Our experiment is shown schematically in Fig. 6. The pump beam is provided by a Chromatix CMX-4 flashlamp-pumped dye laser (1-μs duration pulses), and the probe beam is provided by a 0.8-mW He–Ne laser. The experiments are performed in an open jet of N_2 seeded with 1025-ppm NO_2. Seeding was necessary because N_2 does not have optical absorption in the dye laser spectral range. The dye laser was tuned to 490 nm, where NO_2 has a high absorption. A 4.6-mm i.d. × 25-cm long stainless steel tube was used to form a laminar flow of the gases. The tube was connected to a flowmeter, so that the flow velocity measured by PTDS could be compared with the value given by the flowmeter. The tube was mounted on a translation stage which could be moved along a direction perpendicular to the pump beam. In this way the velocity profile of the jet could be measured. The pump beam was focused by a 20-cm focal length lens at the center of the jet. The ($1/e^2$) radius of the pump beam at the focal spot was measured by the knife-edge method to be 0.3 mm.[14] The probe beam was also focused by a 15-cm focal length lens at the center of the jet. The ($1/e^2$) radius of probe beam was 0.1 mm at the focal spot. The focal spots of the two beams were coincident and intersected at right angles. To vary the probe–pump distance, a mirror mounted on a micrometer-driven translation stage was used to move the pump beam up and down. Moving the pump beam instead of the probe beam was purely a matter of convenience, only the relative motion of the two beams being important. The deflection of the probe beam was measured by a Bi-cell detector (Silicon Detector Corp. model SD 113-24-21) in conjunction with a difference amplifier. The probe beam was arranged on the Bi-cell detector so as to give a null signal in its quiescent position. At the instant of pump laser firing, the probe beam deflected, giving a transient signal at the difference amplifier.

The output of the difference amplifier was fed to a LeCroy WD 8256 transient digitizer for recording of the transient signal. The transient digitizer was interfaced to a Commodore PET microcomputer for signal averaging, if necesary, and data storage.

IV. Results

Figure 7 shows some of our experimental data. The photothermal deflection signals have been plotted as a function of time for overlapping pump and probe beams ($x = 0$) and for various values of the flow velocity. These curves are in excellent agreement with the theoretical curves shown in Fig. 3(a). In Fig. 8 we have plotted the peak values of the deflections $\phi_m(x)$ as a function of the probe–pump-beam distance. The solid curve correponds to $v_x = 0$, the dashed curve is for $v_x = 0.5$ m/s, and the dotted curve was taken for $v_x = 2$ m/s. Comparison with Fig. 2 shows that the general shape of these curves agrees very well with the theoretical predictions. For the $v_x = 0$ curve, the maximum values of $\phi_m(x)$ occur at $x = \pm a/2$. We find that in Fig. 8 the separation between the two peaks is somewhat larger than the pump-beam radius. This discrepancy is due to the nonzero width of the probe beam which has the effect of broadening the curves in Fig. 8[15] and due to the fact that the spatial profile of our pump beam is not a Gaussian.[12] (It has a significant amount of light in higher-order modes.) Comparison of the magnitudes in Figs. 8 and 2 shows that the experimental curves agree with the theoretical ones within ~25%. In view of the experimental uncertainties, this agreement is considered to be very good. These uncertainties include the uncertainty in the calibration (±5%) and reading (~±5% on low ranges) of the flowmeter, a pump-beam spatial profile which was not a Gaussian as assumed by the theory, uncertainties in the beam

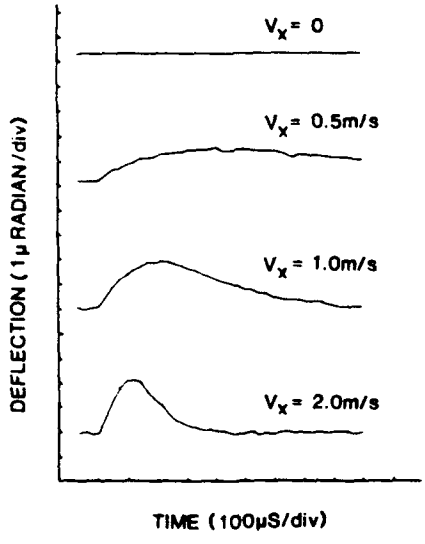

Fig. 7. Photothermal deflection signals plotted as a function of time for overlapping pump and probe beam ($x = 0$) for various values of the flow velocity. The pulse energy of pump laser was 1.65 mJ. Each curve is the result of averaging over 100 laser pulses.

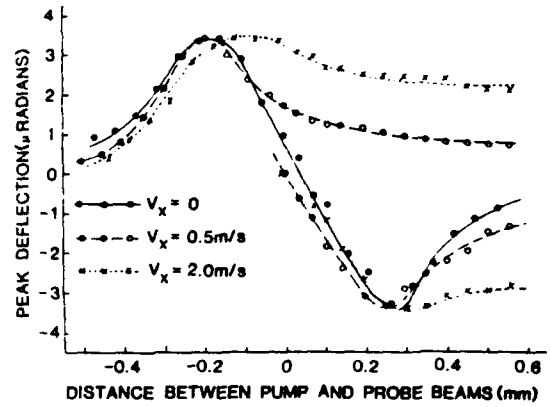

Fig. 8. Peak values of the deflections $\phi_m(x)$ plotted as a function of the probe–pump-beam distance x for $v_x = 0$, $v_x = 0.5$ m/s, and $v_x = 2$ m/s. The pulse energy of the pump laser was 1.4 mJ. Each point represents averaging over 100 pulses.

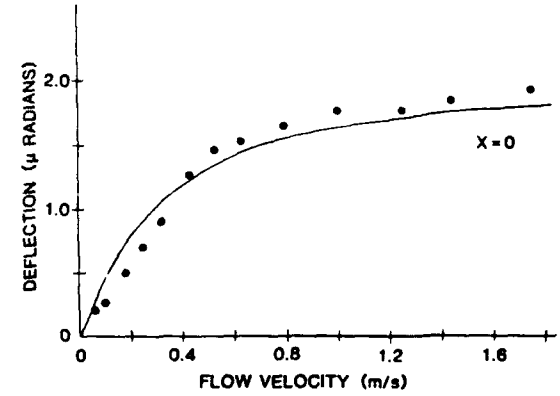

Fig. 9. Deflection signal for overlapping beams $\phi_m(0)$ plotted as a function of the flow velocity. Circles are the experimental data points, and the solid line is the theoretical curve. The pulse energy of pump laser was 0.65 mJ, the pulse length was 1 μs, and the radius of the pump beam was 0.3 mm. Each point was averaged over 100 laser pulses.

position measurements, and uncertainties in the calibration of the position sensitive detector. Better agreement between the theory and experiment can be obtained by minimizing these uncertainties.

Figure 9 shows the deflection signal for overlapping beams $\phi_m(0)$ as a function of the flow velocity. Circles are the experimental data points, while the solid line is the theoretical curve computed from the parameters given in the caption. The flow velocity was derived from the flow rate of the gases and the area of cross section of the jet. It should be emphasized that the solid curve in Fig. 9 is not a fit to the data; it is an absolute curve with no adjustable parameters.

We have also measured the velocity profile of our jet 3 mm above the nozzle, and it is shown in Fig. 10. Flow velocity, as measured by PTDS, is plotted against the position of the jet. Circles are in the experimental data points, while the solid line is the best fit to a curve given by[16]

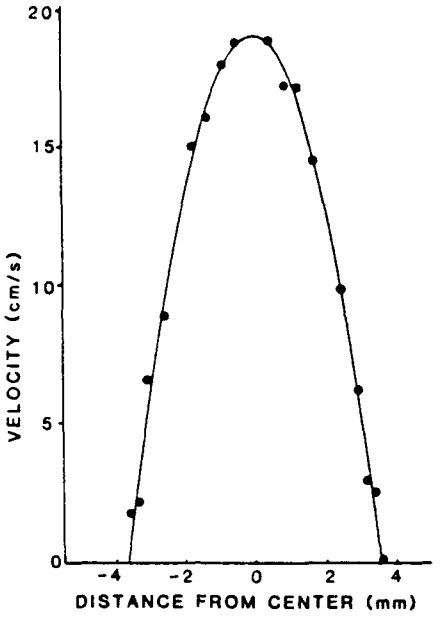

Fig. 10. Velocity profile of a laminar open jet, as measured by PTDS, plotted against the position of the jet. Circles are the experimental data points, and they are the result of averaging over 100 laser pulses. The solid line is the best fit.

$$v(r) = v_0(1 - r^2/R^2). \quad (8)$$

Here v_0 is the velocity at the center of the jet, and R is its radius. The experimental data points match exactly a parabolic velocity profile expected for a laminar flow. The fitted value of R is ~3.5 mm, larger than the inside radius (2.3 mm) of the nozzle, due to expansion of the jet, as expected.

In conclusion, we have shown that the photothermal deflection signal, where the centers of the pump and probe beams exactly coincide, can be used to measure very low gas flow velocities. In our experiments, velocities as low as a few mm/s could be measured. This technique is nonintrusive and has high degrees of spatial and temporal resolution.

We are grateful to A. Rose for assistance. This work was supported by U.S. Air Force Wright Aeronautical Laboratories. K. Hane, who is on leave from the Department of Electronic-Mechanical Engineering of Nagoya University, would like to acknowledge the financial support provided by the Ministry of Education, Culture, and Science of Japan. Y.-X. Nie is on leave from the Institute of Physics of the Chinese Academy of Sciences.

References

1. S. Cheng, M. Zimmermann, and R. B. Miles, "Supersonic-Nitrogen Flow-Field Measurements with the Resonant Doppler Velocimeter," Appl. Phys. Lett. **43**, 143 (1983).
2. B. Hiller and R. K. Hanson, "Two-Frequency Laser-Induced Fluorescence Technique for Rapid Velocity-Field Measurements in Gas Flows," Opt. Lett. **5**, 206 (1985).
3. H. Moosmuller, G. C. Herring, and C. Y. She, "Two-Component Velocity Measurements in a Supersonic Nitrogen Jet with Spatially Resolved Inverse Raman Spectroscopy," Opt. Lett. **9**, 536 (1984); C. Y. She, W. M. Fairbank, Jr., and R. J. Exton, "Measuring Molecular Flows with High-Resolution Stimulated Raman Spectroscopy," IEEE J. Quantum Electron. **QE-17**, 2 (1981).
4. E. K. Gustafson, J. C. McDaniel, and R. L. Byer, "CARS Measurement of Velocity in a Supersonic Jet," IEEE J. Quantum Electron. **QE-17**, 2258 (1981).
5. L. E. Drain, *The Laser Doppler Technique* (Wiley, New York, 1980).
6. J. A. Sell, "Quantitative Photothermal Deflection Spectroscopy in a Flowing Stream of Gas," Appl. Opt. **23**, 1586 (1984).
7. J. A. Sell, "Gas Velocity Measurements using Photothermal Deflection Spectroscopy," Appl. Opt. **24**, 3725 (1985).
8. W. A. Weimer and N. J. Dovichi, "Time-Resolved Crossed-Beam Thermal Lens Measurement as a Nonintrusive Probe of flow Velocity," Appl. Opt. **24**, 2981 (1985).
9. H. Sontag and A. C. Tam, "Time-Resolved Flow-Velocity and Concentration Measurements using a Traveling Thermal Lens," Opt. Lett. **10**, 436 (1985).
10. A. Rose and R. Gupta, "Application of Photothermal Deflection Technique to Flow-Velocity Measurements in a Flame," Opt. Lett. **10**, 532 (1985).
11. V. Zharov and N. M. Amer, "Pulsed Photothermal Deflection Spectroscopy in Flowing Media," in *Technical Digest, Fourth International Topical Meeting on Photoacoustic, Thermal and Related Science*, Ville D'Esterel, Quebec (1985).
12. A. Rose, R. Vyas, and R. Gupta, "Quantitative Investigation of Pulsed Photothermal Deflection Spectroscopy in a Flowing Medium," submitted to Appl. Opt.
13. M. V. Klein, *Optics* (Wiley, New York, 1970).
14. D. K. Cohen, B. Little, and F. S. Luecke, "Techniques for Measuring 1-μm Diam Gaussian Beams," Appl. Opt. **23**, 637 (1984).
15. A. Rose, Ph.D. Dissertation, U. Arkansas (1986).
16. W. Kaufmann, *Fluid Mechanics* (McGraw-Hill, New York, 1963).

Reprinted from Applied Optics, Vol. 25, Page 4626, December 15, 1986

Pulsed photothermal deflection spectroscopy in a flowing medium: a quantitative investigation

A. Rose, Reeta Vyas, and R. Gupta

A comprehensive investigation of pulsed photothermal deflection spectroscopy in a flowing medium has been carried out. A rigorous solution of the appropriate diffusion equation has been obtained, and experiments have been conducted to verify the theoretical predictions. Absolute measurements of the photothermal deflection were made and no adjustable parameters were used in the theory. Very good agreement between the theory and the experiment was obtained.

I. Introduction

Recently there has been extensive interest in the technique of photothermal deflection spectroscopy (PTDS). Since the initial work of Davis,[1] and of Boccara, Fournier, Amer and co-workers,[2-5] extensive new applications have been developed by Tam and co-workers[6-9] and by others.[10] Gupta and co-workers have demonstrated the usefulness of this technique for combustion diagnostics.[11-17] Motivated by this application, here we present results of a comprehensive and quantitative investigation of pulsed PTDS in a flowing medium.

The principle of the PTDS technique is quite simple: A dye laser beam (pump beam) passes through the medium of interest and is tuned to one of the absorption lines of the molecules that are to be detected. The molecules absorb optical energy from the laser beam and, if the pressure is sufficiently high (i.e., if the quenching rates are sufficiently fast compared to the radiative rates), most of the energy quickly appears in the rotational–translational modes of the medium. The dye laser irradiated region thus gets slightly heated, leading to changes in the refractive index of the medium in that region. If the density of the absorbing molecules is uniform over the width of the dye laser beam, the refractive index acquires the same spatial profile as the dye laser beam (e.g., a Gaussian profile if the dye laser is working in the TEM_{00} mode). Now if another laser beam (called the probe beam) overlaps the pump beam, it is deflected due to the changes in the refractive index created by the absorption of the pump beam. This deflection is easily measured by a position-sensitive optical detector. If a pulsed dye laser is used, a transient deflection of the probe beam is obtained. The deflection of the probe beam is proportional to the concentration of the absorbing molecules. Therefore the technique can be used to measure majority and minority species concentrations.[11-13] If the medium is flowing, the heat pulse produced by the absorption of the dye laser travels downstream with the medium. The heat pulse is, of course, accompanied by changes in the refractive index and can be measured by the deflection of a suitably placed probe beam. The flow velocity of the medium can be measured from a measurement of the transit time of the heat pulse between two probe beams downstream from the pump beam.[7,15,18,19] The heat pulse broadens due to thermal diffusion as it travels downstream. The thermal diffusion coefficient of the medium can be measured from the broadening of the signal which, in turn, yields the local temperature of the medium.[14,6] Therefore photothermal deflection spectroscopy is a valuable optical diagnostic technique for varied applications (combustion diagnostics is just one of the applications). Quantitative measurements of species concentrations, temperature, and velocity are more difficult, however, than one might assume from the above discussion. The PTDS signal in a flowing medium depends in a complicated manner on all three parameters (concentration, velocity, and temperature). For example, the amplitude of the signal depends not only on the concentration of the absorbing species but also on the temperature and the flow velocity. The width of the signal depends on both the temperature and the flow velocity. The measurement of the transit time is affected by the broadening due to thermal diffusion. Therefore, a good theoretical and experimental understanding of the size and shape of

The authors are with University of Arkansas, Physics Department, Fayetteville, Arkansas 72701.

Received 25 July 1986.
0003-6935/86/244626-18$02.00/0.

the PTDS signals in a flowing medium is essential for quantitative measurements. For this purpose the heat diffusion equation in a flowing medium must be solved. Although this equation has been solved for various special cases (for example, for a static medium,[5] for negligible thermal diffusion,[20] for very short laser pulses,[7] and for 1-D diffusion,[18]) a rigorous solution, to our knowledge, is not available. Moreover, some of these solutions have been obtained by numerical methods, with the results presented in graphic form. In this paper we present a general solution to this equation. The Green's function method has been used which permits the solution to be written down for any type of pump beam spatial profile which can be expressed analytically. Expressions for PTDS signals under various geometries of the pump and probe beams have been derived. Limits of the validity of approximate solutions have been determined by comparison with the exact solution. Absolute measurements of the photothermal deflection have been made (in well-defined conditions) and a comparison with theory has been done with no adjustable parameters. To our knowledge, these are the first such measurements of the pulsed PTDS signals. Several subtle effects that influence the size and shape of the signals have been found. The work presented here represents the most comprehensive investigation of the pulsed photothermal deflection spectroscopy in fluids to date. The theory is presented in Sec. II, the apparatus is described in Sec. III, the experimental results are given in Sec. IV, and conclusions are drawn in Sec. V.

II. Theory

Let us assume that the pump beam propagates through the medium in the z direction and the medium is flowing with velocity v_x in the x direction, as shown in Fig. 1. The pump beam is assumed to be centered at the origin of the coordinate system. We will consider three cases: Probe beam propagating in the y direction (transverse PTDS) as shown in Fig. 1(a), probe beam propagating in the z direction (collinear PTDS) as shown in Fig. 1(b), and the general case where the probe beam is in the y-z plane and makes an arbitrary angle θ with respect to the pump beam as shown in Fig. 1(c). We wish to derive an expression for the deflection angle $\phi(x,y,t)$ of the probe beam. Our first task (Sec. II.A) would be to determine the temperature distribution created by the absorption of the pump beam and its evolution under thermal diffusion and forced convection (i.e., flow). Deflection of the probe beam will be derived in Sec. II.B, and explicit cases of transverse PTDS, collinear PTDS, and the general case will be considered in Sec. II.C. Some special cases will be considered in Sec. II.D, and an approximate analytical solution will be given in Sec. II.E.

A. Temperature Distribution

The temperature distribution is given by the solution of the differential equation

$$\frac{\partial T(\mathbf{r},t)}{\partial t} = D\nabla^2 T(\mathbf{r},t) - v_x \frac{\partial T(\mathbf{r},t)}{\partial x} + \frac{1}{\rho C_p} Q(\mathbf{r},t), \qquad (1)$$

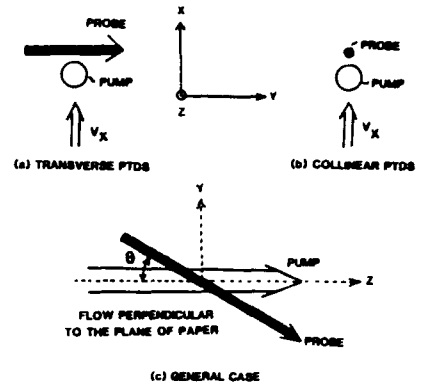

Fig. 1. Pump and probe beam configuration for (a) transverse PTDS, (b) collinear PTDS, and for the (c) general case. The gas flow is in the x direction, the pump beam propagates along the z axis, and the probe beam is in the y-z plane.

where $T(\mathbf{r},t)$ is the temperature above the ambient, D is the diffusivity, ρ is the density, and C_p is the specific heat at constant pressure of the medium. The first, second, and the third terms on the right in Eq. (1) represent, respectively, the effects of thermal diffusion, flow, and the heating due to pump beam absorption. If we assume that the medium is weakly absorbing, the heat produced per unit volume by the absorption of the laser energy is given by

$$Q(\mathbf{r},t) = \alpha I(\mathbf{r},t) = \begin{cases} \dfrac{2\alpha E_0}{\pi a^2 t_0} \exp(-2r^2/a^2) & \text{for } 0 \le t \le t_0, \\ 0 & \text{for } t > t_0. \end{cases} \qquad (2)$$

Here α is the absorption coefficient of the medium and $I(\mathbf{r},t)$ is the intensity of the pump laser beam. The total energy in each pulse is E_0. The spatial profile of the pump beam is assumed to be a Gaussian with $(1/e^2)$ radius a. It is further assumed that the laser pulse turns on sharply at $t = 0$ and turns off sharply at $t = t_0$. The Gaussian spatial profile was chosen because it is the most frequently used profile and because it closely corresponds to our experimental situation. Solutions for other types of spatial profiles can be found in an analogous manner. The assumption of a rectangular temporal profile is a good one, if the rise and fall times of the laser pulse are very short compared with the thermal diffusion time.

Equation (1) is essentially the equation of conservation of energy. For a general solution to the problem one must also consider the conservation of mass and momentum. It is, however, not necessary to consider the latter two if the effect of the pressure pulse[12,21] (photoacoustic effect) accompanying the photothermal signal is ignored. The pressure pulse occurs on a much shorter time scale than the thermal diffusion[12,21] and the energy carried off by the pressure pulse is negligible.[22] Therefore, we will neglect the effect of the pressure pulse on the photothermal signal and will not consider the conservation of mass and momentum here. All three equations will be considered in a forthcoming article on photoacoustic deflection spectroscopy.[23]

Equation (1) was solved in two dimensions, it being assumed that the effect of thermal diffusion along the z axis is negligible. This implies that any inhomogeneities in the medium along the pump beam are negligible. The following boundary conditions are assumed to hold:

$$T(x,y,t)|_{t=0} = 0, \quad T'(x,y,t)|_{t=0} = 0,$$
$$T(x,y,t)|_{x=\pm\infty} = 0, \quad T(x,y,t)|_{y=\pm\infty} = 0. \tag{3}$$

Here T' is the gradient of the temperature. We will use the Green's function method for a solution to Eq. (1). The solution is given by

$$T(x,y,t) = \int_{-\infty}^{+\infty}\int_{-\infty}^{+\infty}\int_{0}^{\infty} Q(\xi,\eta,\tau)G(x/\xi;y/\eta;t/\tau)d\xi d\eta d\tau, \tag{4}$$

where the functional form of $Q(\xi,\eta,\tau)$ is given by Eq. (2), and the Green's function satisfies the differential equation

$$-D\nabla_{xy}^2 G + v_x\frac{\partial G}{\partial x} + \frac{\partial G}{\partial t} = \frac{1}{\rho C_p}\delta(x-\xi)\delta(y-\eta)\delta(t-\tau), \tag{5}$$

with the following boundary conditions:

$$G(\pm\infty/\xi;y/\eta;t/\tau) = 0,$$
$$G(x/\xi;\pm\infty/\eta;t/\tau) = 0, \tag{6}$$
$$G(x/\xi;y/\eta;0/\tau) = 0.$$

The solution of Eq. (5) can be found conveniently by first Fourier transforming Eq. (5) from x,y space to ω_x,ω_y space:

$$(\omega_x^2+\omega_y^2)DG_F - i\omega_x v_x G_F + \frac{\partial G_F}{\partial t} = \frac{1}{2\pi\rho C_p} \times \exp[i(\omega_x\xi+\omega_y\eta)]\delta(t-\tau). \tag{7}$$

Here G_F is the Fourier transform of the Green's function. Equation (7) can be further simplified by taking its Laplace transform from t space to its complementary s space. The result is

$$(\omega_x^2+\omega_y^2)DG_{FL} - i\omega_x v_x G_{FL} + sG_{FL} = \frac{1}{2\pi\rho C_p}\exp[i(\omega_x\xi+\omega_y\eta)] \times \exp(-s\tau), \tag{8}$$

where G_{FL} is the Laplace transform of G_F. Equation (8) is simply an algebraic equation with the solution

$$G_{FL} = \frac{\exp(i\omega_x\xi)\exp(i\omega_y\eta)\exp(-s\tau)}{2\pi\rho C_p[D(\omega_x^2+\omega_y^2) - i\omega_x v_x + s]}. \tag{9}$$

G_F can now be obtained by taking the inverse Laplace transform of Eq. (9):

$$G_F = \frac{\exp(i\omega_x\xi)\exp(i\omega_y\eta)H_\tau(t)}{2\pi\rho C_p}\exp[[i\omega_x v_x - (\omega_x^2+\omega_y^2)D](t-\tau)]. \tag{10}$$

Here $H_\tau(t)$ is the unit step function (Heavyside function):

$$H_\tau(t) = \begin{cases} 0 \text{ for } 0 \le t < \tau, \\ 1 \text{ for } t \ge \tau. \end{cases} \tag{11}$$

The original Green's function is now obtained by taking the inverse Fourier transform of Eq. (10):

$$G = \frac{H_\tau(t)}{4\pi\rho C_p D(t-\tau)}\exp(-[x-[\xi+v_x(t-\tau)]]^2/4D(t-\tau)) \times \exp[-(y-\eta)^2/4D(t-\tau)]. \tag{12}$$

Substitution of Eq. (12) into Eq. (4) leads to the desired temperature distribution, $T(x,y,t)$, as a function of x, y, and t:

$$T(x,y,t) = \frac{2\alpha E_0}{\pi t_0\rho C_p}\int_0^{t_0}\frac{\exp(-2[[x-v_x(t-\tau)]^2+y^2]/[8D(t-\tau)+a^2])}{[8D(t-\tau)+a^2]}d\tau \quad \text{for } t > t_0. \tag{13}$$

Unfortunately, the analytical solution of Eq. (13) is not possible and the integration over τ must be performed numerically. In Fig. 2 we have plotted the spatial profile of the heat pulse, as predicted by Eq. (13), at several times after elapse of the laser pulse. Distance has been plotted in units of the $(1/e^2)$ radius of the pump beam. Equation (13) was integrated using a standard subroutine (called DCADRE) which used the adaptive Romberg method provided by IMSL (International Mathematical and Statistical Library). In Fig. 2 we note that the heat pulse moves downstream with the flow, and as it does, it broadens due to thermal diffusion. The heat pulse is Gaussian in shape initially, that is, it has the same spatial profile as that of the pump beam. At later times its shape does not seem to deviate significantly from a Guassian with larger radius and smaller amplitude.

For future reference, we write below the gradient of the temperature $\partial T/\partial x$ obtained by differentiating inside the integral:

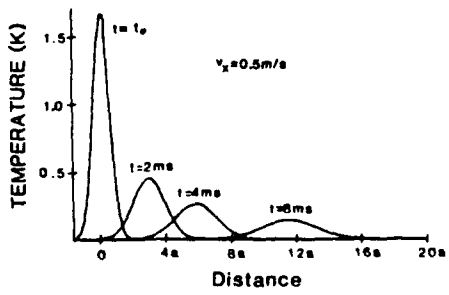

Fig. 2. Spatial profile of the heat pulse in a flowing gas at different times after the end of the excitation pulse. The medium was assumed to be N_2 at room temperature seeded with 1025 ppm of NO_2 (absorption coefficient $\alpha = 0.39\ m^{-1}$) and flowing with velocity $v_x = 0.5$ m/s. The pump laser was assumed to have an energy $E_0 = 1$ mJ in a pulse of $t_0 = 1$-μs duration. $(1/e^2)$ radius of the pump beam was 0.35 mm. For the values of all the other parameters, see Appendix A.

$$\frac{\partial T(x,y,t)}{\partial x} = -\frac{8\alpha E_0}{\pi t_0 \rho C_p}\int_0^{t_0}\frac{x - v_x(t-\tau)}{[8D(t-\tau)+a^2]^2} \times \exp(-2[x - v_x(t-\tau)]^2 + y^2]/[8D(t-\tau)+a^2])d\tau \quad \text{for } t > t_0. \tag{14}$$

B. Probe Beam Deflection

The propagation of an optical beam in an inhomogeneous medium is governed by the equation[24]

$$\frac{d}{ds}\left(n_0\frac{d\delta}{ds}\right) = \nabla_\perp n(\mathbf{r},t), \tag{15}$$

where s represents the beam path, δ is the perpendicular displacement of the beam from its original direction (see Fig. 3), and $\nabla_\perp n(\mathbf{r},t)$ is the gradient of the refractive index perpendicular to the beam path. The refractive index $n(\mathbf{r},t)$ is related to the unperturbed refractive index n_0 by

$$n(\mathbf{r},t) = n_0 + \left.\frac{\partial n}{\partial T}\right|_{T_A} T(\mathbf{r},t), \tag{16}$$

where T_A stands for the ambient temperature. Therefore,

$$\frac{d\delta}{ds} = \frac{1}{n_0}\frac{\partial n}{\partial T}\int_{\text{path}} \nabla_\perp T(\mathbf{r},t)ds, \tag{17}$$

where the integration is carried out over the path of the beam. In our geometry (Fig. 1), and for small deflections, we may simply write the deflection angle ϕ as

$$\phi(x,y,t) = \frac{1}{n_0}\frac{\partial n}{\partial T}\int_{\text{path}}\frac{\partial T(x,y,t)}{\partial x}\,ds. \tag{18}$$

Equation (14) may now be used in Eq. (18) to derive $\phi(x,y,t)$ explicitly.

C. Explicit Expressions for PTDS

1. *Transverse PTDS*

For the transverse PTDS shown in Fig. 1(a), Eq. (18) reduces to

$$\phi_T(x,t) = \frac{1}{n_0}\frac{\partial n}{\partial T}\int\frac{\partial T(x,y,t)}{\partial x}\,dy. \tag{19}$$

Using the explicit expression for $\partial T/\partial x$ from Eq. (14),

$$\phi_T(x,t) = -\frac{1}{n_0}\frac{\partial n}{\partial T}\frac{8\alpha E_0}{\pi t_0 \rho C_p}\int_0^{t_0} d\tau \times\left(\int_{-\infty}^{\infty}\exp[-2y^2/[8D(t-\tau)+a^2]]dy\right) \times\frac{x - v_x(t-\tau)}{[8D(t-\tau)+a^2]^2} \times \exp[-2[x - v_x(t-\tau)]^2/[8D(t-\tau)+a^2]]. \tag{20}$$

The integrand in the y integral vanishes outside an interaction length, which is of the order of $[a^2 + 8D(t-\tau)]^{1/2}$. It is therefore permissible to choose the limits as $\pm\infty$ on this integral. This integral can be solved analytically, with the result

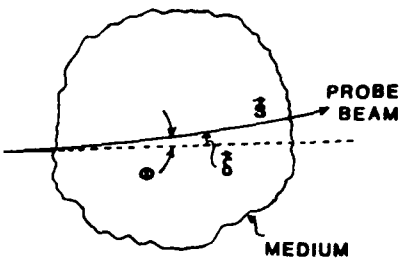

Fig. 3. Diagram showing the relationship between the probe beam path s, perpendicular displacement δ, and the deflection angle ϕ.

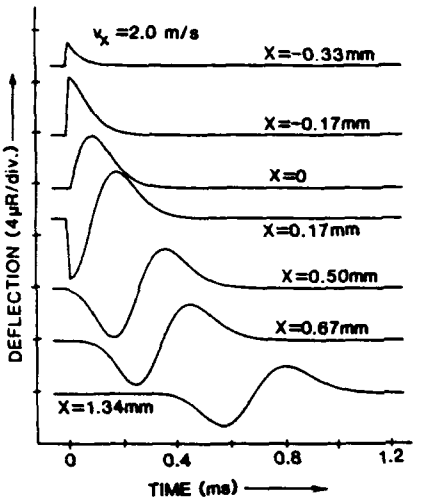

Fig. 4. Photothermal deflection signal shapes in a flowing medium for several different pump-to-probe beam distances. $x = 0$ corresponds to the case when the centers of the two beams coincide. Negative x corresponds to the probe beam being upstream from the pump beam and positive x corresponds to it being downstream. Flow velocity of the medium (N_2 seeded with 1025-ppm NO_2) was assumed to be 2.0 m/s. Laser pulse energy was assumed to be 1.65 mJ, beam radius a was 0.33 mm, and all the other parameters used in this computation are given in the caption for Fig. 2.

$$\phi_T(x,t) = -\frac{1}{n_0}\frac{\partial n}{\partial T}\frac{8\alpha E_0}{\sqrt{2\pi}t_0\rho C_p}\int_0^{t_0}\frac{[x - v_x(t-\tau)]}{[8D(t-\tau)+a^2]^{3/2}} \times \exp[-2[x - v_x(t-\tau)]^2/[8D(t-\tau)+a^2]]d\tau \quad \text{for } t > t_0. \tag{21}$$

Figure 4 shows some of the results predicted by Eq. (21). For this purpose, the integral in Eq. (21) was evaluated using the IMSL subroutine (DCADRE) used earlier to evaluate Eq. (13). In Fig. 4 photothermal deflection has been plotted as a function of time for different positions of the probe beam. x represents the center-to-center distance between the pump and the probe beams. A negative value of x corresponds to the probe beam being upstream from the pump beam while a positive value of x corresponds to the probe beam being downstream. We note that as the probe beam is moved upstream, the signal becomes smaller and narrower quickly because the heat has to diffuse against the gas flow. As the probe beam is moved downstream, the signal gets stronger at first and then

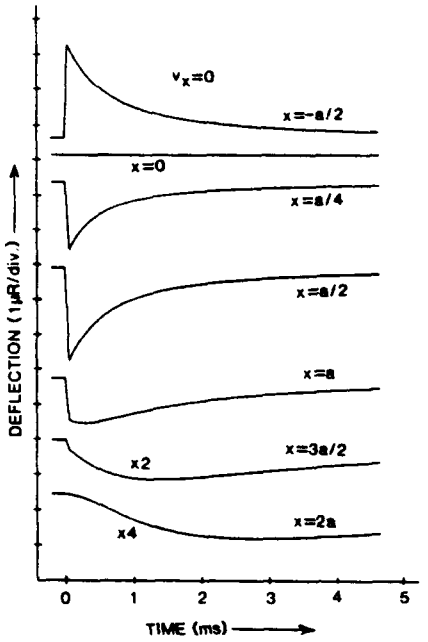

Fig. 5. Photothermal deflection signal in a stationary medium ($v_x = 0$) for several probe-to-pump beam distances as indicated above. Laser energy was assumed to be $E_0 = 1$ mJ and all the other parameters used in this calculation are the same as for Fig. 4. Two curves on the bottom have been expanded by the indicated factors for clarity.

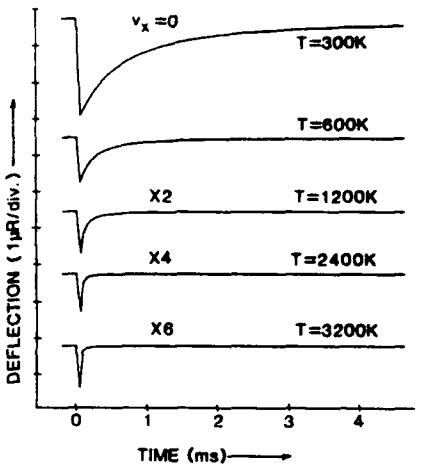

Fig. 6. Dependence of the photothermal deflection signal, in a stationary medium, on the temperature of the medium. In this calculation pump laser radius $a = 0.33$ mm, pump–probe distance $x = a/2$, pump energy $E_0 = 1$ mJ, pulse width $t_0 = 1$ μs, absorption coefficient $\alpha = 0.39$ m^{-1} (corresponding to 1025-ppm NO_2), and the diffusion coefficient D is assumed to vary as $T^{1.7}$ (see Appendix A for other parameters). Curves at elevated temperatures have been expanded by the indicated factors for clarity.

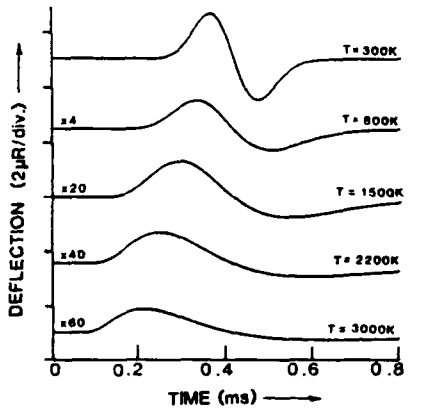

Fig. 7. Dependence of the photothermal deflection signal, in a flowing medium, on the temperature of the medium. Curves at elevated temperatures have been expanded by the factors indicated. The flow velocity of the medium was taken to be 4 m/s, and the probe–pump distance $x = 1.5$ mm. All the other parameters are the same as in Fig. 6.

acquires a shape which is essentially the derivative of the spatial profile of the pump beam (which is assumed to be a Gaussian here). This shape, of course, can be understood easily. As the heat pulse passes by, the probe beam at first experiences a positive gradient of the heat followed by a negative gradient. As x is increased further, the signal becomes broader and smaller due to thermal diffusion. Flow velocity of the medium can be measured in several different ways using these signals. The simplest method is based on the measurement of the time of flight of the heat pulse between two probe beam positions downstream from the pump beam[7,15,18,19] as mentioned earlier. One may also determine the flow velocity by fitting the shape of the PTDS signal.[18,25] Yet another way is to use amplitude of the signal which depends on the flow velocity.[20,26]

Figure 5 shows results similar to that of Fig. 4 but in a stationary medium ($v_x = 0$). In this case, the signal is zero for $x = 0$ because $\partial T/\partial x$ is zero at this point, and reverses sign as x changes sign, as expected. For small values of x ($0 < x < a$) the signal consists of a sharp deflection of the probe beam shortly after the pump laser firing, followed by a gradual return of the probe beam to its original position on the time scale of the diffusion time of the heat out of the probe region. The signal attains its maximum value for $x = a/2$ where the gradient of $T(x,y,t)$ is a maximum. For larger values of x, the peak of the signal occurs later in time, and the signal is broader and weaker, as expected.

Since one of our goals is the application of PTDS to flames, we have investigated the dependence of the signals on the temperature of the medium. Figure 6 shows the PTDS signals in a stationary medium for various temperatures up to 3200 K. In this calculation, the change in the absorption coefficient of NO_2 with temperature has not been taken into account. We note that the signal gets much narrower and weaker as the temperature increases. The diffusion constant has been assumed to increase as $T^{1.7}$ in these plots.[27] The signal gets narrower at elevated temperatures because the heat is able to diffuse through the probe beam much faster. Figure 7 shows similar curves for $v_x = 4$ m/s. We note that in this case the signal becomes weaker and broader as the temperature

increases. The increase in D with temperature manifests itself as broadening of the curves for $v_x \neq 0$ (for nonoverlapping beams) while it manifests itself as narrowing for $v_x = 0$. As the diffusion constant becomes large at elevated temperatures, the PTDS signal becomes more and more asymmetric (the second peak being much broader compared with the first) due to the variation in the thermal diffusion rate during the duration of the signal. The temperature dependence of the amplitude of PTDS signals is summarized in Fig. 8. The temperature dependence of these signals, in general, depends on both the values x and v_x in a complicated manner. However, for $x = a/2$ and $v_x = 0$, we find that the amplitude of PTDS signals can be fitted to a simple power law, $\phi_m \propto T^{-1.1}$ (not shown).

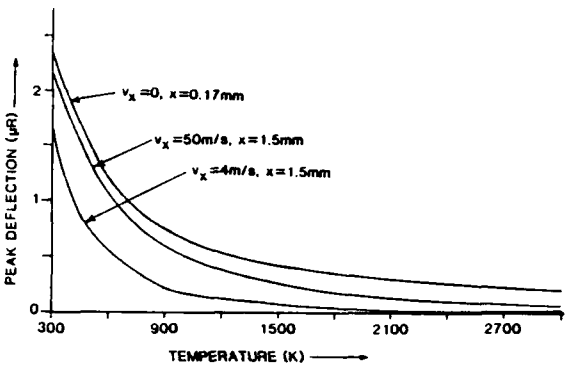

Fig. 8. Dependence of the amplitude of the photothermal deflection signal on temperature of the medium for a few representative values of the flow velocity, as indicated on the curves. In the case of $v_x \neq 0$, the amplitude of the larger peak (see Fig. 6) has been used. All the parameters used in this calculation were the same as in Figs. 6 and 7.

2. *Collinear PTDS*

Consider the collinear PTDS shown in Fig. 1(b) now. Equation (18) reduces to

$$\phi_L(x,y,t) = \frac{1}{n_0}\frac{\partial n}{\partial T}\int \frac{\partial T(x,y,t)}{\partial x}\,dz. \tag{22}$$

Substitution of $\partial T/\partial x$ from Eq. (14) leads to the final result,

$$\phi_L(x,y,t) = -\frac{l}{n_0}\frac{\partial n}{\partial T}\frac{8\alpha E_0}{\pi t_0 \rho C_p}\int_0^{t_0}\frac{|x - v_x(t-\tau)|}{|8D(t-\tau)+a^2|^2} \times \exp(-2[|x - v_x(t-\tau)|^2 + y^2]/[8D(t-\tau)+a^2])\,d\tau, \tag{23}$$

where l is the interaction length. If the probe and pump beams are aligned as shown in Fig. 1(b), y may be set equal to zero in Eq. (23). (Note that in all cases considered in this paper, the probe beam is assumed to be infinitesimally thin.) The signals predicted by Eq. (23) have the same general shape as those predicted by Eq. (21). However, the amplitude of the signals is larger than in the transverse case and it depends on the length of interaction between the probe and the pump beams l. Moreover, the width of the signal in a stationary medium is narrower than for transverse PTDS (see Fig. 10 in the next section). An examination of Figs. 1(a) and (b) shows the physical reasons for the difference in widths. In the case of collinear PTDS, the width of the pump beam in the y direction (for an infinitesimally thin probe beam) does not contribute significantly to the width of $\phi_L(t)$. However, in the case of transverse PTDS, the probe beam samples heat from different parts of the heat source in the y direction. Since it takes longer for the heat to diffuse out of the probe beam for $y \neq 0$ than for $y = 0$, the $\phi_T(t)$ signal is broader.

3. *General Case*

If the pump and the probe beams cross at an arbitrary angle as shown in Fig. 1(c), then

$$\phi(x,y,t) = \frac{1}{n_0}\frac{\partial n}{\partial T}\int \frac{\partial T(x,y,t)}{\partial x}\,(dy^2 + dz^2)^{1/2}, \tag{24}$$

where the path elements dy and dz are related by $dy = -dz\tan\theta$. Therefore Eq. (24) may be written as either

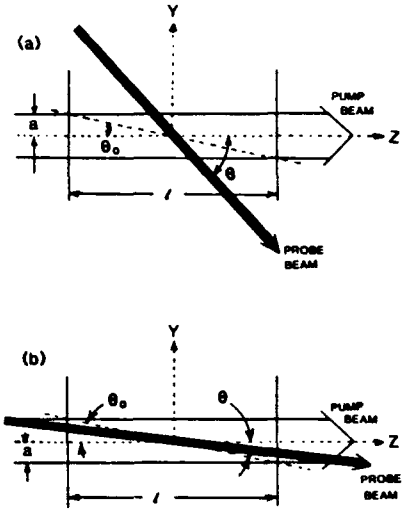

Fig. 9. Diagram showing the configuration of the probe and the pump beams for (a) $\theta > \theta_0$ and (b) $\theta < \theta_0$.

$$\phi(x,\theta,t) = \frac{1}{n_0}\frac{\partial n}{\partial T}\frac{1}{\sin\theta}\int_{-\frac{l}{2}\tan\theta}^{+\frac{l}{2}\tan\theta}\frac{\partial T(x,y,t)}{\partial x}\,dy, \tag{25}$$

or

$$\phi(x,\theta,t) = \frac{1}{n_0}\frac{\partial n}{\partial T}\frac{1}{\cos\theta}\int_{-\frac{l}{2}}^{\frac{l}{2}}\frac{\partial T(x,z\tan\theta,t)}{\partial x}\,dz, \tag{26}$$

where l is the length of the cell, as shown in Fig. 9. Both forms are equivalent. However, Eq. (25) becomes indeterminant for $\theta = 0$ and Eq. (26) becomes indeterminant for $\theta = \pi/2$. Therefore it is more convenient to use Eq. (25) for $\theta \lesssim 2\theta_0$ and to use Eq. (26) for $\theta \gtrsim 2\theta_0$, where the angle θ_0 is defined by

$$l\tan\theta_0 = 2(a^2 + 8Dt)^{1/2}, \tag{27}$$

as shown in Fig. 9. $(a^2 + 8Dt)^{1/2}$ is the diffusion broadened radius of the heat source, which, for convenience, is simply indicated by a in Fig. 9. $2\theta_0$, which corresponds to two times the $(1/e)^2$ radius of the heat source, has been arbitrarily chosen as a convenient

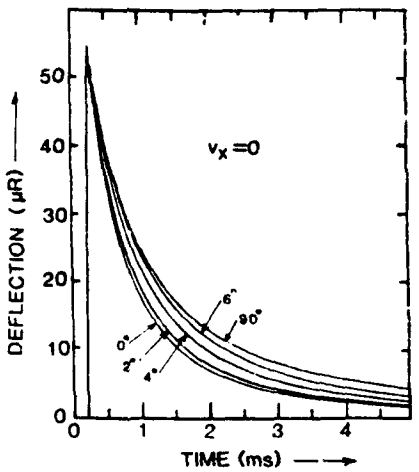

Fig. 10. Dependence of the photothermal deflection signal in a stationary medium on the angle between the pump and the probe beams. In this calculation the following values were used: $a = 0.35$ mm, $x = a/2$, $t_0 = 1$ μs, $l = 1$ cm, $\alpha = 0.39$ m^{-1}, and $T = 300$ K. To display the change in width clearly, the peak values of all the curves have been normalized to the $\theta = 0$ curve. The normalizing factors are 1.2 for $\theta = 2°$, 1.7 for $\theta = 4°$, 2.4 for $\theta = 6°$, and 22.8 for $\theta = 90°$

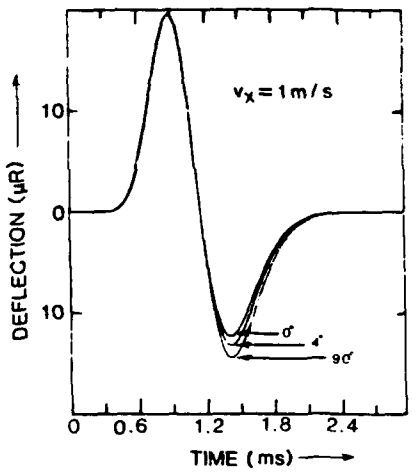

Fig. 11. Dependence of the photothermal deflection signal in a flowing medium on the angle between the probe and the pump beams. In this calculation the following values were used: $v_x = 1$ m/s, $a = 0.35$ mm, $x = 1.0$ mm, $t_0 = 1$ μs, $l = 1$ cm, $\alpha = 0.39$ m^{-1}, and $T = 300$ K. First peaks of all the curves have been normalized to the $\theta = 0$ value. The normalizing factors are 1.3 for $\theta = 4°$, and 16.3 for $\theta = 90°$.

boundary. For $\theta \gtrsim 2\theta_0$ the limits of integration in Eq. (25) may be replaced by $\pm\infty$, as explained in the discussion leading to Eq. (21). $\phi(x,\theta,t)$ may then be written explicitly using Eq. (14) as

$$\phi(x,\theta,t) = -\frac{1}{n_0}\frac{\partial n}{\partial T}\frac{8\alpha E_0}{\sqrt{2\pi t_0 \rho C_p}}\frac{1}{\sin\theta}\int_0^{t_0}\frac{|x - v_x(t-\tau)|}{|8D(t-\tau)+a^2|^{3/2}} \times \exp|-2|x - v_x(t-\tau)|^2/|8D(t-\tau)+a^2||d\tau \quad \text{for } 2\theta_0 \le \theta \le \pi/2 \text{ and } t > t_0, \quad (28)$$

$$\phi(x,\theta,t) = -\frac{1}{n_0}\frac{\partial n}{\partial T}\frac{8\alpha E_0}{\pi t_0 \rho C_p}\frac{1}{\cos\theta}\int_0^{t_0}\frac{|x - v_x(t-\tau)|}{|8D(t-\tau)+a^2|^2} \times \exp|-2|x - v_x(t-\tau)|^2/|8D(t-\tau)+a^2|| \times \left(\int_{-l/2}^{+l/2}\exp|-2z^2\tan^2\theta/|8D(t-\tau)+a^2||dz\right)d\tau \quad \text{for } 0 \le \theta \le 2\theta_0 \text{ and } t > t_0. \quad (29)$$

Figure 10 shows the PTDS signal for various values of θ for $v_x = 0$, $x = a/2$, and $\theta_0 = 4°$. The double integral in Eq. (29) was evaluated by using an IMSL subroutine DBLIN, which also utilizes the adaptive Romberg method. The collinear PTDS signal ($\theta = 0$) is much narrower than the transverse signal ($\theta = 90°$), as mentioned previously. As the angle θ is increased, the signal broadens rapidly at first, and then for $\theta \gtrsim 2\theta_0$ (8°) it attains its broadest width (which is the same as for $\theta = 90°$). In order that the widths of various curves be compared, their magnitudes have been normalized to the same value. Various normalizing factors have been given in the caption and they indicate the change in amplitude of the PTDS signal with angle. If the PTDS signals are to be used for temperature measurements, it is important that the dependence of these curves on θ be fully appreciated. While transverse PTDS is quite insensitive to the angle, a slight misalignment of the pump and probe beams in the case of collinear PTDS can lead to substantial errors. Collinear PTDS also broadens if the beams are misaligned in the y direction (i.e., if $y \neq 0$). Figure 11 shows curves similar to that of Fig. 10 but for $v_x \neq 0$. In this case $x = 3a$, and θ_0 is still 4°. All three curves have been normalized on the first peak, with the normalization factors given in the caption. In this case we find that the signal width is quite insensitive to the angle between the pump and the probe beams.

It should be noted that angle θ_0 in general is a very small angle. Therefore, in the range of validity of Eq. (29), $\theta \simeq 0$, and the z-integral [in Eq. (29)] may be set equal to l in applications where the width of the signal is not of primary importance (e.g., if the signal is not used to deduce the temperature of the medium). In this case we may summarize the results simply as

$$\phi(x,\theta,t) = \begin{cases}\phi_T/\sin\theta \text{ for } 2\theta_0 \le \theta \le \pi/2, \\ \phi_L/\cos\theta \text{ for } 0 \le \theta < \theta_0.\end{cases}$$

D. Special Cases

In the following we will consider some special cases where analytical integration of Eq. (14) is possible. As before, the solutions are valid only for $t > t_0$.

1. *PTDS Signal in the Absence of a Flow* ($v_x = 0$)

In this case Eq. (14) can be integrated [note that Eq. (13) still cannot be integrated] with the result:

$$\frac{\partial T(x,y,t)}{\partial x} = \frac{\alpha E_0 x}{2\pi t_0 \rho C_p D(x^2+y^2)} \times (\exp|-2(x^2+y^2)/|a^2+8D(t-t_0)|| - \exp|-2(x^2+y^2)/|a^2+8Dt||). \quad (30)$$

This result agrees with that of Jackson *et al.*[5] who solved the thermal diffusion equation for a stationary medium. Using Eqs. (19) and (22) we get explicit

expressions for transverse and collinear photothermal deflection signals, respectively,

$$\phi_T(x,t) = -\frac{1}{n_0}\left(\frac{\partial n}{\partial T}\right)\frac{\alpha E_0}{2t_0\rho C_p D}\left(\operatorname{erf}\left\{\left[\frac{2x^2}{a^2+8D(t-t_0)}\right]^{1/2}\right\} - \operatorname{erf}\left[\left(\frac{2x^2}{a^2+8Dt}\right)^{1/2}\right]\right). \quad (31)$$

$$\phi_L(x,y,t) = \frac{l}{n_0}\left(\frac{\partial n}{\partial T}\right)\frac{\alpha E_0 x}{2\pi t_0\rho C_p D(x^2+y^2)} \times \{\exp[-2(x^2+y^2)/[a^2+8D(t-t_0)]] - \exp[-2(x^2+y^2)/(a^2+8Dt)]\}. \quad (32)$$

The predictions of Eqs. (31) and (32) have already been shown in Figs. 5 and 10.

2. *PTD Signal in Flow Dominated Conditions*

If the flow velocity is very large and the PTDS signal is observed downstream from the pump beam on such a short time scale that no appreciable thermal diffusion takes place, we may set $D = 0$ in Eq. (14). This can then be integrated analytically, with the result:

$$\frac{\partial T(x,y,t)}{\partial x} = \frac{2\alpha E_0 \exp(-2y^2/a^2)}{\pi t_0\rho C_p a^2 v_x}\{\exp[-2[x-v_x(t-t_0)]^2/a^2] - \exp[-2(x-v_x t)^2/a^2]\}. \quad (33)$$

Sell[20] has considered the flow dominated situation previously. He was, however, not able to get an analytical solution and his numerical results were presented in a graphic form. Using Eq. (33) in Eqs. (19) and (22), we are, however, able to get explicit expressions for transverse and collinear PTDS signals, respectively, in closed form:

$$\phi_T(x,t) = \frac{1}{n_0}\left(\frac{\partial n}{\partial T}\right)\frac{2\alpha E_0}{\sqrt{2\pi}t_0\rho C_p a v_x}\{\exp[-2[x-v_x(t-t_0)]^2/a^2] - \exp[-2(x-v_x t)^2/a^2]\}, \quad (34)$$

$$\phi_L(x,y,t) = \frac{l}{n_0}\frac{\partial n}{\partial T}\frac{2\alpha E_0 \exp(-2y^2/a^2)}{\pi t_0\rho C_p a^2 v_x} \times \{\exp[-2[x-v_x(t-t_0)]^2/a^2] - \exp[-2(x-v_x t)^2/a^2]\}. \quad (35)$$

It should be noted that in gaseous media Eqs. (34) and (35) are valid only for very large flow velocities. These expressions are useful, however, in liquids where the diffusion rates are very low.

3. *PTDS Signals in the Impulse Approximation*

If the laser pulse duration t_0 is very short compared to the observation time t, the analytical solutions of Eqs. (13) and (14) are possible by simply recognizing that

$$\lim_{t_0 \to 0}\int_0^{t_0} f(\tau)d\tau = f(0)t_0.$$

This gives, for $T(x,y,t)$ and $\partial T(x,y,t)/\partial x$, respectively,

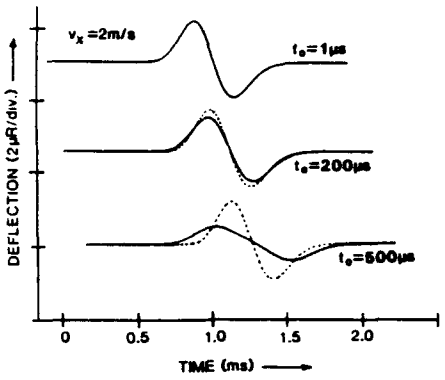

Fig. 12. Comparison of the results of the impulse approximation (dotted curve) with the exact results (solid curve) for three values of the laser pulse length t_0. When only one curve is shown, the two curves overlap. Parameters used in this calculation were $v_x = 2$ m/s, $a = 0.35$ mm, $x = 2$ mm, $\alpha = 0.39$ m^{-1}, and $T = 300$ K. Each dotted curve has been shifted to the right by $t_0/2$ to make the centers of the curves match.

$$T(x,y,t) = \frac{2\alpha E_0}{\pi\rho C_p(8Dt+a^2)} \times \exp\{-2[(x-v_x t)^2+y^2]/[a^2+8Dt]\}, \quad (36)$$

$$\frac{\partial T(x,y,t)}{\partial x} = -\frac{8\alpha E_0}{\pi\rho C_p}\frac{(x-v_x t)}{(a^2+8Dt)^2} \times \exp\{-2[(x-v_x t)^2+y^2]/(a^2+8Dt)\}. \quad (37)$$

This approximate solution is very useful because it shows very clearly the motion of the heat pulse in time (see Fig. 2). The heat pulse moves downstream with velocity v_x and has a Gaussian spatial profile of $(1/e^2)$ width $(a^2 + 8Dt)^{1/2}$, where $8Dt$ gives the broadening due to thermal diffusion. Sontag and Tam[28] recently derived Eqs. (36) and (37) by a phenomenological modification of the Jackson *et al.*[5] solution for a stationary medium. Weimer and Dovichi[25] also obtained a similar solution based on the results of Twarowski and Klinger.[29] It is easy to obtain explicit expressions for the transverse and collinear PTDS using Eqs. (19) and (22), respectively,

$$\phi_T(x,t) = -\frac{1}{n_0}\frac{\partial n}{\partial T}\frac{8\alpha E_0}{\sqrt{2\pi}\rho C_p}\frac{(x-v_x t)}{(8Dt+a^2)^{3/2}} \times \exp[-2(x-v_x t)^2/(a^2+8Dt)], \quad (38)$$

$$\phi_L(x,y,t) = -\frac{l}{n_0}\frac{\partial n}{\partial T}\frac{8\alpha E_0}{\pi\rho C_p}\frac{(x-v_x t)}{(8Dt+a^2)^2} \times \exp\{-2[(x-v_x t)^2+y^2]/(a^2+8Dt)\}. \quad (39)$$

Equations (38) and (39) are very useful expressions because they give the PTDS signals in closed form. One must, however, be aware of the limits of validity of the impulse approximation. Since the results of Sontag and Tam[28] are in widespread use, we have explored the limits of validity of these results and give some important conclusions below.

Figure 12 shows the dependence of the signal on the laser pulse length t_0. These signals were calculated for room temperature (300 K). The solid curves show the

results of the exact theory [Eq. (21)] while the dashed curves show the results of the impulse approximation [Eq. (38)]. The distance between the pump and the probe beams is $x = 2$ mm and the flow velocity is $v_x = 2$ m/s. We note that the agreement between the exact and the approximate results is good for short laser pulses and gets progressively worse for longer pulses, as expected. In all the curves plotted in Fig. 12, the approximate result has been shifted forward in time by $t_0/2$ to make the centers of the curves match. This fact must be kept in mind when using the impulse approximation for velocity measurements. We also note that the approximate results are narrower and larger in magnitude than the exact results. This result must be kept in mind if the approximate expression is to be used for species concentration or temperature measurements. The agreement between the approximate and the exact results, of course, improves as the distance x increases, making the observation time t larger compared to t_0. This result is shown in Fig. 13. The percent error in the magnitude of the signal is plotted against the observation time for various values of t_0. We note, for example, that, if the error is to be kept below 5%, then t/t_0 should be >5.

We have also investigated the dependence of the signals on the flow velocity, as shown in Fig. 14 for $T = 300$ K and $t_0 = 0.5$ ms. The approximate and exact results agree exactly for $v_x = 0$ and $t > t_0$ (the exact results are valid only for $t > t_0$). Note that the approximate results have been shifted by $t_0/2$ as in Fig. 12 to obtain the agreement. As the velocity increases, the agreement between the two results gets progressively worse. Note that in the bottom three curves t/t_0 is held constant (equal to 2) by increasing x as v_x increases. For $v_x t_0 \geq 2a$, the exact signal changes shape drastically, while the approximate signal maintains its shape. This is because a significant part of the heat is carried out of the pump beam-irradiated region by the flow even before the laser pulse is over. As such, the heat pulse spatial profile looks more like a top hat than a Gaussian. We have also investigated the dependence of these signals on temperature (not shown) and we find that, as the temperature increases, the agreement between the approximate and the exact results gets better. We conclude that overall the impact approximation works very well for laser pulse lengths $t_0 \leq 10\ \mu$s, but care must be exercised in its use for longer pulse lengths.

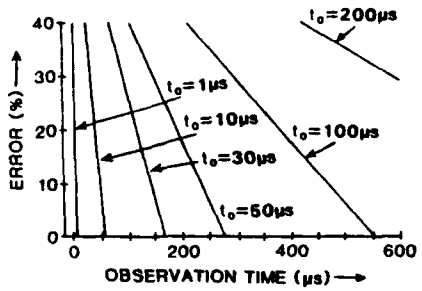

Fig. 13. Percent error in the peak value of the signal introduced by the use of impulse approximation as a function of the observation time of the signal for various values of the laser pulse lengths.

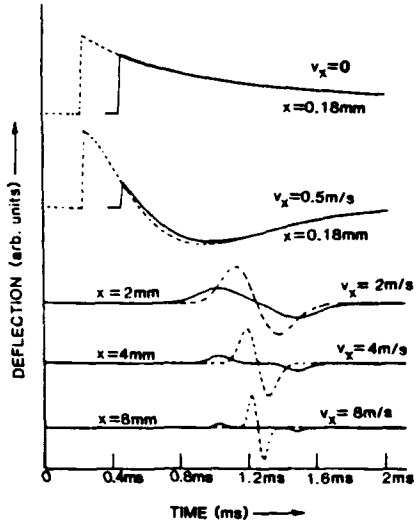

Fig. 14. Comparison of the results of the impulse approximation (dotted curves) with the exact results (solid curves) for different velocities. The dotted curves have been moved to the right by $t_0/2$, as in Fig. 12. In these curves $a = 0.35$ mm, $t_0 = 0.5$ ms, $\theta = 90°$, and $T = 300$ K were used.

E. Approximate Analytical Solution

The forms of Eqs. (30) and (33) suggest that an analytical expression of the following type may be a good approximation to the exact solution:

$$\frac{\partial T(x,y,t)}{\partial x} = \frac{2\alpha E_0}{\pi t_0 \rho C_p [4Dx + v_x a^2 + 4Dv_x(t-t_0)]} \times [\exp(-2[(x - v_x(t-t_0)]^2 + y^2]/[a^2 + 8D(t-t_0)]) - \exp[-2[(x - v_x t)^2 + y^2]/(a^2 + 8Dt)]]. \quad (40)$$

Note that Eq. (40) is simply a conjectured expression that reduces to the exact solutions in the extreme limits, $v_x = 0$ and $D = 0$ [Eqs. (30) and (33), respectively]. Using Eq. (40) we may write down the explicit expressions for the transverse and collinear PTDS signals:

$$\phi_T(x,t) = \frac{l}{n_0}\frac{\partial n}{\partial T}\frac{2\alpha E_0}{\sqrt{2\pi} t_0 \rho C_p [4Dx + v_x a^2 + 4Dv_x(t-t_0)]} \times ([a^2 + 8D(t-t_0)]^{1/2} \times \exp(-2[(x - v_x(t-t_0)]^2/[a^2 + 8D(t-t_0)]) - (a^2 + 8Dt)^{1/2}\exp[-2[(x - v_x t)^2]/(a^2 + 8Dt)]), \quad (41)$$

$$\phi_L(x,y,t) = \frac{l}{n_0}\frac{\partial n}{\partial T}\frac{2\alpha E_0}{\pi t_0 \rho C_p [4Dx + v_x a^2 + 4Dv_x(t-t_0)]} \times (\exp(-2[(x - v_x(t-t_0)]^2 + y^2]/[a^2 + 8D(t-t_0)]) - \exp[-2[(x - v_x t)^2 + y^2]/(a^2 + 8Dt)]). \quad (42)$$

We have explored the limits of validity of Eqs. (41) and (42) by comparing the results given by these equations with the exact results, while these equations reduce to the exact equations in the limits of very low and very high velocities [Eqs. (30) and (33), respectively],

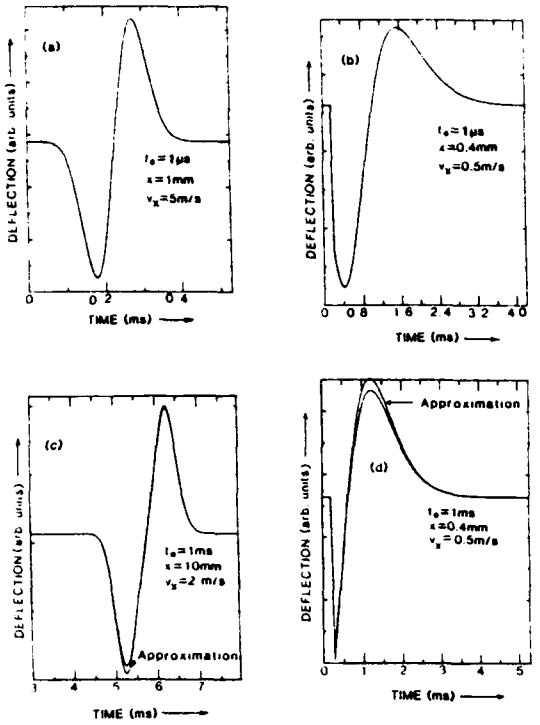

Fig. 15. Comparison of the results of the approximate analytical formula with the exact results for intermediate values of velocity at $T = 3000$ K. In these curves $\theta = 0$ (collinear PTDS), $t_0 = 1$ μs for (a) and (b), and $t_0 = 1$ ms for (c) and (d). Other parameters are given in the diagram. When a single curve is shown, approximate and exact results coincide.

the intermediate velocity range needed to be explored. We find that these equations have a much larger range of validity than the impulse approximation solutions of Sontag and Tam[28] and that of Weimer and Dovichi.[25] We find that at room temperature this expression gives perfect agreement with the exact solution for short laser pulses, for the entire range of v_x and x that we have tried. Two examples are shown in Figs. 15(a) and (b). These curves have been plotted for the collinear case [Eq. (42)] for $t_0 = 1$ μs. Values of v_x and x are given in the diagram. The exact and the approximate solutions lie on top of each other within the widths of the lines. The difference between the two becomes noticeable only when t_0 becomes large. Two cases are shown in Figs. 15(c) and (d) for $t_0 = 1$ ms. Again, the two solutions agree exactly for $v_x = 0$ and for $v_x \gg (Dx)/a^2$ (in our case $v_x > 5$ m/s gives almost perfect agreement). The cases shown in Figs. 15(c) and (d) represent the worst agreement cases, i.e., long pulse and intermediate value of velocity. Similar excellent agreement is obtained for the transverse PTDS. At very high temperatures (3000 K), intermediate velocities (i.e., the worst case), and short pulses the agreement between the exact and the approximate expressions is still perfect for collinear PTDS while it is little worse for transverse PTDS as shown in Fig. 16 for $v_x = 4$ m/s. The agreement, of course, gets better as v_x is increased, because then v_x gets closer to $(Dx)/a^2$. For long pulses (1 ms) the agreement is somewhat worse than that shown here for $t_0 = 1$ μs.

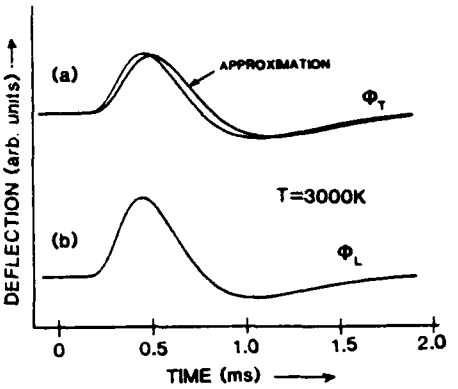

Fig. 16. Comparison of the results of the approximate analytical formula with the exact results for $T = 3000$ K. The parameters used in this calculation were $v_x = 4$ m/s, $t_0 = 1$ μs, $a = 0.35$ mm, and $x = 3.0$ mm. Curves (a) are for transverse PTDS and curves (b) are for collinear PTDS. Two curves in (b) overlap completely.

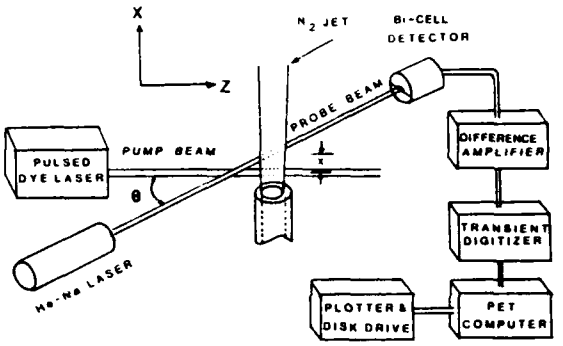

Fig. 17. Schematic illustration of the apparatus. Optical elements (mirrors, lenses, etc.) have been omitted for clarity.

Overall, we conclude that the approximate analytical formula gives excellent agreement with the exact results for a vast range of parameters t_0, x, v_x, and T. In particular, this formula gives good results even for long laser pulse lengths (e.g., $t_0 = 1$ ms and longer) where the impulse approximation breaks down.

III. Apparatus

Our experimental arrangement is shown schematically in Fig. 17. The pump beam was provided by a Chromatix CMX-4 flashlamp pumped dye laser. This laser typically gave 2 mJ of energy in an ~1-μs long pulse. For this experiment, the laser was operated without an etalon and had a bandwidth of ~3 cm^{-1}. A Uniphase 0.8-mW He–Ne laser provided the probe beam. An open jet of N_2 gas was used for the medium. Laminar flow was produced by passing the gas through a 25-cm long path in a 6.2-mm o.d. × 4.6-mm i.d. stainless steel tube. The flow rate of the gas through the tube could be measured by a flowmeter. Since N_2 does not have optical absorption in the dye laser spectral range, it was seeded with 1025-ppm NO_2 which has good optical absorption throughout the visible region. In some of our experiments, a stationary medium was required. In this case, a glass cell of square cross section (1 cm on the side and 4 cm long) was substitut-

ed for the open jet. The cell was filled with atmospheric pressure of N_2 seeded with 1025-ppm NO_2. The dye laser was tuned to 490 nm where NO_2 has a high optical absorption. The deflection of the probe beam was measured by a silicon bicell (Silicon Detector Corp. model SD-113-24-21-021). The difference signal from two halves of the bicell was measured. The probe beam was arranged to produce a null signal at the detector in its quiescent position. Shortly after the firing of the pump laser, the probe beam suffered a transient deflection which was recorded as a difference signal from the bicell. The output of the bicell was amplified (amplifier bandwidth ~2 MHz) and fed to a LeCroy WD8256 transient digitizer. The digitizer was interfaced to a Commodore PET microcomputer for signal averaging, if needed, and for data storage.

The optical elements in the probe and the pump beam paths are not shown in Fig. 17 for clarity. Both beams were focused in the interaction region using lenses. The pump beam was generally focused using a 20-cm focal length lens while the probe beam was focused by a 15-cm focal length lens. No other lenses were used anywhere in the beam paths. The pump and probe beam spot sizes were measured at the focal point using the knife-edge technique.[30] The $1/e^2$ radius of the probe beam at its focal point was ~0.1 mm. The pump beam at its focal point was found to have different dimensions in two orthogonal directions. The $1/e^2$ radii in two orthogonal directions were a few tenths of a millimeter and the exact values are given in the next section. Further comments on the spatial profile of the pump beam will be made in the next section.

Several mirrors were used to steer the beams. For transverse PTDS, the pump and probe beams made an angle of 90° as shown in the figure. For collinear PTDS, a dielectric mirror with 99% reflectivity at 490 nm (45° angle of incidence) and 90% transmission at 633 nm was used to combine the two beams. Other arbitrary angles between the two beams could also be obtained by proper arrangement of mirrors. The distance between the interaction region and the bicell detector (the lever arm of the probe beam) was ~1 m, giving a probe beam spot size of ~1 cm at the detector. For many of our investigations, the distance x between the pump and the probe beams needed to be variable. For this purpose, the probe beam was left unchanged while the pump beam was moved using a mirror mounted on a translation stage. Care was exercised to move the focusing lens with the pump beam, so that the pump beam always passed through the same part of the lens. All position measurements (i.e., measurements of x) were made with reference to the $x = 0$ position, which was determined from the disappearance of the PTDS signal in a stationary medium.

The bicell detector output (volts) was calibrated to yield absolute value of the deflection (radians) in the following way: Deflection of the probe beam at the interaction region results in the displacement of the probe beam spot on the detector. Leaving the probe beam undisturbed, the detector was moved (only the relative displacement of the two being important) in a direction in which the probe beam would normally move using a precision translation stage. Change in the output voltage for a given displacement was noted. The angular displacement of the probe beam is simply the lateral displacement at the detector divided by the lever arm (distance between the interaction region and the detector). The output of the detector was thus calibrated to yield the deflection angle directly. The calibration factor was found to be very sensitive to the precise position of the probe beam spot on the detector. Therefore a new calibration factor was obtained for each experimental run. Based on the observed statistical deviation, our calibration accuracy is believed to be within ±10%. A typical signal of 2 μR generally gave a voltage output at the difference amplifier (with amplifier gain of 5) of ~50 mV.

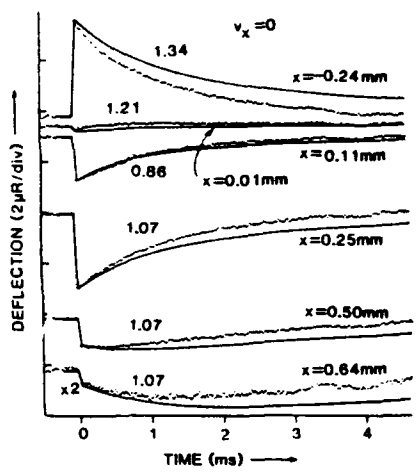

Fig. 18. Photothermal deflection signals for transverse geometry in a stationary medium (closed cell) for various pump-to-probe distances. Dots represent the experimental signals and they have been plotted on an absolute scale except the bottom curve which has been expanded by a factor of 2 for clarity. Solid lines are the theoretical curves computed from Eq. (21) using the parameters in the text. Theoretical curves have been multiplied by the scaling factors given on each curve to facilitate accurate comparison of the shapes of the theoretical and experimental curves. The scaling factors themselves indicate the degree of agreement between theory and experiment for the amplitude of the signals.

IV. Experimental Results

Experiments performed to verify the results of the theoretical model described in Sec. II are described below. The experimental results have been compared with the theoretical results without using any adjustable parameter. Results obtained in a stationary medium will be described first, followed by those obtained in a flowing medium.

A. Results in a Stationary Medium

Figure 18 shows the photothermal deflection signal in a stationary medium (i.e., in a cell) for different values of the distance between the pump and the probe beams. $x = 0$, which corresponds to the centers of the pump and the probe beams being coincident, was de-

termined from the disappearance of the PTDS signal. These data were taken for the transverse geometry ($\theta = 90°$). The solid lines are the theoretical curves while the dots are the experimental points. The experimental results in this figure and in all subsequent figures represent signal averaging over 100 laser shots. Signal averaging was not necessary to observe the signal, it was performed simply to average out the pulse-to-pulse fluctuations in the laser energy. Since the object of this experiment was not to demonstrate the sensitivity of the technique, no attempt was made to optimize the signal-to-noise ratio. Theoretical curves have been calculated using Eq. (21), and no adjustable parameters were used in the theory. All parameters needed were either obtained from tables or were measured. In this calculation we used $v_x = 0$, $a = 0.46$ mm as measured by the knife-edge technique,[30] $t_0 = 1$ μs as measured by a PIN diode, $E_0 = 2$ mJ as measured by a Scientech power/energy meter, and all the other parameters (e.g., $\alpha, D, \rho, C_p, n_0, \partial n/\partial T$) were obtained from the literature and are given in Appendix A. For ease of comparison of signal shapes the theoretical curves in Fig. 18 have been scaled by the factors indicated on each curve to match the experimental curves at $t = t_0$ (which corresponds to the peak of the signal for small values of x). The experimental curves have been plotted on an absolute scale.

First, we note in Fig. 18 that the experimental signal in general agrees quite well with the theory. The probe beam suffers a transient deflection shortly after pump laser firing and returns to its original position on the time scale of thermal diffusion time. The signal vanishes at $x = 0$, reverses sign as one goes from negative x to positive x, and it gets weaker and broader for larger x. Moreover, amplitude of the observed signal agrees quite well with the theoretical predictions (the scaling factors noted on the curves give the degree of agreement between theory and experiment), considering the uncertainties involved (see details below). We note, however, that the widths of the experimental curves are considerably narrower than the theoretical curves. We have made a very careful investigation, both theoretical and experimental, to pinpoint the cause of this anomaly. On the experimental side, we have repeated the experiment numerous times over a six-month period with different mirror and lens configuration (in the pump and the probe beams) each time. Although sometimes a much better agreement between the theory and the experiment than that shown in Fig. 18 was obtained, in general the experimental width remained narrower than the theoretical one. These experiments were also conducted for collinear beams and for arbitrary angles between the pump and the probe beams, and essentially the same conclusions were reached as in the case of transverse PTDS. A thorough investigation of the instrumental effects was also carried out, e.g., the time-scale calibration of the transient digitizer, bandwidth limitations in the difference amplifier. No instrumental effect could be identified which would account for an artificial narrowing of the experimental signals. On the theoretical side, there are only two parameters, the pump beam radius a and the diffusion constant D, which affect the width of the signal in a significant way. To investigate the effect of the uncertainties in the knowledge of these parameters, we plotted the theoretical curves for different values of D and a. We found that D would have to increase by a factor of 2, or a would have to decrease by a factor of 2 to account for the observed width. Both of these possibilities were considered to be well outside of the uncertainties in D and a. From the available literature (see Appendix A for references) we conclude that D is known to within ±5% at room temperature for N_2 gas. The pump beam radius was measured by the knife-edge technique, and it was in complete agreement with that determined independently using the amplitude of the photothermal signal itself (see Appendix C). During the investigation of the beamwidth, we discovered that the $1/e^2$ radius of our pump beam was different in two orthogonal directions (the radius was 0.46 mm in the x direction while it was 0.14 mm in the y direction). This difference also varied somewhat depending on the particular mirror configuration used to manipulate the beam. It is an easy matter to calculate the signal shapes for a beam of elliptical cross section, as shown in Appendix B. In this calculation, the $1/e^2$ radius in the direction of the probe beam displacement (x direction) is assumed to be a, while that in the orthogonal direction (y direction) is assumed to be b. Surprisingly, we find (Appendix B) that for transverse PTDS the signal shape and width are identical to that for a beam of circular cross section of radius a. However, for collinear PTDS, the signal width is narrower for an elliptical beam with $b < a$ (as was true in our case) than for a circular beam of radius a. Since the data presented in Fig. 18 are for transverse geometry, elliptical cross section of the beam cannot be a reason for narrow widths of the observed signals. After eliminating all other possibilities we have concluded that the reason for the disagreement between the widths of the theoretical and the experimental signals is the spatial profile of the pump beam, which is not a Gaussian (see Appendix C) as was assumed in the theory. Our pump beam has quite a large fraction of light in higher-order spatial modes, as could easily be seen by eye in the far field. Moreover, spatial mode structure changed from shot to shot, perhaps due to thermal gradients in the dye solution. The higher-order modes could not be eliminated by an intracavity spatial filter, perhaps due to the flat mirror design of the cavity. In principle, our theory is capable of predicting PTDS signals for any type of spatial profile which can be expressed in analytical form. However, it was considered impractical to calculate the precise shape in our case because we did not know the exact mode structures and the energy distribution among different modes.

Figure 19 shows the comparison of the amplitude (peak value) of the PTDS signal with the theoretical results. The PTDS amplitude has been plotted against the distance between the pump and the probe beams. Circles are the experimental points taken

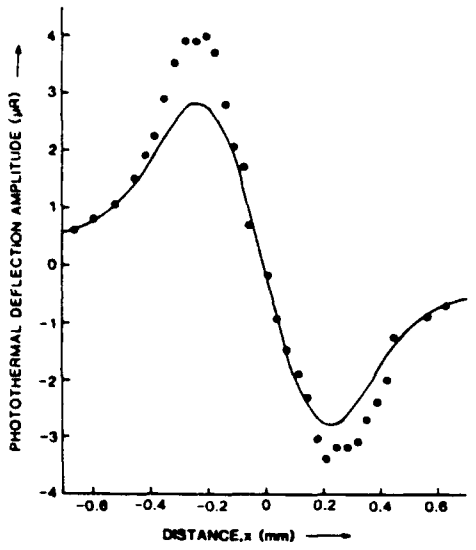

Fig. 19. Peak photothermal deflection signal for transverse geometry plotted as a function of the probe–pump distance. Circles are the experimental points and the solid line is the theoretical prediction using the parameters given in the text in connection with Fig. 18.

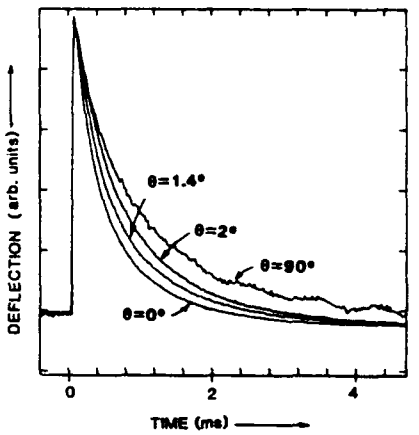

Fig. 20. Effect of the angle between the pump and the probe beams on the width of the photothermal deflection signal. To permit accurate comparison of the widths of different curves, all the curves have been scaled to the same amplitude. The scaling factors are 1.3 (for $\theta = 1.4$), 2.2 (for $\theta = 2°$), and 8.4 (for $\theta = 90°$). The maximum interaction length occurred for the collinear case and it was ~1 cm (width of the cell).

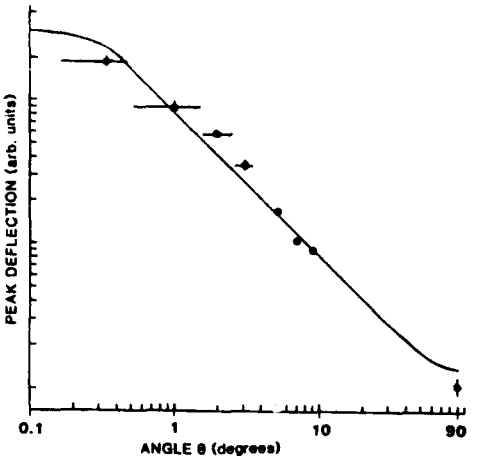

Fig. 21. Effect of the angle between the pump and the probe beams on the amplitude of the photothermal deflection signal. Circles are the experimental data points and the solid line is the theoretical curve. The theoretical curve has been normalized to the experimental data at $\theta = 1°$ for ease in comparison. These data were taken in a cell different from that corresponding to Fig. 20, and the maximum interaction length (corresponding to $\theta = 0°$) was 19 cm.

from the same experimental run as the curves in Fig. 18 and therefore correspond to the same parameters as in Fig. 18. The solid line is the theoretical curve corresponding to the parameters given earlier in connection with Fig. 18. First, we note that the amplitude of the signal agrees very well with the theory. The maximum deviation of the experiment from the theory is in the 30–40% range. Considering that no adjustable parameters have been used anywhere and considering various uncertainties in measurements, we consider this degree of agreement very good. Perhaps the most important source of error is the spatial profile of the pump beam which has been assumed to be a Gaussian in the theory, as mentioned above. Moreover, the probe beam had a nonzero size (0.15-mm $1/e^2$ radius at the interaction region in this case), whereas the theory assumed it to be a single ray (vanishingly small size). The effect of the probe beam diameter on the signal is discussed in Appendix C. Other important uncertainties include those in the calibration of the detector (volts/radian), in the measurement of the beam positions, in the measurement of laser energy (which drifted in addition to the pulse-to-pulse fluctuations), and in the knowledge of the absorption coefficient of NO_2.

Figures 20 and 21 show the effect of changing the angle between the pump and the probe beams. Figure 20 shows the effect on the width of the signal. To make the comparison of different curves easier, all four curves have been normalized to the same amplitude. The normalizing factors are given in the caption. As predicted by the theory, the PTDS signal broadens as the angle between the pump and the probe beams increases, achieving its maximum width for the transverse geometry. Moreover, most of this broadening occurs over a very small angular range, in accordance with the theory. The amplitude of the signal decreases in going from the collinear PTDS ($\theta = 0°$) to the transverse PTDS ($\theta = 90°$), approximately in proportion to the decrease in the interaction length. Smaller SNR for the transverse PTDS compared with the collinear PTDS can clearly be seen in the figure. An exact comparison of the dependence of amplitude of the PTDS signal on the angle between the pump and the probe beams with that expected from the theory is shown in Fig. 21. The circles are the experimental values for the PTDS amplitude (peak value) and the solid line is the theoretical curve. Whenever the error bars cannot be seen, they are within the widths of the points. The error bars in the amplitude correspond to one standard deviation of three runs. The error bars in the angle are estimated uncertainties, and the per-

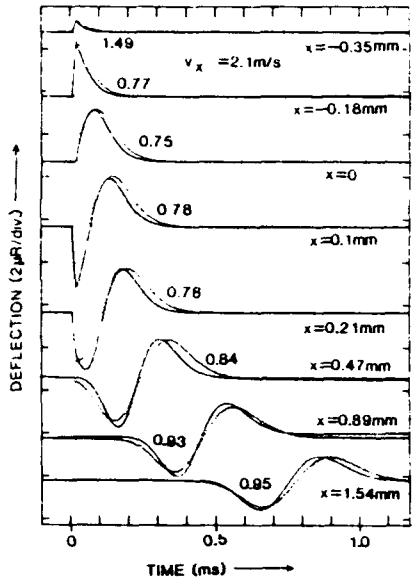

Fig. 22. Photothermal deflection signals for transverse geometry in a flowing medium (open jet of N_2 seeded with NO_2) for different pump-to-probe separations and a fixed flow velocity (2.1 m/s). Dots are experimental data points and they have been plotted on an absolute scale. The solid lines are the corresponding theoretical curves calculated from Eq. (21) using the parameters given in the text. To permit accurate comparison of signal shapes, the theoretical curves have been multiplied by the scaling factors indicated on each curve.

cent uncertainties are, naturally, large for small angles. Since we are only interested in the variation of PTDS amplitude with angle here, the theoretical curve has been normalized to the experimental point at $\theta = 1°$. For technical reasons, these data were taken in a cell different from that for Fig. 20. This cell was ~19 cm long and this fact is reflected in our data. The signal amplitude changes by >2 orders of magnitude corresponding to a change in the interaction length by approximately that factor.

B. Experiments in a Flowing Medium

Experiments were also conducted in a flowing medium (open jet of N_2 with 1025-ppm NO_2) and some of the results are described below. Figure 22 shows the PTDS signals for transverse geometry for various separations between the pump and the probe beams. The flow velocity in the center of the jet was 2.1 m/s. The dots are the experimental data points while the solid curves are the theoretical curves. To permit an accurate comparison of signal shapes, the theoretical signals have been multiplied by the scaling factors indicated on each curve. The experimental results have been plotted on an absolute scale. As before, the scaling factors themselves give the degree of agreement between theory and experiment for the signal amplitudes. Negative x corresponds to the probe beam being upstream from the pump beam while the opposite is true for positive x. $x = 0$ was determined from the disappearance of a negative peak in the signal (note that for $x > 0$ the deflection has a negative as well as a positive peak). Theoretical curves were calculated using the following parameters: $v_x = 2.1$ m/s as measured by a Linde model 4334 flowmeter, $a = 0.25$ mm and $b = 0.12$ mm as measured by the knife-edge technique, $E_0 = 0.8$ mJ as measured by a Scientech power meter, and the $1/e^2$ radius of the probe beam was 0.1 mm. The size of the pump beam in y direction b and the radius of the probe beam were not required in this calculation and are given here for completeness. All other parameters are given in Appendix A. As we noted in Sec. II, the signal has one peak for $x \leq 0$ and it has two peaks for $x > 0$. As the probe beam is moved downstream, away from the pump beam, the signal grows in magnitude and acquires a shape which essentially is a derivative of the spatial profile of the pump beam. In this case the heat pulse is carried downstream by the flow, and the diffusion simply broadens the signal. An examination of the figure shows that the experiment is in excellent agreement with the theory. We find that the 75–90% agreement between the experiment and the theory seen here is typical as long as the probe beam is smaller than the pump beam (probe < 1/2 pump), and as long as the probe beam is not small enough to resolve the higher-order spatial mode structure of the pump beam (see Appendix C). (A discrepancy of ~50% for $x = -0.35$ mm is perhaps due to uncertainty in the measurement of x.) Signal shapes are also in much better agreement with the theoretical predictions than in the case of stationary medium. In a flowing medium the spatial profile of the pump laser appears to be a less important problem. Our flowmeter has a ±5% calibration accuracy and we had a ±5% reading uncertainty for low velocities. We also noticed that the velocity was not completely stable through the run. We feel that a much better agreement of the signal shapes can be obtained using a more accurately measured velocity. As a matter of fact, the PTDS signal itself gives a much better measurement of the velocity[15] than our flowmeter. The bottom curve in Fig. 22 clearly shows that the true velocity was a little smaller than 2.1 m/s (but still within the uncertainty range of the flowmeter). In these investigations, however, no adjustable parameters were used, and therefore the flowmeter reading was used to calculate the theoretical results.

Figures 23 and 24 show the effect of varying the velocity at two different positions of the probe beam. Both sets of data are part of the same experimental run as that in Fig. 22, and therefore they correspond to the same experimental parameters as in Fig. 22 (except for the laser power which drifted slightly). Various velocities as measured by the flowmeter are indicated on each curve. Again, the theoretical curves have been scaled to match the peaks of the experimental curves for ease in the comparison of the signal shapes. The scaling factors are given in the figures. Consider Fig. 23 corresponding to $x = 0$ first. We find that the signal increases monotonically with velocity and therefore it can be used to measure very low flow velocities as demonstrated by Nie *et al.*[26] At zero velocity (not shown) the signal is zero as shown in Fig. 18. We also

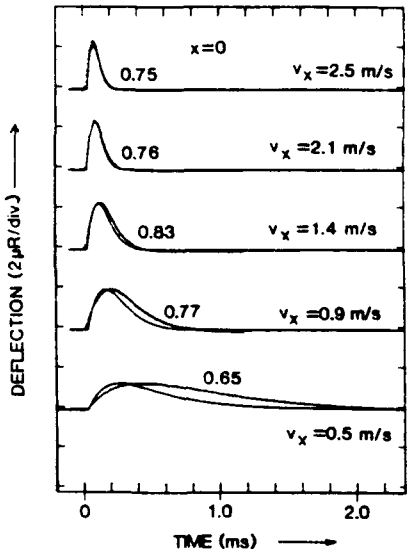

Fig. 23. Photothermal deflection signals for coincident pump and probe beams ($x = 0$) for different flow velocities. Dots represent the experimental signals while the solid lines are the theoretical curves corresponding to the parameters given in the text and scaled by the factors given on each curve.

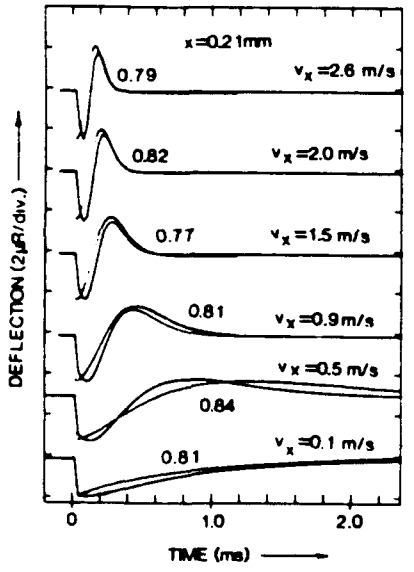

Fig. 24. Photothermal deflection signals similar to those shown in Fig. 23 but for $x = 0.21$ mm. Dots represent experimental points and the solid lines are the theoretical curves scaled by the indicated factors.

note that the signal gets narrower as the velocity increases, in accordance with our intuitive expectations. The agreement between the theory and the experiment is again excellent for relatively high velocities. The agreement gets worse for low velocities. This could be due to two reasons: First, the spatial profile of the pump laser may become more important in determining the signal shapes at low velocities. Second, our velocity measurements (using the flowmeter) at low velocities are more inaccurate. Moreover, at low velocities, the jet spreads out more, making the actual velocity lower than that derived from the flowmeter reading.

Figure 24 shows data similar to that in Fig. 23 for $x = 0.21$ nm. We see a gradual evolution of signal shape from that essentially given by diffusion at very low velocities to the dispersion-type shape for larger velocities. The amplitudes of the experimental signal agree very well with the theoretical predictions, as before. Moreover, the shapes of the signals agree quite well also, except at very low velocities as in Fig. 23, and perhaps for the same reasons. The slight displacement between the experimental and the theoretical signals seen in the top four curves may be primarily due to inaccuracy in the measurements of x and v_x.

V. Conclusions

We have given a complete and comprehensive theoretical description of the pulsed photothermal effect in a flowing medium in its most general form. Special case solutions, whenever available, have been compared with the rigorous theory to determine the limits of validity of the special case solutions. The theoretical results have been verified experimentally. To make an absolute comparison of the theory with experiment, no adjustable parameters were used. In general, the experiment agrees very well with the theory. Many subtle effects which affect the size and shape of the signals have been described.

We are truly grateful to Brian Monson and Yu-Xin Nie for assistance with this experiment. The work was supported by Air Force Wright Aeronautical Laboratories.

Note added in proof: Andrew C. Tam has pointed out (private communication) that the discrepancy between theory and experiment in Fig. 18 may be due to convection induced by the pump beam.

Appendix A

In this Appendix we give the constants that were used in the computation of the theoretical signals. The unperturbed refractive index of N_2 at room temperature and atmospheric pressure was taken to be[31] $n_0 = 1.000294$. The variation of the refractive index with temperature $\partial n/\partial T$ was derived according to the ideal gas law:

$$\frac{\partial n}{\partial T} = \frac{(n_0 - 1)T_0}{T^2}, \tag{A1}$$

and a value of 9.4×10^{-7} K^{-1} was used at room temperature.

The absorption coefficient of NO_2 was derived from the published[32] value of $\alpha \simeq 5 \times 10^{-3}$ cm^{-1} Torr^{-1}. For a 1025-ppm mixture of NO_2 at atmospheric pressure, this gives $\alpha = 0.39$ m^{-1}.

There is extensive literature on the diffusion constant D. We have used the value $D = 2.04 \times 10^{-5}$ m^2/s at room temperature and atmospheric pressure from Ref. 27. Other values in the literature are consistent with this value within experimental errors. The thermal conductivity k is related to D and to ρC_p by the following relation:

$$D = \frac{k}{\rho C_p}. \tag{A2}$$

We have used the value of $k = 2.48 \times 10^{-2}\,\mathrm{J\,m^{-1}\,s^{-1}\,K^{-1}}$ at room temperature (along with that of D) from Ref. 27 to deduce ρC_p.

To calculate PTDS signals at elevated temperatures D was assumed to increase as $T^{1.7}$ and k was assumed to increase as $T^{0.8}$ as deduced from the data of Rutherford *et al.*[27] (between 200 and 1100 K) and extrapolated to higher temperatures. $\partial n/\partial T$ was assumed to follow Eq. (A1).

Appendix B

In this Appendix we derive expressions for photothermal deflection signals when the pump beam has an elliptical cross section. This situation closely corresponds to our experimental situation. This derivation also demonstrates the versatility of our Green's function approach which allows for a solution for any type of spatial profile that can be expressed in analytical form. The derivation shows that for transverse geometry the results are identical to those for a circular beam, while they are different for the collinear case.

In this case the source term, Eq. (2), is modified to

$$Q(x,y,t) = \begin{cases} \dfrac{2\alpha E_0}{\pi a b t_0} \exp\{-2(x^2/a^2 + y^2/b^2)\} & \text{for } 0 \le t \le t_0, \\ 0 & \text{for } t > t_0, \end{cases} \tag{B1}$$

where a is the major radius of the pump beam (assumed to be along the x axis) and b is the minor radius (assumed to be along the y axis). Since the Green's function is independent of the form of the source term, it is still given by Eq. (12). Substitution of Eqs. (B1) and (12) into Eq. (4) gives the desired temperature distribution:

$$T(x,y,t) = \frac{2\alpha E_0}{\pi t_0 \rho C_p} \int_0^{t_0} \frac{\exp\{-2[x - v_x(t-\tau)]^2/[a^2 + 8D(t-\tau)]\}}{[a^2 + 8D(t-\tau)]^{1/2}} \times \frac{\exp\{-2y^2/[b^2 + 8D(t-\tau)]\}}{[b^2 + 8D(t-\tau)]^{1/2}}\, d\tau \qquad \text{for } t > t_0. \tag{B2}$$

We will assume that the probe beam displacement is in the x direction, as before. Again, $\partial T/\partial x$ can be calculated by differentiating inside the integral. We can therefore derive the expressions for transverse PTDS and collinear PTDS using Eqs. (19) and (22), respectively, as we did in Sec. II. The results are, for $t > t_0$,

$$\phi_T(x,t) = -\frac{1}{n_0}\frac{\partial n}{\partial T}\frac{8\alpha E_0}{\sqrt{2\pi} t_0 \rho C_p} \int_0^{t_0} \frac{[x - v_x(t-\tau)]}{[a^2 + 8D(t-\tau)]^{3/2}} \times \exp\{-2[x - v_x(t-\tau)]^2/[a^2 + 8D(t-\tau)]\} d\tau, \tag{B3}$$

$$\phi_L(x,y,t) = -\frac{l}{n_0}\frac{\partial n}{\partial T}\frac{8\alpha E_0}{\pi t_0 \rho C_p} \int_0^{t_0} \frac{[x - v_x(t-\tau)]}{[a^2 + 8D(t-\tau)]^{3/2}} \times \exp\{-2[x - v_x(t-\tau)]^2/[a^2 + 8D(t-\tau)]\} \times \frac{\exp\{-2y^2/[b^2 + 8D(t-\tau)]\}}{[b^2 + 8D(t-\tau)]^{1/2}}\, d\tau. \tag{B4}$$

We find that the expression for transverse PTDS for an elliptical beam is identical to that for a circular beam of radius a, Eq. (21). However, the expression for collinear PTDS is different from the corresponding expression for a circular beam, Eq. (23). Equation (B4) predicts that for an elliptical beam ($b < a$) the signal is stronger and its width is narrower than for the circular case.

Appendix C

In this Appendix we describe the effect of probe beam size on the PTDS signal. We find that, when the probe beam diameter is very small compared with the pump beam diameter, the higher-order mode structure in the spatial profile of our pump beam can easily be seen. However, as the probe beam diameter is increased, this structure cannot be seen due to the loss of resolution. Moreover, as the probe beam diameter is increased, the amplitude of the PTDS signal decreases; this effect becomes quite apparent by the time the probe beam diameter becomes greater than one-half of the diameter of the pump beam.

We start by reexamining Fig. 19. The shape of the curve in Fig. 19 closely corresponds to the derivative of the spatial profile of the pump beam,[33] therefore it can be used to measure its radius as demonstrated by Rose *et al.*[33] The two extrema occur at $x = \pm a/2$, and a simple measurement of the distance between the two extrema gives the pump beam radius. This is found to be 0.47 mm, in good agreement with the results of the knife-edge technique (0.46 mm). As mentioned above, our pump beam was not Gaussian but it was a combination of modes. This mode structure cannot be seen in Fig. 19, because the resolution in the experiment was not high enough to resolve this structure. As mentioned previously, the probe beam radius was 0.15 mm compared with the pump beam radius of 0.46 mm at their focal points (the interaction region). To illustrate this point, Fig. 25 shows a curve similar to Fig. 19, but taken at a different time in different conditions. At this time the pump beam was only mildly focused [Fig. 25(a)] and therefore it was much larger in size (~0.8-mm radius as seen from the diagram) than the probe beam. The crosses are the experimental points and the solid line is the theoretical curve. Only the shape of the curve is important here, therefore the peak of the theoretical curve has been normalized to the experimental data. We can clearly see that the spatial profile of the pump beam has bumps in it and it is not Gaussian by any means. Figure 25(b) shows the measured spatial profile of the same pump beam after it was more tightly focused (~0.4 mm as seen in the diagram). The probe beam diameter remained unchanged. In this case the probe beam did not have enough resolution to be able to resolve the mode structure in the spatial profile of the pump beam. As the pump beam is focused even more tightly (leaving the probe beam size unchanged), the mode structure, of course, remains unresolved; however, the experimental curve becomes broader and smaller than the theoretical curve. Figure 25(c) illustrates this point. Data shown here are from an experimental run different from those shown in Figs. 25(a) and (b), nevertheless,

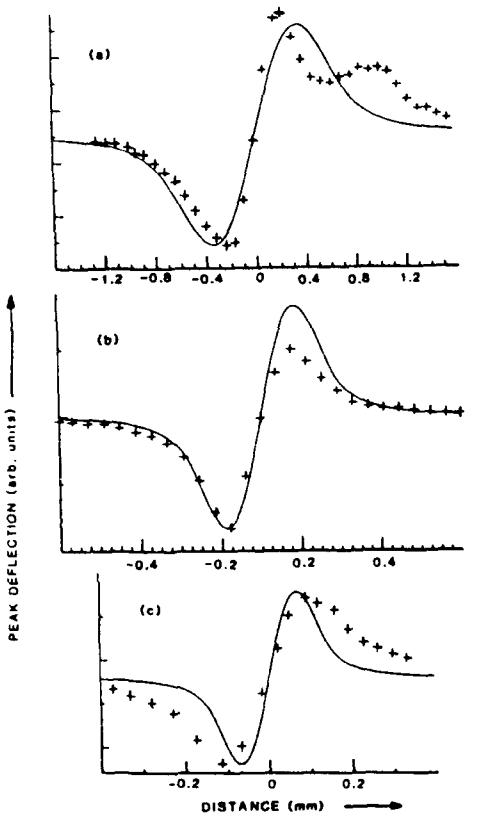

Fig. 25. Diagram showing the effect of the relative sizes of the pump and the probe beams on peak photothermal deflection signal. Crosses are experimental points and the solid lines are the theoretical curves. Theoretical curves have been scaled so that their peaks match the experimental values. Curve (a) is for the case when the pump beam diameter is very large compared with the probe beam diameter. In this case the probe beam is able to resolve the spatial mode structure of the pump beam which is non-Gaussian. In (b) the pump beam has been focused down to ~0.4 mm and the probe beam is no longer able to resolve the structure. When the pump beam size becomes about equal to (or smaller than) the probe beam, the experimental curve becomes broader than the theoretical curve as shown in (c).

they illustrate our point. In this case the pump beam radius was 0.14 mm while the probe beam radius was 0.1 mm (both measured by the knife-edge technique). We see clearly that the experimental curve is broader than the theoretical curve. This effect becomes very obvious by the time the pump beam diameter becomes about equal to the probe beam diameter. When the pump and the probe beams are about equal in size, we find that the amplitude of the experimental signal is about a factor of 2 smaller than the theoretical prediction. This, of course, is totally expected because the theory assumes that the probe beam is a single ray of light. Obviously, for quantitative agreement with theory it is important to keep the probe beam diameter much smaller ($<1/3$) than the pump beam diameter.[34] In our experiments, we were frustrated in these attempts due to the non-Gaussian mode structure of the pump beam which showed up prominently whenever the probe beam size was made too small compared with the pump beam size. We feel that much better agreement between the theory and the experiment can be obtained using a laser with good spatial profile. In our numerous experiments, we have noticed an unmistakable correlation between the quality of our experimental data (i.e., the degree of agreement with the theory) and quality of the spatial profile of the pump beam.

References

1. C. C. Davis, "Trace Detection of Gases Using Phase Fluctuation Optical Heterodyne Spectroscopy," Appl. Phys. Lett. **36**, 515 (1980).
2. A. C. Boccara, D. Fournier, and J. Badoz, "Thermo-Optical Spectroscopy: Detection by the Mirage Effect," Appl. Phys. Lett. **36**, 130 (1980).
3. A. C. Boccara, D. Fournier, W. B. Jackson, and N. M. Amer, "Sensitive Photothermal Deflection Technique for Measuring Absorption in Optically Thin Media," Opt. Lett. **5**, 377 (1980).
4. D. Fournier, A. C. Boccara, N. M. Amer, and R. Gerlach, "Sensitive *in situ* Trace-Gas Detection by Photothermal Deflection Spectroscopy," Appl. Phys. Lett. **37**, 519 (1980).
5. W. B. Jackson, N. M. Amer, A. C. Boccara, and D. Fournier, "Photothermal Deflection Spectroscopy and Detection," Appl. Opt. **20**, 1333 (1981).
6. J. C. Loulergue and A. C. Tam, "Noncontact Photothermal Probe Beam Deflection Measurement of Thermal Diffusivity in a Hot Unconfined Gas," Appl. Phys. Lett. **46**, 457 (1985).
7. H. Sontag and A. C. Tam, "Time-Resolved Flow-Velocity and Concentration Measurements Using a Traveling Thermal Lens," Opt. Lett. **10**, 436 (1985).
8. A. C. Tam, H. Sontag, and P. Hess, "Photothermal Probe Beam Deflection Monitoring of Photochemical Particulate Production," Chem. Phys. Lett. **120**, 280 (1985).
9. H. Sontag and A. C. Tam, "Characterization of Vapor and Aerosol Flows by Photothermal Methods," Can. J. Phys. Sept. 1986, to be published.
10. For a review see A. C. Tam, "Applications of Photoacoustic Sensing Techniques," Rev. Mod. Phys. **58**, 381 (1986).
11. A. Rose, J. D. Pyrum, C. Muzny, G. J. Salamo, and R. Gupta, "Application of the Photothermal Deflection Technique to Combustion Diagnostics," Appl. Opt. **21**, 2663 (1982).
12. A. Rose, J. D. Pyrum, G. J. Salamo, and R. Gupta, "Photoacoustic Spectroscopy and Photothermal Deflection Spectroscopy: New Tools for Combustion Diagnostics," in *Proceedings, International Conference on Lasers '82*, R. C. Powell, Ed. (STS Press, McLean, VA, 1983).
13. S. W. Kizirnis, R. J. Brecha, B. N. Ganguly, L. P. Goss, and R. Gupta, "Hydroxyl (OH) Distributions and Temperature Profiles in a Premixed Propane Flame Obtained by Laser Deflection Techniques," Appl. Opt. **23**, 3873 (1984).
14. A. Rose and R. Gupta, "Combustion Diagnostics by Photodeflection Spectroscopy," in *Twentieth Symposium (International) on Combustion* (Combustion Institute, Pittsburgh, PA, 1984).
15. A. Rose and R. Gupta, "Application of Photothermal Deflection Technique to Flow-Velocity Measurements in a Flame," Opt. Lett. **10**, 532 (1985).
16. A. Rose and R. Gupta, "Application of Photothermal and Photoacoustic Deflection Techniques to Sooting Flames: Velocity, Temperature, and Concentration Measurements," Opt. Commun. **56**, 303 (1986).
17. R. Gupta, "A Quantitative Investigation of Pulsed Photothermal and Photoacoustic Deflection Spectroscopy for Combustion Diagnostics," AIP Conf. Proc. **146**, 672 (1986).
18. J. A. Sell, "Gas Velocity Measurements Using Photothermal Deflection Spectroscopy," Appl. Opt. **24**, 3725 (1985).

19. V. Zharov and N. M. Amer, "Pulsed Photothermal Deflection Spectroscopy in Flowing Media," in *Technical Digest, Fourth International Topical Meeting on Photoacoustic, Thermal, and Related Science*, Ville D'Esterel, Quebec (1985).
20. J. A. Sell, "Quantitative Photothermal Deflection Spectroscopy in a Flowing Stream of Gas," Appl. Opt. **23**, 1586 (1984).
21. A. Rose, G. J. Salamo, and R. Gupta, "Photoacoustic Deflection Spectroscopy: A New Specie-Specific Method for Combustion Diagnostics," Appl. Opt. **23**, 781 (1984).
22. A. C. Tam and H. Coufal, "Pulsed Opto-Acoustics: Theory and Applications," J. Phys. Colloq. C6, **44**, 9 (1983).
23. A. Rose, Y.-X. Nie, and R. Gupta, "A Quantitative Investigation of Pulsed Photoacoustic Deflection Spectroscopy in Gaseous Media," to be submitted to Appl. Opt.
24. See, for example, M. V. Klein, *Optics* (Wiley, New York, 1970).
25. W. A. Weimer and N. J. Dovichi, "Time-Resolved Crossed-Beam Thermal Lens Measurement as a Nonintrusive Probe of Flow Velocity," Appl. Opt. **24**, 2981 (1985).
26. Y.-X. Nie, K. Hane, and R. Gupta, "Measurement of Very Low Gas Flow Velocities by Photothermal Deflection Spectroscopy," Appl. Opt. **25**, 3247 (1986).
27. W. M. Rutherford, W. J. Roos, and K. J. Kaminski, "Experimental Verification of the Thermal Diffusion Column Theory as Applied to the Separation of Isotopically Substituted Nitrogen and Isotopically Substituted Oxygen," J. Chem. Phys. **50**, 5359 (1969).
28. Reference 7. Our result differs from that of Ref. 7 by a factor of 2. We believe that there is an error in Ref. 7.
29. A. J. Twarowski and D. S. Klinger, "Multiphoton Absorption Spectra Using Thermal Blooming," Chem. Phys. **20**, 253 (1977).
30. J. M. Khosrofian and B. A. Garetz, "Measurement of a Gaussian Laser Beam Diameter Through the Direct Inversion of Knife-Edge Data," Appl. Opt. **22**, 3406 (1983).
31. R. Weast, Ed., *Handbook of Chemistry and Physics* (CRC Press, Boca Raton, FL, 1984).
32. V. M. Donnelly and F. Kaufman, "Fluorescence Lifetime Studies of NO_2. I. Excitation of the Perturbed $^2B_2$ State near 600 nm," J. Chem. Phys. **66**, 4100 (1977).
33. A. Rose, Y.-X. Nie, and R. Gupta, "Laser Beam Profile Measurement by Photothermal Deflection Technique," Appl. Opt. **25**, 1738 (1986).
34. A. Rose, "Development of Pulsed Photoacoustic and Photothermal Deflection Spectroscopy as Diagnostic Tools for Combustion," Ph.D. Dissertation, U. Arkansas (1986).

Reprinted from Applied Optics, Vol. 27 page 3914, September 15, 1988

Continuous wave photothermal deflection spectroscopy in a flowing medium

Reeta Vyas, B. Monson, Y-X. Nie, and R. Gupta

A complete and rigorous theoretical treatment of the continuous wave photothermal deflection spectroscopy in a flowing medium is given. The theoretical results have been verified experimentally.

I. Introduction

There is presently extensive interest in the technique of photothermal deflection spectroscopy (PTDS),[1-3] and this technique has found a wide range of applications. In this paper we present a comprehensive and rigorous theoretical treatment of the cw PTDS technique for the most general conditions, i.e., for a flowing medium. The results for a stationary medium appear as a special case. Very interesting results have been found, and these results will extend the range of applications of cw PTDS in fluids. Results of an experiment used to verify the theory are also presented.

The principle of the PTDS technique is as follows: A dye laser beam (pump beam) passes through the medium, and it is tuned to an absorption line of the molecules or atoms of interest. The molecules absorb the laser energy, and in the presence of quenching collisions some of this energy appears in the rotational–translational modes (heating) of the molecules of the medium. If the quenching rates are high compared with the radiative rates, almost all the absorbed energy appears in the heating of the laser irradiated region. The temperature change of the laser irradiated region results in a change of the refractive index of that region. This change in the refractive index can be probed by a second, and weaker, laser (probe beam). In general, the refractive index is nonuniform, and the refractive-index gradient deflects the probe beam. The deflection of the probe beam may be detected conveniently using a position sensitive optical detector. In the case of a cw pump beam, it is generally convenient to intensity modulate the pump beam at some frequency f. In this way, the deflection is also modulated at frequency f, which can then be detected conveniently using a phase sensitive detector.

The only previous theoretical study of the cw PTDS, to our knowledge, is that of Jackson *et al.*[4] These authors, however, consider only a stationary medium. Our study is more general (i.e., a flowing medium), and Jackson *et al.*'s results appear as a special case (flow velocity = 0) in our solutions. Moreover, this treatment of the cw PTDS unifies the theory of cw PTDS with that of pulsed PTDS in a flowing medium, published earlier by Rose *et al.*[5]

The theory of cw PTDS is given in Sec. II. The theoretical results are discussed in Sec. III. The apparatus is described in Sec. IV, and the experimental results are presented in Sec. V.

II. Theory

Figure 1 shows the basic geometry of the pump and probe beams. Two cases are considered: Transverse PTDS, in which the probe beam is perpendicular to the pump beam, and the collinear PTDS, in which the pump and probe beams are parallel. We assume the pump beam to be propagating along the z axis. The origin of the coordinate system lies on the axis of the pump beam. For the transverse PTDS, the probe beam propagates along the y axis, and for the collinear PTDS, the probe beam propagates in the z direction. In both cases, the medium flows with velocity v_x in the x direction. The pump and probe beams do not necessarily intersect, and they may be separated by a variable distance x in the x direction. For the collinear case, they may also be separated by a distance y in the y direction (not shown in Fig. 1). The general case, where the pump and probe beams make an arbitrary angle θ will not be considered here. This case has been treated by Rose *et al.*[5] previously in connection with

The authors are with University of Arkansas, Physics Department, Fayetteville, Arkansas 72701.
Received 22 December 1987.
0003-6935/88/183914-07$02.00/0.

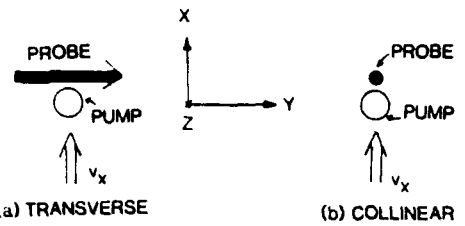

Fig. 1. Pump and the probe beam configuration for (a) transverse and (b) collinear PTDS.

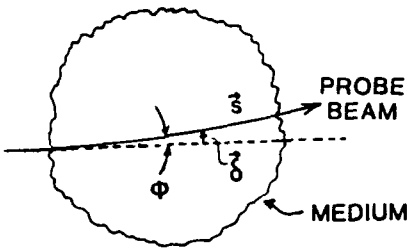

Fig. 2. Deflection of a probe beam.

pulsed PTDS, and expressions for cw PTDS can be derived analogously. Deflection of the probe beam in the x direction $\phi(x,y,t)$ is measured, and our aim is to derive an expression for $\phi(x,y,t)$. The temperature distribution created by the absorption of the pump beam is derived in Sec. II.A, and expressions for the resulting deflection of a pr be beam propagating in this region are derived in Sec. II.B.

A. Temperature Distribution

The temperature distributi:.n created by the absorption of the pump beam in a flowing medium is given by the solution of the differential equation:

$$\frac{\partial T(\mathbf{r},t)}{\partial t} = D\nabla^2 T(\mathbf{r},t) - v_x \frac{\partial T(\mathbf{r},t)}{\partial x} + \frac{1}{\rho C_p} Q(\mathbf{r},t), \tag{1}$$

where $T(\mathbf{r},t)$ is the temperature above the ambient, D is the diffusivity, ρ is the density, and C_p is the specific heat at constant pressure of the medium. The first, second, and third terms on the right-hand side of Eq. (1) represent, respectively, the effects of the thermal diffusion, flow, and heating due to the pump beam absorption. If we assume the medium to be weakly absorbing, the heat produced by the medium per second per unit volume is given by

$$Q(\mathbf{r},t) = \frac{2P_{av}\alpha}{\pi a^2} \exp(-2r^2/a^2)(1 + \cos\omega t), \tag{2}$$

where α is the absorption coefficient of the medium. The laser beam is assumed to have a Gaussian spatial profile with a $1/e^2$ radius a. The laser beam is sinusoidally modulated at a frequency $f = \omega/2\pi$. The average power of the laser beam is P_{av}; i.e., the laser power oscillates between 0 and $P_0 = 2P_{av}$.

Equation (1) has been solved in two dimensions (x and y). Implicit in this is the assumption that there are no inhomogeneities in the medium along the pump beam (z direction). The boundary conditions are

$$\begin{aligned} T(x,y,t)|_{t=0} &= 0, \quad T'(x,y,t)|_{t=0} = 0, \\ T(x,y,t)|_{x=\pm\infty} &= 0, \quad T(x,y,t)|_{y=\pm\infty} = 0, \end{aligned} \tag{3}$$

where the laser is turned on at $t = 0$, and T' represents the gradient of the temperature. The solution of Eq. (1) is given by

$$T(x,y,t) = \int_{-\infty}^{+\infty}\int_{-\infty}^{+\infty}\int_{0}^{\infty} Q(\xi,\eta,\tau)G(x|\xi,y|\eta;t|\tau)d\xi d\eta d\tau, \tag{4}$$

where G is the Green's function appropriate for Eq. (1), and the functional form of Q is given by Eq. (2). The Green's function satisfies the differential equation

$$-D\nabla^2_{\xi,\eta}G + v_x\frac{\partial G}{\partial x} + \frac{\partial G}{\partial t} = \frac{1}{\rho C_p}\delta(x-\xi)\delta(y-\eta)\delta(t-\tau), \tag{5}$$

with appropriate boundary conditions. Rose *et al.*[5] have found the Green's function for Eq. (5) in connection with pulsed PTDS to be

$$G = \frac{H_\tau(t)}{4\pi\rho C_p D(t-\tau)} \exp(-|x - [\xi + v_x(t-\tau)]|^2/[4D(t-\tau)|) \times \exp[-|y-\eta|^2/|4D(t-\tau)|], \tag{6}$$

where $H_\tau(t)$ is the Heaviside unit step function. The Green's function is independent of the source term, Eq. (2), and, therefore, the same Green's function is valid for pulsed PTDS, cw PTDS, modulated cw PTDS, etc. This is indeed the most attractive feature of our theoretical treatment. The temperature distribution can be found easily using Eqs. (4) and (6) for any type of source function, e.g., a laser operating in a TEM_{00} mode or a laser with elliptical Gaussian profile etc. Substitution of Eqs. (6) and (2) in Eq. (4) leads to the desired result

$$T(x,y,t) = \frac{2\alpha P_{av}}{\pi\rho C_p}\int_0^t \frac{(1+\cos\omega\tau)}{[a^2 + 8D(t-\tau)]} \times \exp(-2|[x - v_x(t-\tau)]|^2 + y^2|/[a^2 + 8D(t-\tau)|])d\tau. \tag{7}$$

B. Probe Beam Deflection

The propagation of an optical beam in an inhomogeneous medium is governed by the equation[6]

$$\frac{d}{ds}\left(n_0\frac{d\delta}{ds}\right) = \nabla_\perp n(\mathbf{r},t), \tag{8}$$

where s represents the beam path, δ is the perpendicular displacement of the beam from its original position, as shown in Fig. 2, and $\nabla_\perp n(\mathbf{r},t)$ is the gradient of the refractive-index perpendicular to the beam path. The refractive index $n(\mathbf{r},t)$ is related to the unperturbed refractive index n_0 by

$$n(\mathbf{r},t) = n_0 + \left.\frac{\partial n}{\partial T}\right|_{T_A} T(\mathbf{r},t), \tag{9}$$

where T_A stands for the ambient temperature. Therefore,

$$\frac{d\delta}{ds} = \frac{1}{n_0}\frac{\partial n}{\partial T}\int_{\text{path}} \nabla_\perp T(\mathbf{r},t)ds, \tag{10}$$

where the integration has been carried out over the path of the beam. In our geometry (Fig. 1) and for

small deflections, we may simply write the deflection angle ϕ as

$$\phi(x,y,t) = \frac{1}{n_0}\frac{\partial n}{\partial T}\int_{\text{path}} \frac{\partial T(x,y,t)}{\partial x}\, ds. \tag{11}$$

For transverse and collinear PTDS (Fig. 1), this equation reduces to

$$\phi_T(x,t) = \frac{1}{n_0}\frac{\partial n}{\partial T}\int \frac{\partial T(x,y,t)}{\partial x}\, dy, \tag{12}$$

and

$$\phi_l(x,y,t) = -\frac{1}{n_0}\frac{\partial n}{\partial T}\int \frac{\partial T(x,y,t)}{\partial x}\, dz, \tag{13}$$

respectively. Using Eq. (7) in Eqs. (12) and (13), ϕ_T and ϕ_l may be written explicitly as

$$\phi_T(x,t) = -\frac{1}{n_0}\frac{\partial n}{\partial T}\frac{8\alpha P_{av}}{2\pi\rho C_p}\int_0^t \frac{(1+\cos\omega\tau)[x - v_x(t-\tau)]}{[a^2 + 8D(t-\tau)]^{3/2}} \times \exp\{-2[x - v_x(t-\tau)]^2/[a^2 + 8D(t-\tau)]\}d\tau, \tag{14}$$

$$\phi_l(x,y,t) = -\frac{l}{n_0}\frac{\partial n}{\partial T}\frac{8\alpha P_{av}}{\pi\rho C_p}\int_0^t \frac{(1+\cos\omega\tau)[x - v_x(t-\tau)]}{[a^2 + 8D(t-\tau)]^{2}} \times \exp\{-2[[x - v_x(t-\tau)]^2 + y^2]/[a^2 + 8D(t-\tau)]\}d\tau, \tag{15}$$

respectively, where l is the interaction length for the collinear case. The last step in the evaluation of the temperature [Eq. (7)] and the deflection signal [Eqs. (14) and (15)] is the integration over τ.

The evaluation of these integrals was problematic as the integrand is highly oscillatory due to the presence of a $\cos\omega\tau$ factor, and it rises very steeply near $\tau \approx t$ due to the presence of the exponential factor. To evaluate these integrals, the range of integration 0 to t was divided into three regions: 0 to $0.9t$, $0.9t$ to $0.99t$, and $0.99t$ to t. These regions were further divided into many small intervals. The integral in each of these small intervals was evaluated using Gaussian quadrature of sixty-four points. The length of these intervals was chosen according to the steepness and oscillation frequency of the integrand. They were smaller in the region where the integrand was changing rapidly. For example, for frequencies above 10 Hz, one interval was chosen for each oscillation in the first region (0 to $0.9t$). In the time range, $0.9t$ to $0.99t$, two intervals were chosen for each oscillation. In the third region ($0.99t$ to t) four intervals were chosen for each oscillation. The number of intervals had to be increased further with increasing velocities.

III. Theoretical Results

Figure 3 shows the temperature distribution created by the pump laser beam calculated using Eq. (7). The temperature has been plotted as a function of distance from the center of the laser beam. This distance x is measured in units of the beam radius a for convenience. The four curves correspond to the stationary medium and to the medium moving with flow velocity v_x = 1 cm/s, v_x = 10 cm/s, and v_x = 1 m/s, as labeled. The laser beam is assumed to be unmodulated [$\omega = 0$ in Eq. (7)]. The following values of various parameters

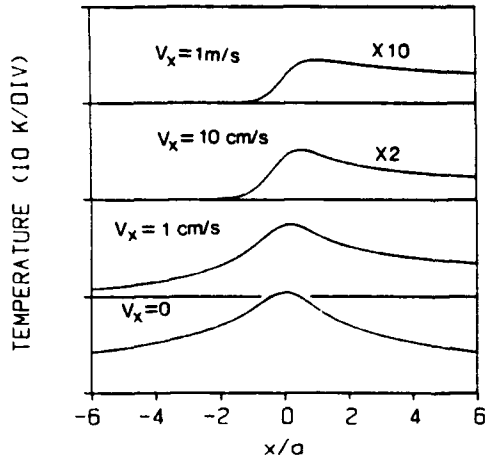

Fig. 3. Temperature distribution produced by a pump beam of power 1 W, $1/e^2$ radius, a = 0.5 mm, in a medium of absorption coefficient α = 0.39 m^{-1}. These temperature distributions have been computed for a stationary medium (v_x = 0) and for three different flow velocities as labeled. Top two curves have been expanded by the indicated factors for clarity.

have been used in this computation (and all subsequent computations presented in this section): Laser beam power P_{av} = 1 W, pump beam radius a = 0.5 mm, absorption coefficient α = 0.39 m^{-1} (corresponding to 1000-ppm NO_2 in atmospheric pressure N_2 and λ = 490 nm), and ρC_p and D are taken to be 1.22×10^3 J m^{-3} K^{-1} and 2.04×10^{-5} m^2 s^{-1}, respectively, corresponding to atmospheric pressure of N_2. All the temperature distributions shown in Fig. 3 have been computed for 5 s after turning on the laser beam. We have studied the temporal evolution of these distributions and find that a true steady state is never reached, particularly in a stationary medium. That is, the temperature keeps rising forever. This is a consequence of the fact that we have assumed the medium to have open boundaries. However, for distances close to the beam, a quasi-steady state is established; that is, the rate of temperature increase becomes negligible after a certain time (a few seconds for a stationary medium). This time shortens considerably as the flow velocity is increased. An examination of Fig. 3 shows that the temperature distribution in a stationary medium extends far beyond the radius of the pump beam. (The temperature distribution extends to infinity at infinite time.) As the flow velocity is increased, the temperature extends farther downstream. Moreover, the magnitude of the temperature rise decreases with increasing velocity, as expected. Since the photothermal deflection signal is proportional to the gradient of the temperature, one would expect the signal to be antisymmetric about x = 0 for the stationary medium and lose the symmetry for nonzero flow velocities. Moreover, the largest signal would be found slightly upstream since the gradient is highest there. On the other hand, the signal would be very small downstream, although the temperature distribution extends quite far downstream, since the gradient is small there. This is in contrast to pulsed PTDS.

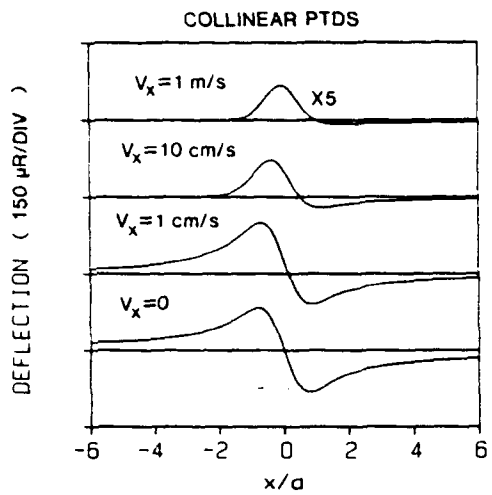

Fig. 4. Collinear PTDS signals corresponding to the temperature distribution shown in Fig. 3.

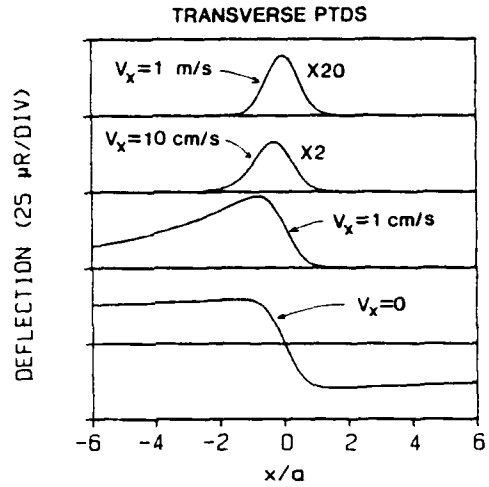

Fig. 5. Transverse PTDS signals corresponding to the temperature distribution of Fig. 3.

Figure 4 shows the steady state PTDS signals for collinear geometry evaluated using Eqs. (15) with $\omega = 0$. In contrast to the temperature distribution, the photothermal deflection signal does reach a steady state. In this computation the interaction length $l = 1$ cm, $(\partial n)/(\partial t) = 9.4 \times 10^{-7}$ K^{-1} appropriate for N_2 at room temperature, and all other parameters are the same as those in Fig. 3. Again, the four curves correspond to $v_x = 0$, 1 cm/s, 10 cm/s, and 1 m/s. As expected, the PTDS signal for $v_x = 0$ is antisymmetric, it loses its symmetry as v_x increases, and the largest signal occurs slightly upstream. Figure 5 shows the PTDS signals for the transverse geometry. These curves follow the same general trend as the collinear ones, except that the signal magnitudes are smaller (due to the shorter interaction length) and that the wings of the signal for $v_x = 0$ extend farther out. The apparent symmetry of the signal for $v_x = 1$ m/s about $x = 0$ is fortuitous.

To measure the PTDS signals, it is generally convenient to modulate the pump beam intensity and detect the oscillating component of the deflection using phase-sensitive (lock-in) techniques. The observed signal is then the rms value of the oscillating component of the deflection. Figure 6 shows the temperature distribution at four different times in the modulation cycle of the pump laser for a modulation frequency of 10 Hz, and $v_x = 10$ cm/s. The solid curve corresponds to the peak of the laser intensity, the dashed curve ($t = 0.15$ s) corresponds to the off portion of the laser intensity, and the other two curves are for the intermediate values of time. The temperature distribution goes through drastic changes with time. What is significant is the fact that outside the pump beam on the downstream side, the gradient of the temperature even changes sign as a function of time. It is important to appreciate this point to understand physically the rms signals. Figure 7 show the deflection for the collinear case at four different times in the modulation cycle, and, as expected, the signal on the downstream

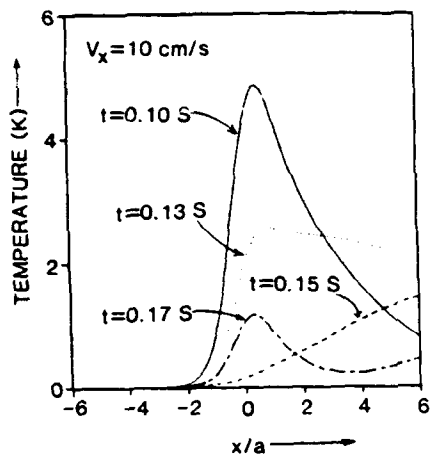

Fig 6. Temperature distribution at four different times in the modulation cycle of the pump laser for $v_x = 10$ cm/s. The modulation period is 0.1 s.

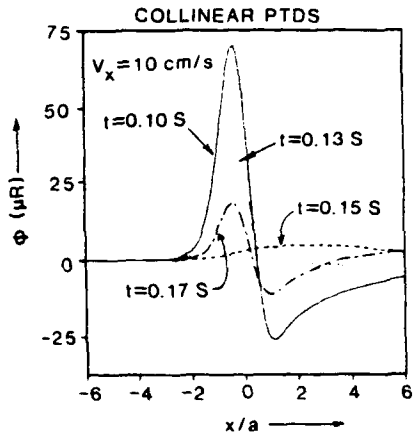

Fig. 7. Collinear PTDS signals at four different times when the pump laser is modulated at $f = 10$ Hz. These signals correspond to the temperature distributions shown in Fig. 6.

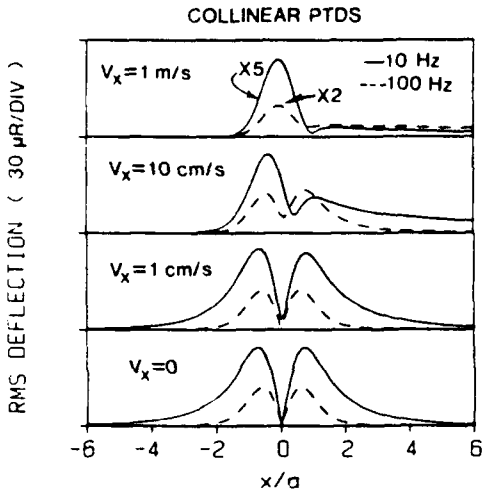

Fig. 8. Root-mean-square values of the deflection signals for the collinear case plotted as a function of the pump-to-probe distance for four different flow velocities, as labeled. Solid curves are for a modulation frequency of 10 Hz, while the dotted curves are for 100 Hz. The top curves have been expanded by the indicated factors for clarity.

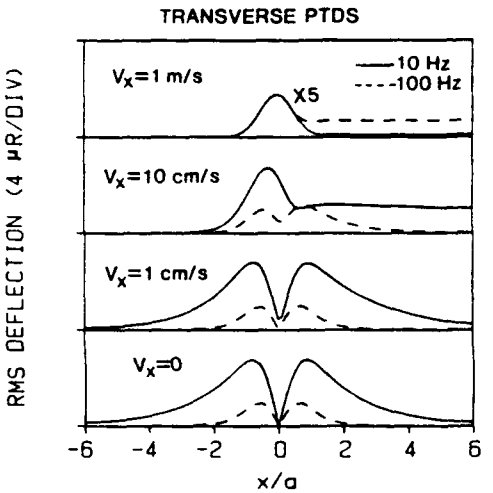

Fig. 9. Root-mean-square values of the deflection signals for the transverse case.

side changes sign as a function of time. Figure 8 shows the rms values of the oscillating part of the deflection signal for the collinear case. Again, four different flow velocities are considered as labeled. As expected, the signals show increasing asymmetry with increasing flow velocity. The solid curves are for a modulation frequency of 10 Hz, while the dashed ones are for 100 Hz. We note that, in general, the signal decreases with increasing modulation frequency. This is because the medium is unable to respond to fast changes due to thermal inertia. Moreover, for a stationary medium, the peak of the signal is pulled closer to the pump beam center with increasing modulation frequency. This is because the heat is only able to diffuse through a short distance during the modulation cycle at a high modulation frequency. Figure 9 shows curves analogous to those of Fig. 8 for the transverse case. In general the signal shapes are similar to those for the collinear case, and the magnitude of the signals is smaller by about an order of magnitude, as expected.

An examination of magnitudes of the signals at $x = 0$ shows that the PTDS signal grows with velocity for low values of the velocity. This fact may be used to measure the flow velocity. This method of flow velocity measurement is analogous to the method demonstrated by Nie *et al.*[7] for the case of pulsed PTDS.

IV. Apparatus

A schematic diagram of the apparatus used for the experiment is shown in Fig. 10. The pump beam was supplied by a Coherent Radiation model CR12 Ar^+ laser tuned to 514 nm. The Ar^+ laser was intensity modulated at a frequency of 10 or 100 Hz using a sine wave from a function generator. The pump beam passed through a glass cell of square cross section (1 × 1 cm). N_2 gas seeded with 1000-ppm NO_2 passed through the cell. NO_2 was added to N_2 to make the gas

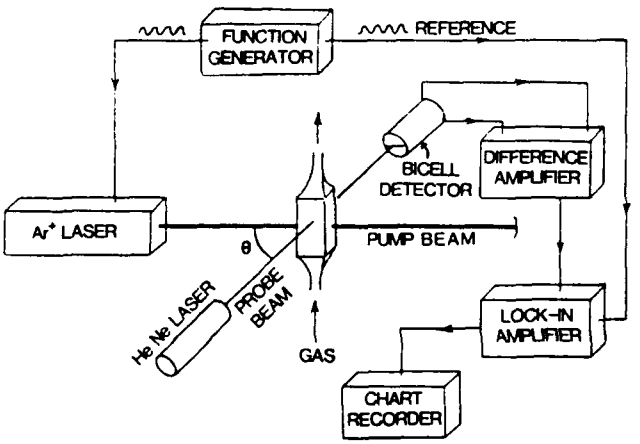

Fig. 10. Schematic illustration of the experiment.

absorb optical radiation in the visible region. The flow rate of the gases through the cell could be controlled with a valve and measured using a flowmeter. The probe beam was supplied by an 0.8–mW Uniphase He–Ne laser operating at 628 nm. In this experiment, the angle θ between the pump and probe beams was arranged to be $\pi/2$ (transverse PTDS). The pump beam could be translated so as to vary the distance x between the pump and probe beams. The deflection of the probe beam was measured by a Silicon Detector Corp. bicell detector. The difference signal from the two cells was measured. A deflection of the probe beam resulted in a change in the difference signal. Since the pump beam was sinusoidally modulated, the difference signal was also sinusoidally modulated. The oscillatory part of the deflection signal was measured using a Princeton Applied Research model HR8 lock-in amplifier. The lock-in amplifier gave a signal proportional to the rms value of the deflection, which was plotted on a chart recorder.

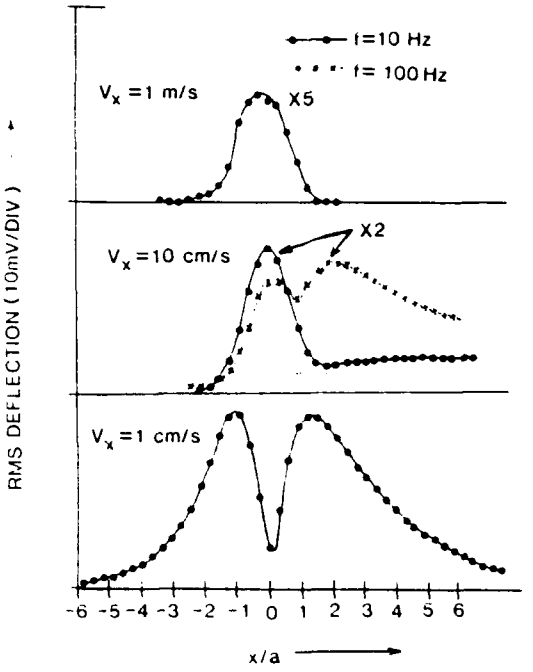

Fig. 11. Measured values of the rms deflections for the transverse case for three different velocities and for modulation frequencies f = 10 and 100 Hz, as labeled. The top three curves have been expanded for clarity, as indicated. These curves correspond approximately to the theoretical curves of Fig. 9.

V. Experimental Results

Figure 11 shows some of the experimental results for the transverse PTDS. The rms values of the deflection are plotted as a function of the distance between the pump and probe beams. This distance has been plotted in units of the pump beam radius. Positive values of x correspond to the probe beam being downstream from the pump beam. Data are displayed for three flow velocities, v_x = 1 cm/s, v_x = 10 cm/s, and v_x = 1 m/s, as labeled. The solid circles correspond to a modulation frequency f = 10 Hz, while the crosses correspond to f = 100 Hz. The lines drawn through the data points are not the result of a fit; they have been drawn to guide the eye. These data were taken with an average pump power P_{av} of 1 W, pump beam radius a was 0.46 mm as measured by the knife-edge technique,[8] and the probe beam radius was estimated to be 0.1 mm. The flow velocity was estimated using the area of cross section of the cell, the gas flow rate as measured by a flowmeter, and the assumption of a laminar flow within the cell. No attempts were made in these experiments to measure the absolute values of the deflection.

An examination of the experimental results shown in Fig. 11 confirms the essential validity of the theoretical results presented in Sec. III. We note that the signal changes shape with increasing velocity in accordance with the theoretical predictions of Fig. 9, and the peak signal amplitude decreases and its position shifts with increasing velocity, as expected. Moreover, the signal decreases with increasing modulation frequency, as predicted by the theory. However, we note that the exact shape of the curve is somewhat different from those shown in Fig. 9, particularly for the case of v_x = 10 cm/s. We believe that the actual flow velocity was larger than 10 cm/s for this case due to inaccuracy in the measurement of the gas flow rate and probably due to some turbulence. There are four observations that support this assertion: (1) The magnitude of the signal is a factor of ~2 smaller than that for v_x = 1 cm/s, while the theory predicts a smaller change. (2) For f = 10 Hz, the ratio of the peak amplitude to that of the tail (downstream side) is ~4, while Fig. 9 predicts it to be ~2.5. (3) Relative magnitude of the f = 100-Hz signal with respect to the f = 10 Hz is higher than predicted. (4) The f = 100-Hz signal has a more prominent tail on the downstream side. All these observations are consistent with a higher flow velocity. Moreover, a different run on a different day (when the pump and the probe beams were at a different place in the cell) did produce a signal for v_x = 10 cm/s, which was consistent with the theoretical predictions, as shown in Fig. 12. However, at that time, data for other velocities were not taken, and only a single curve shown in Fig. 12 is available. In both Figs. 11 and 12, 1 μRad of deflection corresponded to ~7 mV of signal. Therefore, the observed peak signal for v_x = 1 cm/s was ~1.2 μRad, which is of the same order of magnitude as the one predicted theoretically (Fig. 9). Absolute measurements, however, were not attempted for purely technical reasons (uncalibrated flowmeter, possible deviations from laminar flow in the cell, uncalibrated gas composition, etc.). Good general agreement between the theory and experiment, however, does confirm the essential validity of the theory.

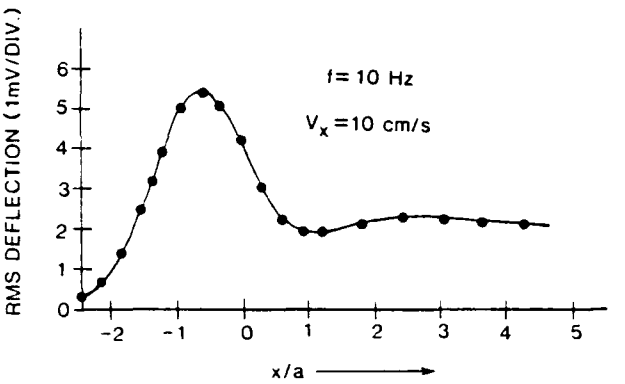

Fig. 12. Measured rms deflection for the transverse case for v_x = 10 cm/s and f = 10 Hz.

To summarize, we have given a complete and rigorous theoretical treatment of the continuous-wave photothermal deflection spectroscopy in a flowing medium, and the theoretical results have been verified experimentally.

This work was supported in part by Air Force Wright Aeronautical Laboratories.

References

1. R. Gupta, "Pulsed Photothermal Deflection Spectroscopy in Fluid Media: A Review," in *Proceedings, International Conference on Lasers '86*, R. W. McMillan, Ed. (STS Press, McLean, VA, 1987).
2. A. C. Tam, "Applications of Photoacoustic Sensing Techniques," Rev. Mod. Phys. **58**, 381 (1986).
3. S. E. Bialkowski, "Pulsed Laser Photothermal Spectroscopy," Spectroscopy **1**, 26 (1986).
4. W. B. Jackson, N. M. Amer, A. C. Boccara, and D. Fournier, "Photothermal Deflection Spectroscopy and Detection," Appl. Opt. **20**, 1333 (1981). Caution must be exercised in using the results given in this paper for the cw case, because the source term $Q(\mathbf{r},t)$ has been assumed to vary as $\cos\omega t$, which results in negative power during the alternate half-cycles.
5. A. Rose, R. Vyas, and R. Gupta, "Pulsed Photothermal Deflection Spectroscopy in a Flowing Medium: A Quantitative Investigation," Appl. Opt. **25**, 4626 (1986).
6. See, for example, M. V. Klein, *Optics* (Wiley, New York, 1970).
7. Y.-X. Nie, K. Hane, and R. Gupta, "Measurement of Very Low Gas Flow Velocities by Photothermal Deflection Spectroscopy," Appl. Opt. **25**, 3247 (1986).
8. J. M. Khosrofian and B. A. Garetz, "Measurement of a Gaussian Laser Beam Diameter Through the Direct inversion of Knife-Edge Data," Appl. Opt. **22**, 3406 (1983).

Appendix 11

Reprinted from Applied Optics, Vol. 25, Page 1738, June 1, 1986

Laser beam profile measurement by photothermal deflection technique

A. Rose, Y.-X. Nie, and R. Gupta

University of Arkansas, Physics Department, Fayetteville, Arkansas 72701.
Received 16 December 1985.
0003-6935/86/111738-04$02.00/0.

Laser beam profile is an important parameter in the field of laser research, development, and applications. Several methods of measuring a laser beam profile have been reported in the literature.[1] These methods consist of photographic methods,[2,3] beam-scan techniques[4–7] (pinhole, slit, and knife-edge), and imaging detector techniques,[8] among others.[9–12] In this letter we report a new method for measuring laser beam profiles using the photothermal deflection technique.[13]

The principle of this method is quite simple: Let the laser beam whose profile is to be measured pass through a region containing an absorbing gas (or a gas mixture). The gas molecules absorb the optical energy from the laser beam and, due to quenching collisions of the absorbing molecules with other molecules of the medium, this energy quickly appears as heating of the laser-irradiated region. This heating leads to changes in the refractive index of the medium in that region. If the density of absorbing molecules is uniform over the width of the laser beam, the refractive index acquires the same spatial profile as the laser beam (for example, a Gaussian profile). We shall refer to the laser beam whose profile is to be measured as the pump beam. Now, if a probe beam, generally a He–Ne laser beam, passes through the pump-beam-irradiated region, it is deflected due to gradients in the refractive index created by the absorption of the pump beam.

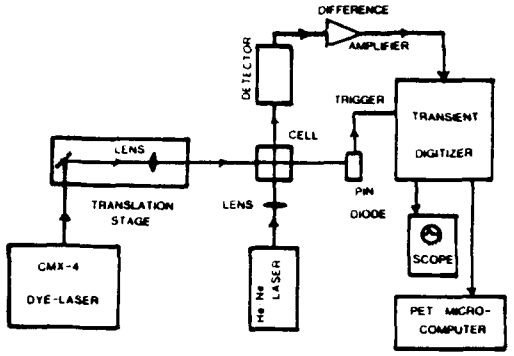

Fig. 1. Schematic diagram of the experiment.

This deflection can be easily measured by a position-sensitive optical detector. If the probe beam is scanned across the pump beam profile, this profile can easily be measured.

Figure 1 shows our experimental setup. A quartz cell with nitrogen at atmospheric pressure was used as the medium. To make the medium absorb the pump beam, 1025 ppm of NO_2 was added to N_2. A Chromatrix CMX-4 flashlamp-pumped dye laser was used as the source of the pump beam. In this work the dye laser was tuned to 490 nm where the absorption of NO_2 is high. The laser produced 2–3 mJ of energy in ~1-μs duration pulses. The pump beam was focused by a 20-cm focal length lens in the center of the quartz cell. The He–Ne laser beam (the probe beam) was also focused at the center of the quartz cell. The focal spot size of the probe beam was arranged to be smaller than that of the pump beam. The focal spots of the two beams were coincident and intersected at right angles at the center of the cell. A micrometer-driven translation stage was used to move the pump beam across the probe beam. Moving the pump beam instead of the probe beam was purely a matter of convenience, only the relative motion of the two beams being important. The deflection of the probe beam was measured by a quadrant detector in conjunction with a difference amplifier. The probe beam was arranged on the quadrant detector to give a null signal in its quiescent position. At the instant of laser firing, the probe beam deflected, giving a transient signal at the difference amplifier. The probe beam returned to its original position on the time scale of the diffusion time of the heat from the irradiated region. The output of the difference amplifier was fed to a LeCroy WD 8256 transient digitizer for recording of the transient signal. The transient digitizer was interfaced to a Commodore PET microcomputer for signal averaging, if necessary, and for data storage.

Figure 2 shows our typical data. Photothermal deflection (PTD) signal amplitude (i.e., the peak value) is plotted against the distance between the centers of the pump and probe beams. The inset shows the time-resolved shape of the PTD signal. The PTD signal amplitude is zero when the centers of the probe and pump beams coincide exactly, and it is maximum when the center-to-center distance between the pump and probe beams is $a/2$ (see below), where a is the $(1/e^2)$ radius of the pump beam. Thus, a simple measurement of the distance between the two peaks in Fig. 2 yields the radius of the pump beam.

A rigorous theoretical treatment of PTD signals is given by Jackson *et al.*[13] We present here, however, an expression for PTDs signal amplitude based on a simple model which is adequate for our purposes. This model has the advantage of elegant simplicity and that a simple analytical solution can be found for any type of spatial profile that can be expressed in an analytical form. Let the pump beam intensity (W/m^2) be given by $I(r)$. We assume that the laser pulse turns on sharply at time $t = 0$ and turns off sharply at $t = t_0$. The peak value of the PTD signal then occurs at $t = t_0$. The heat deposited per unit volume in the laser-irradiated region, $Q(r)$, at $t = t_0$ is given by

$$Q(r) = \alpha I(r) t_0, \tag{1}$$

where α is the absorption coefficient of the medium and we have assumed weak absorption. The temperature rise over the ambient is then given by

$$T(r) = \frac{\alpha I(r) t_0}{\rho C_p}, \tag{2}$$

where ρ is the density, and C_p is the specific heat of the medium. Now if a probe beam is placed a distance r from the center of the pump beam, the deflection of the probe beam is given by[14]

$$\phi(r) = \frac{1}{n_0}\frac{\partial n}{\partial T}\int_{\text{path}} \frac{\partial T}{\partial r}\, ds, \tag{3}$$

where n_0 is the unperturbed refractive index of the medium, $(\partial n/\partial T)$ is the variation of the refractive index with temperature, ds is an element of the probe beam path, and the integration is carried out over the path of the probe beam. We will assume that the interaction length of the probe and pump beams, l, is so small that the variation of $(\partial T/\partial r)$ over the interaction length is negligible. $\phi(r)$ may then be written as

$$\phi(r) = \frac{l}{n_0}\frac{\partial n}{\partial T}\frac{\alpha t_0}{\rho C_p}\frac{\partial I(r)}{\partial r}. \tag{4}$$

We note that the PTD signal amplitude is proportional to the gradient of the spatial profile of the (pump) laser beam. This is true no matter what kind of spatial profile the beam has. Note that in this treatment we have neglected the effects of thermal diffusion, which is justified when the probe and pump beams overlap and the laser pulse duration is

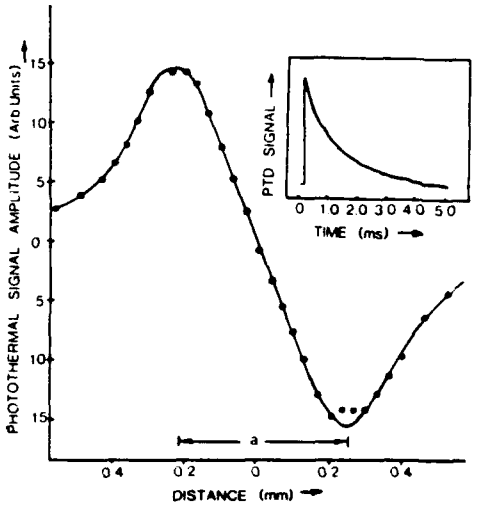

Fig. 2. Photothermal deflection signal amplitude plotted against the center-to-center distance between the probe and pump beams. The circles are the experimental data points and the solid line has been drawn to guide the eye. The $(1/e^2)$ radius of the probe beam used in this investigation was 0.1 mm (as measured by a knife-edge). The inset shows the time-resolved PTD signal.

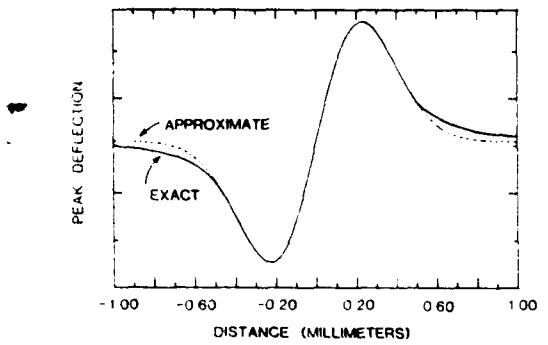

Fig. 3. Theoretical PTD signal amplitude plotted against the probe-to-pump beam distance. The dotted curve is calculated from Eq. (6) in this paper, while the solid curve is calculated from Eq. (28) in Jackson *et al.*[13] Pump-beam radius a was assumed to be equal to 0.45 mm in this calculation.

short compared to the characteristic time scales associated with thermal diffusion.

Let us now assume that the pump beam spatial profile is given by a Gaussian:

$$I(r) = \frac{2E_0}{\pi a^2 t_0} \exp(-2r^2/a^2), \tag{5}$$

where E_0 is the laser energy per pulse, and a is the $(1/e^2)$ radius of the beam. When the pump and probe beams intersect at right angles, the interaction length l is of the order of a. A rigorous calculation[15] shows that the effective interaction length is given by $l = (\sqrt{\pi}/2)a$. Therefore, for a Gaussian pump beam the PTD signal amplitude is given by

$$\phi(r) = -\frac{1}{n_0}\frac{\partial n}{\partial T}\frac{4\sqrt{2}aE_0}{\rho C_p \sqrt{\pi}a^2}\left(\frac{r}{a}\right)\exp(-2r^2/a^2). \tag{6}$$

Figure 3 shows a plot of $\phi(r)$ calculated from Eq. (6) (dotted curve). The solid curve represents $\phi(r)$ calculated from the exact expression of Jackson *et al.*[13] We note that the two curves agree exactly for $|r| \leq a$. The reason for the slight disagreement for $|r| > a$ is obvious: As the probe–pump beam distance increases, the peak of the PTD signal no longer occurs at $t = t_0$. The peak value is affected by thermal diffusion of heat from the interior of the beam and it occurs for $t > t_0$. The difference between the two curves is unimportant for our purposes. An examination of Eq. (6) and Fig. 3 shows that the two extrema of $\phi(r)$ occur at $r = \pm a/2$. Therefore the radius of the beam can be measured by a simple measurement of the distance between the two extrema. It should be noted that it is not necessary to measure the absolute magnitude of the signal; it is the shape of the $\phi(r)$ curve that gives the beam profile. Moreover, it is not necessary to know any of the constants in Eq. (4) or Eq. (6). Eqs. (4) and (6) have been derived assuming that the probe beam size is negligible compared to the pump beam size. Experimentally, we find that good agreement with knife-edge method is obtained if the probe beam diameter is kept smaller than about one-half of the pump-beam diameter. Larger probe beams leads to broadening of the curve in Fig. 2.

A measurement of the separation between the two extrema in Fig. 2 yields $a = 0.47$ mm for the radius of the pump beam at its focal spot. Of course, the spatial profile of the pump beam can be measured at any point along its length, and the method is not restricted to measurements at the focal spot. The radius of the beam at the focal spot as measured by the knife-edge technique[5] gave $a = 0.46$ mm. The two values are in excellent agreement within their respective uncertainties. Since $\phi(r)$ is proportional to the gradient of the pump beam spatial profile, this profile can be retrieved very simply by

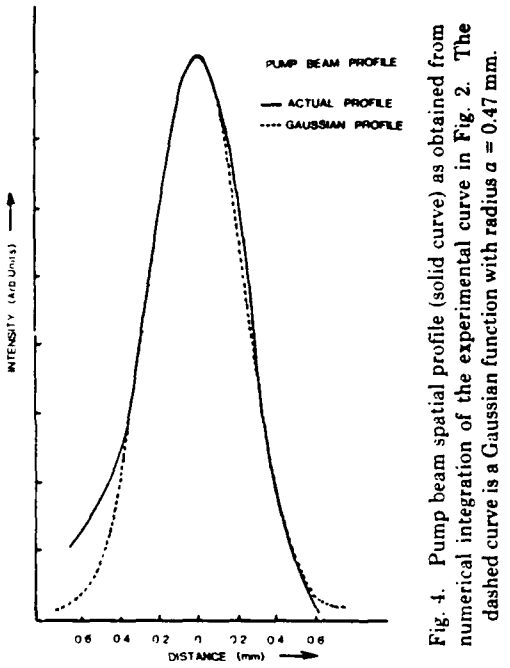

Fig. 4. Pump beam spatial profile (solid curve) as obtained from numerical integration of the experimental curve in Fig. 2. The dashed curve is a Gaussian function with radius $a = 0.47$ mm.

numerical integration of the curve in Fig. 2. The spatial profile of our laser was obtained by adding the successive values of $\phi(r)$ at regularly spaced intervals of r on a pocket calculator, and is shown in Fig. 4 (solid curve). Superimposed on this curve is a Gaussian with $(1/e^2)$ radius of 0.47 mm. We note the spatial profile of our laser is asymmetric and deviates slightly from a true Gaussian profile. When the pump beam profile was measured away from the focal spot, it was found to contain significant amount of light in higher order spatial modes. At the focal spot, however, our probe beam did not have high enough resolution to detect this structure.

It should be noted that it is not necessary to use a transient digitizer for beam profile measurements, since the temporal behavior of the PTD signal is unimportant. A boxcar or simply an oscilloscope may be used to observe the signals. The signals are strong enough that they can easily be observed on an oscilloscope. The method described here may be useful where other methods cannot be used or are inconvenient. For example, the multiphoton ionization technique[12] requires very high laser powers which may not be available, or space limitations or accessibility (for example, inside a vacuum system) may preclude the use of methods like beam-scan techniques.[4–7] The spatial profile of a cw beam can also be measured in an analogous manner. It is useful to point out that NO_2 is a good medium to use in the PTD technique because it has a continuous absorption throughout the visible region of the optical spectrum.

This work was supported by the Air Force Wright Aeronautical Laboratories.

References

1. D. Hull and A. F. Stewart, "Laser Beam Profiles: Experiment and Techniques," Lasers Appl. 4, 71 (1985).
2. I. M. Winer, "A Self-Calibrating Technique for Measuring Laser Beam Intensity Distributions," Appl. Opt. 5, 1437 (1966).
3. D. Milam, "Fluence in 1064-nm Laser Beams: Its Determination by Photography with Polaroid Film," Appl. Opt. 20, 169 (1981).
4. Y. Suzaki and A. Tachibana, "Measurement of the μm Sized Radius of Gaussian Laser Beam Using the Scanning Knife-Edge," Appl. Opt. 14, 2809 (1975).

5. J. M. Khosrofian and B. A. Garetz, "Measurement of a Gaussian Laser Beam Diameter Through the Direct Inversion of Knife-Edge Data," Appl. Opt. **22**, 3406 (1983).
6. D. K. Cohen, B. Little, and F. S. Luecke, "Techniques for Measuring 1-μm Diam Gaussian Beams," Appl. Opt. **23**, 637 (1984).
7. P. J. Shayler, "Laser Beam Distribution in the Focal Region," Appl. Opt. **17**, 2673 (1978).
8. W. L. Smith, A. J. DeGroot, and M. J. Weber, "Silicon Vidicon System for Measuring Laser Intensity Profiles," Appl. Opt. **17**, 3938 (1978).
9. Y. C. Kiang and R. W. Lang, "Measuring Focused Gaussian Beam Spot Sizes: a Practical Method," Appl. Opt. **22**, 1296 (1983).
10. W. B. Veldkamp, "Laser Beam Profile Shaping with Interlaced Binary Diffraction Gratings," Appl. Opt. **21**, 3209 (1982).
11. S.M. Sorscher and M. P. Klein, "Profile of a Focused Collimated Laser Beam near the Focal Minimum Characterized by Fluorescence Correlation Spectroscopy," Rev. Sci. Instrum. **51**, 98 (1980).
12. E. H. A. Granneman and M. J. van der Wiel, "Laser Beam Waist Determination by means of Multiphoton Ionization," Rev. Sci. Instrum. **46**, 332 (1975).
13. W. B. Jackson, N. M. Amer, A. C. Boccara, and D. Fournier, "Photothermal Deflection Spectroscopy and Detection," Appl. Opt. **20**, 1333 (1981).
14. M. V. Klein, *Optics* (Wiley, New York, 1970).
15. A. Rose, R. Vyas, and R. Gupta, "Quantitative Investigation of Pulsed Photothermal Deflection Spectroscopy in Flowing Media," to be published.

Reprinted from Optics Letters, Vol. 13, page 740, September 1988.

Real-time measurement of the spatial profile of a pulsed laser by photothermal spectroscopy

Karen Williams, Paul Glezen, and R. Gupta

Department of Physics, University of Arkansas, Fayetteville, Arkansas 72701

Received February 8, 1988; accepted June 8, 1988

A new method for the measurement of the spatial profile of a pulsed laser is demonstrated. The method is based on the photothermal deflection technique. The spatial profile of a single pulse can be measured in real time.

There is extensive interest in measurements of spatial profiles of pulsed lasers.[1-11] Such measurements are necessary in many diverse fields, such as nonlinear optical processes, laser-induced damage in materials, and development of stable pulsed lasers. In this Letter we demonstrate a new and simple method, based on the technique of photothermal deflection spectroscopy[12,13] (PTDS), to measure the spatial profile of a pulsed laser in real time. The outstanding feature of this technique is that it permits a real-time measurement of each laser pulse. Thus pulse-to-pulse changes in the spatial profile of a laser can be monitored and measured. Since pulse-to-pulse instabilities in pulsed lasers are a widespread problem, and the outcome of many experiments depends critically on the spatial profile of the laser, the development of this technique should prove to be useful. The technique has a wide dynamic range and is nearly nonintrusive.

The photothermal technique is simple in concept and practice, and it is illustrated in Fig. 1. The laser beam whose spatial profile is to be measured (hereafter called the pump beam) passes through a glass cell containing a weak solution of an appropriate dye in a liquid solvent. The dye is chosen such that is partially absorbs the pump beam. The cell is connected to a pump and a reservoir of the dye solution, and the dye solution is continuously circulated through the cell. The laser beam is partially absorbed by the dye solution, which gets slightly heated. The temperature profile of the laser-irradiated region is then a true replica of the intensity profile of the laser beam. The refractive index of the medium in the laser-irradiated region follows the temperature profile, and therefore it acquires a profile that is an image of the laser intensity profile. Since the medium is flowing, this thermal image moves downstream with the flow velocity of the medium. The thermal image broadens owing to thermal diffusion as it moves downstream. However, by a proper choice of the medium, the thermal diffusion broadening can be made negligible compared with the size of the image. In this case, the proper choice is simply a liquid medium rather than a gaseous medium. The thermal image can be probed by a second (and weaker) laser beam, placed a distance x downstream from the pump beam. We refer to this beam as the probe beam. As the thermal image passes by the probe beam, this beam gets deflected by the gradients in the refractive index of the medium created by the absorption of the pump beam. The deflection of the probe beam can easily be monitored by a position-sensitive optical detector. The temporal waveform of the signal is just the derivative of the spatial profile of the pump beam. The temporal waveform can be captured by a transient digitizer. A simple integration of this waveform (which can be accomplished in less than 20 msec) reproduces the spatial profile of the pump beam. Thus the spatial profile of each pulse can be measured in real time.

Assuming that the spatial profile of the pump beam is Gaussian, and that the pulse duration is short (<10 μsec), the PTDS signal shape for the transverse geometry is given by[13-15]

$$\phi_T = -\frac{1}{n_0}\frac{\partial n}{\partial T}\frac{8\alpha E_0}{\sqrt{2\pi}\rho C_p}\frac{(x - v_x t)}{(a^2 + 8Dt)^{3/2}} \times \exp[-2(x - v_x t)^2/(a^2 + 8Dt)]. \quad (1)$$

Appropriate expression for longer pulses can be found elsewhere[14,15] but would not change the essential validity of the conclusions reached here. In Eq. (1), n_0 is the unperturbed refractive index of the medium, $\partial n/\partial T$ is the derivative of the refractive index with respect to temperature evaluated at the ambient temperature,

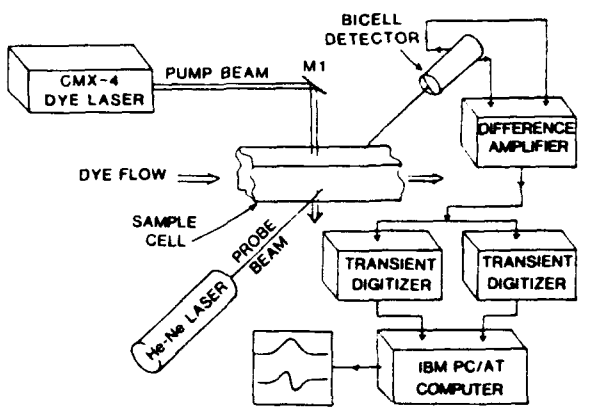

Fig. 1. Schematic illustration of the photothermal deflection experiment for a measurement of the spatial profile of a pulsed laser.

0146-9592/88/090740-03$2.00/0

E_0 is the total energy in the laser pulse, α, ρ, C_p, and D are, respectively, the absorption coefficient, the density, the specific heat at constant pressure, and the diffusion constant of the medium, and a is the $1/e^2$ radius of the pump beam. The flow velocity of the medium is v_x, and x is the distance between the pump and the probe beams. The term $8Dt$ in Eq. (1) represents the broadening of the signal owing to thermal diffusion. For water, $D = 1.4 \times 10^{-7}$ m^2/sec, and if the time of observation $t \simeq 1$ msec (a typical value in our experiments) and $a = 300\ \mu$m, we find that $a^2 \gg 8Dt$. Therefore the term $8Dt$ in Eq. (1) may be neglected in comparison with a^2. For much narrower beams, t may be reduced by increasing the flow velocity v_x so that the above condition remains valid. Under these circumstances, Eq. (1) may be simplified to

$$\phi_T(x, t) = \text{const.} \times \frac{4(x - v_x t)}{a^2} \exp[-2(x - v_x t)^2/a^2]. \tag{2}$$

An examination of Eq. (2) reveals that ϕ_T is simply the derivative of a Gaussian centered at $x = v_x t$. Therefore an integration of $\phi_T(x, t)$ returns the spatial profile of the pump beam, that is,

$$I(x) \propto \int \phi_T(x, t)\mathrm{d}x = v_x \int \phi_T(x, t)\mathrm{d}t. \tag{3}$$

In our experiment, the pump beam was provided by a Chromatix CMX-4 flashlamp-pumped dye laser. This laser produced ~1-μsec-long pulses of radiation, and it was tuned to 490 nm. The sample cell had a cross section of 1 cm × 1 cm and was 5 cm long. A solution of R6G dye in water[16] (1 mg/L) was circulated through the sample cell using a Micropump Model 301902 pump. The pump beam passed through the cell as shown, and it was partially absorbed by the dye solution, creating a thermal image. The thermal image moved downstream with the medium, where it was detected by the probe beam. The probe beam was provided by a Uniphase 0.8-mW He–Ne laser. The pump and the probe beams were transverse to each other and were focused in the region of the sample by lenses of focal lengths 20 and 15 cm, respectively (not shown). The deflection of the probe beam was detected by a Silicon Detector Corporation Model SD-113-24-21-021 bicell detector. The difference signal from the two cells was measured. The probe beam was arranged in such a way that it produced a null signal in the quiescent position of the probe beam. However, shortly after the firing of the pump laser, the deflection of the probe beam was detected as a transient signal from the difference amplifier. This signal was digitized by two LeCroy Model TR8837F transient digitizers connected in parallel. Part of the pump beam was split off by a beam splitter, and it was detected by a P-I-N diode. The output of the P-I-N diode provided the trigger to the transient digitizers. The digitized output was transferred to an IBM PC/AT microcomputer through a LeCroy Model 8901A CAMAC interface. The signals were acquired, stored in the computer, and displayed on the computer monitor using LeCroy Catalyst-Plus software. The signal from one of the digitizers was displayed directly on the computer screen. The identical signal from the other digitizer was first numerically integrated using an assembly-language program and then displayed on the computer screen. This plot represented the spatial profile of the pump beam. In general, it is not necessary to use two digitizers, since it is not necessary to view the raw PTDS data.

Figure 2 shows the typical data. This figure is a reproduction of the computer screen. When these data were taken the laser energy was ~1 mJ. The lower trace shows the raw photothermal deflection data from one of the digitizers. The horizontal scale is 500 μsec/division. The upper trace shows the data from the other digitizer after the data were integrated. Thus the upper trace represents the spatial profile of a single pulse from our laser. A measurement of the beam radius requires that the horizontal scale of the upper trace be known in spatial units (rather than in temporal units). This requires a knowledge of the flow velocity of the medium. Since $\delta x = v_x \delta t$, a knowledge of v_x allows the horizontal axis to be relabeled in spatial units. To this end, v_x was measured for each pulse. The assembly language program mentioned earlier also measured the time interval Δt between the trigger pulse and the arrival time of the PTDS signal at the probe beam (peak of the signal in the upper trace). The velocity was then determined using $v_x = \Delta x/\Delta t$, where Δx was the distance between the pump and the probe beams. Δx was measured once at the beginning of the experiment (and it remained constant throughout the run) in the following way: Mirror M1 was mounted on a calibrated translation stage, and the pump beam was moved until it was concentric ($\Delta x = 0$) with the probe beam. This position was detected by the disappearance of the PTDS signal[14] in a stationary medium (i.e., with the dye pump turned off). This is an extremely sensitive method for the detection of the concentricity of two beams. The calibrated translation stage was moved so as to result in a known Δx (generally ~1 mm).

Fluctuations in the flow velocity, if any, did not affect our measurements, since the velocity was measured for each pulse. The spatial scale (625 μm/division in Fig. 2) was simply determined by multiplying the temporal scale (500 μsec/division) by the measured flow velocity (which was 125 cm/sec in Fig. 2).

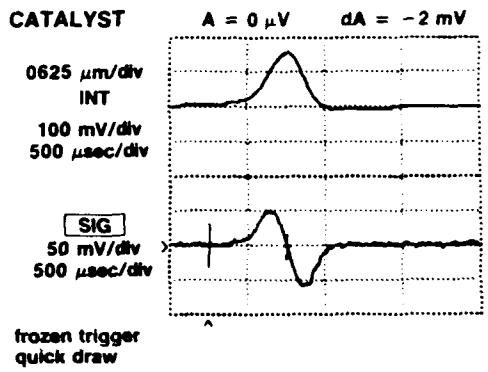

Fig. 2. Typical data. The lower trace is the raw PTDS signal, while the upper trace is the integrated PTDS signal representing the spatial profile of a single laser pulse. The scale for the upper trace is 625 μm/division.

The scale factor, shown to the left of the upper trace (see Fig. 2), was updated every pulse. The procedure for integrating and relabeling the horizontal axis was fast enough that there was no perceptible delay in the display of the integrated data with respect to the raw data. The data (raw as well as integrated) could also be recorded on the hard disk automatically after each pulse for later retrieval. Although we have not done this, a simple modification to the program can be written to fit the experimentally measured profile to a Gaussian (or any other type of profile). As we watched the spatial profile of our laser change from pulse to pulse on the computer screen, we found that the laser had large pulse-to-pulse instabilities. A nearly Gaussian profile of the type shown in Fig. 2 was only obtained about 10% of the time; most of the time the profile had more complicated shapes.

The real advantage of this technique over other techniques is that the spatial profile of an single laser pulse can be measured in real time. Thus pulse-to pulse instabilities, if present, can be monitored. As the laser pulses, the laser profile flashes on the computer screen almost simultaneously. To our knowledge, this is the first technique with this capability. Moreover, a single command at the beginning of the run allows a permanent record of each pulse to be stored automatically on the hard disk for later retrieval. This technique is nearly nonintrusive. If it is required that the spatial profile of a beam be measured while it is being used for an experiment, the sample cell can be inserted between the laser and the experiment and the profile can be monitored while the experiment is being conducted. In other words, since the beam is only partially absorbed by the dye solution, the transmitted beam can be used to do the experiment. Also, there is wide latitude in the power of the beam that can be measured. Moreover, since the amplitude of the PTDS signal is linearly proportional to the laser energy [see Eq. (1)], laser power can also be monitored simultaneously with the beam profile. There are, however, two limitations of the technique. The first limitation is that the probe beam must be considerably narrower than the beam whose profile is to be measured; otherwise the measured profile would be artificially broadened. This can always be arranged except for the very narrow beams. In our experiment, no particular attempt was made to narrow the probe beam. The probe-beam radius was ~0.1 mm, while the pump-beam radius was 0.28 mm. The second, and perhaps more serious, limitation is that a *true* spatial profile is obtained only for Gaussian beams. For other profiles (particularly nonaxisymmetric beams), only an approximate profile is obtained. For nearly Gaussian beams, however, deviation from being Gaussian can be determined quite well. Moreover, for Gaussian beams, the radius can be measured quite accurately. The second limitation is common with that of several other techniques (e.g., the knife-edge technique).

If proper instrumentation (e.g., a transient digitizer interfaced to a computer) is not available for the above experiment, two alternative methods can be used to measure the profile. In the first method, the PTDS signal can be integrated electronically. The integrated signal can then be observed on an oscilloscope. The second method involves a straightforward modification of the PTDS technique. Instead of measuring the gradient of the refractive index, as is done in PTDS, one can measure the change in the refractive index produced by the pump-beam absorption directly. Then it is not necessary to integrate the signal in order to obtain the spatial profile, and a transient digitizer is not necessary. The signal can be observed simply on an oscilloscope. In this method of detection, photothermal phase-shift spectroscopy,[15,17] the sample cell is placed in one arm of a Michelson interferometer. As the thermal image of the pump beam passes by the probe beam, a fringe shift is produced that is detected as an intensity change. For small changes in the refractive index, the signal shape reproduces the laser intensity profile.[15] We have given a quick trial to this method and have observed the signal. However, we have not seriously pursued this method of detection. We merely wish to point out that photothermal phase-shift spectroscopy is an alternative method if the proper instrumentation for PTDS is not available.

This research was supported in part by the U.S. Air Force Wright Aeronautical Laboratories.

References

1. See, e.g., J. M. Fleischer and C. B. Hitz, Lasers Optron. **6**, 60 (1987); R. L. Rypma, Photon. Spectra **21**, 67 (1987); D. Hull and A. F. Stewart, Lasers Appl. **4**, 71 (1988).
2. I. M. Winer, Appl. Opt. **5**, 1437 (1966).
3. D. Milam, Appl. Opt. **20**, 169 (1981).
4. Y. Suzaki and A. Tachiban, Appl. Opt. **14**, 2809 (1975).
5. J. M. Khosrofian and B. A. Garetz, Appl. Opt. **22**, 3406 (1983).
6. D. K. Cohen, B. Little, and F. S. Luecke, Appl. Opt. **23**, 637 (1984).
7. W. L. Smith, A. J. DeGroot, and M. J. Weber, Appl. Opt. **17**, 3938 (1978).
8. Y. C. Kiang and R. W. Lang, Appl. Opt. **22**, 1296 (1983).
9. A. A. McInnes and A. D. Wilson, J. Phys. E **20**, 458 (1987).
10. A. Rose, Y.-X. Nie, and R. Gupta, Appl. Opt. **25**, 1738 (1986).
11. While a two-dimensional video image of the beam may be obtained in real time using, e.g., a solid-state-array camera, a graph of the intensity profile generally cannot be obtained in real time. Also, these method are intrusive and, because of poor resolution, are not useful for focused beams.
12. See, e.g., R. Gupta, in *Proceedings of the International Conference on Lasers '86*, R. W. McMillan, ed. (STS, McLean, Va., 1987), p. 379.
13. H. Sontag and A. C. Tam, Opt. Lett. **10**, 436 (1985).
14. A. Rose, R. Vyas, and R. Gupta, Appl. Opt. **25**, 4626 (1986).
15. R. Gupta, in *Photothermal Investigations of Solids and Fluids*, J. A. Sell, ed. (Academic, New York, to be published).
16. Since this experiment was performed, it has been brought to our attention that other solvents and dyes may be more appropriate for this purpose. Some organic solvents have a much larger $\partial n/\partial T$, and nonfluorescent dyes would convert the absorbed optical energy to heat more efficiently.
17. C. C. Davis, Appl. Phys. Lett. **36**, 515 (1980).

Reprinted from Applied Optics, Vol. 27, page 4701, November 15, 1988

Photothermal lensing spectroscopy in a flowing medium: theory

Reeta Vyas and R. Gupta

A complete and general theoretical description of dual-beam photothermal lensing spectroscopy is given. The results are valid for the most general conditions, that is, for flowing as well as stationary media, and for cw as well as pulsed excitation. For pulsed excitation, the results are valid for arbitrary pulse length. The cw results apply to both modulated as well as unmodulated excitation. Both transverse and collinear geometries are considered.

I. Introduction

In this paper we present the theory of dual-beam photothermal lensing spectroscopy (PTLS) in a fluid medium valid for the most general conditions, that is, for flowing as well as stationary media and for cw as well as pulsed excitation. For pulsed excitation, the pulse length is arbitrary, and for cw excitation both the modulated and the unmodulated sources are considered. Both the transverse and the collinear geometries are considered. A unified treatment of all cases is presented. This is the first comprehensive treatment of this important subject.

The basic idea underlying dual-beam PTLS is shown in Fig. 1. A laser beam (pump beam) propagates through a medium, and it is tuned to one of the absorption frequencies of the medium. The medium absorbs some of the optical energy from the laser beam. If the collision rate in the medium is sufficiently high compared to the radiative rates, most of the energy appears in the translational–rotational modes of the medium within a short period of time. In other words, the laser-irradiated region gets slightly heated. The refractive index of the medium is thus modified. The refractive-index change can be monitored in several different ways.[1] In this paper, we are concerned with a technique that relies on the lensing effect of the medium to monitor the refractive-index change. A weak probe beam passes through the pump-irradiated region, as shown in Fig. 1. Due to the curvature of the refractive index, the probe beam diverges, which can be detected as a change in the intensity of the probe beam passing through a pinhole. In other words, under the influence of the pump beam, the medium acts like a diverging lens. In certain circumstances, the medium acts like a converging lens also. If a pulsed pump laser is used, a transient lens is formed; the probe beam changes shape shortly after the pump beam is fired and returns to its original shape on the time scale of the diffusion of heat from a probe region. If a cw laser is used, it is generally convenient to amplitude modulate its intensity, and the PTLS signal consists of oscillations in the intensity of the probe beam passing through the pinhole. The PTLS takes on more interesting dimensions if a flowing medium is used. The PTLS technique has been discussed extensively in the literature for trace detection of chemicals,[2] and the use of PTLS in a flowing medium has recently been demonstrated for flow velocity measurements.[3] Although the thermal lensing effect may also be observed by monitoring the pump beam itself, in this paper we only consider the dual-beam technique in which the thermal lens is created by the pump beam and monitored by the probe beam.

The photothermal lensing effect was observed accidentally by Gordon *et al.*[4] in 1964 when they placed a cell filled with a liquid sample inside a He–Ne laser cavity. These authors correctly identified the effect and gave a theoretical description of it. In 1973, Hu and Whinnery[5] gave a detailed theoretical description of the effect for an extracavity sample and determined that the maximum signal occurred when the sample cell was placed one confocal distance away from the waist of the beam. They also demonstrated the usefulness of this technique for measurements of small absorptivities. A cw laser was used, and a shutter was employed to effect the change necessary to observe the

The authors are with University of Arkansas, Physics Department, Fayetteville, Arkansas 72701.
Received 6 June 1988.
0003-6935/88/224701-11$02.00/0.

signal. Flynn and collaborators,[6] on the other hand, used a pulsed laser (a Q-switched CO_2 laser) and introduced the dual-beam technique, that is, a pump beam to create a change in the refractive index and a probe beam to monitor the change. They used PTLS to measure V-T/R relaxation rates in CH_3F and other molecules. The dual-beam technique offers significant advantages over the single-beam technique, because the pump and probe beams can be manipulated separately. Twarowski and Kliger[7] in 1977 gave a theoretical description of the pulsed PTLS in the impulse approximation, that is, assuming that the excitation pulse is essentially a delta function. Swofford and collaborators,[8,9] on the other hand, gave the theory of a repetitively pulsed excitation. All the above authors considered only the collinear pump and probe beams since they were interested in maximizing the signal and spatial resolution was not a consideration. Dovichi *et al.*[10] for the first time considered transverse PTLS (probe beam perpendicular to the pump beam) for both single-pulse and repetitively pulsed excitation. Recently, Weimer and Dovichi[9,11] have given the theory of PTLS in a flowing medium for delta-function and repetitively pulsed excitations. Bialkowski[12] has considered the effect of the finite probe beam radius (which in practice may be comparable with the pump beam radius) using a phase-shift method. A very readable account of PTLS is given by Harris and Dovichi,[13] an excellent review is given by Fang and Swofford,[2] and a more recent review is given by Bialkowski.[14]

The work presented in this paper is significant for the following reasons: A coherent treatment of PTLS in the most general conditions is given. A flowing medium is considered. Therefore, the results for a stationary medium are simply a special case (flow velocity = 0). Using the Green's function method, both the cw excitation (with or without modulation) and the pulsed excitation are treated on the same footing. Moreover, the results for the pulsed case are just as valid as for a long pulse as for a delta function pulse. Collinear PTL, which acts like a spherical lens (which may be astigmatic), and transverse PTL, which acts like a cylindrical lens, are treated in a unified way. The treatment is general enough that it includes cases where the axes of the pump and the probe beams do not intersect. Absolute values of the signals are computed for ease of comparison with experiment. Although a few results given here have been published before,[2-14] many other results are new and/or more general. Furthermore, the treatment unifies the theory of PTLS with the theory of photothermal deflection spectroscopy (PTDS) presented earlier.[15]

In Sec. II we derive expressions for the temperature distribution produced by the absorption of pulsed and cw laser beams. Expressions for the focal length of a medium with nonuniform refractive index are derived in Sec. III, and formal expressions for PTLS signal amplitudes are derived in Sec. IV. Explicit expressions for PTLS signals are derived and the results discussed in Sec. V.

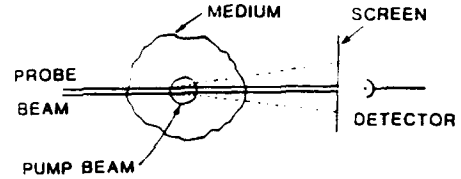

Fig. 1. Schematic illustration of the photothermal lensing effect.

II. Temperature Distribution

The temperature distribution created by the absorption of the pump beam is given by the solution of the differential equation[1]:

$$\frac{\partial T(\mathbf{r},t)}{\partial t} = D\nabla^2 T(\mathbf{r},t) - v_x \frac{\partial T(\mathbf{r},t)}{\partial x} + \frac{1}{\rho C_p} Q(\mathbf{r},t), \tag{1}$$

where $T(\mathbf{r},t)$ is temperature above the ambient, D is the diffusivity, ρ is the density, and C_p is the specific heat at constant pressure of the medium. v_x is the flow velocity of the medium, assumed to be in the x-direction, and $Q(\mathbf{r},t)$ is the source term. The first, second, and third terms on the right in Eq. (1) represent, respectively, the effects of the thermal diffusion, flow, and heating due to the pump beam absorption. If a pulsed laser is used, the heat produced per second per unit volume by the absorption of laser energy $Q(\mathbf{r},t)$ is given by

$$Q(\mathbf{r},t) = \alpha I(\mathbf{r},t) = \begin{cases} \dfrac{2\alpha E_0}{\pi a^2 t_0} \exp(-2r^2/a^2) & \text{for } 0 \le t \le t_0, \\ 0 & \text{for } t > t_0. \end{cases} \tag{2}$$

Here α is the absorption coefficient of the medium and the medium is assumed to be optically thin (weakly absorbing). $I(\mathbf{r},t)$ is the intensity of the beam with total energy per pulse being E_0. The spatial profile of the pump beam is assumed to be a Gaussian with $1/e^2$ radius a. It is further assumed that the laser pulse turns on sharply at $t = 0$ and turns off sharply at $t = t_0$. The assumption of a rectangular temporal profile is a good one, if the rise and fall times of the pulse are very short compared to the thermal diffusion and convection times.

For cw laser beams $Q(\mathbf{r},t)$ is given by

$$Q(\mathbf{r},t) = \frac{2\alpha P_{av}}{\pi a^2} [\exp(-2r^2/a^2)](1 + \cos\omega t), \tag{3}$$

where again the medium is assumed to be optically thin and the laser beam is assumed to have a Gaussian spatial profile with $1/e^2$ radius a. Moreover, the beam is assumed to be sinusoidally modulated at a frequency $f = \omega/2\pi$ to permit phase-sensitive (lock-in) detection. Results for an unmodulated beam may be obtained by simply setting $\omega = 0$ in Eq. (3). The average power of the laser beam is P_{av}, i.e., the laser power oscillates between 0 and $P_0 = 2P_{av}$.

We assume that the pump beam propagates in the z-direction. If there are no inhomogeneities in the medium along the pump beam, Eq. (1) may be solved in two dimensions (x and y). The boundary conditions are

$$T(x,y,t)|_{t=0} = 0;\ T'(x,y,t)|_{t=0} = 0,$$

$$T(x,y,t)|_{x,y\to\pm\infty} = 0;\ T(x,y,t)|_{z\to\infty} = 0, \tag{4}$$

where the laser is turned on at $t = 0$ and T' represents the gradient of the temperature. The solution of Eq. (1) is given by

$$T(x,y,t) = \int_{-\infty}^{+\infty}\int_{-\infty}^{+\infty}\int_{0}^{\infty} Q(\xi,\eta,\tau)G(x/\xi,y/\eta,t/\tau)\,d\xi\,d\eta\,d\tau, \tag{5}$$

where G is the Green's function appropriate for Eq. (1) and the functional form of Q is given by Eq. (2) for a pulsed laser and it is given by Eq. (3) for a cw laser. The Green's function satisfies the differential equation

$$-D\nabla_{r}^{2}G + v_{r}\frac{\partial G}{\partial x} + \frac{\partial G}{\partial t} = \frac{1}{\rho C_{p}}\delta(x-\xi)\delta(y-\eta)\delta(t-\tau) \tag{6}$$

with appropriate boundary conditions. The solution of Eq. (6) has been found by Rose *et al.*[15] in connection with pulsed photothermal deflection spectroscopy to be

$$G = \frac{H_{\tau}(t)}{4\pi\rho C_{p}D(t-\tau)}\exp(-|x-[\xi+v_{r}(t-\tau)]|^{2}/[4D(t-\tau)])$$
$$\times \exp(-(y-\eta)^{2}/[4D(t-\tau)]), \tag{7}$$

where $H_{\tau}(t)$ is the unit step function. Substitution of Eq. (7) in Eq. (5), along with Eqs. (2) or (3), lead to the desired temperature distributions

$$T(x,y,t) = \frac{2\alpha E_{0}}{\pi t_{0}\rho C_{p}}\int_{0}^{t_{0}}\frac{1}{[8D(t-\tau)+a^{2}]}$$
$$\times \exp[-2[|x-v_{r}(t-\tau)]^{2} + y^{2}]/[8D(t-\tau)+a^{2}]]\,d\tau \quad \text{for } t > t_{0} \tag{8}$$

for the pulsed case, and

$$T(x,y,t) = \frac{2\alpha P_{av}}{\pi\rho C_{p}}\int_{0}^{t}\frac{(1+\cos\omega\tau)}{[8D(t-\tau)+a^{2}]}$$
$$\times \exp(-2[|x-v_{r}(t-\tau)|^{2}+y^{2}]/[8D(t-\tau)+a^{2}])\,d\tau \tag{9}$$

for the cw case. Equations (8) and (9) must be evaluated numerically except in certain special cases. Equations (8) and (9) have been derived for a laser with a Gaussian spatial profile for convenience and also because this type of profile is most commonly used. However, our method is completely general, as the Green's function is independent of the source term. Expressions analogous to Eqs. (8) and (9) for other types of spatial profile may be derived in a similar manner.

III. Focal Length of the Thermal Lens

In this section we derive expressions for the focal length of the thermal lens. Consider a medium of length l with refractive index $n(x,y)$ which varies with x and y, as shown in Fig. 2. This figure illustrates the case where the refractive index increases with x, although the results have general applicability. $x = y = 0$ corresponds to the axis of the pump beam. We assume that the length of the medium l is very small

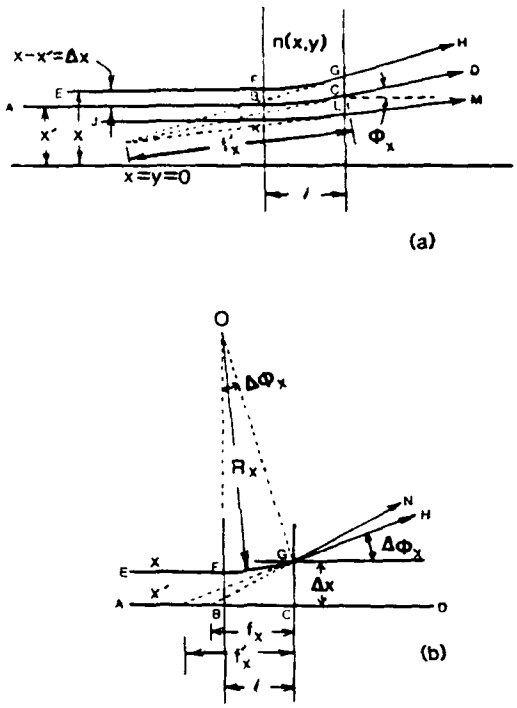

Fig. 2. Focal length of a thermal lens.

compared with the focal length of the medium (thin lens approximation). An optical beam (probe beam) centered at x' is incident normally at the left interface, follows a curved trajectory inside the medium, and arrives at the right interface making an angle ϕ_x with the normal, as shown in Fig. 2(a). *ABCD* represents an optical ray at the center of the probe beam. *EFGH* and *JKLM* represent two other optical rays in the probe beam at distances $\pm\Delta x$ from the center of the probe beam. The deflection of the rays is caused by a nonuniform refractive index (nonzero $\partial n/\partial x$). If $\partial n/\partial x$ itself varies with x (nonzero $\partial^{2}n/\partial x^{2}$), the deflection ϕ_x varies with x. The situation can be analyzed as a deflection of the probe beam by an angle $\phi_x(x')$ and a focusing (a defocusing) with focal length f'_x, as shown in the figure. Our aim is to derive an expression for f'_x.

The propagation of an optical ray in an inhomogeneous medium is given by the ray equation[16]

$$\frac{d}{ds}\left(n_{0}\frac{d\delta}{ds}\right) = \nabla_{\perp}n(x,y,t), \tag{10}$$

where s represents the path of the optical beam, δ is the deviation of the beam from its original path, and $\nabla_{\perp}n(x,y,t)$ is the gradient of the refractive index perpendicular to the beam path. We have made an approximation in Eq. (10) by replacing $n(x,y,t)$ by the unperturbed refractive index n_0 on the left-hand side. Consider the deflection of the ray in the x-direction:

$$\frac{d}{ds}\left(n_{0}\frac{d\delta_{x}}{ds}\right) = \frac{\partial n}{\partial x} \tag{10a}$$

or

$$\phi_{x}(x,y) = \frac{1}{n_{0}}\int\frac{\partial n}{\partial x}\,ds. \tag{11}$$

where $\phi_x(x,y)$ is the deflection angle. The refractive index $n(x,y)$ may be expanded in a Taylor series about a point on the axis of the probe beam (x',y'):

$$n(x,y) = n(x',y') + (x - x')\left(\frac{\partial n}{\partial x}\right)_{x',y'} + (y - y')\left(\frac{\partial n}{\partial y}\right)_{x',y'} + \frac{(x - x')^2}{2}\left(\frac{\partial^2 n}{\partial x^2}\right)_{x',y'} + \frac{(y - y')^2}{2}\left(\frac{\partial^2 n}{\partial y^2}\right)_{x',y'} + (x - x')(y - y')\left(\frac{\partial^2 n}{\partial x \partial y}\right)_{x',y'} + \cdots \quad (12)$$

The use of Eq. (12) in Eq. (11) yields

$$\phi_x(x,y') = \frac{1}{n_0}\int \left(\frac{\partial n}{\partial x}\right)_{x',y'} ds + \frac{1}{n_0}\int (x - x')\left(\frac{\partial^2 n}{\partial x^2}\right)_{x',y'} ds, \quad (13)$$

where we have neglected the higher order terms. We may write $\phi_x(x,y')$ as

$$\phi_x(x,y') = \phi_x(x',y') + (x - x')\frac{\partial \phi_x}{\partial x}. \quad (14)$$

Substitution of Eq. (14) in Eq. (13) leads to

$$\phi_x(x',y') = \frac{1}{n_0}\int \left(\frac{\partial n}{\partial x}\right)_{x',y'} ds, \quad (15a)$$

$$(x - x')\frac{\partial \phi_x}{\partial x} = \frac{1}{n_0}\int (x - x')\left(\frac{\partial^2 n}{\partial x^2}\right)_{x',y'} ds. \quad (15b)$$

Equation (15a) simply represents the deflection of the probe beam. For the present discussion, it is of no interest to us, and we shall ignore it. Equation (15b) represents the focusing of the beam, and we shall rewrite it in terms of the effective focal length of the medium. To this end, we rewrite Eq. (15b) as

$$\frac{d}{ds}(\Delta\phi_x) = \frac{1}{n_0}\left(\frac{\partial^2 n}{\partial x^2}\right)_{x',y'} \Delta x, \quad (16)$$

where $\Delta x = (x - x')$, and $\Delta\phi_x = \phi_x(x) - \phi_x(x')$ is illustrated in Fig. 2(b). In this diagram the center ray $ABCD$ is shown by a straight line, since we are ignoring the deflection of the beam given in Eq. (15a). Referring to this diagram we note that

$$\frac{1}{f_x} = \frac{\Delta\phi_x}{\Delta x}, \quad (17)$$

and the radius of curvature R_x is given by $ds = R_x d(\Delta\phi_x)$. We immediately identify the left side of Eq. (16) as $1/R_x$. Moreover, $R_x\Delta\phi_x \simeq l$; therefore,

$$\frac{1}{f_x} = -\frac{l}{R_x \Delta x} = -\frac{1}{n_0}\left(\frac{\partial^2 n}{\partial x^2}\right)_{x',y'} l. \quad (18)$$

Actually, due to refraction at the right interface, the ray does not travel along GH; it travels along GN. Therefore, the effective focal length is given by f_x, where f_x is given by f_x/n_0. Therefore, we obtain

$$\frac{1}{f_x} = -\left(\frac{\partial^2 n}{\partial x^2}\right)_{x',y'} l. \quad (19)$$

In photothermal spectroscopy, the variation in the refractive index is caused by the temperature change. Therefore, we may write $n(x,y,t)$ as

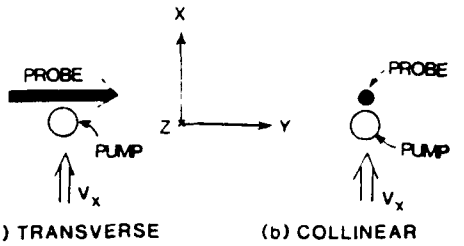

Fig. 3. Pump–probe beam configuration for (a) transverse, (b) collinear photothermal lensing spectroscopy.

$$n(x,y,t) = n_0 + \left.\frac{\partial n}{\partial T}\right|_{T_A} T(x,y,t), \quad (20)$$

where T_A is the ambient temperature. Therefore, f_x may be written as

$$\frac{1}{f_x} = -\frac{\partial n}{\partial T}\left(\frac{\partial^2 T}{\partial x^2}\right)_{x',y'} l. \quad (21)$$

Finally, if $(\partial^2 T/\partial x^2)$ is not constant over the path of the probe beam, Eq. (21) may be generalized as

$$\frac{1}{f_x} = -\frac{\partial n}{\partial T}\int_{\text{path}} \left(\frac{\partial^2 T}{\partial x^2}\right)_{x',y'} ds. \quad (22)$$

A similar expression for f_y may be found analogously.

We consider two situations as illustrated in Fig. 3. We assume that the pump beam propagates along the z axis, and the medium is flowing in the x-direction, as previously stated. Two cases considered are: Transverse PTLS shown in Fig. 3(a), in which the probe beam propagates in the y-direction, and the collinear PTLS shown in Fig. 3(b), in which the probe beam propagates in the z-direction. In both cases, the probe beam may be displaced with respect to the pump beam in the x-direction by an arbitrary distance x'. The case of an arbitrary angle between the pump and probe beams will not be considered here. The case of an arbitrary angle can be treated in a manner analogous to that discussed by Rose *et al.*[15] in connection with photothermal deflection spectroscopy. Referring to Fig. 3, it is obvious that in general an astigmatic lens is formed in a flowing medium. In particular, a cylindrical lens is formed in the case of a transverse PTLS. For the cases illustrated in Fig. 3 we may write f_x and f_y for the collinear PTLS as

$$\frac{1}{f_x} = -\frac{\partial n}{\partial T} l \left(\frac{\partial^2 T}{\partial x^2}\right)_{\substack{x=x' \\ y=0}}, \quad (23a)$$

$$\frac{1}{f_y} = -\frac{\partial n}{\partial T} l \left(\frac{\partial^2 T}{\partial y^2}\right)_{\substack{x=x' \\ y=0}}. \quad (23b)$$

Similarly, for the transverse PTLS, the focal lengths f_x and f_z are given by

$$\frac{1}{f_x} = -\frac{\partial n}{\partial T}\int \left(\frac{\partial^2 T}{\partial x^2}\right)_{x=x'} dy, \quad (24a)$$

$$\frac{1}{f_z} = 0. \quad (24b)$$

IV. Detection of the Thermal Lens

In this section an expression for the change in the intensity of a probe beam passing through a thermal lens is derived. A typical configuration for the detection of a thermal lens is shown in Fig. 4. The thermal lens is placed a distance z_1 in front of the probe beam waist. A screen with a pinhole is placed a distance z_2 in front of the thermal lens. The intensity of the probe beam passing through the pinhole of radius b is observed by a photodetector. To begin, we assume that the thermal lens has cylindrical symmetry with respect to the probe beam. Later we will generalize the results to include astigmatic lenses. Let w_0 be the $1/e^2$ radius of the probe beam at its waist and w_1 and w_2 be the radii at the positions of the thermal lens and the screen, respectively. When the thermal lens is activated (by turning on the pump beam), w_2 changes, resulting in a change of intensity at the detector. Our aim is to derive an expression for the signal $s(t)$ in terms of the focal length $f(t)$ of the thermal lens, where $s(t)$ is defined as

$$s(t) = \frac{P_{det}(t) - P_{det}(0)}{P_{det}(0)}. \tag{25}$$

$P_{det}(t)$ is the power at the detector at time t. Time $t = 0$ represents the instant before the laser is turned on. For the cw case, the time t at which the observation is made is generally large compared with the thermal diffusion time. For the pulsed case, t is greater than t_0. Assuming that the probe beam has a Gaussian spatial profile, the radial intensity distribution of the probe beam at the screen is given by

$$I(r) = \frac{2P}{\pi w_2^2} \exp(-2r^2/w_2^2), \tag{26}$$

where P is the power of the probe beam. Then

$$P_{det} = \int_0^b I(r) 2\pi r dr \simeq 2P \frac{\pi b^2}{\pi w_2^2}. \tag{27}$$

The signal $s(t)$ is then given by

$$s(t) = \frac{w_2^2(0) - w_2^2(t)}{w_2^2(0)}, \tag{28}$$

where we have replaced $w_2(t)$ by $w_2(0)$ in the denominator because the change in the radius of the beam is small.

$w_2(t)$ may be found using the $ABCD$ law.[17] The complex beam parameter q_2 at the position of the screen is given in terms of the parameter q_0 at the beam waist by

$$q_2 = \frac{Aq_0 + B}{Cq_0 + D}, \tag{29}$$

where A, B, C, and D are the elements of the transformation matrix representing translation by a distance z_1, focusing by a lens of focal length f, and a translation by a distance z_2, that is,

$$\begin{bmatrix} A & B \\ C & D \end{bmatrix} = \begin{bmatrix} 1 & z_2 \\ 0 & 1 \end{bmatrix} \begin{bmatrix} 1 & 0 \\ -1/f & 1 \end{bmatrix} \begin{bmatrix} 1 & z_1 \\ 0 & 1 \end{bmatrix}. \tag{30}$$

The complex beam parameter q is defined as

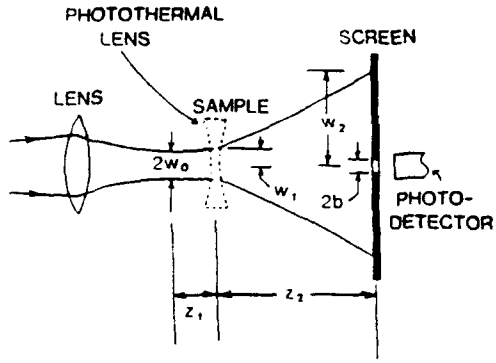

Fig. 4. Detection of a photothermal lens.

$$\frac{1}{q} = \frac{1}{R} - \frac{i\lambda}{\pi n w^2}, \tag{31}$$

where R is the radius of the phase front, n is the refractive index of the medium, and λ is the wavelength of the probe beam. Using Eqs. (29)–(31), $w_2^2(t)$ is found to be

$$w_2^2(t) = w_0^2 \left[\left(1 - \frac{z_2}{f}\right)^2 + \frac{1}{z_0^2} \left(z_1 + z_2 - \frac{z_1 z_2}{f}\right)^2 \right], \tag{32}$$

where $z_0 = \pi n w_0^2/\lambda$ is the confocal distance. Remembering that at $t = 0$, $f(0) = \infty$, we may use Eq. (32) in Eq. (28) to obtain the final expression for $s(t)$ as

$$s(t) = \frac{2z_2}{f(t)[z_0^2 + (z_1 + z_2)^2]} \times \left[z_1^2 + z_0^2 + z_1 z_2 - \frac{z_2}{2f(t)} (z_0^2 + z_1^2) \right]. \tag{33}$$

In the following we will use the approximation that $z_2 \gg z_1$ and $z_2 \gg z_0$ (which can generally be arranged) and that $f(t) \gg z_1$ and z_0 (which is generally the case). Under these assumptions, Eq. (33) is greatly simplified:

$$s(t) = \frac{2z_1}{f(t)}. \tag{34}$$

Consider now an astigmatic thermal lens. In this case the beam radius w_2 is different in two orthogonal directions. Equation (27) modifies to

$$P_{det} = 2P \frac{\pi b^2}{\pi w_x w_y}, \tag{35}$$

where w_x and w_y are the beam radii in the x and the y directions, respectively. The signal $s(t)$ is then given by

$$s(t) = \frac{w_x(0)w_y(0) - w_x(t)w_y(t)}{w_x(0)w_y(0)}. \tag{36}$$

Under the assumptions $z_2 \gg z_1$ and $z_2 \gg z_0$, Eq. (32) may be simplified to yield

$$w_x(t) = \frac{w_0 z_2}{z_0} \left[1 - \frac{z_1}{f_x(t)} \right] \tag{37}$$

and a similar expression for $w_y(t)$. Substitution of Eq.

(37) in (36), along with the assumptions $f_y(t) \gg z_1$ and $f_x(t) \gg z_1$, leads to the final expression

$$s(t) = \frac{z_1}{f_x(t)} + \frac{z_1}{f_y(t)}, \tag{38}$$

where $f_x(t)$ and $f_y(t)$ are given by Eqs. (23a) and (23b).

V. Results

In this section explicit expressions for PTLS signals are derived and the theoretical results are discussed. Implicit in our treatment is the assumption that the pump beam diameter remains constant over the interaction length. Pulsed PTLS is discussed in Sec. V.A while cw PTLS is discussed in Sec. V.B.

A. Pulsed PTLS

1. *Collinear Case*

The PTLS signal is given by Eq. (38) where f_x and f_y are given by Eqs. (23a) and (23b). Substitution of $T(x,y,t)$ from Eq. (8) leads to the final expression

$$s_l(x,t) = \frac{8\alpha E_0 l z_1}{\pi\rho C_p t_0}\left(\frac{\partial n}{\partial T}\right)\int_0^{t_0} \frac{1}{[a^2 + 8D(t-\tau)]^2} \times \left\{2 - \frac{4[x - v_x(t-\tau)]^2}{[a^2 + 8D(t-\tau)]}\right\} \times \exp\{-2[x - v_x(t-\tau)]^2/[a^2 + 8D(t-\tau)]\}d\tau, \tag{39}$$

where we have dropped the prime on x for convenience. The τ-integral cannot be evaluated analytically, and it must be evaluated numerically. We have evaluated Eq. (39) using the method of 64-point Gaussian quadrature. The equation may also be conveniently evaluated using a subroutine named DCADRE available in the International Mathematical and Statistical Library (IMSL). The results are shown in Figs. 5 and 6. Before we discuss Figs. 5 and 6, it is worth noting that Eq. (39) can be expressed in a closed form for very short laser pulses (impulse approximation). If the laser pulse is very short, we may use

$$\lim_{t_0 \to 0} \int_0^{t_0} f(\tau)d\tau = f(0)t_0 \tag{40}$$

to express $s_l(x,t)$ as

$$s_l(x,t) = \frac{8\alpha E_0 l z_1}{\pi\rho C_p}\left(\frac{\partial n}{\partial T}\right)\frac{1}{(a^2 + 8Dt)^2}\left[2 - \frac{4(x - v_x t)^2}{(a^2 + 8Dt)}\right] \times \exp[-2(x - v_x t)^2/(a^2 + 8Dt)]. \tag{41}$$

Equation (41) is very convenient as it is in closed form. However, caution must be used in its use for laser pulses of ≥ 10 μs duration (see below). Rose *et al.*[15] have discussed the limits of validity of impulse approximation in connection with photothermal deflection spectroscopy.

Figure 5 shows the collinear PTLS signals in a stationary medium. The medium is assumed to be N_2 at atmospheric pressure, seeded with 1000-ppm NO_2 to make the medium absorbing in the visible region (absorption coefficient $\alpha = 0.39\ m^{-1}$ at 490 nm). In this medium $\rho C_p = 1218\ J\ m^{-3}\ K^{-1}$, $D = 2.04 \times 10^{-5}\ m^2\ s^{-1}$, $n_0 = 1.000294$, and $\partial n/\partial T = 9.4 \times 10^{-7}\ K^{-1}$. The pump laser is assumed to give 1-μs long pulses. The interaction length of the pump and the probe beams is $l = 1$ cm. The pump beam radius a is assumed to be 0.5 mm. The probe beam radius does not enter the calculation. However, it is assumed to be much smaller than the pump beam radius. Five different curves corresponding to five different positions of the probe beam are plotted. Consider the curve corresponding to $x = 0$ (the pump and the probe beams coaxial) first. The

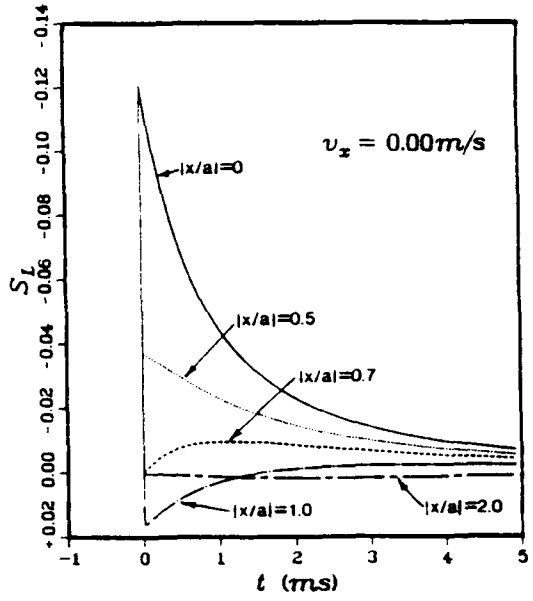

Fig. 5. Pulsed collinear PTLS signals in a stationary medium. The signal is plotted as a function of time for various pump–probe separations. The laser energy was assumed to be 6 mJ, and all other parameters used in this calculation are given in the text.

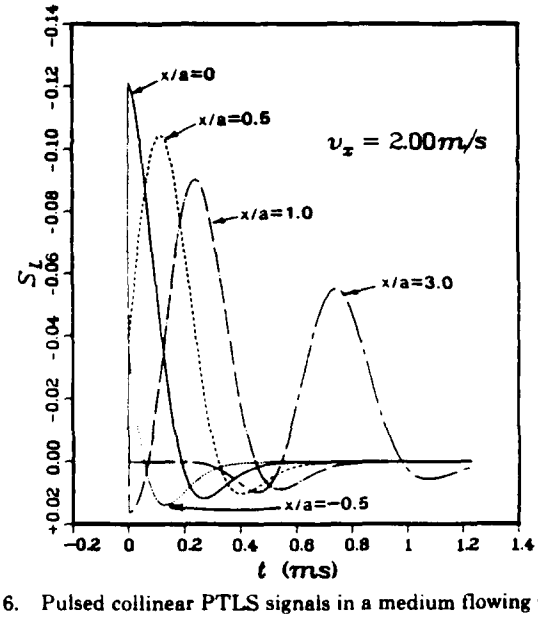

Fig. 6. Pulsed collinear PTLS signals in a medium flowing with a velocity of 2 m/s. Negative x corresponds to the probe beam being upstream from the pump beam.

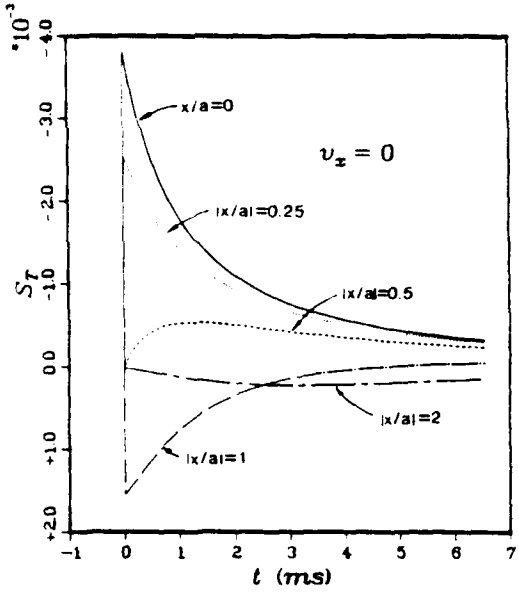

Fig. 7. Pulsed transverse PTLS signals in a stationary medium.

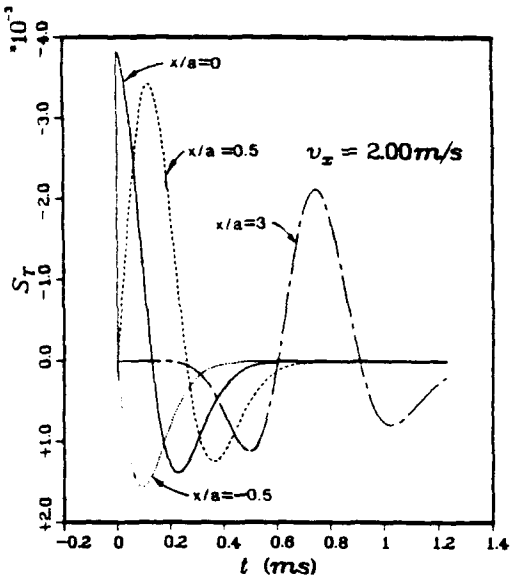

Fig. 8. Pulsed transverse PTLS signals in a flowing medium.

shape of the signal suggests that the intensity at the detector is sharply reduced at the instant of pump laser firing ($t = t_0$) and returns to its original value on the time scale of the thermal diffusion time. The decrease in the intensity at the detector [negative value of $s_L(t)$] suggests that the photothermal lens formed is a diverging lens. As $|x|$ is increased, the power of the thermal lens decreases until it is zero at $|x| = 0.707a$. s_L goes to zero at $t = t_0$ but regains a nonzero value for $t > t_0$ due to the diffusion of heat from the interior of the pump beam irradiated region. For $|x| > 0.707a$, the signal sign inverts, indicating that the thermal lens formed is a converging lens. When the probe beam is outside the pump beam ($x \geq 2a$), the signal becomes very small and its peak value occurs late in time.

Figure 6 shows the collinear PTLS signal in a medium flowing with velocity $v_x = 2$ m/s. All other parameters used in this calculation are the same as those for Fig. 5. Again, five curves are shown for different values of the pump–probe distance x, as labeled. The figure shows that a photothermal lens is formed, which is diverging in the center ($|x| < 0.707a$) and converging in the wings ($|x| > 0.707a$). The lens travels downstream with the flow of the medium. The probe beam samples this lens as the lens goes past it. The entire lens is observable at $x = 3a$, as shown. The asymmetric wings result from the thermal diffusion.

2. *Transverse PTLS*

In transverse PTLS, a cylindrical lens is formed, and, using Eq. (24a), the signal $s_T(x,t)$ is given by

$$s_T(x,t) = \frac{z_1}{f_1} = -z_1 \left(\frac{\partial n}{\partial T}\right) \int \left(\frac{\partial^2 T}{\partial x^2}\right) dy, \tag{42}$$

where $T(x,y,t)$ is given by Eq. (8). Since the integrand is nonzero only in a dimension of the order of $(a^2 + 8Dt)^{1/2}$, one may set the limits of integration in Eq. (42) to be from $-\infty$ to $+\infty$. The y-integral can then be evaluated exactly, with the result

$$s_T(x,t) = \frac{8\alpha E_0 z_1}{\sqrt{2}\pi\rho C_p t_0} \left(\frac{\partial n}{\partial T}\right) \int_0^{t_0} \frac{1}{[a^2 + 8D(t-\tau)]^{3/2}} \times \left\{1 - \frac{4[x - v_x(t-\tau)]^2}{[a^2 + 8D(t-\tau)]}\right\} \times \exp\{-2[x - v_x(t-\tau)]^2/[a^2 + 8D(t-\tau)]\} d\tau. \tag{43}$$

The τ-integral in general must be evaluated numerically except for very short laser pulses. For short pulses (impulse approximation), $s_T(x,t)$ may be written down in closed form using Eq. (40) as

$$s_T(x,t) = \frac{8\alpha E_0 z_1}{\sqrt{2}\pi\rho C_p} \left(\frac{\partial n}{\partial T}\right) \frac{1}{(a^2 + 8Dt)^{3/2}} \left\{1 - \frac{4(x - v_x t)^2}{(a^2 + 8Dt)}\right\} \times \exp[-2(x - v_x t)^2/(a^2 + 8Dt)]. \tag{44}$$

The predictions of Eq. (43) are shown in Figs. 7 and 8. The method of 64-point Gaussian quadrature was used to evaluate the τ-integral, although the IMSL subroutine DECADRE could also have been used.

Figure 7 shows the results for a stationary medium, while Fig. 8 shows the results for a flowing medium. All parameters used in these calculations are the same as those for Figs. 5 and 6. The general shape of these curves is similar to that of collinear PTLS. However, the magnitude of the signal is much smaller due to the reduced interaction length in the transverse case, and the lens becomes a converging lens for $|x| > 0.50$. Moreover, the relative strength of the converging lens (wings of the lens) is larger than in the collinear case.

The curves shown in Figs. 5–8 were computed for a laser pulse which was short (1 μs) compared to the thermal diffusion and convection times. In this case the predictions of Eqs. (41) and (44) do not differ significantly from those of Eqs. (39) and (43), respectively. However, for long laser pulses, the signal shapes are drastically modified. The distinguishing

feature of our theoretical treatment is that it is valid for arbitrarily long pulses. Figure 9 shows the transverse PTLS signal shapes for a laser pulse of 0.5-ms duration. Four curves for four different flow velocities are shown. Time $t = 0$ corresponds to the start of the laser pulse. For each value of the velocity, a pump–probe distance was chosen so as to make the curves fall in the same time range for convenience in the display. All parameters, except t_0, used in this calculation were the same as in the previous diagrams. Again, the method of 64-point Gaussian quadrature was used to evaluate the τ-integral. The integrals in the $0 \le t \le t_0$ range were evaluated by replacing the upper limit (t_0) by t. Consider the $v_x = 0$ curve first. The signal increases in the time range $0 < t < 0.5$ ms because the laser pulse is on during this time interval. In the presence of a flow, the signal starts changing shape as a/v_x becomes comparable to t_0. For $t_0 > a/v_x$, the signal shapes are totally different from those shown in Fig. 8. The physical reason for the change in shape, of course, is that a significant amount of heat is convected during the time that the laser pulse is on, and the shape of the thermal image is more like a top hat than a Gaussian.

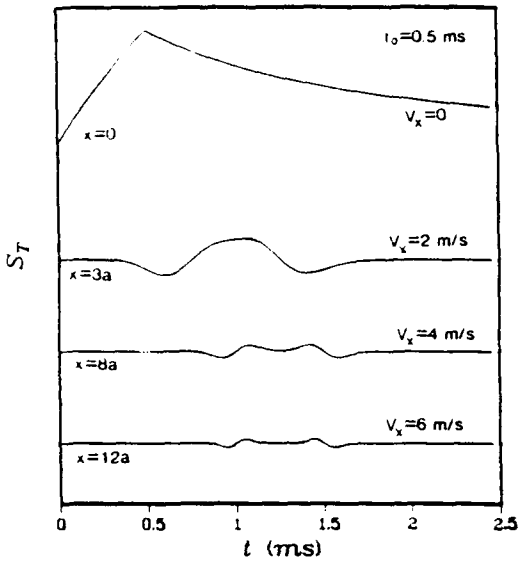

Fig. 9. PTLS signal shapes for a long laser pulse ($t_0 = 0.5$ ms) for four values of the flow velocity, as labeled. Time $t = 0$ corresponds to the start of the laser pulse. The signal has been plotted in arbitrary units.

B. Continuous-Wave PTLS

The collinear PTLS signal is given by Eq. (38) where f_1 and f_3 are given by Eqs. (23a) and (23b). Substitution of $T(x,y,t)$ from Eq. (9) leads to the desired result

$$s_L(x,t) = \frac{8\alpha P_0 l z_1}{\pi\rho C_p}\left(\frac{\partial n}{\partial T}\right)\int_0^t \frac{|(1+\cos\omega\tau)|}{[a^2+8D(t-\tau)]^{\frac{1}{2}}} \times \left\{2 - \frac{4[x-v_x(t-\tau)]^2}{[a^2+8D(t-\tau)]}\right\} \times \exp\{-2[x-v_x(t-\tau)]^2/[a^2+8D(t-\tau)]\}d\tau. \quad (45)$$

The transverse PTLS signal is given by Eq. (42) in conjunction with Eq. (9). The result is

$$s_T(x,t) = \frac{8\alpha P_0 z_1}{\sqrt{2}\pi\rho C_p}\left(\frac{\partial n}{\partial T}\right)\int_0^t \frac{|(1+\cos\omega\tau)|}{[a^2+8D(t-\tau)]^{\frac{1}{2}}} \times \left\{1 - \frac{4[x-v_x(t-\tau)]^2}{[a^2+8D(t-\tau)]}\right\} \times \exp\{-2[x-v_x(t-\tau)]^2/[a^2+8D(t-\tau)]\}d\tau. \quad (46)$$

Equations (45) and (46) must be evaluated numerically. The evaluation of these integrals was problematic as the integrand is highly oscillatory due to the presence of the $\cos\omega\tau$ factor, and it rises very steeply near $\tau \approx t$ due to the presence of the exponential factor. To evaluate these integrals, the range of integration 0 to t was divided into three regions: 0–$0.9t$, $0.9t$–$0.99t$, and $0.99t$–t. These regions were further divided into many small intervals. The integral in each of these small intervals was evaluated using a Gaussian quadrature of 64 points. The length of these intervals was chosen according to the steepness and oscillation frequency of the integrand. They were smaller in the region where the integrand was changing rapidly. For example, for frequencies above 10 Hz, one interval was chosen for each oscillation in the first region (0–$0.9t$). In the time range $0.9t$–$0.99t$ two intervals were chosen for each oscillation. In the third region ($0.99t$–t) four intervals were chosen for each oscillation. The number of intervals had to be increased further with increasing velocities.

Before discussing the steady state PTLS signals, it is instructive to examine the temporal evolution of the temperature distribution and that of the signal. Since Eq. (9) for $T(x,y,t)$ and Eqs. (45) and (46) for $s(x,t)$ cannot be integrated analytically for the general case, let us consider the simple case of $v_x = 0$, $\omega = 0$, and $x = y = 0$. Integration of Eq. (9) then yields

$$T(x=y=0,t) = \frac{\alpha P_0}{4\pi\rho C_p D}\ln\left(1+\frac{2t}{t_c}\right). \quad (47)$$

where the time constant t_c is defined as $t_c = a^2/4D$. We note that the temperature continues to rise as t increases, that is, a true steady state is never reached (although the rate of increase is very small for $t \gg t_c$). This is a consequence of the fact that we have assumed our sample to have no boundaries. Now consider the collinear signal at $x = y = 0$ for $v_x = 0$ and $\omega = 0$. Integration of Eq. (45) yields

$$s_L(x=y=0,t) = \frac{2\alpha P l z_1}{\pi\rho C_p D a^2}\left(\frac{\partial n}{\partial T}\right)\frac{1}{(1+t_c/2t)}. \quad (48)$$

In contrast to the temperature, the PTLS signal does reach a steady state.

Consider now the evolution of the temperature distribution, as shown in Fig. 10 for four positions. The laser is turned on at $t = 0$, and it is modulated at 100 Hz. The medium is again assumed to be N_2 at atmospheric pressure seeded with 1000-ppm NO_2, and it is assumed to be moving with a flow velocity of 1 cm/s. Throughout this paper, the negative values of x represent upstream positions while the positive values rep-

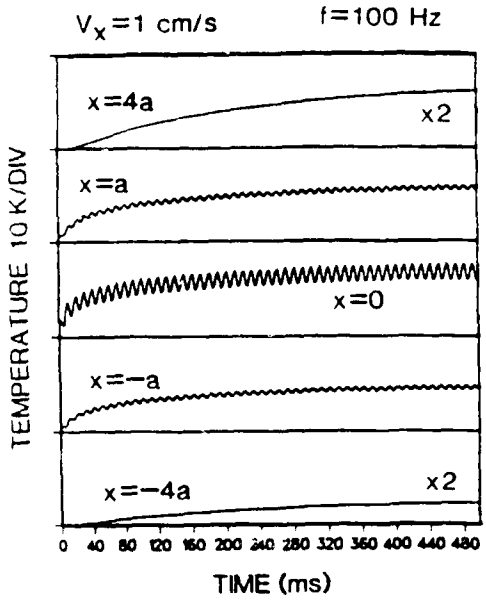

Fig. 10. Temporal evolution of the temperature at several positions in the medium. The cw laser was assumed to be modulated at 100 Hz and was turned on at $t = 0$. $x = 0$ corresponds to the axis of the pump beam. The top and bottom curves have been expanded by factors of 2 for clarity.

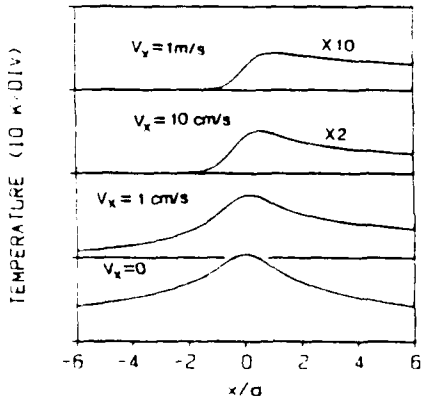

Fig. 11. "Steady state" temperature distributions in the medium (atmospheric pressure of N_2 seeded with 1000-ppm NO_2) created by an unmodulated cw laser. The laser power was assumed to be 1 W, and its $1/e^2$ radius was assumed to be 0.5 mm. All other parameters have been given previously in connection with pulsed PTLS. The top two curves have been expanded by the indicated factors for clarity.

resent downstream positions. We note that it takes the temperature a long time to reach "equilibrium," as expected. Moreover, as one gets farther from the center of the beam, the time it takes to reach "equilibrium" gets longer. Also, the modulation amplitude decreases very significantly as $|x|$ is increased. The effect of the flow velocity can also be seen in Fig. 10, and it is most significant for $|x| > a$. For larger flow velocities, there is no temperature distribution (above the ambient) outside the pump beam on the upstream side. Also, the temperature distribution approaches "equilibrium" much faster as the flow velocity is increased.

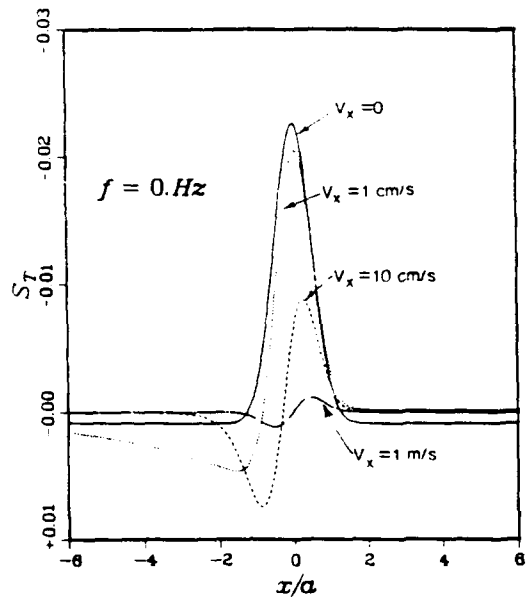

Fig. 12. Transverse cw PTLS signals corresponding to the temperature distribution shown in Fig. 11 for several flow velocities.

Figure 11 shows the temperature distribution 5 s after turning on the pump beam for several flow velocities as labeled. In this plot, the laser is assumed to be unmodulated [$\omega = 0$ in Eq. (9)]. An examination of Fig. 11 shows that the "steady state" temperature distribution extends far beyond the radius of the pump beam. As the flow velocity is increased, the temperature distribution becomes more and more asymmetric and the temperature extends farther downstream. Moreover, the magnitude of the temperature rise decreases with increasing velocity, as expected. Since the PTLS signal is proportional to the second derivative of the temperature, a nonuniform variation of the temperature with distance is required to generate a signal. Therefore, one might even obtain a larger PTLS signal on the upstream side than on the downstream side.

Figure 12 shows the PTLS signals from an unmodulated laser beam as a function of the position of the probe beam. The signal for the transverse case is plotted for four different flow velocities ($v_x = 0$, 1 cm/s, 10 cm/s, and 1 m/s). Consider the signal in the stationary medium ($v_x = 0$) first. The signal is symmetric about $x = 0$, as expected. The center of the laser irradiated region acts like a diverging lens, while the wings act like weak converging lenses. As the flow velocity is increased, the signal becomes asymmetric. The irradiated region on the upstream side behaves like a converging lens, while that on the downstream side behaves like a diverging lens. Collinear PTLS signals are similar to the transverse ones, except that they are larger due to the larger interaction length.

Generally it is convenient to amplitude modulate the pump beam so that lock-in detection (phase sensitive detection) can be used. Figure 13 shows the rms value of PTLS signal for the transverse case when the laser was modulated at 10 Hz and had an average

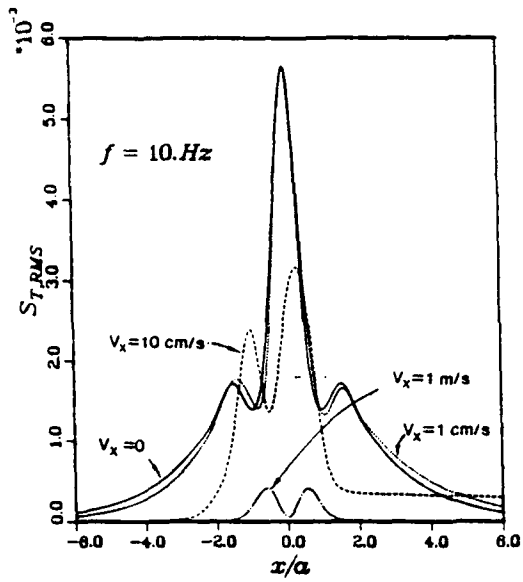

Fig. 13. Root mean square values of transverse PTLS signals for a modulation frequency of 10 Hz.

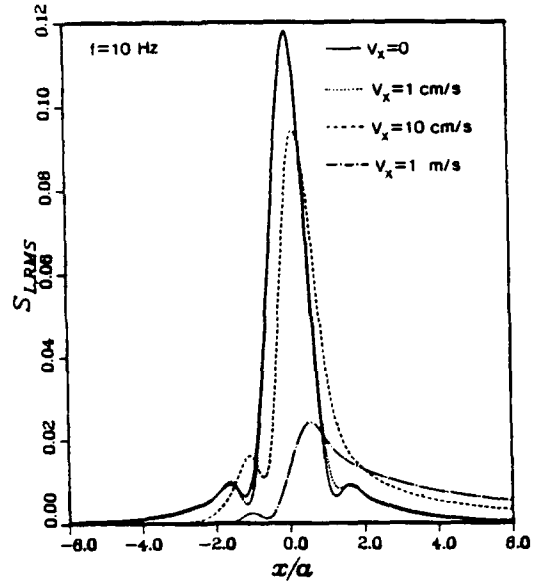

Fig. 15. Root mean square values of collinear PTLS signals for f = 10 Hz. Interaction length was assumed to be 1 cm.

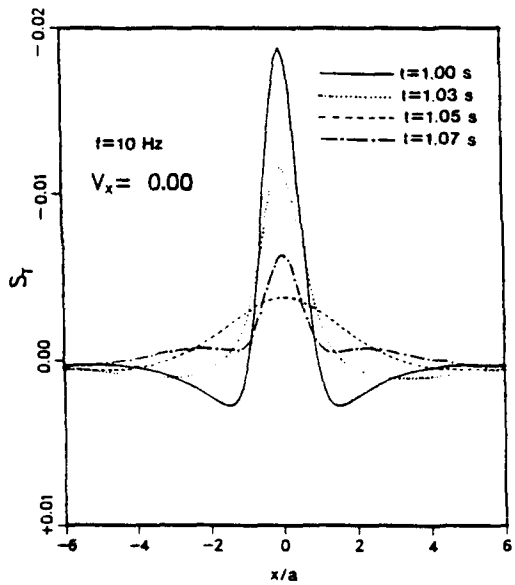

Fig. 14. Transverse PTLS signals at four times in the modulation cycle of the laser. t = 1.00 s corresponds to the peak of the laser intensity, and t = 1.05 s corresponds to the off portion of the modulation cycle.

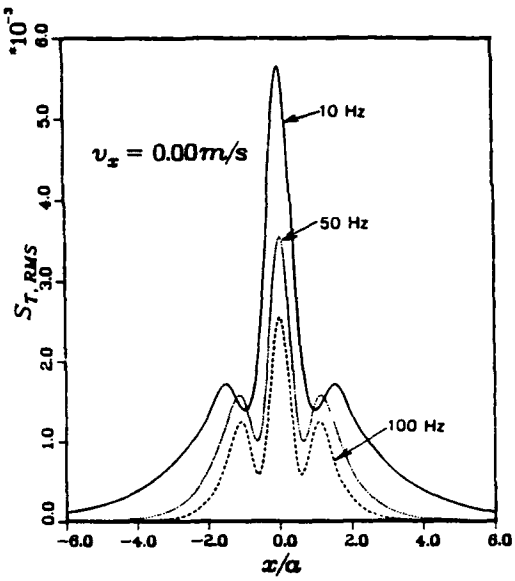

Fig. 16. Dependence of the rms transverse PTLS signals on the modulation frequency of the laser in a stationary medium.

power of 1 W. This diagram and all subsequent diagrams have been plotted for parameters given in the caption to Fig. 11. The signal is plotted as a function of the position of the probe beam for four different flow velocities, as labeled. As expected, the signal is symmetric about $x = 0$ for $v_x = 0$ and becomes increasingly asymmetric as v_x is increased. The apparent symmetry of the v_x = 1 m/s curve about $x = 0$ is fortuitous. To understand the shapes of these signals, it is necessary to consider the variation of PTLS signals with time. The PTLS signals for $v_x = 0$ (and f = 10 Hz) at four different times in the modulation cycle of the pump laser are shown in Fig. 14. The t = 1.00-s curve corresponds to the peak of the pump intensity, while the t = 1.05-s curve corresponds to the off portion of the laser intensity. Drastic changes in the signal shape with time occur. First, we note that at the peak of the pump cycle (t = 1.00 s) the wings (converging lens portion) are much more pronounced than for the unmodulated case (Fig. 12). Moreover, the thermal lens in the wings oscillates between being a converging lens and a diverging lens. Of course, this information is lost in the rms signal. Similar curves for the other flow velocities were plotted to understand the shapes of the rms signals (not shown). Curves for the collinear PTLS are

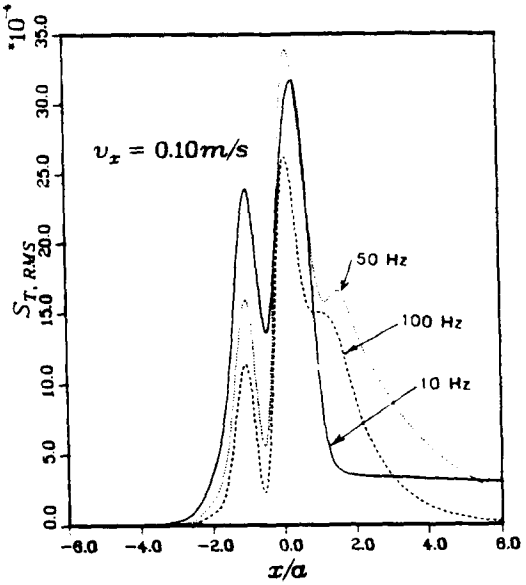

Fig. 17. Curves similar to those shown in Fig. 16 for v_x = 10 cm/s.

shown in Fig. 15. The signal amplitudes are larger, of course, but the signal shapes are also quite different from the corresponding transverse case. Again, one must examine the variation in the instantaneous signal shapes with time to understand the rms signal shapes. The modulation frequency also has a profound effect on the signal shapes. For a stationary medium, increasing the modulation frequency simply reduces the magnitude of the signal and reduces the spatial extent of the signal, as shown in Fig. 16. However, for nonzero flow velocities, the signal shapes are modified drastically as shown in Fig. 17.

VI. Summary

We have given a comprehensive theoretical description of photothermal lensing spectroscopy valid for the most general conditions.

This work was supported in part by Air Force Wright Aeronautical Laboratories.

References

1. R. Gupta, "Theory of Photothermal Effect in Fluids," in *Photothermal Investigations of Solids and Fluids*, J. A. Sell, Ed. (Academic, New York, 1988).
2. H. L. Fang and R. L. Swofford, "The Thermal Lens in Absorption Spectroscopy," in *Ultrasensitive Laser Spectroscopy*, D. S. Kliger, Ed. (Academic, New York, 1983).
3. W. A. Weimer and N. J. Dovichi, "Time-Resolved Crossed-Beam Thermal Lens Measurements as a Noninstrusive Probe of Flow Velocity," Appl. Opt. **24**, 2981 (1985).
4. J. P. Gordon, R. C. C. Leite, R. S. Moore, S. P. S. Porto, and J. R. Whinnery, "Long-Transient Effects in Lasers with Inserted Liquid Samples," J. Appl. Phys. **36**, 3 (1965).
5. C. Hu and J. R. Whinnery, "New Thermooptical Measurement Method and A Comparison with Other Methods," Appl. Opt. **12**, 72 (1973).
6. F. R. Grabiner, D. R. Siebert, and G. W. Flynn, "Laser Induced Time-Dependent Thermal Lensing Studies of Vibrational Relaxation: Translational Cooling in CH_3F," Chem. Phys. Lett. **17**, 189 (1972).
7. A. J. Twarowski and D. S. Kliger, "Multiphoton Absorption Spectra Using Thermal Blooming. I. Theory," Chem. Phys. **20**, 253 (1977).
8. R. L. Swofford and J. A. Morrell, "Analysis of the Repetitively Pulsed Dual-Beam Thermooptical Absorption Spectrometer," J. Appl. Phys. **49**, 366 (1978).
9. H. L. Fang and R. L. Swofford, "Analysis of the Thermal Lensing Effect for an Optically Thick Sample—A Revised Model," J. Appl. Phys. **50**, 6609 (1979).
10. N. J. Dovichi, T. G. Nolan, and W. A. Weimer, "Theory of Laser-Induced Photothermal Refraction," Anal. Chem. **56**, 1700 (1984).
11. W. A. Weimer and N. J. Dovichi, "Time-Resolved Thermal Lens Measurements in Flowing Samples," Anal. Chem. **57**, 2436 (1985).
12. S. E. Bialkowski, "Photothermal Lens Aberration Effects in Two Laser Thermal Lens Spectrophotometry," Appl. Opt. **24**, 2792 (1985).
13. J. M. Harris and N. J. Dovichi, "Thermal Lens Calorimetry," Anal. Chem. **52**, 695A (1980).
14. S. E. Bialkowski, "Pulsed Laser Photothermal Spectroscopy," Spectroscopy **1**, 26 (1986).
15. A. Rose, R. Vyas, and R. Gupta, "Pulsed Photothermal Deflection Spectroscopy in a Flowing Medium: A Quantitative Investigation," Appl. Opt. **25**, 4626 (1986).
16. See, for example, A. K. Ghatak and K. Thyagarajan, *Contemporary Optics* (Plenum, New York, 1978).
17. A. Yariv, *Introduction to Optical Electronics* (Holt, Rinehart & Winston, New York, 1976).